

Alma Mater Studiorum – Università di Bologna
in cotutela con Communauté Université Grenoble Alpes

DOTTORATO DI RICERCA IN
Scienze della Terra, della Vita e dell’Ambiente

Ciclo XXIX

Settore Concorsuale di afferenza: 04/A3

Settore Scientifico disciplinare: GEO/04

**Exploring Holocene climate signals recorded in stalagmites from
Bosnia**

- a multi proxy approach coupling petrography and geochemistry-

Presentata da: Veronica Chiarini

Coordinatore Dottorato

Barbara Mantovani

Relatore

Jo De Waele

Relatore

Fabien Arnaud

Correlatore

Isabelle Couchoud

Esame finale anno 2017

CONTENTS

ABSTRACT	14
I. INTRODUCTION	16
II. STATE OF THE ART	20
2.1 Present day climate: ocean and atmospheric circulation patterns in the central Mediterranean with particular focus on the Adriatic area.....	21
2.1.1 Atmospheric circulation.....	21
2.1.2 Ocean circulation in the Adriatic Sea	22
2.2 The Holocene in the Periadriatic area.....	24
2.2.1 Lateglacial-Holocene transition and early Holocene (~13,000 - 8,200 yr cal BP).....	25
2.2.1.1 <i>The Younger Dryas</i>	25
2.2.1.2 <i>The onset of the Holocene</i>	26
2.2.2 Middle Holocene (8,200 – 4,200 yr cal BP)	28
2.2.3 Late Holocene (4,200 yr cal BP – present day)	31
2.2.4 Short summary of Holocene climate fluctuations in the Periadriatic area.....	36
2.3 Hints of history: human presence and activities in the Balkans during the last 11,000 years.....	37
2.4 Speleothems as palaeo-environmental records.....	40
2.4.1 Formation of carbonate stalagmites	40
2.4.1.1 <i>Precipitation of calcium carbonate in cave environments.....</i>	40
2.4.1.2 <i>Factors involved in speleothem growth</i>	41
2.4.2 Isotopes in the study of carbonate speleothems	43
2.4.2.1 <i>Dating speleothems</i>	44
2.4.2.2 <i>Oxygen and carbon stable isotopes: clues for past environmental changes</i>	46
2.4.2.2.1 The environmental significance of stable oxygen isotope ratios ($\delta^{18}\text{O}$).....	46
2.4.2.2.2 The environmental significance of stable carbon isotope ratios ($\delta^{13}\text{C}$).....	48
2.4.2.2.3 How $\delta^{13}\text{C}$ and $\delta^{18}\text{O}$ are recorded in speleothems.....	49
2.4.3 Trace elements in speleothems and their relevance in palaeo-climate and palaeo-environmental studies	51
2.4.3.1 <i>Trace elements transfer through the karst and their incorporation into calcite</i>	51
2.4.3.2 <i>Palaeo-environmental meaning of speleothems trace element composition</i>	52
2.4.4 Stalagmite petrography and its capability in providing environmental information	53
2.4.4.1 <i>Columnar Fabric</i>	54
2.4.4.1.1 Columnar Compact (C).....	54
2.4.4.1.2 Columnar Open (Co).....	55
2.4.4.1.3 Columnar Elongated (Ce)	55
2.4.4.1.4 Spherulitic type growth in columnar fabrics.....	55
2.4.4.1.5 Columnar Microcrystalline (Cm).....	55
2.4.4.2 <i>Dendritic Fabric</i>	56
2.4.4.3 <i>Micrite (M)</i>	56

2.4.4.4 <i>Microsparite (Ms)</i>	57
2.4.4.5 <i>Mosaic Calcite (Mc)</i>	57
2.4.4.6 <i>Implication of calcite fabric micrologging for stable isotope profile interpretation.</i>	58
III. STUDY AREA	60
3.1 Cave settings and sampling location.....	61
3.2 Atmospheric circulation and stable isotope composition.....	64
3.3 Present day climate and vegetation	64
IV. MATERIALS AND METHODS	66
4.1 Brief sample description.....	67
4.2 Monitoring of cave parameters and present day precipitation	69
4.2.1 Cave monitoring and precipitation sampling	69
4.2.2 Air mass backtrajectory analyses	70
4.3 Analyses performed on the Bosnian stalagmites.....	71
4.3.1 U-Th dating and age modeling.....	71
4.3.2 Stable isotopes.....	74
4.3.3 Trace elements	76
4.3.4 Petrography	77
4.3.5 Statistical analyses used for comparing petrography and geochemical signals in stalagmites BS14 and BS15	78
4.3.6 Analyses applied specifically to the black layer	79
4.3.6.1 <i>Fluorescence microscope</i>	79
4.3.6.2 <i>Micro-Raman spectroscopy analyses</i>	79
4.3.6.3 <i>Fourier Transform Infrared Spectroscopy (FTIR)</i>	80
4.3.6.4 <i>Scanning Electrom Microscope (SEM) analyses</i>	80
V. RESULTS	82
5.1 Monitoring data: cave dynamics and precipitation stable isotope composition	83
5.1.1 Cave dynamics	83
5.1.2 Precipitation and drip water stable isotope composition	85
5.1.3 Air mass back trajectories of daily precipitation in Sarajevo	86
5.2 Petrography	88
5.2.1 Calcite textures in stalagmite G5	88
5.2.2 Calcite textures in stalagmite BS8	88
5.2.3 Calcite textures in stalagmite BS9	89
5.2.4 Classification of BS14 and BS15 textures for petrography micrologging.....	90
5.3 Ages of the bosnian stalagmites	95
5.3.1 Stalagmite G5.....	95

5.3.2 Stalagmite BS8.....	96
5.3.3 Stalagmite BS9.....	97
5.3.4 Stalagmite BS14.....	98
5.3.5 Stalagmite BS15.....	100
5.4 Stable oxygen and carbon isotope composition.....	105
5.4.1 $\delta^{13}\text{C}$ and $\delta^{18}\text{O}$ variability along the growth axis of the studied stalagmites	105
5.4.2 Tests for fractionation conditions during calcite precipitation	107
5.5 Trace element concentration in stalagmite BS15	110
5.6 Statistical approach used to couple petrography and geochemical signals in stalagmites BS14 and BS15	113
5.7 The black layer	117
5.7.1 Fluorescence microscopy	117
5.7.2 FTIR and micro-Raman results.....	117
5.7.3 SEM observations and analyses.....	118
VI. DISCUSSION	128
6.1 Processes behind the isotopic signal of precipitation and its transfer to the karst environment.....	129
6.1.1 Introduction	129
6.1.2 Stable isotope composition of modern precipitation in Zagreb and their relation with atmospheric physical parameters	129
6.1.3 Present day atmospheric circulation in Sarajevo and its influence on the isotopic signal of precipitation	134
6.1.4 Cave hydrology and sensitivity to external changes.....	138
6.1.5 Conclusions.....	142
6.2 Age of the studied stalagmites.....	143
6.2.1 Introduction.....	143
6.2.2 Age-depth model of stalagmite G5 and rejected ages.....	143
6.2.3 Age-depth model of stalagmite BS8 and rejected ages.....	144
6.2.4 Age-depth model of stalagmite BS9 and rejected ages.....	146
6.2.5 Age-depth model of stalagmite BS14 and rejected ages.....	148
6.2.6 Age-depth model of stalagmite BS15 and rejected ages.....	151
6.2.7 Comparison between stalagmite growth rates	152
6.2.8 Conclusions.....	153
6.3 Petrographical and geochemical changes in the Bosnian stalagmites.....	154
6.3.1 Introduction.....	154
6.3.2 Trace element variations in stalagmite BS15.....	155

6.3.3 Stable isotope variability in the studied stalagmites. Reliability and significance of the recorded signals.....	158
6.3.3.1 <i>Hendy test and replication test: disequilibrium or equilibrium fractionation?</i>	158
6.3.3.2 <i>Evidence from trace elements in stalagmite BS15 for stable isotope interpretation</i>	163
6.3.4 Petrography variations and their relation to environmental changes.....	164
6.3.4.1 <i>Chemical and physical parameters influencing fabric variation in stalagmites BS14 and BS15</i>	164
6.3.4.2 <i>Palaeo-environmental information recorded by calcite fabrics</i>	167
6.3.4.3 <i>Petrography variations in stalagmites BS8 and BS9</i>	169
6.3.5 Conclusions.....	173
6.4 The Bosnian Holocene record	174
6.4.1 Introduction.....	174
6.4.2 Interpretation of the analysed record in terms of palaeo-environmental changes during the Holocene in Bosnia	174
6.4.2.1 <i>Millennial-scale climate trends through the Holocene</i>	174
6.4.2.2 <i>Multi-decadal- to centennial-scale climate changes</i>	179
6.4.3 Comparison with other records and signal interpretation in the wider context of climate variations in the central Mediterranean and the Balkan region	186
6.4.4 Conclusions.....	194
6.5 Archaeological evidence	195
6.5.1 Introduction.....	195
6.5.2 Timing of the black layer in the Mračna Pećina stalagmites.....	195
6.5.3 Origin of the black layer	197
6.5.4 Conclusions.....	200
VII. CONCLUSIONS.....	201
FINAL REMARKS AND FUTURE DEVELOPMENTS	203
SYNTHESIS IN ITALIAN - Sintesi in Italiano	204
SYNTHESIS IN FRENCH – Synthèse en Français	209
ACKNOWLEDGEMENTS.....	214
References	215

LIST OF FIGURES

Section II

Fig. 2.1 – Jet stream variation in relation to positive and negative NAO mode.....	21
Fig. 2.2 – Eastern Mediterranean Sea circulation patterns. From Siani et al., 2013.....	23
Fig. 2.3 – Location of the Periadriatic records reporting Holocene climate reconstructions.....	24
Fig. 2.4 – Summary of Holocene hydrological fluctuations in the Periadriatic area. Only general trends are considered.....	37
Fig. 2.5 – Map on the Roman Empire invasions.....	38
Fig. 2.6 – Left: speleothems fed by fracture flow dominated paths (Orlovača Cave, Bosnia and Herzegovina). Right: speleothems fed by diffuse flow dominated paths (Pozzo Cucù Cave, Italy).....	42
Fig. 2.7 – Oxygen isotopes.....	43
Fig. 2.8 – ²³⁸ U and ²³² Th decay chain.....	45
Fig. 2.9 – Rainout effect on $\delta^2\text{H}$ and $\delta^{18}\text{O}$ in precipitation (Hoefs, 1997; Coplen et al., 2000).....	47
Fig. 2.10 – Stable oxygen isotope fractionation in the hydrological cycle and in water paths towards cave environments. (From Lachniet, 2009).....	48
Fig. 2.11 – Spatial distribution of C4 fraction of vegetation (from Still et al., 2003).....	49
Fig. 2.12 – Scheme of possible sources of trace elements found in speleothem calcite.....	51
Fig. 2.13 – Thin section images of stalagmite fabrics.....	57
Fig. 2.14 – Fabric classification and coding proposed in Frisia (2015).....	59

Section III

Fig. 3.1 – Mračna Pečina and Govještica cave entrance locations.....	61
Fig. 3.2 – Map of Mračna Pečina cave and partial map of Govještica cave (by Gruppo Speleologico Bolognese). Red circles indicate the areas where the stalagmites were found.....	63
Fig. 3.3 – Major vegetation zones in Europe (Encyclopaedia Britannica, Inc).....	65
Fig. 3.4 – Average monthly precipitation (blue boxes: time interval 1992-2015) and average monthly temperature (red line: time interval 1992-2015).....	65

Section IV

Fig. 4.1 – Polished sections of the studied stalagmites.....	68
Fig. 4.2 – Mračna Pečina cave map. The red circle: area where the stalagmites were collected; D1 and D2: monitored drip sites; G1, G2 and G3: location of glass plates; T1: location of the temperature data logger.....	69
Fig. 4.3 – Position of dating and stable isotope samples on the polished sections of stalagmites BS8 and BS9.....	71

Fig. 4.4 – Position of dating and stable isotope samples on the polished sections of stalagmites G5, BS14 and BS15.....	72
Fig. 4.5 – MicroProto systems Micromill 2000 used for sampling stalagmites surfaces for both stable isotopes and U-Th analyses.....	74
Fig. 4.6 – Trace element track on BS15 slab.....	76
Fig. 4.7 – Thin sections of stalagmites BS8, BS9, BS14 and BS15.....	77
Fig. 4.8 – Left: image of BS15 polished section; the holes marked by progressive numbers correspond to the samples drilled for stable isotope analyses. Right: image of thin section corresponding to the stalagmite portion on the left.....	77
Fig. 4.9 – Red squares indicate the position where powder samples have been drilled along the black layer in stalagmites BS14 and B15.....	80
Fig. 4.10 – The red square indicates the area on the surface of BS14 where one of the powder samples of the black layer was drilled.....	81
Fig. 4.11 – Copper tape on BS15 slab.....	81

Section V

Fig. 5.1 – pH, water temperature (°C) and specific electrical conductance (SEC) of monitored drip sites. N.m = not measured. D1 and D2: drip sites monitored with a stalagmite; G1, G2 and G3: drip sites where a glass tablet was positioned for growth rate monitoring.....	83
Fig. 5.2 – $\delta^{18}\text{O}$ composition of rainfall sampled in Sarajevo and drip sites D1, D2, G1 and G3 (see Tab. 5.2).....	86
Fig. 5.3 – Example of backtrajectories performed on rainy days in Sarajevo showing the predominant patterns of winter and summer air mass trajectories (left) and the different and less frequent air mass trajectories mainly found in spring, autumn and summer (right).....	87
Fig. 5.4 – Image of stalagmite BS8 thin section under natural (right) and polarised light (left).....	89
Fig. 5.5 – Image of stalagmite BS9 thin section under natural (left) and polarised light (right).....	90
Fig. 5.6 – Microphotographs of composite crystals identified in stalagmite BS15 thin section.....	91
Fig. 5.7 – Fabric subdivision and classification (normal and polarised light) modified from Frisia (2015).....	92
Fig. 5.8 – Thin section images of stalagmite BS15. Red circles indicate Ccm laminae presenting a brownish coating and evident signals of dissolution of the underlying calcite.....	93
Fig. 5.9 – Petrography curve and lamination curve for stalagmites BS14 and BS15.....	95
Fig. 5.10 – U-Th ages for stalagmite G5. Results are represented in relation to their distance from the stalagmite top.....	96
Fig. 5.11 – U-Th ages for stalagmite BS8. Results are represented in relation to their distance from the stalagmite top.....	97
Fig. 5.12 – U-Th ages for stalagmite BS9. Results are represented in relation to their distance from the stalagmite top.....	98
Fig. 5.13 – U-Th ages for stalagmite BS14. Results are represented in relation to their distance from the stalagmite top.....	99
Fig. 5.14 – U-Th ages for stalagmite BS15. Results are represented in relation to their distance from the stalagmite top.....	100

Fig. 5.15 – Oxygen stable isotope ratio along the growth axis of stalagmites BS8, BS9, BS14, BS15 and G5.....	105
Fig. 5.16 – Stable carbon isotope variation along the growth axis of stalagmites BS8, BS9, BS14, BS15 and G5.....	106
Fig. 5.17 – $\delta^{13}\text{C}$ - $\delta^{18}\text{O}$ diagrams. Left: stalagmites G5, BS9, BS14 and BS15. Right: data restricted to the part above above 51 mm from the top (black rhombohedra; BS8 - 1) and below 51 mm from the top (grey rhombohedra; BS8-2) in stalagmite BS8.....	107
Fig. 5.18 – Hendy test results for stalagmites BS8, BS14 and BS15.....	109
Fig. 5.19 – Trace element concentrations in stalagmite BS15 expressed as 31-point moving averages (coloured lines) and millimetric averages (black and grey bold lines). Results are expressed in ppm.....	112
Fig. 5.20 – Isotope-fabric plots for BS14 and BS15 stalagmites.....	114
Fig. 5.21 – Discriminant function for the classified petrography groups using two variables ($\delta^{18}\text{O}$ and $\delta^{13}\text{C}$) for stalagmites BS14 (left) and BS15 (right).....	115
Fig. 5.22 – Discriminant function for the classified petrography groups using four variables ($\delta^{18}\text{O}$, $\delta^{13}\text{C}$, Mg and Sr) for stalagmite BS15.....	116
Fig. 5.23 – Microphotographs of the black layer in BS15 stalagmite (10 mm from the top; red bracket). Left: natural light. Right: luminescence emitted under UV lamp excitation.....	117
Fig. 5.24 – FTIR analyses of the black layer in both stalagmites BS15 (black) and BS14 (red).....	118
Fig. 5.25 – Analysis of the black layer in stalagmite BS15 by micro-raman.....	118
Fig. 5.26 – Chemical results by SEM analysis of the black layer in BS15 stalagmite.....	119
Fig. 5.27 – Picture obtained with the SEM secondary detector on powder from the black layer of stalagmites BS14 (left) and BS15 (right). The dark area between the grains is the substrate on which the powder was set.....	119
Fig. 5.28 – Results from chemical cartography performed on the black layer powder samples of stalagmites BS14 and BS15.....	120
Fig. 5.29 – SEM image of BS14ext powder sample. Red lines delimitate groups of crystals covered by a dark coating.....	121
Fig. 5.30 – Above: SEM image of BS14ext powder sample on which the points chosen for chemical mapping are indicated with red squares. Below: results of chemical mapping corresponding to the chosen points.....	122
Fig. 5.31 – Above: SEM image of calcite coarse powder of the black layer; left: secondary detector picture; right: chemical mapping according to Ca and C concentration directly plotted on the analysed surfaces. Below: results of the chemical mapping showing the intensities of peaks corresponding to the detected elements.....	123
Plate 1 – Polished surface of stalagmite G5. Potential hiatuses are indicated in red. Black squares represent dated samples. The black line on the central growth axis represents the stable isotope profile.....	124
Plate 2 – Polished surface of stalagmite BS8. Potential hiatuses are indicated in red. Thin section images corresponding to these surfaces are reported on the right. Black squares represent dated samples. The black lines on the central growth axis represent the stable isotope profile. H1, H2 and H3 indicate the laminae on which the Hendy test was performed.....	125

Plate 3 – Polished surface of stalagmite BS9. Potential hiatuses are indicated in red. Thin section images corresponding to these surfaces are reported on the right. Black squares represent dated samples. The black lines on the central growth axis represent the stable isotope profile.....	126
Plate 4 – Polished surface of stalagmites BS14 (above) and BS15 (below). Potential hiatuses are indicated in red. Thin section images corresponding to these surfaces are reported on the right. Black squares represent dated samples. The black lines on the central growth axis represent the stable isotope profile. H1, H2 and H3 indicate the laminae on which the Hendy test was performed.....	127

Section VI

Chapter 6.1

Fig. 6.1.1 – Average monthly precipitation and temperature in Sarajevo and Zagreb over the period 2000-2012 (data from www.worldweatheronline.com).....	130
Fig. 6.1.2 – Comparison between Global Meteoric Water Lines (GMWL; Craig, 1961), Mediterranean Meteoric Water lines (MMWL; Gat and Carmi, 1970), Zagreb and Sarajevo local water lines.....	130
Fig. 6.1.3 – Average monthly $\delta^{18}\text{O}$ composition of precipitation in Zagreb plotted in function of precipitation (mm; above) and temperature ($^{\circ}\text{C}$; below).....	131
Fig. 6.1.4 – Weighted average $\delta^{18}\text{O}$ for each temperature class plotted versus the average temperature for each class (GNIP data from Zagreb).....	132
Fig. 6.1.5 – Weighed average $\delta^{18}\text{O}$ for each precipitation class plotted versus the average precipitation for each class (GNIP data from Zagreb).....	132
Fig. 6.1.6 – Comparison of smoothed data (moving averages on 15 points) of: monthly precipitation (blue curve), $\delta^{18}\text{O}$ (green curve), temperature (red curve), and the NAO index (black curve) for the Zagreb station.....	133
Fig. 6.1.7 – Data smoothing (moving averages on 25 points) of monthly precipitation (blue curve), $\delta^{18}\text{O}$ (green curve), temperature (red curve), and NAO index (black curve).....	134
Fig. 6.1.8 – Relation between daily temperature (from www.wunderground.com) and $\delta^{18}\text{O}$ of sampled precipitation in Sarajevo.....	135
Fig. 6.1.9 – Black dots: $\delta^{18}\text{O}$ composition of sampled precipitation. The orange box corresponds to samples collected during the meteorological autumn (1 st September – 30 th November), the light blue box the ones collected during the meteorological winter (1 st December – 28 th February), the green one the samples collected during the meteorological spring (1 st March – 31 st May) and the light yellow one samples collected in summer (1 st June – July).....	136
Fig. 6.1.10 – Daily temperature (purple squares) and $\delta^{18}\text{O}$ (blue points) in Sarajevo. Temperatures have been obtained from www.wuunderground.com	137
Fig. 6.1.11 – Backtrajectory analyses performed on February 29th, 2016.....	137
Fig. 6.1.12 – Average monthly temperature (red line: time interval 1992-2015; black dashed line: year 2015) and average monthly precipitation (blue boxes: time interval 1992-2015; black squared boxes: year 2015).....	138
Fig. 6.1.13 – pH and specific electrical conductivity (SEC) measurements for drip sites D1, D2, G1 and G3 in Mračna Pećina Cave.....	139
Fig. 6.1.14 – $\delta^{18}\text{O}$ composition of precipitation events sampled in Sarajevo (black dots and line) and of drip water collected at monitored drip sites D1 (blue), D2 (pink), G1 (yellow) and G3 (light blue) in Mračna Pećina cave....	141

Chapter 6.2

Fig. 6.2.1 – Age-depth model of stalagmite G5.....	144
Fig. 6.2.2 – Age-depth model of stalagmite BS8.....	145
Fig. 6.2.3 – Thin section of BS8 corresponding to BS8-2e dating sample under normal (right) and polarised light (left).....	146
Fig. 6.2.4 – Age-depth model of stalagmite BS9.....	147
Fig. 6.2.5 – Thin section of stalagmite BS9 corresponding to the sampling position of samples BS9-3a and BS9-4a.....	148
Fig. 6.2.6 – Age-depth model of stalagmite BS14.....	149
Fig. 6.2.7 – Thin section image corresponding to the area where samples BS14-t and BS14-3d were drilled.....	150
Fig. 6.2.8 – Petrography corresponding to sample BS14-1d.....	150
Fig. 6.2.9 – Age-depth model of stalagmite BS14.....	151
Fig. 6.2.10 – Growth rate (mm/yr) according to age-depth models for all the studied stalagmites.....	153

Chapter 6.3

Fig. 6.3.1 – Comparison between Sr, Mg and P variation in BS15 and its growth rate (mm/yr) according to the calculated age-depth model.....	156
Fig. 6.3.2 – Left: linear correlation between $\delta^{13}\text{C}$ and $\delta^{18}\text{O}$ in stalagmites G5, BS9, BS14 and BS15; Right: linear correlation between $\delta^{13}\text{C}$ and $\delta^{18}\text{O}$ in stalagmite BS8, for its upper part (above 51 mm from the top; black romboheda) and lower part (below 51 mm from the top; grey romboheda).....	159
Fig. 6.3.3 – Comparison of $\delta^{18}\text{O}$ (left) and $\delta^{13}\text{C}$ (right) records in the two coeval stalagmites BS15 (black line) and BS9 (red line).....	161
Fig. 6.3.4 – $\delta^{18}\text{O}$ mid-to-late Holocene time-series of stalagmites BS15, BS9, BS14 and BS8. The blue and green boxes shades indicate tentative correlations among the different records.....	161
Fig. 6.3.5 – $\delta^{18}\text{O}$ profiles versus age of stalagmites BS8 and G5. Yellow and orange boxes indicate possible correlations among the two records during the first half of the Holocene.....	162
Fig. 6.3.6 – Growth rate (mm/yr), trace element concentrations (Sr, P, Mg: 31 points moving average and average calculated every millimetre in correspondence with the stable isotope profile) $\delta^{13}\text{C}$, calcite fabrics and $(^{234}\text{U}/^{238}\text{U})_{\text{A}}$ variations in stalagmite BS15. The grey box highlights a portion of higher growth rate corresponding to increased Sr content, lower $\delta^{13}\text{C}$ values, and decreased Mg content.....	163
Fig. 6.3.7 – Average monthly precipitation (blue boxes: time interval 1992-2015); potential monthly infiltration (blue line); average monthly temperature (red line: time interval 1992-2015) and potential evapotranspiration (PET; black dotted line).....	165
Fig. 6.3.8 – $\delta^{13}\text{C}$ and $\delta^{18}\text{O}$ profiles and micrologging curve for stalagmites BS14 (left) and BS15 (right).....	166
Fig. 6.3.9 – Isotope-fabric plots for BS14 and BS15 stalagmites.....	166
Fig. 6.3.10 – Stable isotope profiles compared with calcite fabrics in stalagmite BS9.....	170

Fig. 6.3.11 – Stable isotope profiles compared with calcite fabrics in stalagmite BS8.....	172
--	-----

Chapter 6.4

Fig. 6.4.1 – $\delta^{13}\text{C}$ (green) and $\delta^{18}\text{O}$ (red) profiles in stalagmite G5.....	175
Fig. 6.4.2 – $\delta^{13}\text{C}$ (green) and $\delta^{18}\text{O}$ (red) profiles in stalagmite BS8.....	176
Fig. 6.4.3 – Comparison between $\delta^{18}\text{O}$ (left) and $\delta^{13}\text{C}$ (right) variation recorded during the first half of the Holocene in stalagmites BS8 (blue) and G5 (black).....	177
Fig. 6.4.4 – Comparison of $\delta^{18}\text{O}$ (left) and $\delta^{13}\text{C}$ (right) variations between the four Mračna Pečina stalagmites.....	178
Fig. 6.4.5 – Middle to late Holocene $\delta^{13}\text{C}$ (green) and $\delta^{18}\text{O}$ (red) profiles in stalagmite BS15, BS8, BS9 and BS14, Mg (ppm) concentration variations and petrography variations in BS15.....	179
Fig. 6.4.6 – Early to middle Holocene $\delta^{13}\text{C}$ and $\delta^{18}\text{O}$ profiles for stalagmites BS8 (blue) and G5 (black).....	180
Fig. 6.4.7 – $\delta^{18}\text{O}$ profiles of stalagmites BS8 (top part), BS9, BS14 and B15 covering the second half of the Holocene.....	183
Fig. 6.4.8 – $\delta^{13}\text{C}$ profiles of stalagmites BS8 (top part), BS9, BS14 and B15 covering the second half of the Holocene.....	184
Fig. 6.4.9 – $\delta^{13}\text{C}$, $\delta^{18}\text{O}$ petrography and lamination curves of stalagmites BS14 and BS15 covering the second half of the Holocene.....	185
Fig. 6.4.10 – $\delta^{13}\text{C}$ (green) and $\delta^{18}\text{O}$ (red) profiles of stalagmite BS8 and South Adriatic Sea Surface Temperature ($^{\circ}\text{C}$) (Siani et al., 2013); winter and summer insolation variations at 30°N during the Holocene (Berger and Loutre, 1991).....	187
Fig. 6.4.11 – $\delta^{18}\text{O}$ (red) and $\delta^{13}\text{C}$ (green) profiles in stalagmite BS8 and total organic carbon (TOC %; blue) and organic matter $\delta^{13}\text{C}$ (black) of Lake Ohrid (Lacey et al., 2015).....	189
Fig. 6.4.12 – $\delta^{13}\text{C}$ and $\delta^{18}\text{O}$ profiles of stalagmite BS8 and $\delta^{13}\text{C}$ profile of stalagmite CC26 from Corchia Cave (Zanchetta et al., 2007).....	190
Fig. 6.4.13 – $\delta^{13}\text{C}$ profiles of stalagmites BS9 and BS15 and total organic carbon (TOC %) and organic matter $\delta^{13}\text{C}$ of Lake Ohrid (Lacey et al., 2015).....	192
Fig. 6.4.14 – $\delta^{13}\text{C}$, $\delta^{18}\text{O}$ and petrography changes in stalagmite BS15 and NAO oscillation reconstruction for the last 5.2 ka (Olsen et al., 2012).....	193

Chapter 6.5

Fig. 6.5.1 – Ages of the black layer in stalagmites BS8, BS9, BS15 and BS14 according to their age-depth models. The yellow box indicates the ages that are contemporaneous.....	195
Fig. 6.5.2 – U-Th results for stalagmites BS8, BS9, BS14 and BS15 of samples below and above the black layer.....	196
Fig. 6.5.3 – Mn and Fe results from laser ablation on stalagmite BS15.....	197
Fig. 6.5.4 – Thin section images (plain polarised light) of the black layer in stalagmites BS14, BS15, BS8 and BS9.....	198
Fig. 6.5.4 – SEM image of calcite coarse powder sampled in the black layer.....	198

LIST OF TABLES

Section IV

Tab. 4.1 – Distance from the stalagmite top of the laminae sampled for HENDY test in stalagmites BS8, BS14 and BS15 and number of calcite powder samples drilled for each lamina.....	74
---	----

Section V

Tab. 5.1 – pH, water temperature (°C) and specific electrical conductance (SEC) of monitored drip sites. N.m = not measured. D1 and D2: drip sites monitored with a stalagmite; G1, G2 and G3: drip sites where a glass tablet was positioned for growth rate monitoring.....	84
Tab. 5.2 – Stable isotope results of precipitation in Sarajevo (labelled with an S) and drip water from Mračna Pećina Cave (G and D samples. Monitored drip sites are indicated in Fig. 4.1 in Chapter IV).....	85
Tab. 5.3 – U-Th results for stalagmite BS8.....	101
Tab. 5.4 – U-Th results for stalagmites BS9 and G5.....	102
Tab. 5.5 – U-Th results for stalagmites BS14.....	103
Tab. 5.6 – U-Th results for stalagmites BS15.....	104
Tab. 5.7 – Oxygen and carbon stable isotope variation along single laminae of BS8, BS14 and BS15 stalagmites.....	108
Tab. 5.8 – Trace elements analysed in stalagmite BS15 by laser ablation.....	111
Tab. 5.9 – Results from Kruskal-Wallis test performed among fabric groups according to $\delta^{18}\text{O}$ and $\delta^{13}\text{C}$ in stalagmites BS14 and BS15.....	113
Tab. 5.10 – Bonferroni test results between petrography groups in stalagmites BS14 and BS15 for $\delta^{18}\text{O}$ and $\delta^{13}\text{C}$ ratios.....	114
Tab. 5.11 – Discriminant analysis results for stalagmites BS14 and BS15. Petrography class have been discriminated according to their $\delta^{18}\text{O}$ and $\delta^{13}\text{C}$ composition.....	115
Tab. 5.12 – Discriminant analysis results for stalagmite BS15. Petrography class have been discriminated according to their $\delta^{18}\text{O}$, $\delta^{13}\text{C}$, Sr and Mg composition.....	116

Section VI

Tab. 6.1.1 – Average $\delta^{18}\text{O}$ composition of drip water samples collected between September 2015 and July 2016 and precipitation events collected in Sarajevo; average seasonal $\delta^{18}\text{O}$ composition of the collected water samples (autumn and winter – spring and summer); $\delta^{18}\text{O}$ composition of drip water in winter; average $\delta^{18}\text{O}$ composition of precipitation in winter.....	140
Tab. 6.3.1 – Trace elements analysed in stalagmite BS15 by laser ablation. LOD represents the instrument detection limit.....	57

ABSTRACT

The Mediterranean area is a densely populated region characterised by an extremely complex atmospheric circulation, which is particularly sensitive to any modification of air mass dynamics. Thus, the understanding of past climate fluctuations in this area is of great importance to gain insight in the pattern of regional climate variability in response to hemispheric and global climate changes. The central Mediterranean area displayed contrasting climatic responses to atmospheric circulation re-organization following the last glacial period. In particular, drier/wetter conditions in the northern/southern regions respectively, lasted until about 4.5 ka, followed by a trend towards an inversion of these conditions. This trend, which is evident in marine and continental records from the Italian Peninsula and the Adriatic Sea, is less witnessed in the Balkans, where few Holocene climate reconstructions are available. In order to better understand Holocene climate dynamics in the Balkan Peninsula, five stalagmites were collected from two Bosnian caves (Govještica and Mračna Pećina; Prača Valley). Speleothems are indeed excellent archives of past climate and environment thanks to their deposition in stable environments, protected from most surface weathering processes. Rainfall and cave monitoring (in Mračna Pećina Cave) was set up in order to understand present day cave hydrology and better interpret how the environmental and/or climate signals are transmitted to the speleothem through the karst system. Both drip water and rainfall samples were collected for stable isotope analyses ($\delta^{18}\text{O}$ and δD). All stalagmites were dated using the U-Th disequilibrium, measured by MC-ICPMS, and age-depth models were derived from a Bayesian-Monte Carlo treatment of the ages with stratigraphic constraints. $\delta^{18}\text{O}$ and $\delta^{13}\text{C}$ were analysed along the growth axis. Indeed, these values can provide information about temperature, precipitation regime and vegetation cover if calcite is deposited close to isotopic equilibrium conditions. Unfortunately, stable isotope profiles were noisy and not interpretable straightforwardly. Therefore, a multi proxy approach was adopted, coupling stable isotope and trace element profiles with detailed petrographic observations. This allowed for the interpretation of geochemical proxies and petrography variations in relation to hydrological changes. In particular, a trend towards relatively drier conditions appears since about 4 kyr, suggesting a local response to climate change similar to the one of the southern Mediterranean sites. A marginal part of this project involved the examination of a dark laminated deposited around 1.2 ka in the 4 samples from Mračna Pećina cave. This layer, appearing fluorescent under the fluorescence optic microscope, was not identified using the FTIR and micro Raman techniques, but only with SEM observation, which demonstrated its soot nature.

La Méditerranée est une région densément peuplée, caractérisée par une circulation atmosphérique extrêmement complexe et particulièrement sensible aux modifications de dynamique des masses d'air. Ainsi, la compréhension des fluctuations climatiques passées dans cette région est d'une grande importance pour mieux comprendre les modalités de la variabilité climatique régionale en réponse aux changements hémisphériques et globaux. La zone méditerranéenne centrale a présenté des réponses climatiques contrastées à la réorganisation de la circulation atmosphérique suivant la dernière période glaciaire. En particulier, dans les régions du sud/nord des conditions plus sèches/humides, ont duré jusqu'à environ 4,5 ka, suivies d'une tendance vers une inversion de ces conditions. Cette tendance, qui se manifeste dans les archives marines et continentales de la péninsule italienne et de la mer Adriatique, est moins attestée dans les Balkans, où peu de reconstructions climatiques de l'Holocène sont disponibles. Afin de mieux comprendre la dynamique du climat dans la péninsule des Balkans pendant l'Holocène, cinq stalagmites ont été collectées dans deux grottes de Bosnie (Govještica et Mračna Pećina, Prača Valley). En effet, les spéléothèmes sont d'excellentes archives du climat et des environnements passés, grâce à leur dépôt dans des environnements stables et protégés de la plupart des processus d'altération qui existent à la surface. Un monitoring de la pluie et en grotte (Mračna Pećina) a été mis en place afin de comprendre la dynamique actuelle des égouttements en grotte et de mieux interpréter la façon dont les signaux environnementaux et/ou climatiques sont transmis aux spéléothèmes à travers le système karstique. Des échantillons d'eau d'infiltration et de précipitations ont été recueillis pour les analyses d'isotopes stables ($\delta^{18}\text{O}$ et δD). Tous les stalagmites ont été datés en utilisant le déséquilibre U-Th, mesuré par MC-ICPMS, et les modèles d'âge en fonction de la profondeur ont été calculés par un traitement Bayésien-Monte Carlo des âges avec

contraintes stratigraphiques. Les analyses des isotopes stables ($\delta^{18}\text{O}$ et $\delta^{13}\text{C}$) ont été réalisées le long de l'axe de croissance. En effet, ces valeurs peuvent fournir des informations sur la température, le régime des précipitations et la couverture végétale à condition que la calcite soit déposée dans des conditions proches de l'équilibre isotopique. Malheureusement, les profils des isotopes stables se sont avérés très bruités et pas interprétables directement. Ainsi, une approche multi-proxy a donc été adoptée en couplant les profils des isotopes stables avec des observations pétrographiques détaillées et les variations de concentration des éléments traces. Ceci a permis d'interpréter les variations des indicateurs géochimiques et de la pétrographie en termes de changements d'hydrologie. En particulier, une tendance vers des conditions plus sèches apparaît depuis environ 4 ka, ce qui suggère une réponse locale au changement climatique similaire à celle des sites du sud de la Méditerranée.

Une partie marginale de ce projet a été consacrée à l'examen d'un dépôt sombre datant de ~1,2 ka dans les échantillons de Mračna Pećina. Cette lamina, apparaissant fluorescente sous le microscope optique à fluorescence, n'a pas été identifiée au moyen des techniques FTIR et micro Raman. Cependant, les observations au MEB ont permis de définir qu'il s'agissait d'un dépôt de suie.

Il Mediterraneo è una regione densamente popolata caratterizzata da una circolazione atmosferica estremamente complessa, particolarmente sensibile alle più piccole modifiche delle dinamiche tra le masse d'aria. La comprensione delle fluttuazioni climatiche del passato in questa regione è quindi di grande importanza al fine di comprendere le variazioni climatiche a scala regionale in risposta ai cambiamenti climatici globali. La zona del Mediterraneo centrale è stata caratterizzata da risposte climatiche contrastanti in seguito alla riorganizzazione della circolazione atmosferica dopo l'ultimo periodo glaciale. In particolare, un clima umido/arido si è instaurato nelle regioni meridionali/settentrionali fino a circa 4,5 mila anni fa, seguito da un andamento opposto. Questa tendenza climatica è evidente nei record marini e continentali della penisola italiana, mentre è meno chiara nei Balcani, dove sono disponibili poche ricostruzioni paleo climatiche. Al fine di comprendere meglio le dinamiche climatiche nella penisola balcanica nel corso dell'Olocene, cinque stalagmiti sono state campionate in due grotte bosniache (Govještica e Mračna Pećina; Valle di Prača). Gli speleotemi sono eccellenti archivi paleoclimatici e paleoambientali grazie alla loro formazione in ambienti relativamente stabili, protetti dai processi erosivi che avvengono all'esterno. Un programma di monitoraggio delle precipitazioni e dei parametri fisici in grotta (nella grotta Mračna Pećina) è stato messo a punto con lo scopo di comprendere le dinamiche idrologiche odierne e di interpretare come i segnali ambientali e/o climatici vengono trasmessi agli speleotemi attraverso il sistema carsico. Campioni d'acqua, sia di precipitazione, sia di stillicidio, sono stati raccolti per le analisi della composizione isotopica ($\delta^{18}\text{O}$ e δD).

Le stalagmiti sono state datate col metodo U-Th. Le date così ottenute sono state utilizzate per calcolare i modelli età-profondità utilizzando un metodo che accoppia la statistica Bayesiana al metodo Monte Carlo. Gli isotopi stabili ($\delta^{18}\text{O}$ e $\delta^{13}\text{C}$) della calcite sono stati analizzati lungo l'asse di crescita delle stalagmiti. Questi valori, infatti, possono fornire informazioni sulla temperatura, sul regime delle precipitazioni e sulla copertura vegetale, a patto che la calcite precipiti in condizioni di equilibrio isotopico. Purtroppo però, i profili isotopici di queste stalagmiti sono risultati essere affetti da un'elevato rumore di fondo, che ne ha resa complicata l'interpretazione. Pertanto, è stato adottato un approccio multi-proxy, accoppiando i profili isotopici con la variazioni degli elementi in traccia e i cambiamenti di tessitura dei cristalli di calcite. Questo approccio ha consentito l'interpretazione dei proxy geochimici e delle variazioni petrografiche in termini idrologici. In particolare, un trend verso condizioni relativamente aride è stato osservato negli ultimi 4 mila anni, suggerendo una risposta climatica locale simile a quella registrata nei siti del Mediterraneo meridionale.

Una parte marginale di questo progetto ha coinvolto l'esame di una lamina scura depositasi circa 1,2 mila anni fa nei 4 campioni prelevati nella grotta Mračna Pećina. Questo orizzonte, apparso fluorescente al microscopio ottico a fluorescenza, non è stato identificato utilizzando le tecniche FTIR e micro-Raman, ma solamente attraverso l'osservazione al SEM, che ha permesso di identificarlo come un deposito di fuliggine..

I. INTRODUCTION

The Mediterranean area is a transitional zone between the European temperate and African tropical zones (Magny et al., 2013). The complex atmospheric circulation of this region is responsible for its strong sensitivity to climate fluctuations (Giorgi, 2006): even small changes in air mass dynamics can have significant hydrological consequences at the regional scale. Considering the population density in this region, it is of fundamental importance to understand local responses to climate changes occurred in the past, in order to better predict possible future trends.

During the Holocene interglacial period, the central Mediterranean area displayed contrasting responses to climate changes related to the atmospheric circulation re-organization following the last glacial period. In particular, northern sites experienced relatively dry conditions during the early to middle Holocene followed by increased precipitation during the late Holocene, while the southern ones experienced the opposite trend. The border between these two different climate responses has been assumed to be at $\sim 40^{\circ}\text{N}$ (Magny et al., 2013). However, whereas these contrasting trends have been recorded by marine and continental records of the Italian Peninsula, the palaeoclimate dynamics in the Balkans are less documented. In this region, few Holocene climate reconstructions are available, suggesting a more gradual onset of the Holocene than in the Italian Peninsula. Although less marked than in the Italian records, contrasting climate responses seem to have been recorded also in this region. However, the availability of only few studies in the central and northern Balkan regions does not allow for the identification of the boundary between the different climate responses to atmospheric processes. A combination of orbital, ice-sheet and solar forcing influenced the atmospheric re-organization after the glacial period, leading to the development of a NAO-type circulation at $\sim 5\text{ka}$, which is thought to have caused the contrasting north-south patterns in the last 4.5 ka; however the eventual role of atmospheric circulation patterns other than NAO in the identified palaeohydrological dynamics is not clear (Magny et al., 2013).

In the context of Holocene climate reconstructions in the central Mediterranean basin, the western-central Balkans are a strategic target for 1) the identification of the boundary between the north-south contrasting climate responses and 2) the investigation of the eventual role played by eastern Europe atmospheric circulation in palaeohydrological variations. Aiming to investigate Holocene climate dynamics of this region, in this study we focused on five stalagmites sampled in Mračna Pećina and Govještica caves (Prača Valley, Bosnia and Herzegovina), covering almost the entire Holocene interglacial. These two caves, which belong to a karst system developed in the Romanija plateau, are located at a latitude of 43°N , thus resulting an interesting target for the exploration of Holocene climate fluctuations.

Among the continental archives of past climate and environmental changes, carbonate stalagmites are considered excellent materials thanks to the characteristics of the environments in which they are found and to the processes that lead to their formation. Indeed, these natural archives are deposited in relatively stable underground environments protected from surface weathering processes, allowing them to potentially grow continuously over long periods of time. These speleothems are formed by calcium carbonate precipitated from water infiltrating the soil and the bedrock before reaching the cave. When calcite is deposited, it incorporates the U transported by the infiltrating water that starts decaying into its daughter products, allowing for a potentially precise radiometric dating of these materials. During their growth they can also record external changes over seasonal to multi-millennial time periods. Indeed, the speleothem parent drip water transfers some information related to both atmospheric and soil processes into the karst, and ultimately into the precipitated carbonate. This can be deduced from calcite oxygen and carbon stable isotope ratios, trace element concentration and petrographic features (Fairchild and Baker, 2012 and reference therein; Frisia, 2015). The interpretation of isotopic signals in terms of palaeoclimate fluctuations relies on calcite precipitation close to equilibrium conditions and on the absence of post-depositional alterations. When these conditions are met, the oxygen isotope fractionation between water and calcite depends only on temperature, which in cave environments is usually stable and reflects the average temperature at the surface. This value can then provide information on the original isotopic composition of infiltrating water, which in turns depends on several factors more or less directly related to climate. The stable carbon isotope composition of calcite is instead influenced by the isotopic signature of soil pCO₂ which is related to the type and density of vegetation cover and soil microbial activity.

However, even when calcite precipitates under disequilibrium conditions, climate-related signals may still be preserved, but their interpretation is not straightforward.

Environmental and/or climate fluctuations can also produce variations in the type and concentration of trace elements leached from soil and bedrock and then incorporated into calcite crystal lattice and in speleothem texture (e.g. Fairchild and Treble, 2009; Frisia, 2015). Thus, coupling all the information that can be extrapolated from stalagmite geochemistry and petrography can improve the interpretation of the paleoenvironmental and/or palaeoclimate signals recorded by these archives.

In this thesis the multi-proxy study of the five Holocene Bosnian stalagmites is presented.

This work is divided into seven main sections, comprising the thesis introduction and conclusions. An up-to-date review of Holocene climate reconstructions in the central Mediterranean area is

treated in the second section, together with a detailed overview over on carbonate speleothems as archives for palaeoclimate information.

In the third section, the study area is presented with the geological setting and present day vegetation and climate dynamics.

The five studied stalagmites and the methods used in this research project are described in the fourth section. In the fifth one, results of the in-cave and precipitation monitoring and stalagmite geochemical analyses together with petrography observations are presented. The sixth section is entirely dedicated to the discussion of the obtained results. This part is divided into 5 minor chapters regarding, respectively, present-day hydrology of the monitored cave and the transfer of precipitation isotopic signature to the karst, the palaeoenvironmental significance of the petrographical and geochemical variations in the stalagmites, the palaeoclimatic and/or palaeoenvironmental reconstruction of this record, and, finally, the origin of a dark lamina deposited close to the top of four of the five samples.

II. STATE OF THE ART

2.1 Present day climate: ocean and atmospheric circulation patterns in the central Mediterranean with particular focus on the Adriatic area

2.1.1 Atmospheric circulation

Located in the transitional zone between the humid western and central European domain and the arid North African desert belt (Düneloh and Jacobeit, 2003), the Mediterranean area presents an extremely complicated atmospheric circulation influenced by teleconnection patterns, which have been investigated by several authors. The Northern Hemisphere patterns which play an important role in defining the climate over Europe and the Mediterranean are: the North Atlantic Oscillation (NAO), the East Atlantic pattern (EA), the Scandinavian pattern (SCAN), the East Atlantic/Western Russia pattern (EA/WR) and the Arctic Oscillation (AO), all characterised by changes in their behaviour throughout the year (Casanueva et al., 2014; Kingston et al., 2015 and reference therein). At a more global scale, Gaetani et al. (2007) investigated the possible influence of the West Africa Monsoon on the Mediterranean climate. This pattern can cause a strengthening of the North Atlantic subtropical anticyclone (Rodwell and Hoskins, 2001) leading to heat waves over the Mediterranean basin during periods of particular strong monsoonal season. This occurs through the intrusion of the Libyan anticyclone in the Mediterranean region and the strengthening of the Hadley cell circulation. However, according to Krichak and Alpert (2005) and other authors, the two prominent teleconnection patterns affecting the Mediterranean area are the North Atlantic Oscillation (NAO) and the East Atlantic/Western Russian pattern (EA/WR). During positive phases of the NAO, whose influence is stronger in winter, westerly winds are strengthened and storm tracks are shifted poleward, bringing drier conditions over the Mediterranean. Conversely, during phases of negative winter NAO are characterised by general wetter conditions (Krichak and Alpert, 2005; Fig. 2.1).

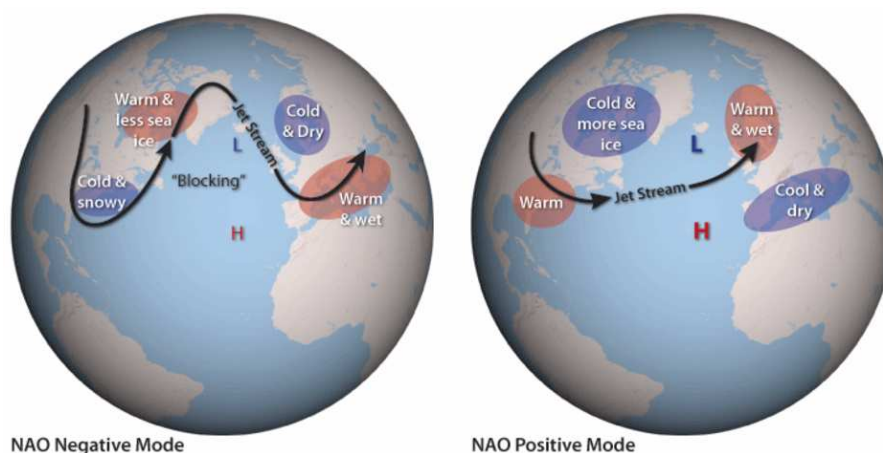


Fig. 2.1 – Jet stream variation in relation to positive and negative NAO mode (figure adapted from AIRMAP by Ned Gardiner and David Herring, NOAA).

The EA/WR pattern is characterised by predominant northerlies onto Europe over the Baltic Sea area during its positive phases, bringing drier conditions; instead, wetter climate in the Mediterranean is inferred for negative EA/WR phases. This particular pattern, according to Krichak and Alpert (2005) might be strictly related to the NAO whose strengthening might indirectly induce the formation of the EA/WR pattern bringing important dry air masses over the Eastern Mediterranean.

According to this general circulation picture, the Adriatic area is located between the subtropical high-pressure zone and the mid-latitude or westerlies belt (Orlić et al., 1992). The latter dominate the region for most of the year, disturbed in summer by the dominance of the subtropical high-pressure zone. However, Hellerman and Rosenstein (1983) and May (1982) infer a dominant easterly component over the northern and middle Adriatic. Winter and summer are characterised respectively by the main presence of the Bora wind (blowing from NE) and the Sirocco (from SW) and by the Etesian winds from NW (Orlić et al., 1992). At present, maximum precipitation occurs in late autumn while the driest period occurs in summer. In summer there is not a great difference in temperatures between the northern and the southern parts with mean temperatures spanning between 22 and 26°C, but it is in winter that the contrast becomes more important with colder conditions in the north (about 2°C) and markedly warmer ones in the southern parts (about 10°C; Orlić et al., 1992). Relative humidity is generally higher in the northern area during the coldest season, with highest values during late autumn, while the southern portion presents a relative humidity minimum in all seasons (Artegiani et al., 1997). Mean air temperature reaches the highest values in July and the lowest ones in January.

2.1.2 Ocean circulation in the Adriatic Sea

The Adriatic Sea is a semi-enclosed elongated and relatively shallow basin orientated N-NW/S-SE, presenting an increasing depth towards the Otranto Strait. The northern portion reaches a maximum depth of about 100 m, dropping quickly to 200 m just south of Ancona (Jabuka Pit); the deepest portion reaches 1200 m depth in the South Adriatic Pit rising again in the Otranto strait, where the Adriatic opens to the Ionian Sea (Orlić et al., 1992). The Po River represents the major fresh water source in the Adriatic, while other smaller contributions come from the Apennine and the Balkan rivers. The northern portion of the Adriatic is thus characterised by a surface circulation mainly controlled by the Po River seasonal discharge, which plays an important role in freshening the waters of this semi-closed basin influencing the circulation also at its southern end (Siani et al., 2013). In addition, in winter a NE wind (the Bora) plays an important role in modifying the

conditions of the region and generating a cold, dense water mass accumulating in the western flanks and dividing southwards into two branches: one sinking to the bottom of the Jabuka Pit and the other proceeding southward (Orlić et al., 1992). The complex circulation pattern modulated by the freshwater input and the formation of dense deep water in the northern and the central Adriatic, results in a cyclonic movement of surface waters that partially separate the northern and the southern portions of the basin. This is probably further enhanced by the freshwater input also from the northern regions of the Balkans (Orlić et al., 1992). This pattern can be found also in intermediate layers where the Modified Levantine Intermediate Water (MLIW) enters along the eastern coast while the cold water originating in the northern Adriatic flows southwards along the western coast. In the south Adriatic there is a continuous outflow at the Otranto Strait below the inflowing of the MLIW and the Ionian waters, giving an important contribution of the formation of the Eastern Mediterranean Deep Water (EMDW) (Fig. 2.2).

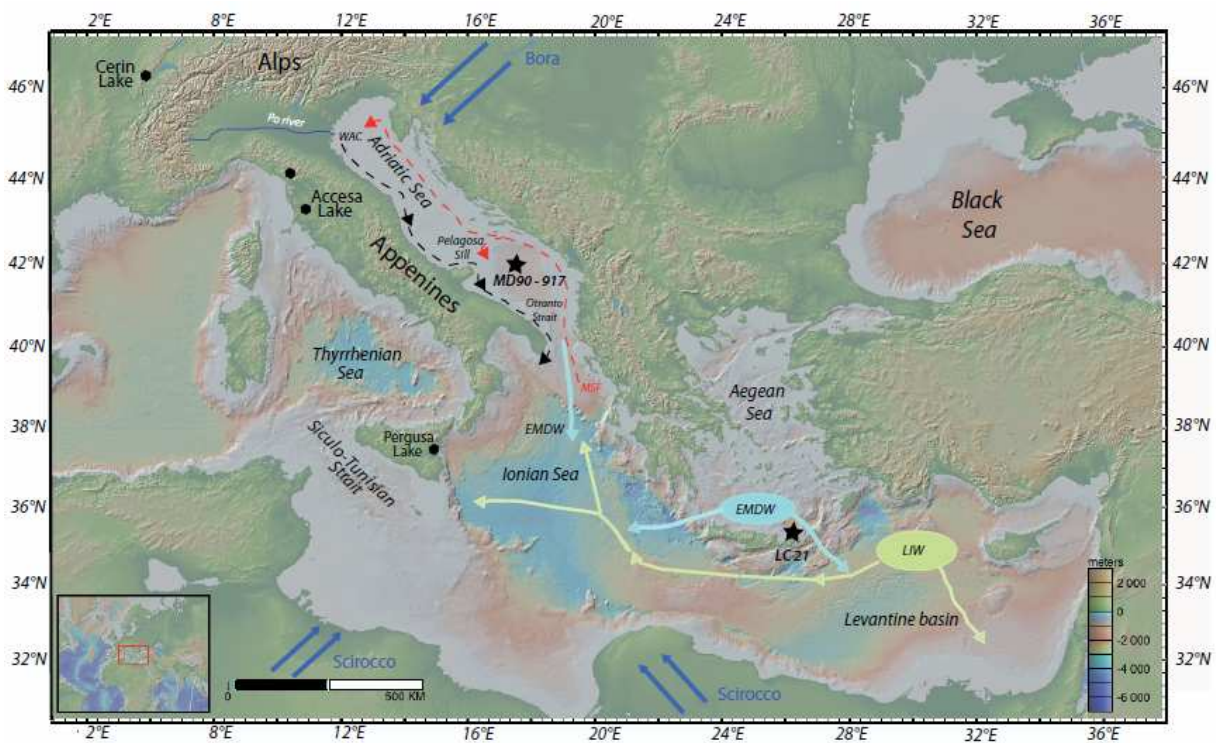


Fig. 2.2 – Eastern Mediterranean Sea circulation patterns. From Siani et al., 2013.

These dynamics highlights that the Adriatic long-term variability is driven by the winter formation of dense water masses and their partial removal by deep ocean currents (Orlić et al., 1992). But while winter is the most important period for this cold and dense water formation, the Adriatic waters are freshened during spring and summer by the river runoff (Artegiani et al., 1997). Even if the current variability is thought to be the major responsible of this circulation pattern, winds are more and more considered as important driving forces for the seasonal formation of dense water (Artegiani et al., 1997).

2.2 The Holocene in the Periadriatic area

In this chapter a summary of Holocene climate reconstructions available in the Periadriatic area is developed. The considered records are shown in Fig. 2.3. This summary is subdivided into three phases (Early Holocene, Middle Holocene and Late Holocene) following the temporal subdivision for the Holocene proposed in Walker et al. (2012).

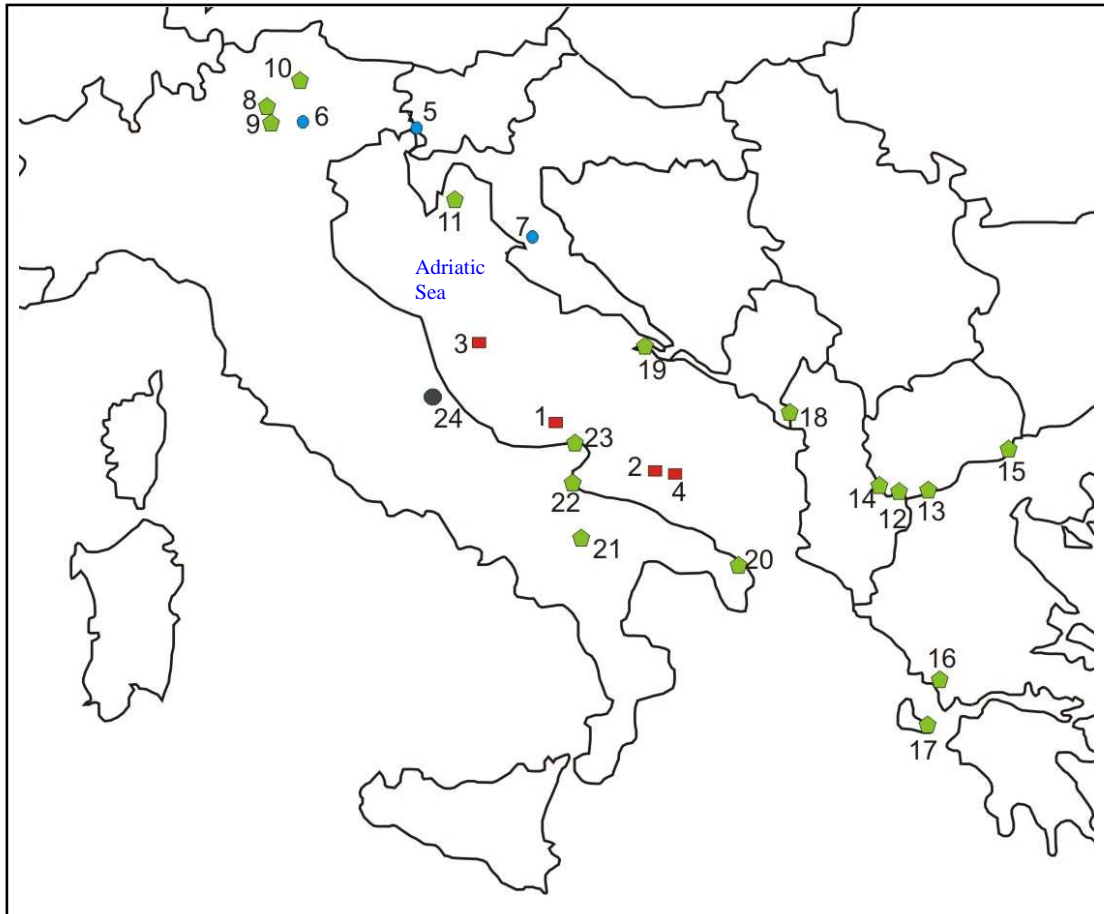


Fig. 2.3 – Location of the Periadriatic records reporting Holocene climate reconstructions.

Red squares → marine cores; 1: core RF93-30 (Oldfield et al., 2003); 2: core MD90-917 (Siani et al., 2013; Combourieu Nebout et al., 2013); 3: core CM-92-43 (Ariztegui et al., 2000; Asioli et al., 2001); 4: core AD91-17 (Sangiorgi et al., 2003). Blue dots → speleothems; 5: Grotta Savi (Belli et al., 2013); 6: Grotta di Ernesto (Scholz et al., 2013); 7: Modric Cave (Rudzka et al., 2012); Green pentagons → lakes; 8: Lake Ledro (Joannin et al., 2013; Peyron et al., 2012); 9: Lake Frassino (Baroni et al., 2006); 10: Lake Lavarone (Filippi et al., 2007); 11: Lake Vrana (Schmidt et al., 2000); 12: Lake Ohrid (Wagner et al., 2009; Vogel et al., 2010); 13: Lake Prespa (Panagiotopoulos et al., 2013; Cvetkoska et al., 2014); 14: Lake Maliq (Denèfle et al., 2000; Bordon et al., 2009); 15: Lake Dojran (Francke et al., 2013); 16: Lake Voulkaria (Jahns, 2005); 17: Alikes Lagoon (Avramidis et al., 2012); 18: Lake Shkodra (Zanchetta et al., 2012); 19: Isle Mljet (Wunsam et al., 1999); 20: Lago Alimini Piccolo (Di Rita and Magri, 2009); 21: Lago Grande di Monticchio (Allen et al., 2002); 22: Lago Salso (Di Rita et al., 2011); 23: Lago Battaglia (Caroli and Caldara, 2007). Black dot → glacier; 24: Calderone glacier (Giraudi et al., 2005).

2.2.1 Lateglacial-Holocene transition and early Holocene (~13,000 - 8,200 yr cal BP)

2.2.1.1 The Younger Dryas

During the Younger Dryas (YD) the Adriatic area (~12,800 – 11,700 yr cal BP; Ariztegui et al., 2000) was characterised by a semi-desert vegetation reflecting cold and dry climate conditions (e.g Watts et al., 1996; Magri and Sadori, 1999, Denèfle et al., 2000; Allen et al., 2002; Bordon et al., 2009; Kotthoff et al., 2011; Combourieu-Nebout et al., 2009; Combourieu-Nebout et al., 2013; Fletcher et al., 2010; Desprat et al., 2013). Cold sea surface temperatures (SSTs) have been identified in the south Adriatic Sea and the lowest mean temperature for the coldest month (5-7°C lower than the preceding and following periods) has been detected at about 12,000 yr cal BP (core MD 90-917; Siani et al., 2013; Combourieu-Nebout et al. 2013). At the same time, subtropical foraminifera species, which characterised the Adriatic Sea waters during the Bølling Allerød oscillation, disappeared and cold and productive waters with low fresh water input are inferred (core CM92-43; Ariztegui et al., 2000; Asioli et al., 2000). At about 12,500 yr cal BP, the Po river discharge increased, while between about 12,000 and 11,700 yr cal BP, climate improved, with increased moisture availability and the replacement of semi-desert plants with arboreal associations. This change is accompanied with higher discharge rates from the Apennine rivers in the Adriatic Sea (Combourieu-Nebout et al., 2013), probably related to the melting phase identified both in the Alps and in the Apennines by Maisch (1982).

Inland, the northern area of the Adriatic region experienced a period with high seasonal rainfall variability with high autumnal recharge and long winters. At Grotta Savi (Friuli Venezia Giulia, NE Italy), Belli et al. (2013) recognised the beginning of the Younger Dryas in a drastic decrease of stalagmite lamina thickness. According to Belli et al. (2013) and Grisogono and Belušić (2009), the cooler and drier conditions that characterised the YD in this region might be related to an increase in the Siberian High resulting in the strengthening of the Bora wind. In Northern Italy, pollen records from Lake Ledro (NE Italy) and diatom records from Lake Lavarone confirm the presence of a cold and dry climate phase during this period (Joannin et al., 2013; Filippi et al., 2007). Unfortunately, no palaeoclimatic lake record from south-eastern Italy covers this period, preventing the possibility of comparison with climate fluctuations recorded in north-eastern region of the Balkan region

In contrast with the trend recorded in northeastern Italy and in the south Adriatic Sea, sediment analyses at Lake Vrana (coastal lake in central Croatia) suggest the onset of more humid conditions during the Younger Dryas (Schmidt et al., 2000). Moving southwards along the Adriatic regions of

the Balkan Peninsula, climatic evidence of the Younger Dryas is not always clear. At Lake Ohrid (Albania), this peculiar climatic period is not well recorded, while it is marked by increased seasonality of precipitation with arid conditions in winter and wetter conditions in summer at the nearby Lake Maliq (Albania-Montenegro) (Vogel et al., 2010; Bordon et al., 2009). Lake-level reduction, wind stress and possibly wider catchment erosion have been recognised at Lake Prespa a bit earlier (~13,100 – 12,300 yr cal BP; Cvetkoska et al., 2014). Lake Dojran (Albania-Greece) seems to have registered this period with a higher resolution allowing a subdivision of the Younger Dryas in two phases: the first one (~12,500-12,100 yr cal BP) showed cold and dry conditions, while climate improved a little bit during the second one (~12,100-11,500 yr cal BP) with slightly higher summer temperatures and more humid conditions (Francke et al., 2013). The second phase, in particular, is remarkable by its correspondence with the increased river discharge from the Italian peninsula recognised in the south Adriatic core MD90-917 by Combourieu-Nebout et al. (2013).

2.2.1.2 The onset of the Holocene

According to several authors (Ariztegui et al., 2000; Asioli et al., 2000; Combourieu-Nebout et al., 2013; Siani et al., 2013) the onset of the Holocene in the region occurred at about 11,500 yr cal BP. The studies regarding the marine cores from the South Adriatic Sea highlight soft climate deteriorations in the basin after the improvement recognised at the end of the Younger Dryas. This phase was followed by amelioration at about 11,000 yr cal BP, when mixed deciduous forests started developing (Combourieu-Nebout et al., 2013). The beginning of the deposition of Sapropel S1 at about 9,000 yr cal BP recognised in the south Adriatic sea clearly marks a period of increased precipitation, especially in the southern parts of the Mediterranean Basin (e.g. Sangiorgi et al., 2003; Ariztegui et al., 2000); the sea surface temperatures started increasing, reaching a maximum at about 8,400 yr cal BP (Siani et al., 2013). A cold spell at about 8,200 yr cal BP in the south Adriatic SSTs has been associated with the interruption of Sapropel S1 deposition and corresponds to the main sea water salinity decrease recorded during the early Holocene (Siani et al., 2013). This cold phase is also confirmed by the increase of high altitude pollen taxa in the south Adriatic core AD91-17 (Giunta et al., 2003) although Sangiorgi et al. (2003) did not detect this SSTs cooling.

- **Adriatic side of the Italian peninsula**

The early Holocene climate improvement in northern Italy presents warmer temperatures associated with generally low moisture availability. Climate amelioration and a weakened seasonality are also recorded in NE Italy at the beginning of the Holocene (Grotta Savi; Belli et al., 2013). At about 10.8

and 10.1 ka, two cold events led the stalagmite to stop growing twice (Belli et al. 2013). In contrast, at Lake Ledro a slight increase of summer precipitation and of vegetation development occurred at about 10.800 yr cal BP, while lake levels remained generally low (Magny et al., 2012; Joannin et al., 2013). Afforestation and warmer temperatures have been recorded also at Lake Lavarone, while a general dry period is highlighted at Lake Frassino (Filippi et al., 2007; Baroni et al., 2006). At Lake Ledro, at about 9,300 yr cal BP, the expansion of montane trees is accompanied by a relative rise in lake level and temperature decrease, while at Lake Frassino dry conditions persisted (Baroni et al., 2006; Joannin et al., 2013). The lake level rise recorded at Lake Ledro at about 8,200 yr cal BP, in apparent contrast with the drier conditions reported in the South Adriatic Sea, can be associated with cold and dry winters and cool and wet summers according to Peyron et al. (2013). Southwards along the Adriatic side of the Italian peninsula, at Lago Grande di Monticchio, the afforestation process started at about 10,000 yr cal BP (Sadori and Narcisi, 2001). This process was soon followed by the increase of *Abies* in the temperate deciduous forest composition after 9,900 yr BP suggesting a wetter and/or cooler climate (Allen et al., 2002), which would agree with the increased moisture inferred during the deposition of the Sapropel S1.

- **Adriatic side of the Balkan region**

On the Adriatic side of the Balkans, the onset of the Holocene was more gradual and cool summers have been reported at Lake Maliq until about 9,800 yr cal BP (Denèfle et al., 2000). After 11,000 yr cal BP relatively humid climate conditions and slightly warmer summers are reported at Lake Ohrid (Vogel et al., 2010). Increasing lake Prespa levels during the early Holocene support the hypothesis of higher moisture availability in the region (Cvetkoska et al., 2014). The same trend with increased moisture, warmer summer and vegetation development was recorded also at Lake Dojran (Albania - Greece; Francke et al., 2013). In Croatia, enhanced moisture is inferred only from about 8,400 yr cal BP (Wunsam et al., 1999), while at Lake Maliq the temperate deciduous forest deteriorates between about 8,300 and 8,100 yr cal BP due to a return to drier and cooler conditions (Bordon et al., 2009). At Lake Prespa, the period between 10,000 and 8,000 yr cal BP is marked by a general arid phase. A markedly cold and dry spell is observed at 8,400 yr BP (Panagiotopoulos et al., 2013; Cvetkoska et al., 2014). At Lake Dojran cool conditions were still present between 10,700 and 8,300 yr cal BP with a trend of increasing humidity. Denser vegetation developed from about 9,000 yr cal BP declining after 8,700 yr cal BP with a return towards cooler temperatures (Francke et al., 2013). The increase of *Pistacia* in Greece between about 9,000 and 8,000 yr cal BP and its disappearance at about 8,000 yr cal BP confirms the climate deterioration observed in other records

of this region (Willis, 1994). Still in Greece, at Lake Voulkaria, between 10,500 and 8,300 yr cal BP the landscape appeared semi-open with deciduous oaks accompanied by significant amounts of *Pistacia* (Jahns, 2005; Di Rita and Magri, 2012). At Alikes Lagoon (Greece), open vegetation is inferred between 8,450 and 8,100 yr cal BP with general low rainfall (Avramidis et al., 2012). A decline in forest cover between 8,300 and 8,100 yr cal BP is the most prominent event in this period (Di Rita and Magri, 2012).

2.2.2 Middle Holocene (8,200 – 4,200 yr cal BP)

After the climate deterioration centred at about 8,200 yr cal BP, in the Adriatic basin forest openings are reported until about 7,500 yr cal BP, while at 7,700 yr cal BP increase of conifer population in the mixed deciduous forest probably occurred in the northern regions of the basin (south Adriatic core MD90-917; Combourieu-Nebout et al., 2013). A period of particularly cool SSTs has been recorded between about 7,300 and 6,300 yr cal BP, interrupted by two warm spells at 7,100 and 6,500 yr cal BP, the first of which is also associated with an increase in water salinity (Siani et al., 2013). The highest values of precipitation in the basin were reached between about 8,000 and 7,500 yr cal BP, when both annual and summer precipitation increased during the deposition of Saproel S1b in the south-eastern Mediterranean basin. In particular, at ~7,700 yr cal BP a long humid season with low summer and winter temperatures occurred during a period of decreased salinity, SSTs cooling and increased Po river discharge (~7,800-7,500 yr cal BP), while from ~7,000 yr cal BP increasing annual precipitation with less Po river influence and increased Apennine river discharge probably occurred (Combourieu-Nebout et al., 2013; Siani et al., 2013). At about 6,800 yr cal BP, SSTs increased reaching their maximum values between ~6,900 and 5,600 yr cal BP and stabilising at values similar to the present ones. This trend, associated with enhanced salinity, suggests the beginning of a drier phase in the South Adriatic (Sangiorgi et al., 2003; Siani et al., 2013; Sangiorgi et al., 2003). A short phase of decreased salinity indicating a brief period of enhanced river discharge occurred between about 5,000 and 4,800 yr cal BP, while foraminifera evidence suggests the onset of warmer conditions in the central Adriatic Sea (Piva et al., 2008).

- **Adriatic side of the Italian peninsula**

In north-eastern Italy, between about 8.0 and 7.3 ka, strong seasonality is inferred (Grotta di Ernesto; Scholz et al., 2012). From 8,200 yr cal BP, a lake level rise coupled with increased summer precipitation is recorded at Lake Ledro (Peyron et al. 2013). Considering temperature

reconstructions from pollen concentration, the period around 7,700 yr cal BP shows minima in annual temperatures and average temperatures of the warmest month, while dry and/or cold spells are identified at ~7,000 - 6,400 - 5,000 and 4,200 yr cal BP (Combourieu-Nebout et al., 2013). Cold temperatures between 7.8 and 7.6 ka are also confirmed by the record from Grotta di Ernesto (NE Italy), where high hydrological instability occurs between ~6.6 and 4.2 ka (Scholz et al., 2012). At 7,300 and 7,100 yr cal BP, two lake level rise events are recognised at Lake Ledro (Magny et al., 2012), the second of which corresponds to a warm spell identified by Siani et al. (2013) in the South Adriatic Sea. Phases with warm winters are recognised in north-eastern Italy at ~7.9, 7.4, 6.5, 5.5, and 4.9 ka (Grotta di Ernesto; Scholz et al., 2012). Summer cooling is recorded at Lake Ledro from about 7,000 until 4,600 yr cal BP together with a mean low water table until about 4,500 yr cal BP, with the exception of two lake level rise events at 5,850 and 5,300 cal years BP (Peyron et al., 2013). Human activity at this site is recorded from about 6,700 yr cal BP but remains low until about 4,100 yr cal BP (Joannin et al., 2013). In northern Italy, from about 5,700 until 4,100 yr cal BP, a general cooler and wetter interval is recorded with an increase in flooding activity at about 4,500 yr cal BP (Lake Ledro; Joannin et al., 2013; Peyron et al., 2013). In this context, Lake Frassino record appears controversial: here the end of the early Holocene arid phase seems to occur at about 7,000 yr BP and wetter conditions are recorded until about 5,000 yr cal BP. The alternation of dry and wet phases followed, with dry events centred at ~5,800 and 4,500 yr cal BP during a period of general wetter conditions (Baroni et al., 2006).

In southern Italy, the presence of *Alnus* at Lago Grande di Monticchio, from about 7,100 yr cal BP, suggests the onset of warmer and probably drier conditions (Allen et al., 2002). In Apulia (Lake Battaglia) typical Mediterranean vegetation is present at ~6,000 yr cal BP with a trend towards a progressive drying from about 4,200 yr cal BP (Caroli and Caldara, 2007). At Lago Salso (Laguna di Salpi; Tavoliere delle Puglie) between 6,350 and 4,050 yr cal BP, a marshland was present while extensive broad-leaved forests were located at higher elevations inland (Di Rita et al., 2011). The same trend towards more arid conditions is recorded at Lake Alimini Piccolo (southern Apulia). Here from 5,600 to 5,200 yr cal BP, seasonal desiccation is recorded. From 5,200 to 4,350 yr cal BP, the climate was more humid than today at this site, while between 4,800 and 4,500 yr cal BP, evergreen taxa decreased. This period was followed by a drop in pollen composition from 4,359 until 3,900 yr cal BP that has not been associated with human activity (Di Rita and Magri, 2009, 2012). At Lago Salso (Laguna di Salpi; Tavoliere delle Puglie) between 6,350 and 4,050 yr cal BP the area corresponded to a marshland while extensive broad-leaved forests were located at higher elevations inland (Di Rita et al., 2011).

- **Adriatic side of the Balkan region**

At about 8,000 yr cal BP, in the north-western Balkans, a phase of deciduous oak forest expansion is recorded, suggesting mild and relatively wet conditions (Lake Vrana - Croatia; Schmidt et al., 2000). At 7,300 yr cal BP, pollen concentrations in Slovenia dropped to values similar to the ones at the beginning of the Holocene, suggesting a cool/dry phase (Andric, 2007). At about 7,100 yr cal BP in Croatia (Isle of Mljet) a short phase of aridity is identified, followed by increased precipitation until about 6,300 yr cal BP (Wunsam et al., 1999). According to Horvatinčić et al. (2003) it was only from ~7,000 yr cal BP that in the northern Balkans the climatic conditions favourable to the formation of tufa occurred, together with a regeneration of the forest in Slovenia (Andric, 2007). At Isle of Mljet (Lake Malo Jezero, Croatia) a transitional phase towards a Mediterranean climate is recorded between 6,300 and 5,500 yr cal BP (Wunsam et al., 1999). In particular, according to Colombaroli et al. (2009) the transition from deciduous to evergreen forest in the Croatian coast that occurred at about 6,400 yr cal BP, lived a temporary decline between 5,600 and 5,200 yr cal BP associated with increased fire activity. The second event corresponds to drier climate conditions recorded at Lake Vrana (Northern Dalmatia) followed by a new expansion of evergreen forest at about 4,300 yr cal BP (Schmidt et al., 2000).

In the central/southern Balkans the Holocene climate improvement finally started bringing warmer summers, while winters remained cool at least until 7,500 yr cal BP (Lake Ohrid; Vogel et al., 2010). From about 7,800 yr cal BP warmer winter conditions and lower available moisture are also seen at Lake Maliq (Bordon et al., 2009). After the climate deterioration recorded at about 8,400 yr cal BP at Lake Prespa, the climate improved bringing warmer and wetter conditions; between about 7,900 and 6,000 yr cal BP this lake was characterised by a phase of high lake level (Panagiotopoulos et al., 2013; Cvetovska et al., 2014). At Lake Dojran the climate deterioration that started at about 8,700 ended at about 7,900 yr cal BP with a progressive development of vegetation and increased moisture conditions. This phase was followed by relatively high lake levels between ~7,900 and 4,300 yr cal BP, even if between 6,000 and 4,300 yr cal BP warmer temperatures and more arid conditions are inferred (Francke et al., 2013). At Lake Ohrid warmer and drier conditions characterise the period after 6,500 yr cal BP, interrupted by a cold spell at 4,300 yr BP (Vogel et al., 2010). At the same time, dry conditions are recorded at Lake Shkodra, while, in contrast with these findings, at Lake Maliq a water level rise is recorded at about 4,200 yr cal BP (Zanchetta et al., 2007; Fouache et al., 2010). Moving southwards in Greece, at Lake Voulkaria (Greece; Jahns, 2005) between 8,300 and 5,500 yr cal BP there is a decrease in *Pistacia* associated with increase in deciduous taxa. Between ~5,500 and 2,900 yr cal BP, the decrease in deciduous cover is interpreted

as a more important human activity in the area. Still in Greece, at Alikes Lagoon, between 8,100 and 7,800 yr cal BP a reforestation occurred with increases in arboreal and Mediterranean taxa. This period was followed by a decrease in temperate taxa between ~7,800 and 6,300 yr cal BP. From this period until about 5,000 yr cal BP there is an increase of wet environments and Mediterranean arboreal communities (mild and moist winters and dry warm summers; Avramidis et al., 2012; Di Rita and Magri, 2012).

2.2.3 Late Holocene (4,200 yr cal BP – present day)

After the opening of the forest observed at 4,500 yr cal BP, a cold and moist event is recorded about 500 years later in the South Adriatic Sea. At the same time, in the central Adriatic, increased fluvial input occurred. In addition, Sangiorgi et al. (2003) recognise a decrease in alkenone temperatures (SSTs) of the central Adriatic together with an increase in high altitude trees between 4,100 and 3,000 yr cal BP, suggesting a phase of cooler and/or wetter climate conditions. In particular, after a cooling of SSTs at 3,500 yr cal BP, a warming is inferred with most significant changes between ~3,500 and 2,000 yr cal BP. This period was characterised by a general decline in tree cover in the Adriatic Basin (from about 3,000 yr cal BP), with high rates of deforestation at 2,400 yr cal BP (late Bronze Age; Sangiorgi et al., 2003). In the Central Adriatic (core RF 93-30; Oldfield et al., 2003), human interference with natural vegetation is recorded from about 3,600 yr cal BP, reaching a maximum intensity of deforestation at about 3,000 yr cal BP. Even if this trend could be related to anthropogenic pressure on the landscape, the presence of *Pistacia* from about 3,500 yr cal BP together with the increase of *Olea* and of herbaceous taxa could be consistent with a climate change towards decreased summer precipitation, in the wider frame of the drying trend which characterised the southern Mediterranean regions during the late Holocene (core MD 90-917; Combourieu-Nebout et al., 2013). Thus, a possible coupling of human activities with natural climate change should be considered. After this period, a slow recovery of deciduous forest occurred between about 3,000 and 1,500 yr cal BP, even if evidence of cultivation was still present (Oldfield et al., 2003).

According to Siani et al. (2013), at the same location in the southern Adriatic, periods of reduced salinity are recognised between about 3,000 and 2,700 yr cal BP, 2,000 and 1,800 yr cal BP, at ~1,400 and 1,200 yr cal BP and between 600 yr cal BP and present day. These events could be related to enhanced runoff of the Po river according to $\delta^{13}\text{C}$ values of *Globigerina bulloides* and *G. Sacculifer* changes (Piva et al., 2008; Siani et al., 2013). To support this interpretation, periods of enhanced Po river discharges have also been identified by several studies during the last 5,500 yr cal BP (Correggiari et al., 2005; Stefani and Vincenzi, 2005; Amorosi et al., 2008; Rossi and

Vaiani, 2008). Sangiorgi et al. (2003) found an important cooling at 2,000 yr cal BP and between 1,800 and 1,600 yr cal BP after the peak of high temperatures occurred between 2,500 and 2,100 yr cal BP. These temperature changes are probably related to modifications in the water column stratification possibly driven by changes in Po river outflow. In this context, an apparently cold alkenone SST temperature might reflect enhanced river outflow.

According to Piva et al. (2003) between about 5,300-4,000, 3,800-2,400 and 2,100-600 yr cal BP peaks in *Globigerina sacculifer* correspond to warm intervals recognised in the Mediterranean (“Copper Age”, “Bronze Age”, “Roman Age” and the “Medieval Warm Period”). In addition, two cool and wet oscillations are recognised at 3,200 and 2,800 yr cal BP. The first of these cool phases has also been recognised by Sangiorgi et al. (2003) in the South Adriatic Sea. The last occurrence of *Globigerina sacculifer* occurred at about 550 yr cal BP, approximating the beginning of the Little Ice Age (LIA). Besides, the LIA coldest phases, at 1,690-1,630 AD and 1,810-1,820 AD, correspond with two peaks of *Valvulineria complanata* in the Adriatic cores (Kinzl, 1932; Mayr, 1964; Lamb, 1980; Veggiani, 1986). During this period enhanced river runoff is recorded (Piva et al., 2008).

The lack of evidence of the beginning of the Neoglacial period in the north-central Mediterranean from about 4,500-4,000 yr BP recorded in the salinity record of the south Adriatic Sea has to be highlighted (Zanchetta et al., 2012; Siani et al., 2013). At 2,400 yr cal BP a modest increase in sedimentation in the central Adriatic could be related to increased rural settlement during Samnite and Roman times, however, the period between 2,400 and 640 yr cal BP is probably characterised by a decrease in fluvial runoff which corresponds to a period of forest recover and reduced terrigenous input. In the Central Adriatic core RF 93-30 there is no evidence of human impact during the Roman Period (Oldfield et al., 2003). Another important decline in forest cover happened around 1,100 yr cal BP and became more important around 700 to 600 ca yr BP. The late Holocene landscape in the central Adriatic, especially during the Medieval Age, is thus characterised by reduced forest cover and important agricultural activities with the tendency for the Mediterranean evergreen woodland to degrade to shrubs.

- **Adriatic side of the Italian peninsula**

Considering north-eastern Italy, at lake Ledro, lake levels remained low at least until 4,100 yr cal BP (Joannin et al., 2013), even if an increasing flood activity started at ~4,500 yr cal BP (Joannin et al., 2013; Peyron et al., 2013). At Lake Frassino the recorded arid period came to its end with fluctuations between dry and wet conditions between 5,000 and 2,600 yr cal BP, with dry events

centred at 4,500 and 3,600 and 2,800 yr cal BP; between 3,000 and 2,600 yr cal BP the onset of drier conditions is inferred (Baroni et al., 2006). At 3.7 ka at Grotta di Ernesto a phase of warm winter conditions is recorded (Scholz et al., 2012). At Lake Ledro, maximum in summer precipitation is recorded at about 4,000 cal years BP (Peyron et al., 2013). Here, a general cooler and wetter interval is identified between 5,700 and 4,100 yr cal BP (*Quercus* and *Abies*) with a considerable increase in flood activity starting at ~4,500 yr cal BP (Joannin et al., 2013; Peyron et al., 2013). After an abrupt rise, the lake level remained generally high, with higher level events at 3,300 - 2,600 - 1,700 - 1,200 and 400 yr cal BP. The maximum mean elevation of the lake level was reached during the period from 2,800 yr cal BP onwards (Magny et al., 2012).

Nicolussi et al. (2005) identified in tree rings from the eastern Alps periods of higher altitude tree line at 5,460-5,300 and 4,740-4,540 yr cal BP. Human presence at Lake Ledro remained low at least until 4,100 yr cal BP, after which it increased considerably (Joannin et al., 2013); at Lake Lavarone high human impact is recorded during the Late Holocene with high deforestation and cultivation while after the end of the Roman Empire the vegetation started to grow more naturally again (Filippi et al., 2007).

In the southern Apennines, Giraudi et al. (2005) recognised the expansion of the Calderone glacier after 4,520-4,090 yr cal BP. Between ~1,300 and 970 yr cal BP minima winter temperatures 0.9°C higher than today are inferred, while between ~3,720 and 3,380 yr cal BP periglacial features occurred in soils. The lowest minima winter temperatures were registered after 525-275 and 175-150 yr cal BP. Environmental changes coherent with the two cooling cycles of the North Atlantic dated 2,800 and 1,400 yr cal BP are recognised (Bond et al., 1997; Giraudi et al., 2005). Again, talking about Apennine glaciers, the Calderone glacier, that disappeared during early-mid Holocene, had some expansion phases at 2,855-2,725, 1,410-1,290 and 640-580 yr cal BP. Periglacial features in phase with the Calderone advancement, have been found around 3,360-3,270, 2,950-2,760, 1,400-1,270, 1,070-940 and 920-670 yr cal BP. At Lago Grande di Monticchio the presence of *Abies* recorded during the early and mid Holocene started decreasing until its disappearance at around 3,000 cal years BP: this could point to both climate change and human forest exploitation (Allen et al., 2002). Between 3,000 and 1,000 yr cal BP *Quercus* recovered and *Olea* increased, while during the last 1,000 cal years BP wooden taxa pollen concentration fell considerably; during the last 2,000 yr cal BP human activity became more important in the area (Allen et al., 2002).

In southern Italy, in the “Tavoliere delle Puglie”, environmental transformations occurred between 4,050 and 3,800 yr cal BP: in this area, around 4,050 yr cal BP a near-closed lagoon became a lake with the complete disappearance of salt-marsh water foraminifera at 3,700 yr cal BP, while at a regional scale an abrupt deforestation started at about 4,000 yr cal BP (Di Rita et al., 2011).

Anthropogenic disturbances of vegetation due to agricultural activities are reported at least from 3,500 yr cal BP, when the southern slope of the Gargano already appeared completely deforested as it is today, suggesting that the forest opening recorded at ~4,000 yr cal BP had a long-lasting effect, increased by local human activity (Di Rita and Magri, 2012). At Lago Battaglia (Apulia) a progressive drying is inferred from about 4,200 yr cal BP; in particular between 4,000 and 2,700 yr cal BP fire frequency is thought to have increased, probably related to warmer and drier climate according to pollen records (Caroli and Caldara, 2007). At about 3,500 yr cal BP the vegetation recovered with the expansion of *Pinus*. The presence of *Fagus* points to probably wetter conditions between 2,700 and 2,190 yr cal BP, while agricultural activities and fire occurrence became more important (Caroli and Caldara, 2007). A similar trend is seen also at the nearby Alimini Piccolo Lake (Southern Apulia). A decrease in pollen concentration occurred from 4,350 to 3,900 with a minimum at 4,100 yr cal BP, suggesting the ongoing of a drying process (Di Rita and Magri, 2009). Between about 3,900 and 2,100 yr cal BP, a new forest expansion occurred with an increase in evergreen shrubs (Di Rita and Magri, 2012). At around 3,600 yr cal BP there is an important increase in *Olea* that could be related to both human presence and climate, while from about 2,600 yr cal BP the area became more exploited by humans (Di Rita and Magri, 2009). The spreading of *Pinus* at about 2,400 yr cal BP in the region could have been human induced (Grüger and Thulin, 1998). During the Roman occupation at Lake Alimini Piccolo between about 2,500 and 1,500 yr cal BP deforestation increased with the development of agricultural activities. During the last 2,000 yr cal BP the opening of the landscape is mainly human-driven. Around 1,900 yr cal BP an exponential growth of *Olea* has been detected together with an increase of fires (Di Rita and Magri, 2009). The opening of the landscape registered at Lake Battaglia, particularly important during the roman period, was followed by a vegetation development between about 1,500 and 1,000 yr cal BP, preceding the last phase of deforestation recorded in this record.

- **Adriatic side of the Balkan region**

On the Balkan side, in Croatia, climate conditions similar to present day ones have been recognised during the late Holocene. At Lake Ohrid, a regional warmer and drier climate is inferred between 6,500 and 2,400 yr cal BP, but colder climate conditions (decrease in precipitated calcite) are recognised from 4,300 to 3,000 yr cal BP (Vogel et al., 2010). At the coastal lake Shkodra, between 4,200 and 3,700 yr cal BP decreased calcite precipitation leads to the hypothesis of drier climate (Zanchetta et al., 2012), while at lake Maliq an abrupt rise at 4,200 yr cal BP is inferred (Fouache et al., 2010), with a second rise event at 2,600 yr cal BP. At Lake Shkodra the percentage of arboreal

plants remained rather stable for the whole period with minima at ca. 4,000 - 2,900 - 1,450 and 370 yr cal BP (Sadori et al., 2015). Southward, at Lake Dojran, the high humidity suggested by the high lake levels from 7,900 to 4,300 yr cal BP is followed by more arid conditions (Francke et al., 2013). In particular between 4,300 and 2,800 yr cal BP great instability is seen. At 4,000 yr cal BP a short phase of dry conditions is recognised (maybe related to the 4.2 kyr event; Francke et al., 2013). This phase was followed by more humid conditions. After the short cooling recognised at Lake Ohrid, a return to conditions similar to present day is seen until 2,400 years BP, when human presence became important in the area; from 1,000 to 300 years BP and at about 100 years BP possible drier conditions are deduced from a decrease in organic matter and increased precipitated calcite (Vogel et al., 2010). These oscillations could be referred to the Medieval warm period and the Little Ice Age, even if it is not possible to disentangle the eventual human interference on the signal (Wagner et al., 2009). At Lake Shkodra the late Holocene is punctuated by prominent dry events identified at 4,100-4,000, 3,500, 3,300, 1,850, 1,400, 1,150 and between 750 and 200 yr cal BP, while enhanced rainfall is inferred between about 4,500-4,100 and 2,600-2,100 yr cal BP and 1,800-1,500, 1,350-1,250, 1,100-800 and 90 cal years BP suggesting a relatively high climatic instability (Zanchetta et al., 2012). A period of increased calcite precipitation is recorded in the lake sediments from 1,250 yr cal BP, after a period of low concentration since ~3,700 yr cal BP (Zanchetta et al., 2012). Microcharcoal influx shows a peak at 4,200 yr cal BP followed by a second episode of fire at 2,900 yr cal BP (Sadori et al., 2015). The pollen record of this lake does not show any important vegetation change except a slight decreasing trend from the bottom to the top sequence, with more significant changes only in the last 700/800 years (Sadori et al., 2015). Regional fires were important at 4,200, 3,000 yr cal BP and in the last 1,600 yr, mainly related to human activity. Traces of local fires have been identified at 4,400, 2,750-2,100 and 1,300-1,200 yr cal BP. Changes possibly related to dry periods occurred at 4,000, 2,900 and 1,450 yr cal BP (Sadori et al., 2015). Two periods of increased humidity have been found, one before 4,100 yr cal BP and the second at 1,300 yr cal BP. The humidity occurring before 4,100 yr BP was followed by a decrease of precipitation at 4,300 yr cal BP. High humidity associated with a warmer phase is inferred between 2,700 and 1,200 yr cal BP, a part from a dry episode around 1,900-1,850 yr cal BP (Sadori et al., 2015). In the northern Balkans at Modrić Cave (Croatia; Rudzka et al., 2012) dry conditions are recorded at about 512 ± 76 AD and 900 ± 76 AD, while relatively wet conditions are recorded during the period between $1,348 \pm 59$ and $1,580 \pm 96$ AD. At Lake Prespa the situation is characterised by more stable conditions with lake levels remaining high until about 1,900 yr cal BP with no evidence of the events recorded in closeby sites (Cvetkoska et al., 2014; Mayewsky et al., 2004). Here, increased human deforestation is inferred after 2,000 yr cal BP, while the last 1,900 yr

cal BP have been characterised by lake level fluctuations; increased moisture is inferred between 1,000 and 50 cal ka BP, while there are some evidence for increased temperatures followed by subsequent drying and lake level decline between 1,500 and 600 yr cal BP (Panagiotopoulos et al., 2013; Aufgebauer et al., 2012; Leng et al., 2013). At Lake Dojran between 2,800 and 1,200 yr cal BP a decreasing lake level is inferred; this period was apparently characterised by a slight cooling. From 1,200 to 900 yr cal BP, more humid and warmer conditions and higher lake levels are inferred. From 900 yr cal BP until today lake level fluctuations are related to human influence; the warm medieval period seems to be followed by cooler temperatures (Francke et al., 2013). From this period onward the human influence is particularly strong, except for the period between 2,500 and 2,200 yr cal BP, during which the decrease of anthropic pressure in the area allowed a regeneration of the deciduous woodland. During the Roman period, a decrease in *Olea* and a slight increase in evergreen vegetation occurred, while with the Byzantine times a new increase in *Olea* increased again (Jahns, 2000; Di Rita and Magri, 2012).

2.2.4 Short summary of Holocene climate fluctuations in the Periadriatic area

The extremely complex picture exposed in the previous chapters shows how diverse locations reacted differently in terms of both temperature and hydrology to the onset of the Holocene. However, inside this detailed context, general trends have been identified, in line with the contrasting patterns observed in the central Mediterranean Basin by Magny et al. (2013). Indeed, relatively dry conditions are found in the northern sites of both the Italian and Balkan Peninsula followed by a transitional phase which bring generally wetter conditions during the late Holocene. Southern site in both the Italian and Balkan Peninsula experience the opposite (Fig. 2.4). However the exact limit between these opposite responses is not clear.

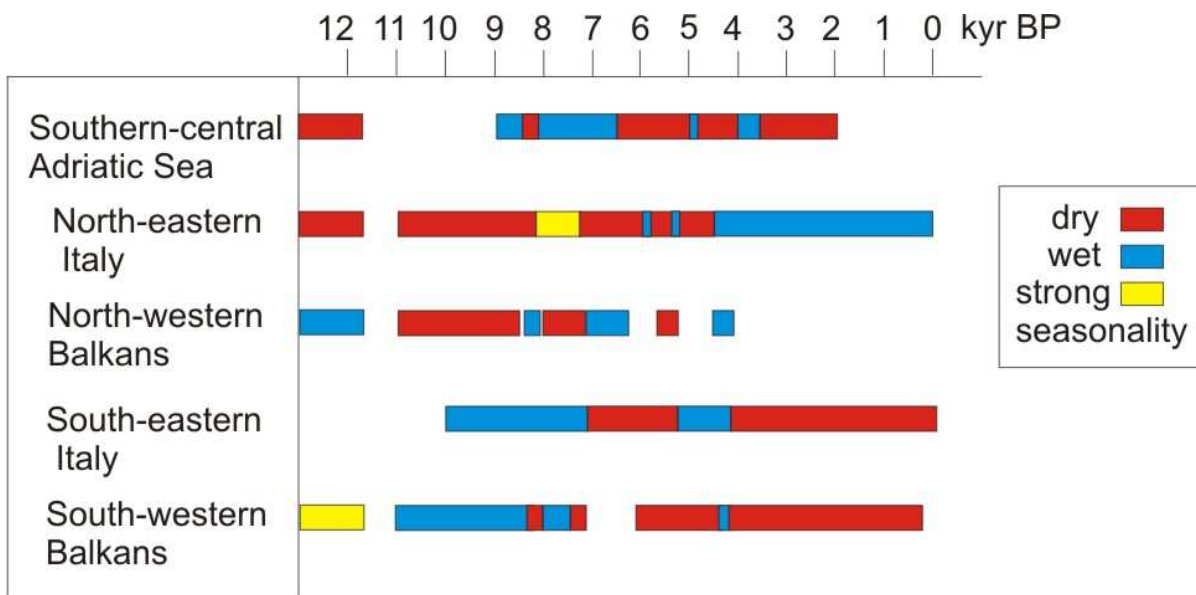


Fig. 2.4 – Summary of Holocene hydrological fluctuations in the Periadriatic area. Only general trends are considered.

2.3 Hints of history: human presence and activities in the Balkans during the last 11,000 years

The Balkans are characterised by a mountain environment, which played an important role in rural development. This kind of environment contributed to the birth of isolated communities making cultural exchanges difficult. Located at the border between western and eastern Europe, this area has always been a crossroad between different cultures and religions. Despite the difficult territory, its strategic position as a point of access to the North Adriatic Sea together with the mineral resources (i.e. silver, gold, copper and iron), present especially in the actual Bosnia and Herzegovina, made this region an interesting territory for conquerors.

The first modern humans appeared in the Balkan region approximately 46,000 yr BP, as documented at Bacho Kiro, Bulgaria (Bailey, 2000). During the last ice age this territory was not covered in ice and permafrost, providing a survival niche for both fauna and deciduous vegetation (Willis, 1994; Bailey, 2000). The main human activities during this period consisted in foraging, gathering, hunting and fishing, causing a marginal if not negligible effect on the natural landscape evolution. This period was characterised by high mobility of people across the regional landscape, concentrating their activities in sheltered places (caves and rock-shelters; Chapman 1990; Whittle, 1996; Bailey, 2000). These characteristics were kept through the post-glacial and early Holocene when the density of human communities was still low. From about 8,500 BP changes occurred in human habits. The first stable settlements developed and the manufacturing of tools and containers

increased. Group of humans started building wooden constructions and stable settlements, increasing their influence on the natural landscape (Bailey, 2000). Despite the southern and eastern Balkans, where stable villages started being built, in the western Balkans (i.e. Serbia) temporary settlements have been found (Bailey, 2000). At the same time activities related to breeding and agriculture developed, especially from about 7,500 yr BP. From this time, constructions evolved into more complex structure-forming permanent villages, while breeding slightly shifted from ovicaprids to cattle. The seasonal grazing herds' movements developed in the previous millennia continued and new areas were occupied (Bailey, 2000). At the same time, cereal cultivation intensified. Expansion of cultivated area has been detected in different archaeological sites, together with increased metal mining and manufacturing (i.e. Chapman, 1990; Tringham & Stevanovic,

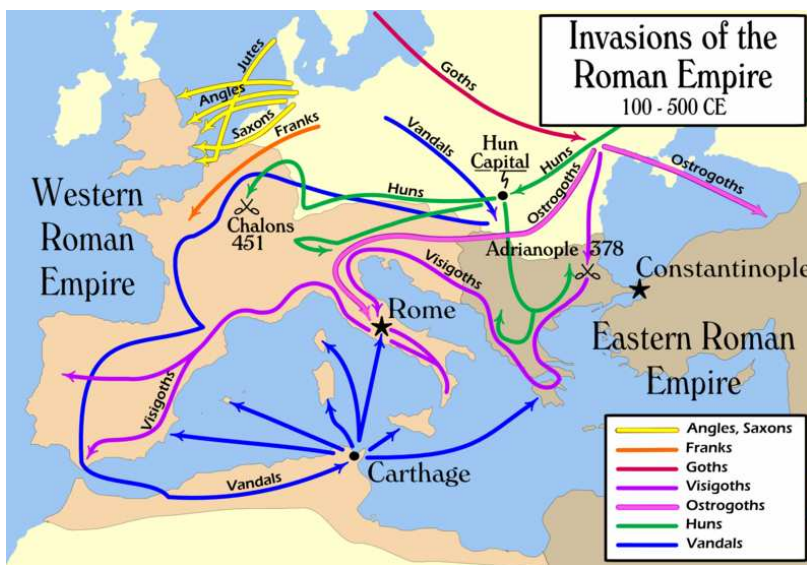


Fig. 2.5 - Map of the Roman Empire invasions.

By User:MapMaster (Own work) [CC BY-SA 2.5 (<http://creativecommons.org/licenses/by-sa/2.5>)], via Wikimedia Commons.

1990). The development of these activities may thus have had a less negligible impact on natural landscape evolution with increased deforestation. However this impact may have played a role only at a scale restricted to the more populated areas. During the VIth millennia the number of stable villages decreased in this region, probably in relation to the increasing size of grazing herds. Together with this, a diminished mining activity

occurred during this period, followed by a further increase in the next millennia (Bailey, 2000). Despite this general frame, only few late Neolithic archaeological sites have been found in the Bosnian mountains (i.e. Visoko Basin, Schroedter et al., 2012). Also mining activities developed later than elsewhere in the Balkans: according to Begemann and Schmitt-Strecker (2005) copper ores of central Bosnia were not exploited during the Early Bronze Age; only few permanent settlement structures have been observed in the timeframe between 3,600 and 3,400 yr BP (Gavranović, 2012). From this period onward these settlements expanded and developed. The presence in the region of iron ores allowed the continuity of settlements in central Bosnia at the passage from the Late Bronze Age to the Iron Age (~3,000-2,900 BP). This period faced the development of different cultures in the Balkans. Traces of the presence of the Cetina culture in the

area of Sarajevo were found (Govedarica, 2006). This culture, which mainly developed on the coastal area of the Adriatic Sea during the Early Bronze Age (~4,200-3,500 BP), may have been in contact with other tribes in the Balkan inland territory, a region that did not correspond to the environment where this culture developed (Govedarica, 2006). Among the several cultures, which developed in the Balkans, between the Late Bronze Age and the Iron Age the Glasinac culture occupied an important role in the area comprising the southern Croatia, Serbia, Bosnia and Hercegovina and Montenegro. This culture can be associated with the Autariatae, one of the most important Illyrian tribes (Stipčević, 1977). Illyrian tribes were the dominant culture in the region until the Roman occupation, which occurred during the IIth century BC. These tribes, which vanished around the VIIth century AD, were mainly devoted to agriculture, animal breeding and mining, activities which were kept and increased during the Roman occupation, while trade started playing an important role in the region, thus augmenting the anthropic pressure on natural landscape (e.g. deforestation related to increased agriculture). After the division of the Roman Empire (325 AD), the area became part of the Byzantine Empire. During the IVth and Vth centuries AD a violent period occurred in the Balkans due to the controversies between the Romans and the Goths (German tribes which invaded central and southern Europe) which led to the collapse of the Western Roman Empire. Between the Vth and VIIIth centuries AD massive migration of different populations from north-eastern Europe occurred in the Roman Empire territories (Hines et al., 1999). The most important German tribe whose migration followed a direction parallel to the Adriatic coast along the Balkans is represented by the Visigoths (Fig. 2.5). During the VIIth century a demographic decline affected the Balkans (Curta, 2013). After the fall of the Western Roman Empire, the western Balkans became part of the Ostrogoths Reign (Vth century AD), whose territories were conquered again by the Byzantines (VIIth century AD). The Balkan region remained under the Byzantine domain until the conquest of the same territories by the Ottoman Empire, which ruled the area from the XIIIth to the beginning of the XIXth centuries AD.

2.4 Speleothems as palaeo-environmental records

Among the continental materials which can record past climate and/or environmental fluctuations, speleothems are considered excellent archives, thanks to their formation in relatively stable underground environments, protected by erosion and weathering occurring at the surface. Information related to air mass and precipitation dynamics and temperature can be transferred to the speleothem calcite over seasonal to multi-millennial time scale through precipitation stable oxygen isotope composition. When water infiltrates the soil and bedrock, it can be enriched by further information related to hydrology, soil activity and type and density of vegetation cover. These are transferred to the percolating water by the stable carbon isotope composition of soil CO₂ and trace elements, which are leached from the soil and bedrock, and then incorporated into the speleothem calcium carbonate. The recorded information can be precisely time-constrained with radiometric dating. However, the interpretation of speleothem geochemistry in terms of palaeoclimate/palaeoenvironmental reconstructions is not straightforward since several processes can mask and modify the original signals. Indeed, petrography observations are essential for the identification of post-depositional modifications. In addition, calcite textures can be influenced by cave hydrology and concentration of foreign particles as well, thus representing a further tool for the identification of past environmental and/or climate fluctuations. In the following paragraphs an overview of the processes leading to speleothem formation and their recording of climate and/or environmental signals is presented.

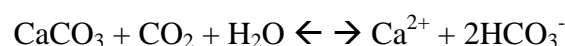
2.4.1 Formation of carbonate stalagmites

2.4.1.1 *Precipitation of calcium carbonate in cave environments*

Carbonate stalagmites are speleothems which form on cave floors from water infiltrating the overlying soil and karst bedrock.

The high soil pCO₂ (higher than the atmospheric one due to root respiration and microbial activity) can increase the acidity of infiltrating water and, thus, its aggressiveness towards the carbonate bedrock, which is dissolved (Witkamp and Frank, 1969). When the water enters the cave, the lower pCO₂ of the cave atmosphere causes the CO₂ degassing which in turns triggers the solution supersaturation and the subsequent precipitation of calcium carbonate.

This process follows the general karst equilibrium reaction for carbonate written below:



The deposition of calcium carbonate from the percolating water is thus related to its degree of saturation with respect to calcite (e.g. Fairchild and Baker, 2012). Thus, the difference in $p\text{CO}_2$ between soil and cave air is a key control on both the amount of rock dissolved and the calcite precipitation rate. If percolating water encounters vadose areas with lower $p\text{CO}_2$ before entering the cave, it may reach calcite saturation and precipitate calcite along its path towards the cave. This phenomenon, which mainly occurs during dry periods, is called prior calcite precipitation (PCP; e.g. Fairchild and McMillan, 2007).

2.4.1.2 Factors involved in speleothem growth

The process behind speleothem formation is only apparently simple. Several variables can play a role in speleothem formation acting at different time scales, from the seasonal and annual scale to the multi-decadal and multi-millennial one.

Surface temperature fluctuations are among the seasonal variations that most influence speleothem growth (Fairchild and Baker, 2012). As explained above, calcite precipitation is related to the $p\text{CO}_2$ contrast between soil and cave air. Air exchange between the cave atmosphere and the external environment can lead to the removal of cave air CO_2 (i.e. cave ventilation), thus enhancing differences between drip water and cave atmosphere $p\text{CO}_2$. In temperate climates, this process is mainly controlled by seasonal variations in surface temperature. Cave air temperature tends to be rather constant through the year at values that average the mean annual surface temperature (e.g. Wigley and Brown, 1976; Moore and Sullivan, 1978). In temperate climates, in summer, when surface temperature is higher, a poor if not negligible air exchange with the external environment occurs, causing an ineffective CO_2 removal. In winter the opposite occurs: due to the low surface temperature, the warmer cave air tends to exit the cavity, while the cold and fresh external air enters the cave, causing a lowering of cave air $p\text{CO}_2$. This phenomenon increases the calcite supersaturation of cave dripwater favouring speleothem formation during this season (Fairchild and Baker, 2012). In case of small seasonal temperature changes, the CO_2 removal can be controlled by periods of high precipitation as recorded in Altamira Cave by Sánchez-Moral et al. (1999) where CO_2 winter-summer exchange is reversed, with more exchanges with the atmosphere in summer via the epikarst.

Considering decadal-to multi-millennial scale changes climatic controls can interfere with speleothem growth (e.g. McDermott et al., 2001; Frisia et al. 2003; Genty et al., 2003; McDermott et al., 2004; Fairchild and Baker, 2012). Variations in temperature and precipitation, for example, may trigger modification in natural vegetation cover, thus changing soil CO_2 production and the subsequent saturation of the percolating waters (i.e. directly affecting stalagmite growth). In

addition long-term variations of those parameters may affect the aquifer recharge and cause changes in cave ventilation, making the air exchange between the cave and the surface less or more efficient. The recording of external signals in speleothems can be further complicated by cave hydrology dynamics: the type of water flow plays a fundamental role in determining speleothem characteristics. The two extremes are represented by diffuse and fracture flow (Fig. 2.6).



Fig. 2.6 – Left: speleothems fed by fracture flow dominated paths (Orlovača Cave, Bosnia and Herzegovina). Right: speleothems fed by diffuse flow dominated paths (Pozzo Cucù Cave, Italy)

The first one usually generates candlestick stalagmites with slow and regular drip rates, and is more subject to mixing effects, which may buffer short term atmospheric signal. The second one is more connected to external variations and is more susceptible to large variability of its drip rate, leading to the formation of wider stalagmites and other kind of speleothems (Williams, 2008; Fairchild and Baker, 2012). However, even in stable aquifers, short-term increases in discharge can cause infiltration events. If this happens, seasonal variations can be reflected in that of dripwaters (e.g. Alpine environments where winter rainfall and snowfall are usually associated with lighter $\delta^{18}\text{O}$ and individual events can be associated with reduced growth rate and reduced saturation index; Fairchild and Baker, 2012).

Given the complexity of the flow paths, speleothems coming from the same cave chamber may display different signals due to differences in hydrology, while showing the same characteristics related to cave ventilation.

2.4.2 Isotopes in the study of carbonate speleothems

Chemical elements are identified by the number of protons forming the atomic nucleus (atomic number). However the same element can comprehend some “variants” characterised by a different number of neutrons, still keeping the same atomic number. These “variants” are called isotopes. Since the sum of the number of protons and neutrons of a nucleus is called mass number, isotopes are characterised by the same atomic number and different mass number (e.g. Fig. 2.7).

Isotopes can be divided into two main categories: stable and radioactive isotopes.

Stable isotopes present a stable mass number, which does not change through time. On the contrary radioactive isotopes, which are also referred to as radionuclides, do not preserve their mass number through time since they tend to decay emitting radiations. Radioactive isotopes, which are usually expressed as ratios with their daughter products, are able to provide temporal information of a particular process. Knowing the decaying series of a particular isotope, its half-life time and the decaying constant, it is possible to determine when the decaying started, if daughter products are preserved and radioactive stock is not renewed (in a closed-system), thus enabling the age determination of several materials (e.g. U/Th, ^{14}C).

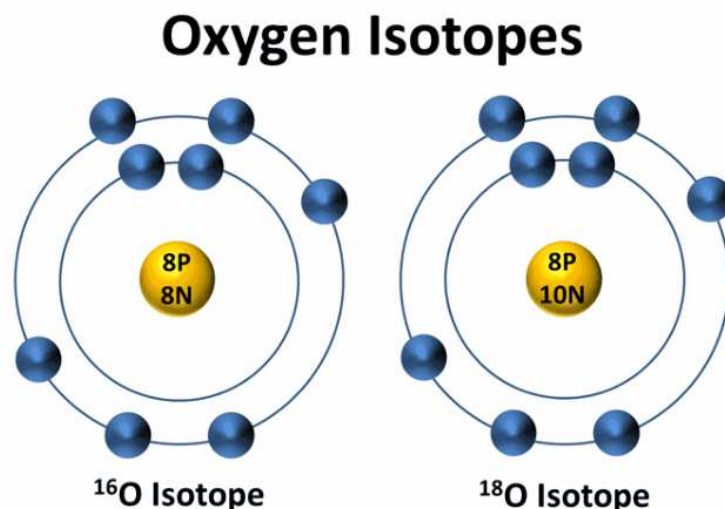


Fig. 2.7 – Oxygen isotopes. On the left the isotope presenting 8 neutrons and 8 protons, whose mass number is 16; on the right the isotope presenting 10 neutron and a mass number of 18. (From www.ces.fau.edu).

Stable isotopes are instead expressed as ratios between heavier and lighter nuclides of a certain element. The relative abundance of different isotopes of the same element can represent a reliable signature of the nature and/or origin of the process that involved these elements. Stable isotope partitioning between two different substances or phases is expressed through the fractionation factor. This parameter, which is called α , represents the ratio between the heavier and lighter

isotopes (R) of the same element in the two considered substances (i.e. $\alpha_{(B-A)} = R_B/R_A$). The fractionation process between two phases can occur at both equilibrium and disequilibrium (i.e. kinetic) conditions.

Equilibrium fractionations consist of isotope partitioning between two substances in chemical equilibrium (i.e. closed system in case of phase changes). In this case the heavier isotopes tend to concentrate into compounds or phases in which they are most stably bound. In kinetic fractionation, which can occur in open systems during phase changes, heavier isotopes tend to move more slowly and the isotopic fractionation tends to favour the lighter ones. Thus, while equilibrium fractionation is related to isotopes bond stability, kinetic fractionation is related to their relative speed. Equilibrium fractionation can be easily predicted from the knowledge of the fractionation factor, which characterises a particular process. On the contrary, kinetic fractionation requires a deeper knowledge of the variables involved in the process, which further complicates the interpretation of signals relative to determinate processes occurred in the past (White, 1997; Lachniet, 2009).

2.4.2.1 Dating speleothems

Among the several characteristics which make carbonate speleothems excellent materials for past climate investigations, the potentiality of been precisely dated providing reliable and continuous chronologies is one of the most important. Different dating techniques can be used, each of them presenting some limitations.

- **Radiocarbon dating**

Radiocarbon (^{14}C) originating in the upper atmosphere is transferred to carbonate speleothems through the CO_2 dissolved in percolating waters. ^{14}C has a half-life of 5715 years, which would be suitable for the study of relatively young samples (<40 kyr). However part of the ^{14}C of speleothem calcite is derived from hostrock dissolution thus deforming/distorting the original atmospheric signal. Since the percentage of bedrock-derived carbon (“dead carbon”) varies in speleothems, this method is not considered reliable when its proportion in the studied speleothem can not be evaluated (e.g. Genty and Massault, 1999; Genty et al., 1999; Genty et al., 2001). However this method can be useful to date young samples, which postdate the 1960s, since the aerial nuclear tests performed in this period created a spike in atmospheric ^{14}C (the “bomb pulse”) which can be recognised in carbonate speleothems (e.g. Hodge et al., 2011).

- **U-series dating**

The most used technique for speleothem dating is based on the U transfer from the soil to the speleothem via the groundwater and its subsequent decay into daughter products (Fig. 2.8).

The ^{238}U - ^{230}Th decay series is the most used for speleothem dating providing accurate dates for the last 400 kyr. Two prerequisites for stalagmite dating using the U-Th disequilibrium method are: 1) the presence of a closed system in relation to calcite precipitation and 2) a negligible detrital Th contamination. The major source of uncertainty is given by the ratio between the detrital radiogenic and stable Th ($^{230}\text{Th}/^{232}\text{Th}$). The threshold value of this ratio, which allows considering U-Th ages reliable, is between 100 and 300 (Li et al., 1989; Richards and Dorale, 2003). The effect of detrital Th contamination can be corrected to some extent using a stratigraphic approach as described in Hellstrom (2006) and/or basing the correction on the ratio of regional clays or bulk earth.

For older samples ^{238}U - ^{206}Pb decaying series is used, allowing for age determination of samples several million years old (e.g. Woodhead et al., 2006).

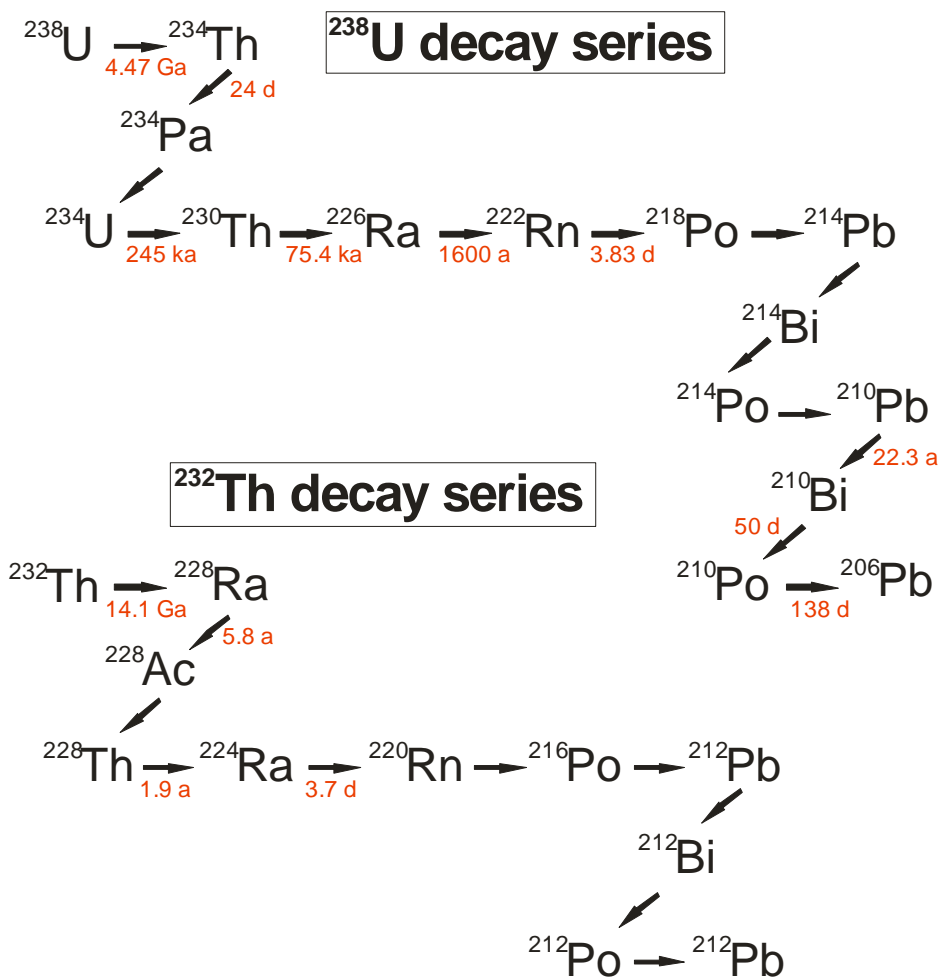


Fig. 2.8 – ^{238}U and ^{232}Th decay chain. Half lives are shown in red. From Fairchild and Baker, 2012, built on data from Dicken (2005) and Geyh and Schleicher (2000).

2.4.2.2 Oxygen and carbon stable isotopes: clues for past environmental changes

2.4.2.2.1 The environmental significance of stable oxygen isotope ratios ($\delta^{18}\text{O}$)

One of the most studied stable isotope ratios in palaeo-environmental studies involving carbonate material is the $^{18}\text{O}/^{16}\text{O}$ one.

This value is always reported against a standard that is represented by the VSMOW (Vienna Standard Mean Ocean Water) for water and the VPDB (Vienna PeeDee Belemnite) for carbonates. It is noted as (Sharp, 2007):

$$\delta^{18}\text{O} (\delta^{18}\text{O} (\text{‰})) = 1000 \times [((^{18}\text{O}/^{16}\text{O})_{\text{sample}} - (^{18}\text{O}/^{16}\text{O})_{\text{standard}}) / (^{18}\text{O}/^{16}\text{O})_{\text{standard}}]$$

The significance of this value relies on the processes behind its partitioning in atmospheric precipitation. The first variable, which influences precipitation stable oxygen isotope composition, is related to mean ocean isotopic composition. Ocean water is the largest H_2O reservoir and its stable isotope composition directly affects precipitation $\delta^{18}\text{O}$. At the global scale, the major factor that influences ocean $\delta^{18}\text{O}$ composition is the amount of ice at the Earth Poles. Indeed, ice sheets tend to concentrate lighter oxygen isotopes, since their origin is related to both low temperatures and increased high latitude snow precipitation, which is particularly depleted in ^{18}O (e.g. Rohling, 2013). At a more regional scale, ocean $\delta^{18}\text{O}$ changes are mainly related to strong evaporation (e.g. in the tropics), precipitation amount and river runoff (Lachniet, 2009). In particular since the lighter ^{16}O tends to evaporate first, intense evaporation can leave the ocean surface isotopically heavier. On the contrary, important river runoff would have the opposite effect lowering the ocean surface $\delta^{18}\text{O}$ ratios due to the input of isotopically lighter freshwater (Lachniet, 2009).

The ocean $\delta^{18}\text{O}$ signal is transmitted to moisture through evaporation. As stated above, this process causes a first modification in $\delta^{18}\text{O}$ ratios since lighter isotopes tend to evaporate first, resulting in a more ^{18}O depleted moisture if compared to the source. In presence of relative humidity of 100% this process occurs under equilibrium conditions and the fractionation corresponds to 9.34‰ at 25°C (Lachniet, 2009). However, at lower relative humidity also kinetic fractionation occurs which is a function of the percentage of relative humidity. Once in the atmosphere the moisture can face condensation, a process that occurs at equilibrium conditions and tends to favour the heavier ^{18}O isotopes, thus lowering the $\delta^{18}\text{O}$ ratios of the remaining vapour. The progressive condensation of water vapour in the atmosphere causes a lowering of precipitation $\delta^{18}\text{O}$ composition. This process, known as Rayleigh distillation, is particularly effective with decreasing temperatures, increasing altitude, increasing latitude and distance from the oceanic source (e.g. Yurtsever, 1975; Fig. 2.9 and 2.10).

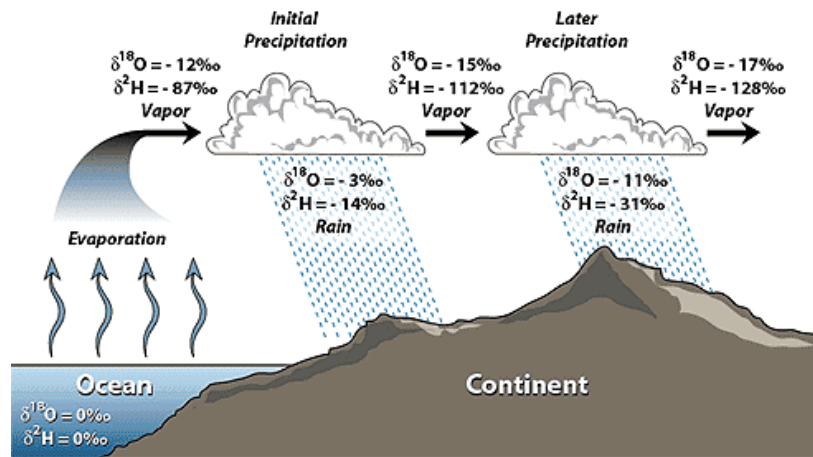


Fig. 2.9 – Rainout effect on $\delta^2\text{H}$ and $\delta^{18}\text{O}$ in precipitation (Hoefs, 1997; Coplen et al., 2000). From [https:// web.sahra.arizona.edu](https://web.sahra.arizona.edu).

Studying the $\delta^{18}\text{O}$ composition of precipitation it is thus possible to identify changes in the primary moisture source composition and/or in atmospheric air mass trajectories.

Precipitation $\delta^{18}\text{O}$ is transmitted to the karst environment through the infiltrating water. Oxygen of carbonate bedrock has a different $\delta^{18}\text{O}$ signature than the percolating water. However, the stable oxygen isotope composition of HCO_3^- derived from limestone dissolution equilibrates isotopically with percolating water allowing for the transmission of the imprinted climate signal. This process is time-dependent but generally occurs fast (hours or one day) compared to the travel time of infiltrating water to the cave, thus enabling the preservation of climate-related information (Dreybrodt, 2008; Dreybrodt and Scholz, 2011).

Further processes that may complicate $\delta^{18}\text{O}$ ratios interpretation must be considered. Once in the soil, evaporation can further modify moisture $\delta^{18}\text{O}$ composition triggering ^{18}O enrichments (e.g. Allison, 1982; Tank and Feng, 2001), an effect that is particularly evident in arid climates. In addition, the mixing in the soil zone of moisture derived from different precipitation events may buffer the original signal (Lachniet, 2009). Considering speleothem feeding systems, Bar Matthews et al. (1996) tried to modulate the isotopic signal related to the different flow paths finding more negative $\delta^{18}\text{O}$ for the diffuse (fissure) flow dominated water if compared to the fracture flow dominated one, making this system less sensitive to atmospheric changes. However, both paths were characterised by more positive values if compared to the atmospheric ones due to mixing effects (Fairchild and Baker, 2012). Thus, while karst water is potentially an important climate-related information reservoir, all the possible processes that can mask the original climate imprint must be taken into account while interpreting its $\delta^{18}\text{O}$ ratios.

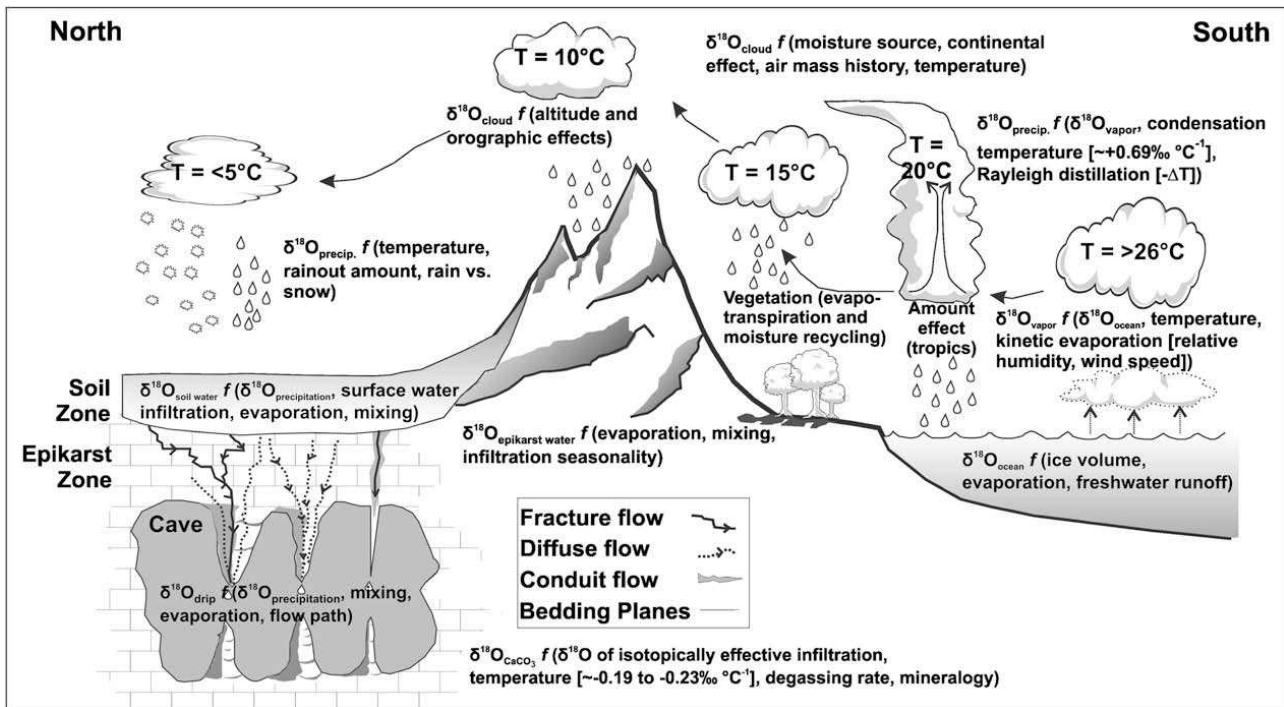


Fig. 2.10 – Stable oxygen isotope fractionation in the hydrological cycle and in water paths towards cave environments. (From Lachniet, 2009).

2.4.2.2.2 The environmental significance of stable carbon isotope ratios ($\delta^{13}\text{C}$)

Another isotopic ratio that is used in the study of past climate change signals recorded in cave carbonate deposits is the stable carbon isotope ratios, which is referred to as:

$$\delta^{13}\text{C} (\delta^{13}\text{C} (\text{‰})) = 1000 \times \left[\frac{(^{13}\text{C}/^{12}\text{C})_{\text{sample}} - (^{13}\text{C}/^{12}\text{C})_{\text{standard}}}{(^{13}\text{C}/^{12}\text{C})_{\text{standard}}} \right]$$

This isotopic ratio, which is transmitted to the karst through the infiltrating water, is mainly influenced by the isotopic composition of both the atmospheric and the soil derived CO_2 and in a minor way by bedrock composition. Soil derived CO_2 comprises CO_2 produced by both root respiration and microbial activity whose relative influence is still not yet well understood (Fairchild and Baker, 2012). While the bedrock stable carbon isotope ratio is stable, the soil activity signal can be dynamic (Dorale and Liu, 2009). Atmospheric CO_2 presents heavier carbon isotope ratios if compared to the vegetation root respiration products.

The $\delta^{13}\text{C}$ ratios related to CO_2 produced by root respiration is dependent on both the vegetation density and the photosynthetic path: indeed plants can be divided into three important groups using different photosynthetic pathways leading to different carbon isotopes fractionation. These groups are represented by the C3, C4 and CAM plants, which trigger average $\delta^{13}\text{C}$ values respectively of -26‰, -12‰ and intermediate values between the two (Deines, 1986; Cerling and Quade, 1993). While C3 plants are mainly found in temperate climates, C4 are light demanding plants adapted to

water stress and are mainly found in arid climates (Fig. 2.11, Cerling and Quade, 1993; Still et al., 2003). Some succulent plants (e.g. Cacti) instead represent the CAM group (i.e. crassulacean acid metabolism) (Smith, 1982). Thus in the central European area, at present, vegetation is dominated by C3 plants. Their photosynthetic paths lead to stored soil CO₂ isotopic ratios 18‰ depleted in respect to the δ¹³C of the atmospheric CO₂ (Farquhar et al., 1982).

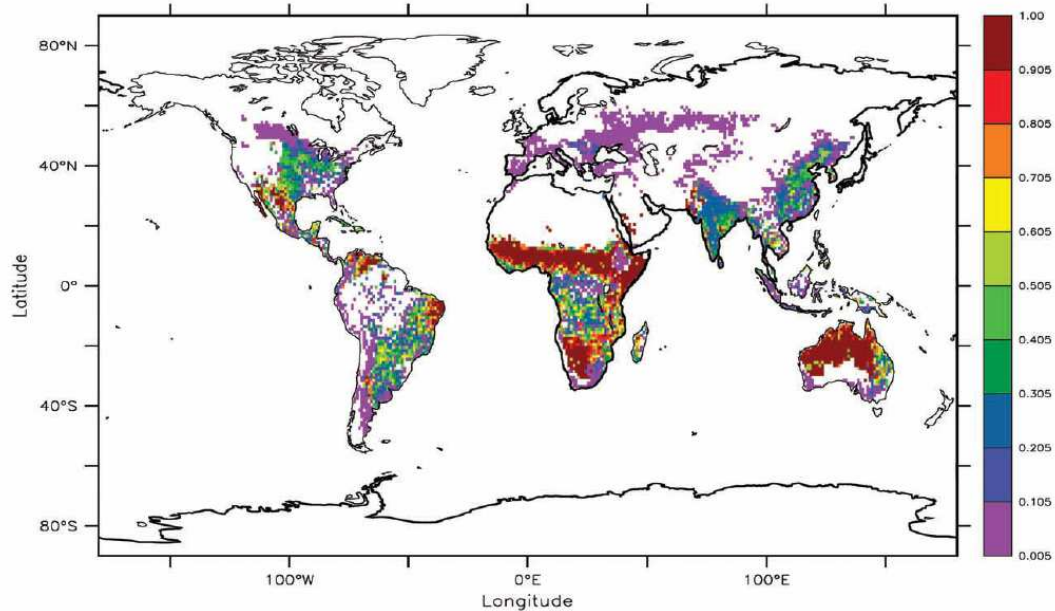


Fig. 2.11 – Spatial distribution of C4 fraction of vegetation (from Still et al., 2003)

2.4.2.2.3 How δ¹³C and δ¹⁸O are recorded in speleothems

Once reached the cave environment, infiltrating water can lead to carbonate speleothem formation (Paragraph 2.4.1). δ¹⁸O and δ¹³C signals carried by the parent dripwater are transmitted to speleothems through the deposition of calcium carbonate.

However, during this process both values can face further modifications that can mask the imprinted environmental signal. In order to have those signals recorded in a stalagmite, calcium carbonate precipitation must occur at isotopic equilibrium with the parent solution. Precipitation close to equilibrium conditions likely occurs when there is sufficient time for the isotope exchange reactions to take place (Hendy, 1971; Sharp, 2007; Lachniet, 2009): under these conditions, δ¹⁸O ratios can return to the equilibrium values through a slow isotope exchange with water in the hydration/dehydration processes of CO₂ (Afeck and Zaarur, 2014; Dreybrodt, 2011), which is an extremely slow process; when this happens, isotopic fractionation between water and calcite depends on cave temperature (e.g. Hendy, 1971; Kim and O’Neil, 1997; Kim et al., 2007). The relation between δ¹⁸O and temperature ranges from -0.18 to -0.23‰/°C at temperatures of 5°C and 35°C respectively (Lachniet, 2009). While temperature impacts δ¹³C fractionation less extensively,

this isotopic value is more sensitive to in-cave CO₂ degassing and CO₂ exchange with the cave atmosphere occurring when calcite precipitates at the speleothem surface. The latter process causes an irreversible ¹³C enrichment in the DIC (dissolved inorganic carbon) in the solution (Afeck and Zaarur, 2014; Dreybrodt, 2011). However, strong and/or rapid CO₂ degassing can trigger kinetic fractionation also in δ¹⁸O values causing enrichments of both δ¹⁸O and δ¹³C ratios (Hendy, 1971; Wiedner et al., 2008). Dreybrodt & Scholz (2011) and Hansen et al. (2013) demonstrated how the rate of outgassing is related to the thickness of the water film on speleothems, preventing complete δ¹⁸O DIC re-equilibration in thin water films. Considering that the occurrence of disequilibrium conditions in DIC isotope ratios is recorded in the precipitating calcite, speleothems forming from thin films of fluid, which are the result of long drip intervals, may experience enriched δ¹³C and δ¹⁸O values (Mühlinghaus et al., 2007; Riechelmann et al., 2013; Caddeo et al., 2015).

Hendy (1971) was the first who tried to examine δ¹³C and δ¹⁸O variations in speleothem calcite in relation to cave conditions, looking for a criterion able to individuate disequilibrium fractionation in speleothem calcite. According to his study, two conditions must be met by stalagmites grown under equilibrium conditions:

- 1) the absence of covariance between δ¹³C and δ¹⁸O along the stalagmite growth axis and the stalagmite growing laminae;
- 2) the absence of strong δ¹⁸O variation along growth laminae.

Thus, if these two criteria are met, the isotopic signal recorded in a stalagmite can be considered reliable for past climate interpretation.

This approach has been considered valid for several years and is still used to test for stalagmite equilibrium conditions. However, this method is not considered fully reliable for testing the preservation of climate signals in speleothem calcite as, for example, several other authors have recognised the role played by climate fluctuations in causing covariation of δ¹³C and δ¹⁸O (i.e. vegetation changes associated with climate changes; Cerling, 1984; Dorale et al., 1992; 1998). In addition, the variation of δ¹⁸O values along single laminae, suggesting the occurrence of disequilibrium fractionation, is not sufficient to demonstrate the absolute absence of equilibrium condition along the central growth axis (where samples for stable isotope analyses are taken). Furthermore, extremely thin lamination may prevent a sampling precise enough to be representative of a single growth lamina. For these reasons, the look for replication of the stable isotope profiles among coeval stalagmites from the same cave is considered more reliable in determining the preservation of the original climate signal (Wang et al., 2001; Dorale and Liu, 2009).

2.4.3 Trace elements in speleothems and their relevance in palaeo-climate and palaeo-environmental studies

In geochemistry, elements that have a low concentration (usually less than 0.1 %) in the analysed material are referred to as “trace elements”. In carbonate speleothems, they mainly consist of all the elements that can be leached from the soil and bedrock by the infiltrating water and then incorporated into calcium carbonate crystal lattice; minor contributors to speleothem trace element

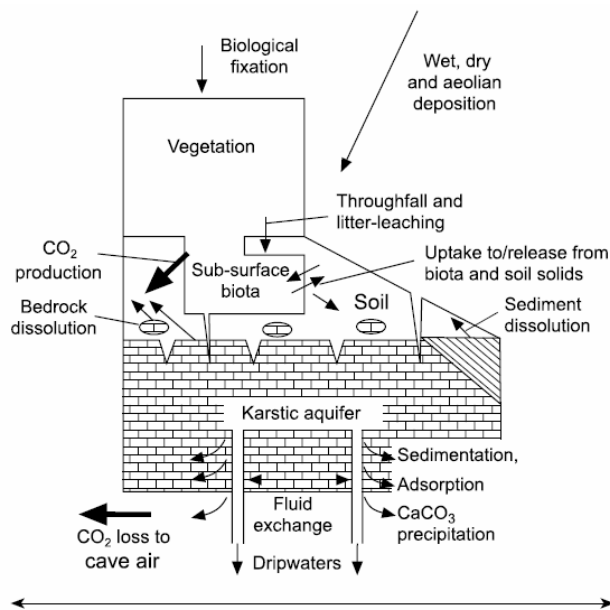


Fig. 2.12 – Scheme of possible sources of trace elements found in speleothem calcite. The arrows indicate fluxes as particulate, colloids or solutes (from Fairchild and Treble, 2009).

composition can be atmospheric input and sea-salt aerosol (e.g. S and Sr; Goede et al., 1998; Fairchild and Treble, 2009; Fairchild and Hartland, 2010; Fig. 2.12). Anthropogenic activity may be a further source of trace elements, since pollutants derived from agricultural and/or industrial activities can be transferred into the karst environment and incorporated into speleothem calcite (e.g. Perrette et al., 2008; Wynn et al., 2010; Allan et al., 2015).

Trace element composition of speleothems depends on the element abundance and mobilization, the hydrochemical processes in the unsaturated zone overlying the cave and partitioning at the water-calcite interface

(Roberts et al., 1998; Fairchild and Treble, 2009; Fig. 2.12). A deep understanding of the mechanisms behind trace element variations allows for the identification of environmental and/or hydrological changes during the period of growth of the studied stalagmites.

A brief overview of the transfer mechanisms and the palaeoenvironmental significance of the most studied trace elements in speleothems is reported below.

2.4.3.1 Trace elements transfer through the karst and their incorporation into calcite

Trace element enrichment in groundwater is mainly related to their chemical mobilization and hydrological processes influencing water infiltration (Fairchild and Treble, 2009).

These elements can be derived by different sources with distinctive dissolution behaviour and they can be taken in charge as solutes (e.g. Mg and Sr) or as particulate and ion aggregates (especially trace metals). Groundwater residence time and flow paths play an important role in both type and

concentration of trace elements. In particular, low flow conditions allow for leaching less soluble elements: as a reflection of this, water entering deep caves is usually more enriched in trace elements than in shallower ones (Perrin, 1997); the same can be said for longer residence times related to drier environments (Fairchild and Baker, 2012). On the contrary, fast flows favour the mobilization of particles and coarse NOM (natural organic matter; cf. Hartland et al., 2012), which can transfer both organic molecules and crystallite or amorphous solids like Fe, Mn or Al oxides (Buffle et al., 1998; Lead and Wilkinson, 2006).

When the infiltrating water precipitates calcite, its load in trace elements can be incorporated into the calcite crystal lattice where divalent cations can substitute Ca^{2+} ions and/or, together with other ions, attach to lattice kink sites (Burton et al., 1951; Fairchild and Baker, 2012). Trace elements (in particular trace metals) can also concentrate in layers rich in organic matter which usually present a brownish/dark colour visible in stalagmite polished sections and in speleothem thin sections (e.g. Fairchild et al., 2001; Richter et al., 2004; Borsato et al., 2007).

2.4.3.2 Palaeo-environmental meaning of speleothems trace element composition

The understanding of the variables influencing trace element mobilization and incorporation into speleothem calcite can provide information related to local hydrology variations even at the seasonal scale (e.g. Huang et al., 2001; Treble et al., 2003; Borsato et al., 2007).

Mg and Sr are among the most studied elements incorporated into speleothem calcite. Mg can be leached from soil and/or bedrock where Mg-bearing carbonate/metamorphic/igneous rocks (e.g. dolomites, ophiolites) are present. Its leaching is directly related to groundwater residence time which can be modulated by the alternation of drier and wetter conditions: indeed drier conditions induce longer residence times and allow for selective leaching of Mg from soil or host rock (Plummer, 1997; Fairchild et al., 2000). However, Mucci and Morse (1990) demonstrated that temperature influences variations in Mg concentration as well. Indeed Mg incorporation into calcite is temperature-dependent and higher temperature leads to higher Mg concentration in speleothems (Verheyden, 2004 and reference therein).

On the contrary, Sr incorporation into calcite crystal lattice is not temperature dependent (Mucci and Morse, 1990). This element seems to be related to calcite precipitation rate, where higher concentrations would indicate faster speleothem growth (Fairchild et al., 2001; Gabitov and Watson, 2006). However this does not always occur (e.g. Borsato et al., 2007).

All trace elements can also be influenced by processes linked to calcite precipitation along the water path before reaching the cave.

A negative correlation between Mg and Sr can be indicative of the alternation of drier (higher Mg and lower Sr) and wetter (lower Mg and higher Sr) phases, reflecting, in some cases, annual

ciclicity (e.g. Roberts et al., 1998; Treble et al., 2003). On the contrary, Huang et al. (2001) observed a positive correlation between Mg and Sr in annual laminae of a stalagmite from Ernesto Cave (Italy), interpreting this signal as a combination of selective leaching of Mg from soil and bedrock and prior calcite precipitation.

Another element that can provide information about environmental processes during calcite speleothem growth is P. Its concentration in speleothems is commonly interpreted as related to vegetation die-back or microbial mats. The mobility of P in soils is higher at pH between 4 and 6 (Giesler et al., 2005), conditions that usually occur in summer (Sartori et al., 2005). However, P is commonly re-adsorbed by the lower alkaline soil layer, maintaining its mobility only in presence of extremely rapid infiltration (Borsato et al., 2007). Thus, laminae portion rich in this element are often deposited during autumn in temperate climates (e.g. Huang et al., 2001; Borsato et al., 2007). At the same time, rapid infiltration events may also favour the transfer of trace metals (e.g. Y, Pb, Zn and Cu), that are attached to natural organic matter (NOM) (e.g. Borsato et al., 2007; Hartland et al., 2012). Their concentration fluctuations in speleothem calcite may thus provide information about the timing and magnitude of rainfalls, especially where strong seasonality of precipitation occurs (Hartland et al., 2012).

2.4.4 Stalagmite petrography and its capability in providing environmental information

In carbonate speleothems, calcite crystal arrangements are related to environmental conditions due to water flow, supersaturation state of parent drip water, presence of impurities and cave air humidity and pCO₂. Changes in these parameters cause variations in crystal nucleation, which result in particular textures. Thus, in order to improve the comprehension of environmental fluctuations recorded in speleothems, the importance to understand the conditions behind each fabric formation is clear.

The calcite crystal growth mechanisms and changes in crystal habits, related to cave and drip water conditions, have been poorly investigated in the distant past, finding evidence of changes in calcite habits related to parent drip water supersaturation state and flow rate and possible influences of foreign particles (e.g. Boistelle, 1982; Sunagawa, 1984; Dreybrodt, 1988; Gonzalez et al., 1992; Genty, 1992). Subsequently, the idea that speleothem fabric variations might have been a potential reservoir of environmental information has been investigated by Frisia et al. (2000) and Frisia and Borsato (2010). These authors intensely analysed the parameters influencing speleothem textures and recognised five main fabrics (columnar, dendritic, micrite, microsparite and mosaic calcite) that

develop under particular conditions of drip water supersaturation and flow rates. The resulting classification has been improved and coded in Frisia (2015) to provide a universal and relatively objective tool for fabric classification and its conversion into numerical values; thus allowing the comparison between different proxies of the same speleothem record and different records as well. Indeed Frisia (2015) described the five main fabrics and their associated patterns assigning to each of them a progressive number from the one reflecting more stable conditions of drip rate and supersaturation to the one related to the highest instability. These fabrics and the associated environmental conditions are described below.

2.4.4.1 Columnar Fabric

Columnar fabric has been observed by Kendall and Broughton (1978) and is considered the most common fabric in carbonate speleothems (Frisia and Borsato, 2010). Crystals are elongated along the main growth axis and are characterised by serrated boundaries. In the past this fabric has also been called “palisadic” by Genty and Quinif (1996). It occurs in caves under different temperature conditions (from 5 to $> 25^{\circ}\text{C}$) and is characteristic of relatively low calcite supersaturation state (SI_{cc} from about 0.1 to 0.35; Frisia et al., 2000). The eventual presence of organic matter (colloids) or foreign particles, drip rate variability and changes in drip water chemistry are responsible for the associated patterns in which the columnar fabric can be subdivided. Microscopically it can be divided into five sub-types described by Frisia (2015) as follows (Fig. 2.13).

2.4.4.1.1 Columnar Compact (C)

This sub-type is characterised by a regular crystal stacking forming compact aggregates without the presence of intercrystalline porosity. Crystals have a length-to-width ratio $\leq 6:1$ and are characterised by regular intercrystal boundaries (e.g. Folk, 1965). They rarely exhibit marked competitive growth phenomena with the exception of the upper surface of major depositional hiatuses (Kendall, 1993; Frisia et al., 2000). The eventual lamination does not disturb the compact crystal stacking, even if flat crystal terminations are often associated with dark and organic-rich laminae, promoting the idea of a possible local dissolution related to organic matter oxidation (Frisia, 2015). This fabric forms under a thin film of fluid under relatively slow and constant drip rate (from 0.1 to ~ 3 ml/min), enhanced degassing, high water pH (~ 8.4), low calcite supersaturation ($\text{SI}_{\text{cc}} = 0.2 \pm 0.15$), low Mg concentration in parent drip water and negligible presence of particles and/or colloids (Kendall and Broughton, 1978; Frisia and Borsato, 2010).

2.4.4.1.2 Columnar Open (Co)

The main difference, which distinguishes this fabric from the columnar compact is the presence of high intercrystalline porosity, marked by linear inclusions or pores. It forms under a thicker film of fluid, higher drip rate and less efficient degassing compared to the compact type (Kendall, 1993; Frisia et al., 2000).

2.4.4.1.3 Columnar Elongated (Ce)

This fabric, that is common in flowstones, is characterised by crystals with a length-to-width ratio exceeding 6:1 (Folk, 1965). Competitive growth phenomena are more widespread than in the other columnar types. According to Gonzalez et al. (1992) its formation requires high water flows on the speleothem surface and presence of Mg in parent water (Mg/Ca from 0.85 to 2.8). Frisia et al. (2000) reported the presence of this fabric in temperate climate under constant drips, low calcite supersaturation state (SI_{cc} between 0.1 and 0.35) and Mg/Ca ratios higher than 0.3. Examples of lateral overgrowth in this fabric associated with micrite rich layers have been described by Frisia (1996). A similar pattern has been recognised as diagenetic in fresh water stromatolites examined by Freytet and Verrecchia (1999). The presence of lateral overgrowth in elongated calcite crystals associated with micrite may therefore imply diagenesis in flowstone layers.

2.4.4.1.4 Spherulitic type growth in columnar fabrics

This particular fabric consists of columnar polycrystals with a length-to-width ratio higher than 6:1 characterised by undulatory extinction. This sub-type can be further subdivided into two sub-fabrics called “fascicular optic” and “radial”. The first assumes the appearance of a sector of a spherulite or a fan with crystals bending outwards, the latter is instead characterised by converging fast vibration directions. Observations on speleothems suggest an important role of Mg (Mg/Ca > 0.35) and higher calcite supersaturation states (SI_{cc} between 0.3 and 0.5) for its development (Mattey et al., 2010; Neuser and Richter, 2007; Frisia, 2015). Considering the role of Mg in the formation of this fabric, it is arguably reasonable to infer these two sub-fabrics as indicative of Prior Calcite Precipitation (PCP) and/or prolonged water residence time in Mg-rich aquifers during dry periods (Frisia, 2015).

2.4.4.1.5 Columnar Microcrystalline (Cm)

This fabric, mainly observed in stalagmites in Alpine settings, is characterised by flame-like polycrystals with length-to-width ratio < 6:1 and uniform extinction. The peculiarity that distinguishes this fabric from the compact one is the presence of highly irregular boundaries between the polycrystals associated with a high inter- and intra-crystalline porosity. This particular

fabric, usually fine laminated, forms under higher discharge rates than the compact one but with higher variability, comparable low supersaturation and strong input of foreign detrital or colloidal particles associated with major infiltration events (Frisia et al., 2000). According to Frisia (2015), the microcrystalline pattern is typical in temperate regions characterised by high seasonal contrast in temperatures, precipitation and vegetation activity. Considering the Alpine settings where this fabric has been recognised, flushing of organic matter may reflect the autumnal season, when a combination of low degassing and low supersaturation occurs. This can result in the development of the observed regular layer of foreign particles at the growing surface. An additional requirement of this process is the presence of an environment where seasonal cave ventilation occurs, allowing for a less efficient exchange between cave air and atmosphere during the season of higher colloidal flushing (Frisia, 2015).

2.4.4.2 Dendritic Fabric

This fabric is characterised by composite crystals organised in branches resulting in the peculiar aspect of a grid. It forms under relatively low calcite saturation conditions (SI_{cc} between 0.2 and 0.4) and high discharge rates with strong fluctuations, including the alternation of periods of high drip rate and prolonged dry seasons during which the speleothem surface dries out completely (Frisia et al., 2000; Frisia and Borsato, 2010).

This pattern has been observed in stalagmites grown close to cave entrances and in the flanks of speleothems formed by the microcrystalline fabric. Its formation may be related to environments with important exchanges between cave air and external atmosphere and in case of prolonged outgassing. The finding of important microbial colonies on the tops of active stalagmites presenting this fabric suggests a possible microbial influence in its precipitation (Frisia, 2015), with important implication for the preservation of the original geochemical signal.

2.4.4.3 Micrite (M)

This fabric consists of tiny crystals (max 2 μm) that appear dark in PPL (plain polarised light) and dark brown in XPL (cross polarised light) (Frisia, 2015). Considering previous studies on continental and stromatolitic-like carbonates, this fabric may be indicative of bio-influenced processes (Kaźmierczak et al., 1996; Banks et al., 2010; Borsato et al., 2000; Frisia and Borsato, 2010; Alonso-Zarza and Wright, 2010; Frisia et al., 2012). In speleothems it might be the result of microbial colonisation of the speleothem surface during relatively dry periods (Frisia et al., 2012). However, also processes involving condensation-corrosion of pre-existing calcite may create micrite as a result of diagenesis (Cañaveras et al., 2001); it is, therefore, not clear whether micrite is

a primary or a diagenetic fabric, even if it is possible that micrite in carbonate speleothems reflects biomediated processes during periods of relatively low discharge (Frisia et al., 2012).

2.4.4.4 *Microsparite (Ms)*

Microsparite is composed of small crystals (between 2 and 30 μm) with anhedral or subeuhedral habits, usually organised in mosaic aggregates. It is considered a diagenetic fabric as it can be the result of micrite transformation by aggrading neomorphism (Folk, 1965; Folk and Assereto, 1976). This fabric may be the result of syn-depositional dissolution and recrystallization of micrite layers related to oxidation of organic matter. Its formation may also be favoured by the discharge resuming after dry periods (Frisia, 2015).

2.4.4.5 *Mosaic Calcite (Mc)*

It consists of large (between 30 μm and 1 cm) euhedral to sub-euhedral crystals and often includes ghosts of needles that represent calcite replacement of aragonite. This fabric has also been associated with dissolution and precipitation of former low-Mg calcite (Frisia et al., 2012; Fairchild and Baker, 2012). It is thus considered a diagenetic fabric even when evidence of previous aragonite precipitation is not present. In general, this fabric is indicative of speleothems with poor or no preservation of the original geochemical signals.

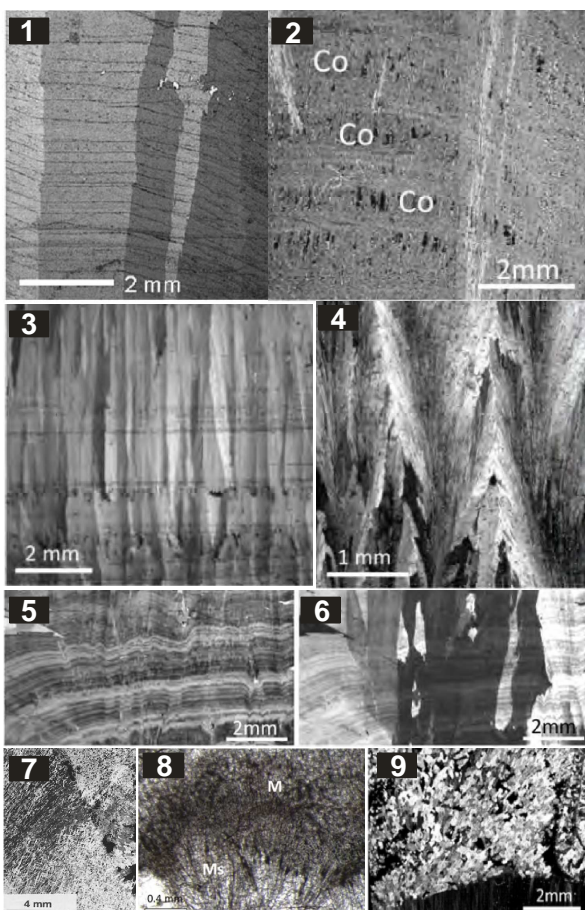


Fig. 2.13 – Thin section images of stalagmite fabrics. 1: Compact columnar calcite; 2: open columnar calcite; 3: elongated columnar calcite; 4: fascicular optic calcite; 5: microcrystalline calcite; 6: microcrystalline calcite (XPL); 7: Dendrite; 8: Micrite and Microsparite calcite; 9: Mosaic calcite (XPL). Modified from Frisia et al. (2000), Frisia and Borsato (2010) and Frisia (2015).

2.4.4.6 Implication of calcite fabric micrologging for stable isotope profile interpretation

The calcite crystals in speleothems can assume the different fabrics described above in function of environmental variations that cause fluctuations in water availability, seasonality of precipitation, vegetation cover and cave air pCO₂. However these factors, besides causing variations in calcite fabrics, may also cause a possible stable isotope signal alteration via the calcite deposition out of equilibrium conditions. In addition, considering both the mechanisms at the base of stable isotope ratio recording in speleothem calcite and the processes that lead to each fabric formation, it is feasible to infer the presence of a possible link between stable isotope ratios and calcite fabrics. Evidence of stable isotope ratio variations related to the occurrence of particular fabrics and the associated outgassing conditions have been reported in literature (e.g. McDermott et al., 1999; Frisia et al., 2000; Belli et al., 2013). An example is the $\delta^{13}\text{C}$ shift towards more positive values associated with dendritic fabric (compared to compact fabric layers in the same specimen) or the more negative $\delta^{13}\text{C}$ values characterizing the columnar compact calcite if compared to the open type in relation to the longer outgassing during its formation (McDermott et al., 1999; Belli et al., 2013). Based on these observations, Frisia (2015) proposed the general classification of calcite fabrics in speleothems described above suggesting a transformation of calcite types into numerical values that can be adapted to each specific case (Fig. 2.14). This procedure allows for the construction of a microstratigraphic log enabling rapid analysis of fabric changes through time and a direct comparison with other climate proxies explored in the studied speleothems, as stable carbon and oxygen isotope ratios *in primis*. She also proposed a new way to represent data called the IsoFab plot. It consists in the representation of average $\delta^{13}\text{C}$ and $\delta^{18}\text{O}$ ratios and their standard deviations grouped for each recognised fabric class of a studied speleothem. She explored the potential of this representation in identifying possible stable isotope anomalies providing information about potential disequilibrium precipitation, since both fabric and disequilibrium conditions may be influenced by the same factors. According to Frisia (2015), this plot, used in conjunction with a comparison between coded fabrics and stable isotope ratios, may be considered a valuable tool to test for equilibrium calcite deposition similar to the well known Hendy test (Hendy, 1971) and the replication tests proposed by Dorale and Liu (2009).

The correct identification of the fabrics forming a studied speleothem and their correlation with stable oxygen and carbon isotope ratios may therefore be of fundamental importance in disentangling climate and hydrological signals recorded in the stable isotope profiles and in the identification of possible disequilibrium condition during calcite precipitation.

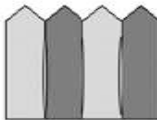


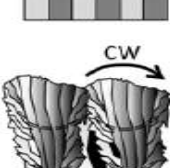




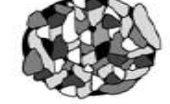




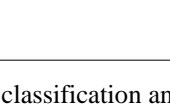
		Type	Symbol (code)	Characteristics	Environment of formation
		Columnar	C (1)	l/w ratio <6:1; competitive growth at interfaces; straight to serrated boundaries; uniform extinction; common "flat" terminations or protruding rhombohedra terminations (~ 2µm high)	Relatively slow and constant drip; Sicc <0.35; Mg/Ca <0.3; pH up to 8.4; low impurity content
		Columnar open	Co (2)	l/w ratio <6:1; competitive growth at interfaces; incomplete coalescence of crystals; high intercrystalline porosity, commonly linear; uniform extinction.	Drip rate > than in C; Sicc up to 0.35; Mg/Ca <<0.3; pH 7.5 up to 8.
		Columnar elongated	Ce (3)	l/w ratio > 6:1; competitive growth at interfaces; preferential growth of acute rhombohedron; incomplete coalescence of crystals; protruding terminations common; uniform extinction. May show lateral overgrowths, in particular in the presence of impurity-rich layers.	Drip rate constant; Sicc 0.1 to 0.4; Mg/Ca > 0.3.
		Ce with lateral overgrowth	Ce _o (4)		Ce _o : relatively fast flow; presence of particulate. Diagenesis?
		Columnar fascicular optc	Cfo (5)	Polycrystals l/w ratio > 6:1; undulatory extinction diverge away from substrate when rotating table is turned CCW; split crystal growth (spherulitic type); downward concave curvature.	Low drip rate or laminar flow; Sicc 0.5; Mg/Ca > 1.5; typical in stalagmites & flowstones formed in caves cut in dolomite
		Columnar radialial	Crf (5.5)	Polycrystals l/w ratio > 6:1; undulatory extinction converge away from substrate when rotating table turned CW; split crystal growth; upward concave curvature.	
		Columnar microcrystalline	Cm (6)	Polycrystals l/w < 6:1; irregular intercrystalline boundaries; uniform extinction with "patches" due to cross-cutting by adjacent crystals; high intracrystalline microporosity; typical of laminated speleothems.	Variable drip rate (seasonal); Sicc up to 0.35; Mg/Ca < 0.3; drip/flow carrying colloidal particles.
		Dendritic	D (7)	Branching polycrystals; scaffold-like appearance "warp and waft"; irregular intercrystalline boundaries; high intercrystalline porosity.	Variable drip rate; Sicc up to 0.4. Mg/Ca possibly similar to Cm; strong degassing; presence of particulate/ foreign ions. Bio-influenced precipitation
		Micrite	M (8)	Crystals < 2µm; stromatolitic-like structure; clotted structure. Common geometric selection above micrite layers.	Bio-influenced. Low flow/dry. Condensation/corrosion?
		Microsparite	Ms (9)	l/w ratio ~ 1:1; crystal size > 2µm < 30µm; commonly associated with micrite. Fabric-destructive replacement.	Diagenesis. Aggrading neomorphism (micrite to microsparite)
		Replacive microsparite	Ms _{ara} (10)	l/w ratio ~ 1:1; Crystal size > 2µm < 30µm; retention of aragonite fabric.	Diagenesis. Mimetic replacement
		Mosaic calcite	Mc (11)	l/w ratio ~ 1:1; crystal size > 30µm. Fabric destructive.	Diagenesis. If replacing calcite, no relicts of a former unstable phase are visible.
		Mosaic calcite with aragonite needles	Mc _{an} (12)	l/w ratio ~ 1:1; Crystal size > 30µm; Fabric destructive; preserves relicts of aragonite, commonly needles.	Diagenesis. Commonly related to the transformation of speleothem aragonite into calcite

Fig. 2.14 – Fabric classification and coding proposed in Frisia (2015)

III. STUDY AREA

3.1 Cave settings and sampling location

Mračna Pećina (also known as Banja Stijena) and Govještica caves are both located on the left side of the narrow valley cut by the Prača River ($43^{\circ}46'20.8''$ N; $18^{\circ}53'14.5''$ E and $43^{\circ}46'26.2''$ N; $18^{\circ}53'18.9''$ E), about 40 km East of Sarajevo (Bosnia and Herzegovina; Fig. 3.1).

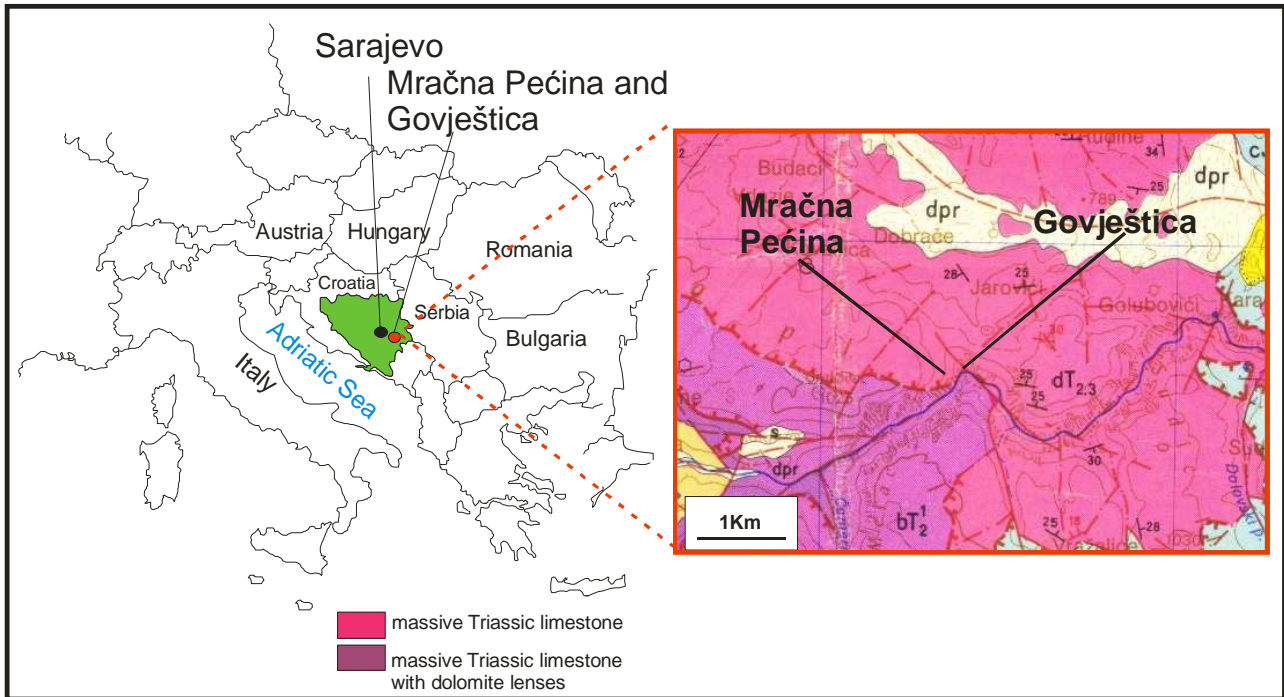


Fig. 3.1 – Mračna Pećina and Govještica cave entrance locations (1:100000 geological map, Vujnović and Marić, 1973-1981).

Before describing cave settings and sampling locations, a short digression on cave names is needed. Indeed, Mračna Pećina cave is also known as Banja Stijena. The latter name was the one preferred by the exploring team and for this reason all samples coming from this cave have been labelled as “BS”. However, the name preferred for the cave register of Bosnia and Herzegovina is Mračna Pećina. For this reason from this point onward I will refer to this cave using this name.

Both caves has developed at the foot of the Romanija Plateau, which reaches the highest elevation of 1500 m a.s.l. in its western part, while the central and southern parts overlying the caves reach an elevations between 800 and 1,000 m a.s.l. The Romanija massif consists of a Triassic succession of basal sandstone followed by massive limestone with ammonites, crinoids and lenses of dolomite, reef limestone and light grey limestone with megalodonts and dolostone.

The Mračna Pećina Cave network develops in the Triassic massive limestone and is characterised by a W-E orientation, coherent with a major thrust line that separates the massive reef limestone from the massive limestone containing ammonites and dolomites (Fig. 3.1). This cave was discovered at the beginning of the 20th century; an artificial entrance and concrete stairs were built

between the First and Second World War to allow tourists to access the first chamber (Daneš, 1921). The artificial entrance is located at 597 m a.s.l., about 20 m above the Prača River, at the foot of a limestone cliff. The natural entrance, now occluded by a rockfall, is located on the north-eastern upper side of the first chamber, not far from the artificial entrance. The cave comprises a chamber 10 m wide and up to 6 m high, decorated with stalactites and flowstones, and located close to the entrance. A series of galleries totalling 1,148 m in length occurs on the same principal level, with a total depth with respect to the entrance of 37 m. In the entrance area, a dark coating is ubiquitous on the cave walls, and is probably related to the use of torches during tourist visits at the beginning of the last century.

Govještica Cave is a resurgence located few hundred metres downstream the Mračna Pečina Cave at the elevation of 580 m a.s.l.. It develops in the same Triassic massive limestone where Mračna Pečina is found with a major NW/SE orientation, parallel to a fault marked on the 1:100 000 geological map (1973-1981); few minor branches develop with a N-S orientation. Thus, this fault may have played a major role in Govještica speleogenesis. This cavity drains the water infiltrating on the Romanija plateau. The explored galleries of Govještica Cave develop for about 10 km. The difference in elevation between the highest and the lowest point is 138 m.

Four (BS8, BS9, BS14 and BS15) out of the five studied stalagmites were found already broken near to the main chamber of Mračna Pečina Cave (between 50 and 100 m from the artificial entrance; Fig. 3.3). Although it was not possible to reconstruct their original position, the presence of a dark coating on their surfaces, similar to the one deposited on the cave walls and other stalagmites in this area, suggests their original allocation in this portion of the cave. One sample (G5) was instead found in the “Sala delle Ossa” (hall of bones) in Govještica cave (Fig. 3.2).

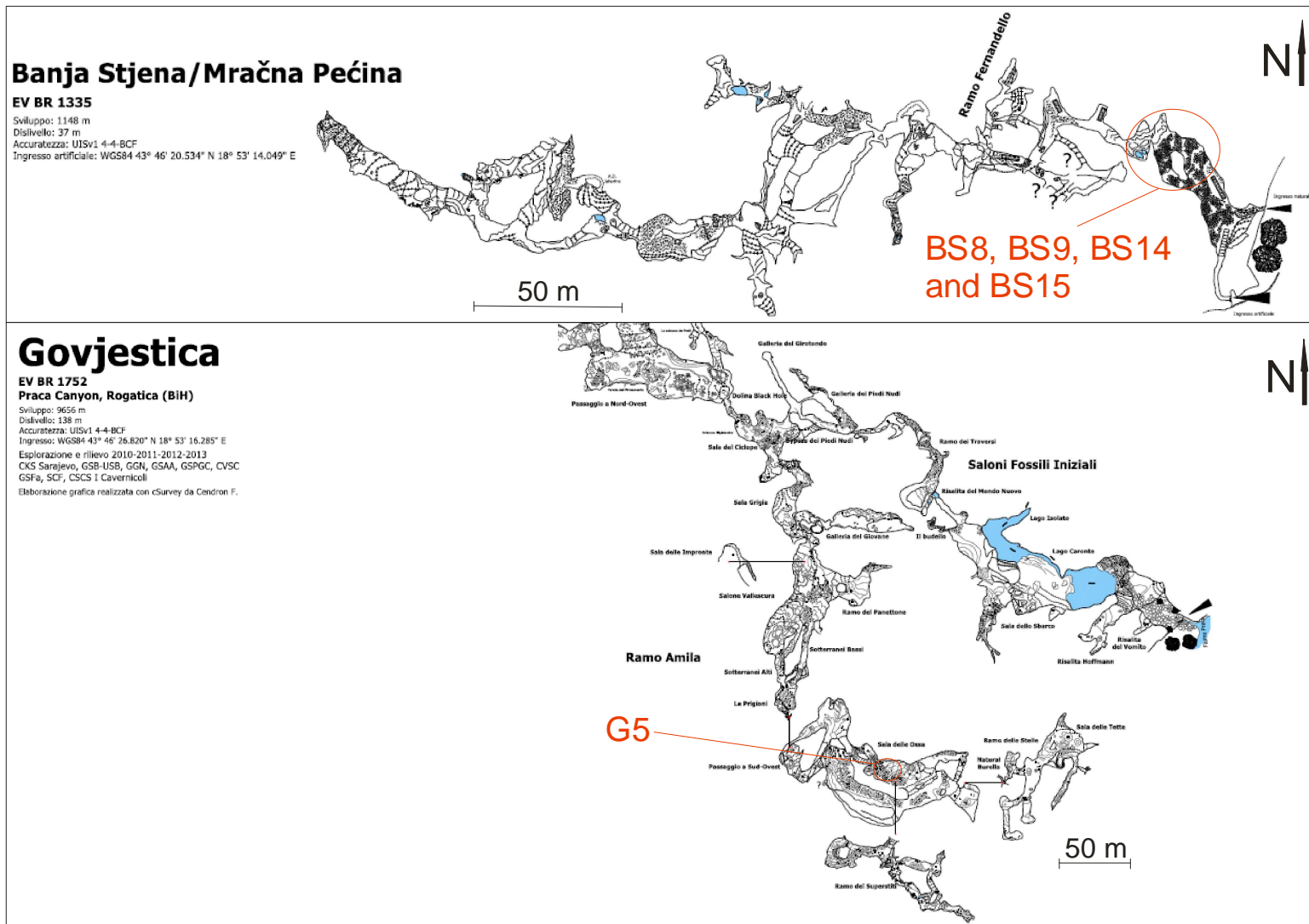


Fig. 3.2 – Map of Mračna Pečina cave and partial map of Govjesticca cave (by Gruppo Speleologico Bolognese). Red circles indicate the areas where the stalagmites were found.

3.2 Atmospheric circulation and stable isotope composition of precipitation

The atmospheric circulation on the Balkan Peninsula, situated in the central portion of the Mediterranean basin, is influenced by the complex circulation pattern described in section II. In particular, according to Pučnik (1980), moisture bearing maritime polar and tropical air masses, originating respectively in the North Atlantic Ocean and in the Azores, and dry continental polar and tropical air masses, originating in Northern and Eastern Europe and Northern Africa, influence the weather in the central-northern areas of the Balkans. The combined impact of those patterns and the orography of the region determines the presence of a mixture of continental, mountain and Mediterranean influences in the Western Balkans (Zupan Hajna, 2012).

Stable isotope composition of precipitation in the Balkans was investigated by Vreča et al. (2006). This study, based on data provided by the Global Network of Isotopes in Precipitation (GNIP) stations situated along the coast and inland in Slovenia and Croatia, is mainly related to temperature variation rather than precipitation amount, in agreement with the general trend observed in temperate regions at middle latitudes. However, stronger relation between stable oxygen isotope variation in precipitation and temperature has been found in the inland stations ($\delta^{18}\text{O}$ variation in function of temperature: $0.37\text{‰}/^{\circ}\text{C}^{-1}$) if compared to the coastal ones ($\delta^{18}\text{O}$ variation in function of temperature: $0.15\text{‰}/^{\circ}\text{C}^{-1}$) which present a less strong seasonal temperature contrast, showing a decreasing trend with increasing mean annual temperature (Vreča et al., 2006).

3.3 Present day climate and vegetation

The Balkan Peninsula presents different climate belts in relation to the local topography and distance from the Adriatic Sea. While the areas along the Adriatic coast present a Mediterranean climate that becomes a sub-Mediterranean one towards the North, the inland areas are mainly dominated by a continental climate (Vreča et al., 2006; Fig. 3.3).

The present day climate in the Sarajevo area is temperate, with warm summers and cold and snowy winters. Rainfall is distributed all year round with the absence of a proper dry season. Annual precipitation in Sarajevo region reaches 946 ± 160 mm, while mean annual temperature is 10.9 ± 0.7 °C (for the time interval 1992-2015; Sarajevo weather station, Federal Institute of Hydrometeorology BIH; Fig. 3.4). The landscape on the Romanija Plateau is characterised by conifer-dominated woods and pastures, while the Prača valley where the cave entrance is located hosts deciduous vegetation.

Nowadays, the surface above the cave is affected by grazing and timber cutting (Milanolo et al., 2013). Evidence of human occupation and activities in the area dates back to the Neolithic period (Srejović, 1994).



Fig. 3.3 – Major vegetation zones in Europe (Encyclopaedia Britannica, Inc). Mediterranean forest along the Balkan coast is the result of the Mediterranean climate present in this area, which becomes more continental inland.

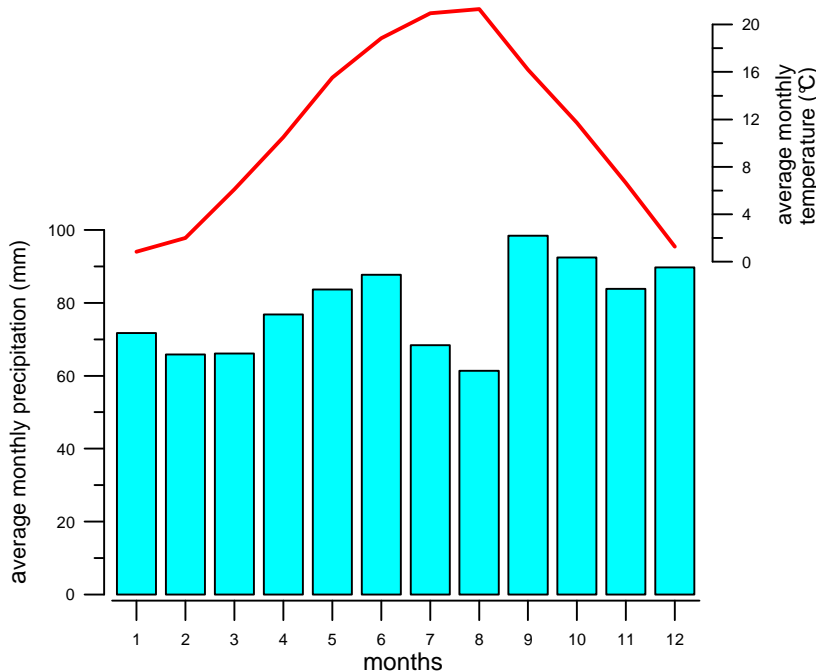


Fig. 3.4 – Average monthly precipitation (blue boxes: time interval 1992-2015) and average monthly temperature (red line: time interval 1992-2015) Data from the Sarajevo weather station, Federal Institute of Hydrometeorology (Bosnia and Herzegovina).

IV. MATERIALS AND METHODS

4.1 Brief sample description

For conservation purposes, the impossibility to target directly on the field the most promising samples and the availability of huge quantities of broken materials, only broken stalagmites were collected for this study. Among the sampled stalagmites, five Holocene samples were identified with preliminary U-Th dating. Unfortunately, the original position of these samples was not identified. Stalagmites have been longitudinally cut along the vertical growth axis using a wet-saw in the laboratory of the University of Bologna. Each half has been polished and scanned at high resolution (Fig. 4.1).

- **Stalagmite G5 (Govještica Cave):**

It presents a candle shape and is 37 cm tall. The diameter varies between 8 cm in its largest portion and 4.4 cm in its narrowest one. This sample is made of compact and translucent columnar calcite without visible lamination.

- **Stalagmites BS8, BS9, BS14 and BS15 (Mračna Pećina Cave):**

- **BS8:** this candle-shaped stalagmite is formed of clear and relatively compact calcite. This sample is 14.5 cm tall, with a regular diameter of about 5.5 cm. Its lamination is faint in upper part and wavy and irregular in its lower part. Three brownish surfaces are clearly visible and may represent growth interruptions. Four additional sharp surfaces are visible in the polished section and will be further investigated in petrographic thin sections. A dark and sharp lamina is clearly visible close to the top of this stalagmite.
- **BS9:** this stalagmite also displays a candlestick shape. This sample is 14 cm tall and only 3 cm wide. The bottom 4.8 cm are made of whitish and porous calcite which presents an extremely faint and irregular lamination made of thin, wavy and vertically spaced surfaces of more compact calcite. The rest of the stalagmite is composed of relatively compact brownish/yellowish calcite characterised by faint lamination. In addition, the alternation of relatively thick and irregular whitish and porous layers is seen. A dark interval is clearly visible close to the top of this sample.
- **BS14:** this sample is made of compact brownish/yellowish calcite associated with flat and regular lamination formed of the alternation of more compact and translucent calcite and relatively porous and more opaque layers. Whitish and porous calcite is present along the flanks of the lower portion of this stalagmite, where in some intervals it expands toward the central axis. Two surfaces are associated with

slight changes in growth axis and may represent growth interruptions. This stalagmite presents a cone shape (9 cm tall and average diameter of 7.5 cm). A dark layer is visible close to its very top.

- **BS15**: this sample presents a general aspect similar to the previous one. It also displays compact brownish/yellowish calcite associated with flat and regular lamination. Whitish and porous calcite is present along the flanks of the stalagmite, but in contrast to BS14, the central portion appears more compact and undisturbed. BS15 presents a quasi-rectangular section, 10 cm tall with a regular diameter of ~ 6.5 cm. A dark layer, similar to the one observed in the three previous samples, is found close to the top.

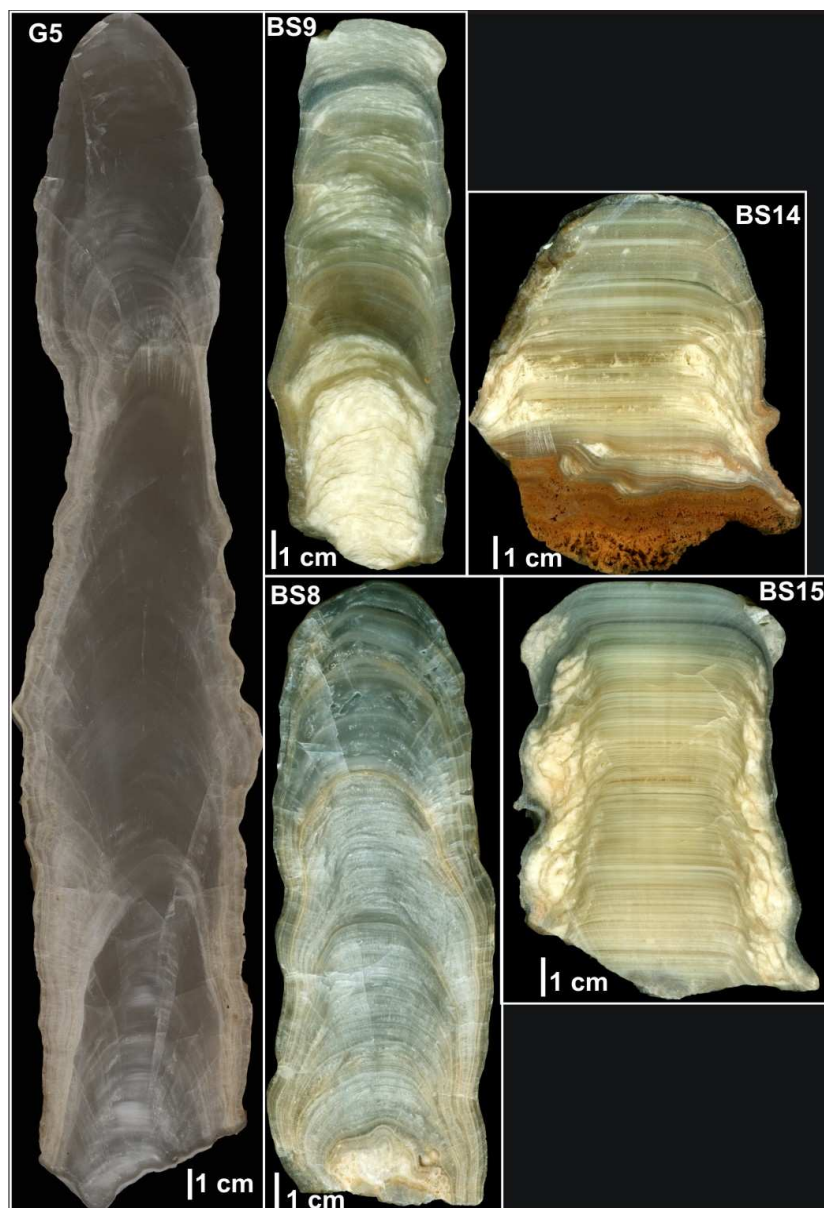


Fig. 4.1 – Polished sections of the studied stalagmites. G5 comes from Govještica Cave; BS8, BS9, BS14 and BS15 come from Mračna Pečina Cave.

4.2 Monitoring of cave parameters and present day precipitation

4.2.1 Cave monitoring and precipitation sampling

In order to understand the cave hydrology, in-cave parameters of Mračna Pečina cave and precipitation monitoring was set up in May 2015. Monitoring instruments were not positioned where stalagmite G5 has been found in Govještica cave, due to the difficult access and the impossibility to guarantee periodic visits to this portion of the cave. A Driptych Pluvimate© and an iButton® temperature data logger were positioned in an open area near the cave entrance, as the area directly above the cave was not accessible.

Two drip-counting Stalagmates© (D1 and D2), registering data every 30 minutes, were positioned in two different areas of Mračna Pečina cave: one in the chamber where the samples were collected, and one deeper in the cave. Three glass plates have also been positioned under active dripping sites to measure calcite precipitation rate (G1, G2 and G3). A temperature logger (iButton®) was set close to D1 site (Fig. 4.2).

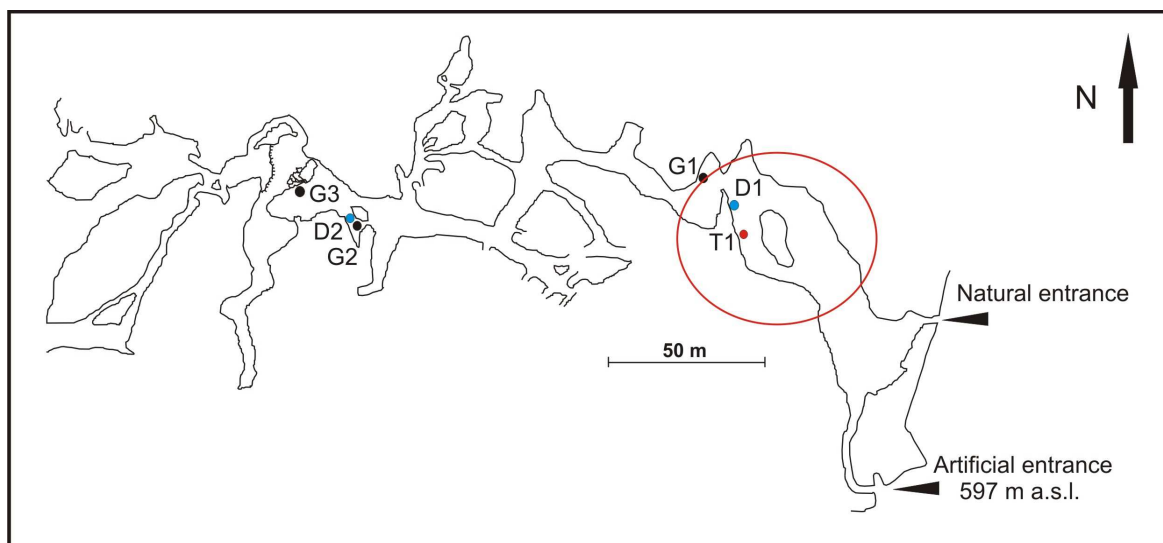


Fig. 4.2 - Mračna Pečina cave map. The red circle: area where the stalagmites were collected; D1 and D2: monitored drip sites; G1, G2 and G3: location of glass plates; T1: location of the temperature data logger.

Before placing the glass plates in monitoring sites, they had been left in the oven at 105°C for 2, 4 and 16 hours. Each time they had been cooled in silica gel for 30 minutes and weighed. The same procedure was repeated every time they had been removed from monitoring sites. The difference in weight was used to estimate the calcite deposition rate at those sites. The cave was visited 6 times in 2015 and 2016 to collect data from the loggers. During those visits, drip water pH and conductivity were measured using, respectively, a WTW LF196, a Lutron pH-222 and a Mettler Toledo SevenGO DUO. Water temperature was measured as well. In addition, drip water for stable isotope

analyses was sampled at each drip site. In order to investigate stable isotope composition of present day precipitation and understand the signal transmitted to the karst system, major precipitation events were sampled in Sarajevo for stable isotope ratio analyses ($\delta^{18}\text{O}$ and $\delta^2\text{H}$). All water samples were collected in 7 ml glass vials filled without leaving air bubbles to prevent evaporation. All samples were stored at a temperature between 0 and 4°C before being analysed. Precipitation stable isotope results have been then compared with drip water stable isotope ratios.

4.2.2 Air mass backtrajectory analyses

Air mass trajectories are among the factors affecting precipitation $\delta^{18}\text{O}$ values. Modification of atmospheric circulation can directly affect precipitation patterns at regional and local scale and the imprinted isotopic signature as well. Prolonged changes in air mass circulation may thus influence both dynamics and chemistry composition of water infiltrating the karst system, thus influencing stalagmite growth and their chemistry.

In order to investigate the atmospheric dynamics behind precipitation patterns in this region, air mass back trajectories of present day precipitation in Sarajevo were performed. Daily precipitation in Sarajevo was obtained from both the Federal Hydrometeorological Institute of Sarajevo and our own monitoring. Back trajectories were performed using the HYSPLIT (Hybrid Single-Particle Lagrangian Integrated Trajectory) model provided online by the NOAA ARL (National Oceanographic and Atmospheric Administration Air Resources Laboratory) (Stein et al., 2015). Following the approach adopted in Baldini et al. (2010), back trajectories were calculated at three atmospheric levels corresponding to 1500, 3015 and 5575 m a.s.l. (i.e. 850, 700 and 500 hPa). The first two levels were chosen as an approximation of the levels from which precipitation forms, the last one to investigate the presence of atmospheric shearing instabilities (Baldini et al., 2010; http://www.arl.noaa.gov/HySPLIT_FAQ.php). This automated system calculates trajectories at a synoptic scale. It starts from wind field data generated by the global data assimilation system (GDAS) and reconstructs the horizontal and vertical coordinates for each hour along a trajectory, as well as other meteorological variables (Baldini et al., 2010). Back trajectories were computed for a running time of 96 hours. Graphic representations resulting from back trajectory reconstructions, which are returned plotted on geographical maps, were analysed to look for possible seasonal trends in air mass movements. These observations were compared with isotope composition of daily precipitation sampled in Sarajevo, searching for possible links between air mass provenance and precipitation stable isotope ratios, aiming to understand the factors involved in precipitation stable isotope values modification. The understanding of these dynamics, together with a good knowledge

of signals transmission to the karst environment is of great importance for the interpretation of environmental and/or climate signals recorded in speleothem calcite.

4.3 Analyses performed on the Bosnian stalagmites

4.3.1 U-Th dating and age modeling

Ages of all stalagmites have been determined with the U-Th disequilibrium method.

Thirteen preliminary U-Th dates (2 in BS8, 2 in BS9, 4 in BS15, 3 in BS14 and 2 in G5) were performed, sampling calcite prisms of about 150 mg with a dentist drill. Additional dating (19 for BS8, 9 for BS9, 15 for BS14, 17 for BS15 and 13 in G5; Fig. 4.3-4.4) was performed on calcite powders, weighing between 50 and 70 mg, in order to improve sampling spatial resolution; they were sampled with a CNC drilling machine (MicroProto systems MicroMill 2000). All samples were prepared and analysed at the School of Earth Science - University of Melbourne (Australia), according to the methodology described in Hellstrom (2003) and modified in Drysdale et al. (2012).

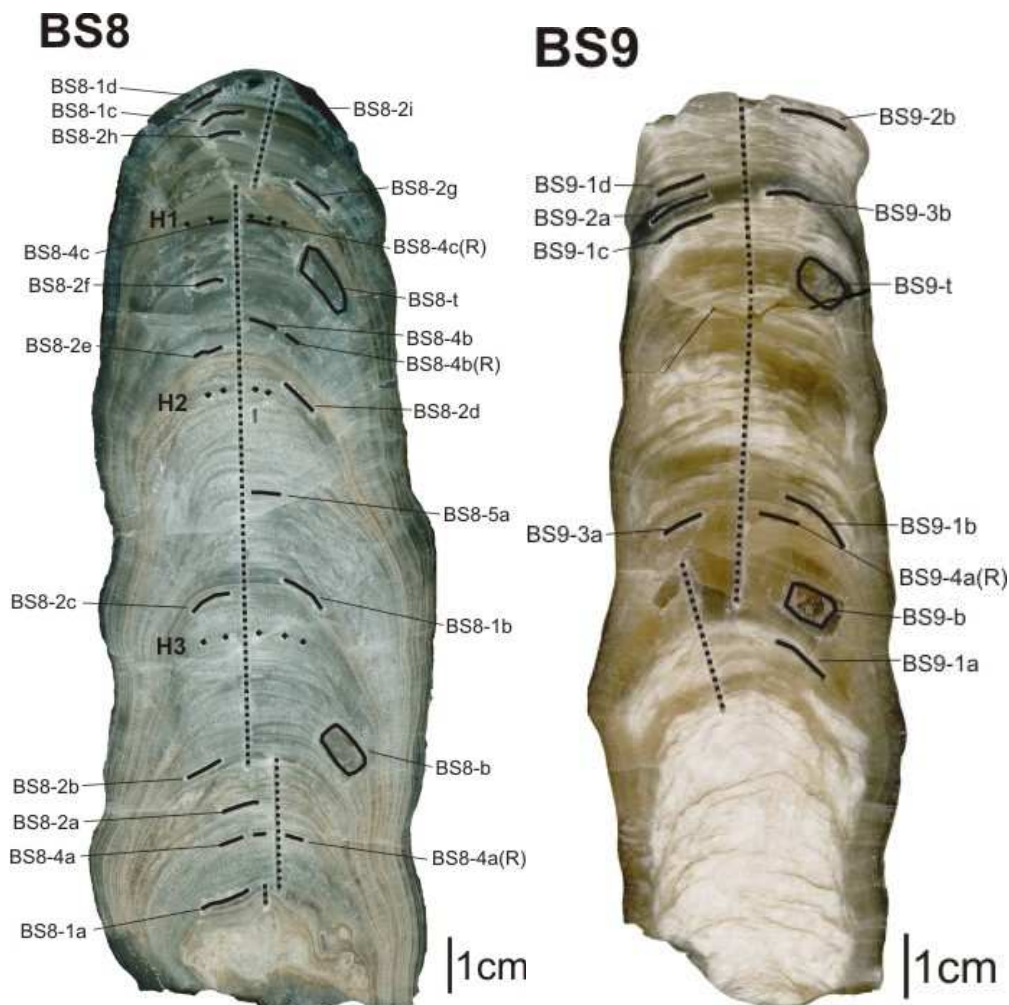


Fig. 4.3 – Position of dating and stable isotope samples on the polished sections of stalagmites BS8 and BS9. Labels indicate samples for U-Th dating. Black dotted lines indicate the stable isotope tracks along the growth axis. H1, H2 and H3 indicate the laminae sampled for the Hendy test (black dots).

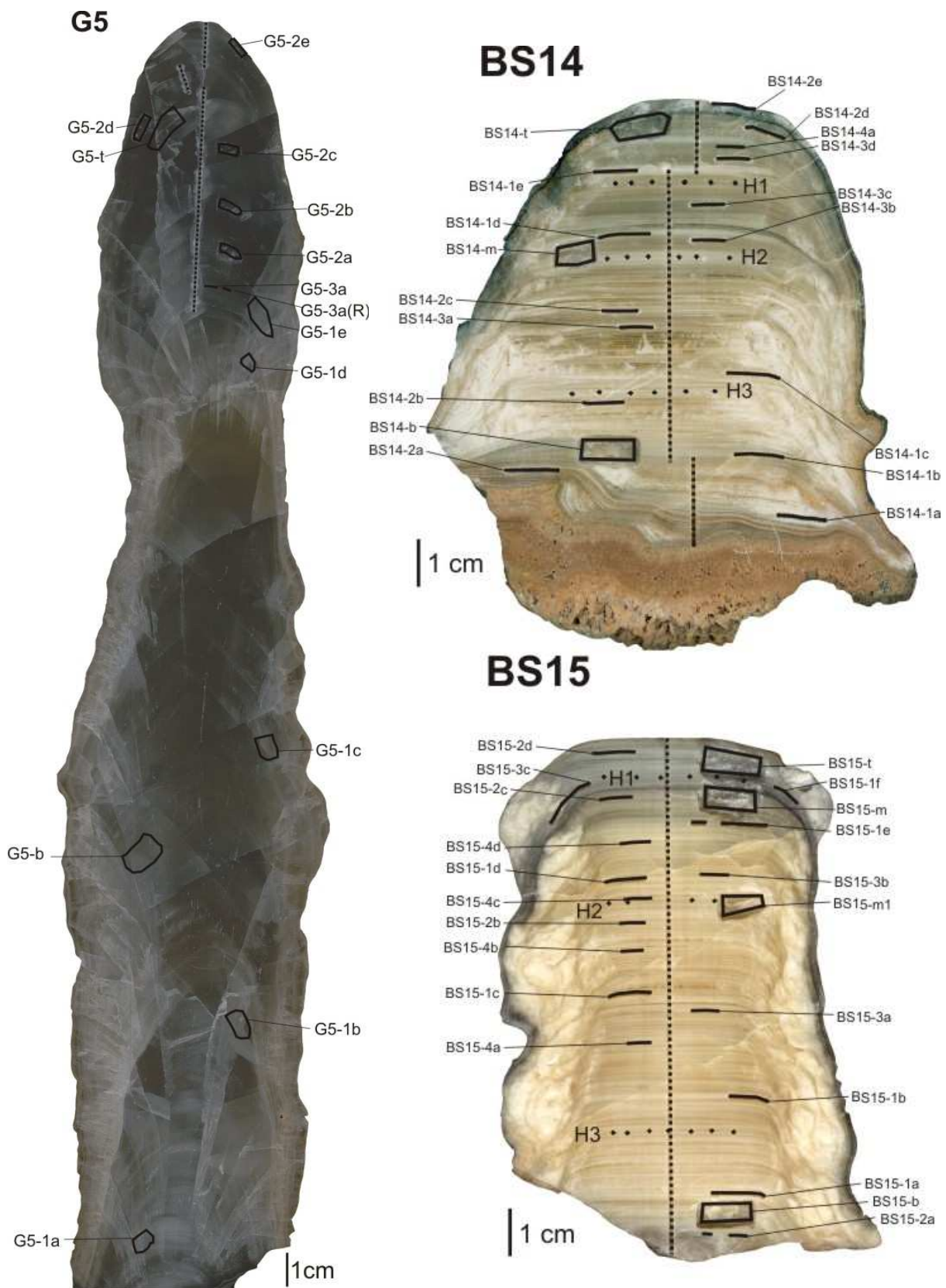


Fig. 4.4 – Position of dating and stable isotope samples on the polished sections of stalagmites G5, BS14 and BS15. Labels indicate samples for U-Th dating. Black dotted lines indicate the stable isotope tracks along the stalagmite growth axes. H1, H2 and H3 indicate the laminae sampled for the Hendy test (black dots) in stalagmites BS14 and BS15.

Uranium is transported to the karst environment via the infiltrating water, it is incorporated into speleothem calcite and decays radioactively to thorium and other daughters products (Fairchild and Baker, 2012). If the system remains closed (i.e. there are no post-depositional modifications involving addition or loss of U and Th isotopes) and there is no initial thorium in the drip water forming the speleothem, it is possible to calculate the time of calcite deposition.

Uranium and thorium were separated from the bulk of the carbonate matrix through a procedure involving the dissolution of the sample and addition of a mixed spike that enables to constrain the yield of the procedure. This procedure was performed in the clean laboratory of the School of Earth Science of the University of Melbourne. A clean room accessible only with special garments is indeed necessary to prevent the introduction of external contamination during sample preparation, which may prevent the achievement of reliable results. 22 calcite dating samples were prepared at a time together with one “blank” sample and a standard. Calcite samples were accurately weighed and placed in 7 ml plastic beakers paying attention not to introduce cross contamination among them. The “blank” sample is an empty plastic beaker which is then prepared using the same procedure as for calcite dating samples and serves to identify the eventual presence of any mistake and/or contamination occurred during sample preparation. The standard is a calcite powder sample whose age is known (in this case 400,000 years old) and that is used to calibrate dating results. All samples were dissolved using concentrated HNO₃ and then diluted with distilled water. The resulting solutions were added with a spike of known $^{236}\text{U}/^{233}\text{U}/^{229}\text{Th}$.

The spiked samples were poured through columns filled with TRU-Spec resin. Uranium-thorium pure fraction was then separated from the carbonate matrix with repeated washes of HNO₃, HCl and HCl-HF through the columns. HNO₃ and HCl acids are necessary to remove the calcium carbonate from the column resin; HCl-HF allows for the collection of U-Th compound in 3 ml vials, which had been left to dry overnight on a hot plate set at the temperature of ~ 80°C.

The isotopic ratios were analysed with a Nu Instruments Plasma multi collector – inductively coupled plasma – mass spectrometer (MC-ICP-MS) at the School of Earth Science (University of Melbourne), following the methodology established in Hellstrom (2003) and refined in Drysdale et al. (2012). Considering the presence of high detrital contamination affecting the analysed samples, the obtained raw ages have been corrected according to the stratigraphic approach described in Hellstrom (2006) using a $^{230}\text{Th}/^{232}\text{Th}$ initial activity ratios of 0.30 ± 0.25 (2σ) for BS8, 0.45 ± 0.30 for BS9, 0.30 ± 0.20 for BS14, 0.65 ± 0.19 for BS15 and 1.5 ± 1.5 for G5. The calculation of initial $^{230}\text{Th}/^{232}\text{Th}$ activity ratios is based on a Monte Carlo simulation which allows for the identification of the best Th correction to apply for the correct age calculation (Hellstrom, 2006). Corrected ages have been then used to calculate age-depth models for the studied stalagmites. These have been

calculated from a Bayesian-Monte Carlo treatment of the U-Th ages performed using a model developed by John Hellstrom at the University of Melbourne. Only major hiatuses have been considered in these models since it is possible to enter growth interruptions only when at least four U-Th ages are available between two hiatuses. A deeper description of these models is presented in Results and Discussion Chapters.

4.3.2 Stable isotopes

Precipitation $\delta^{18}\text{O}$ composition can be directly and/or indirectly influenced by climate-related



Fig. 4.5 – MicroProto systems Micromill 2000 used for sampling stalagmites surfaces for both stable isotopes and U-Th analyses.

processes. This isotopic signal can be transferred to the karst environment through percolating water. During its journey from the soil to the cave, the $\delta^{13}\text{C}$ composition of water can be influenced by soil CO_2 , which in turns depends on soil activity and type of vegetation cover (see Paragraph 2.4.2.2.2). Stable isotope composition of infiltrating water can then be recorded in the precipitated calcite, if calcium carbonate deposition occurs at equilibrium conditions. Thus, stalagmite $\delta^{13}\text{C}$ and $\delta^{18}\text{O}$ composition can change during the speleothem deposition in relation to

Stalagmite	Lamina - distance from top	Number of samples
BS8	H1 – 26.5 mm	5
	H2 – 56.5 mm	4
	H3 – 99 mm	6
BS14	H1 – 16.5 mm	6
	H2 – 31.5 mm	6
	H3 – 59 mm	6
BS15	H1 – 8 mm	6
	H2 – 32.5 mm	6
	H3 – 79 mm	7

Tab. 4.1 – Distance from the stalagmite top of the laminae sampled for Hندی test in stalagmites BS8, BS14 and BS15 and number of calcite powder samples drilled for each lamina.

environmental and/or climate changes. In order to investigate $\delta^{13}\text{C}$ and $\delta^{18}\text{O}$ variations recorded during the period of growth of the studied stalagmites, samples for stable oxygen and carbon isotope analyses were drilled along the vertical growth axis with a 1 mm increment. About 2 mg of powder were collected for each sample, using a 1 mm diameter drill bit mounted on a CNC drilling machine (MicroProto systems MicroMill 2000; Fig. 4.5) at EDYTEM laboratory – Université Savoie Mont Blanc.

However, it must be considered that only calcite precipitation close to equilibrium conditions can lead to the parent drip water isotopic signals preservation. Unfortunately, these conditions are unlikely met in cave

In order to look for the presence of strong disequilibrium fractionation affecting speleothem calcite of the studied stalagmites, samples designed for the Hendy test (1971) were drilled along three distinct laminae, every 3 to 5 mm, in BS8, BS14 and BS15, using a 0.6 diameter drill bit (Tab. 4.1). This test was not performed in stalagmites BS9 and G5 because of the impossibility to sample with precision along the same lamina due to the lack of clear lamination in these samples (Fig. 4.3 - 4.4). The Hendy test is based on the assumptions that 1) the lack of covariation between $\delta^{13}\text{C}$ and $\delta^{18}\text{O}$ along both the sample growth axis and the sampled lamina and 2) the presence of constant $\delta^{18}\text{O}$ values along the sampled lamina are two prerequisite for calcite precipitation at equilibrium conditions. However limits of this method have been highlighted by several authors (e.g. Cerling, 1984; Dorale et al., 1992; 1998; Dorale and Liu, 2009). As a more robust tool to test for the absence of strong disequilibrium fractionation Dorale and Liu (2009) proposed the replication test, which consists in comparing stable isotope profiles of coeval stalagmites sampled in the same cave. This test has also been performed and is further discussed in Chapter 6.3.

All carbonate isotope samples were prepared and analysed at the School of Geography, University of Melbourne (Australia). For the growth-axis samples, about 0.7 to 0.8 mg of powder were weighed into glass vials using a Mettler Toledo XS105 analytical balance. Batches of 105 samples each were prepared and analysed. These batches consisted of 3 racks containing 132 stalagmite powder samples and 37 standards (21 'New1' (Carrara marble standard), 2 'New12' (powdered omogeneous calcite prism of unknown origin), 2 'NBS-18' (international reference standard) and 12 'NBS-19' (international reference standard)). All samples of each single batch were purged with helium to remove the atmospheric gases (carbon dioxide and oxygen in particular), a procedure lasting about 8 hours for each batch. The samples were then acidified using 0.5 ml of 105% H_3PO_4 and left 30 minutes at 70°C in a Nu Instruments NuCarb sample preparation unit to allow for a complete dissolution of the carbonate powder.

The CO_2 gas produced by carbonate powder dissolution was then carried into an Analytical Precision AP2003 continuous-flow isotope-ratio mass spectrometer using an ultra high purity (99.9995%) helium carrier gas. External reproducibility was better than 0.05‰ and 0.10‰ for C and O respectively.

For the Hendy test samples, about 0.05 to 0.10 mg of calcite powder were weighed into glass vials. The atmospheric gases were removed from the vials using the same procedure described above and then 0.5 ml of 105% H_3PO_4 at 70°C were added to allow for a complete dissolution. The sample gas CO_2 was admitted into the ion source under vacuum and analysed on a Nu Instruments Perspective dual-inlet isotope-ratio mass spectrometer. External reproducibility was 0.03‰ and 0.06‰ for C and O respectively. Sample data from both instruments were normalised to

the V-PDB scale using the two in-house calcite standards ('NEW1' and 'NEW12'), previously calibrated against the international reference standards NBS-18 and NBS-19.

4.3.3 Trace elements

When water infiltrates the soil and bedrock, it can take in charge several elements as solutes or particulates and ion aggregates. The type and concentration of the trace element content in groundwater is related to both their availability (i.e. type of source) and hydrochemical processes occurring in the epikarst (see Paragraph 2.4.3). These elements can then be incorporated into speleothem calcite providing insights over hydrological processes from the seasonal to the multi-decadal/multi century scale. Among the Bosnian stalagmites, only BS15 was chosen for trace element analyses, since it was considered the most promising and most suitable sample. Its compact texture and the presence of a fine and relatively regular lamination without marked growth interruptions suggested the possibility of having trace element variations recorded at the lamina scale. Trace element concentrations have been analysed continuously along the vertical growth axis of a slab cut from stalagmite BS15 (Fig. 4.6) at the School of Earth Sciences, University of Melbourne. This analyses was performed using a HelEx ("HeliumExcimer") laser ablation system, equipped with a customised Resonetics Resolution 193 nm Arf laser system, in conjunction with an Agilent 7700x quadrupole ICP-MS instrument as described in Woodhead et al. (2007) and Drysdale et al. (2012). This system operates in a helium atmosphere to minimise sample re-deposition during ablation; however the sample-bearing flow is mixed with argon within the cell to promote more efficient sample transport path (Woodhead et al., 2007 and reference therein).

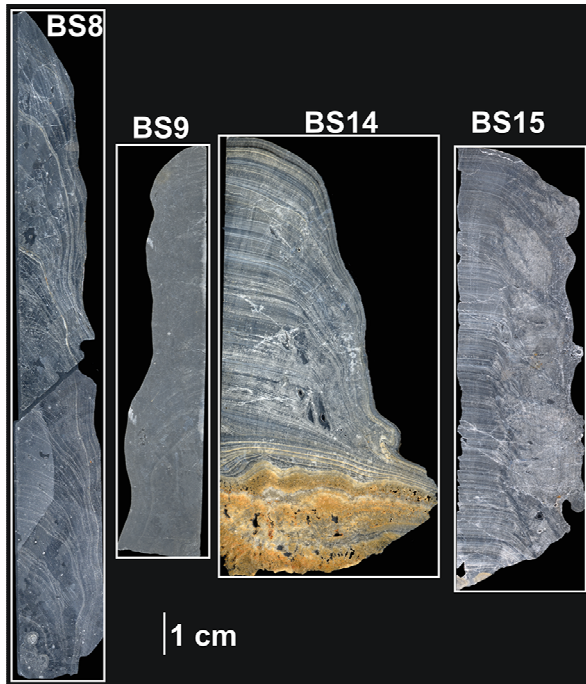
The polished speleothem surface was pre-ablated with a 188 μm laser spot and an intensity of 10 Hz in order to eliminate surface contamination. An 8 x 140 μm laser spot size and a pulse rate of 10 Hz were used for the analyses, which were carried out in a high purity helium atmosphere. One continuous track was performed at the velocity of 30 $\mu\text{m}/\text{s}$, covering the entire length of stalagmite BS15. In order to compare the data with the isotopic values and facilitate the statistical analyses, an average value for each element has been calculated at a millimetre interval corresponding to the stable isotope profiles. Correlation coefficients have been calculated between individual trace elements and between the trace element and stable isotope values



Fig. 4.6 – Trace element track on BS15 slab.

4.3.4 Petrography

All stalagmites were cut along their vertical growth axis. The two halves were polished for



stratigraphic observation and subsequently scanned at high resolution. Growth discontinuities were identified as a guideline for dating in order to assess the duration of hiatuses. Broad description of polished surfaces is provided in Paragraph 4.1.

In order to deeper investigate crystal shapes and arrangements, identify the eventual presence of post-depositional modifications, confirm the hiatuses observed on the polished surfaces and investigate the eventual presence of further growth interruptions, thin sections for petrographic observations have been realised. In particular five thin sections, two containing the full lengths of

Fig. 4.7 – Thin sections of stalagmites BS8, BS9, BS14 and BS15.

BS14 and BS15 stalagmites and three containing, respectively, BS8 and BS9 stalagmites, were made

(Fig. 4.7). Any thin section was realised on stalagmite G5 due to its compactness and the absence of evident changes in crystals arrangements. In addition, since only the upper part of G5 was studied, it was preferred not to perform destructive manipulations on this sample.

Petrography was studied on an Olympus BH-2 BHS polarizing microscope. Pictures of magnified thin sections have been taken with a Leica MC 120 HD camera mounted on the microscope.

Growth discontinuities were identified and calcite textures were recognised and classified following the criteria proposed in Frisia et al. (2000), Frisia & Borsato (2010) and Frisia (2015).

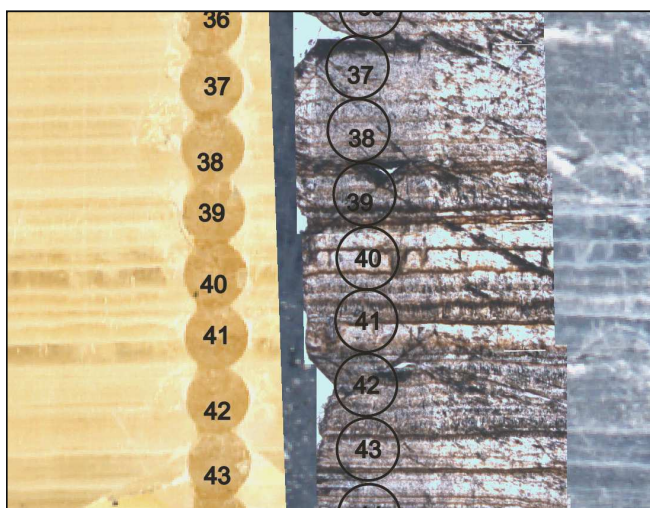


Fig. 4.8 – Left: image of BS15 polished section; the holes marked by progressive numbers correspond to the samples drilled for stable isotope analyses. Right: image of thin section corresponding to the stalagmite portion on the left. Black circles represent the position where samples for stable isotope analyses were drilled and to which a value corresponding to the columnar microcrystalline texture sub-classification was associated with allow for a direct comparison between stable isotope profiles and petrography.

For stalagmites BS14 and BS15 a detailed petrography micrologging was performed: crystallite arrangements have been classified at the millimetre scale, adapting the classification proposed in Frisia (2015) to the specific case. At the lamina scale, calcite textures were classified on the basis of: 1) the composite crystallite boundary geometries, from which intra-crystalline microporosity has been deduced; and 2) inter-crystalline porosity features (i.e. pores orientation and geometry and their relative distribution). From this, a sub-classification scheme for the columnar microcrystalline texture was built for this case study. Following the hierarchical classification of fabrics proposed by Frisia (2015), a ranking was associated with each fabric subtype, expressing a progressive increase of inter- and intra-crystalline porosity within the microcrystalline subtypes, which is related to the presence of impurities directly affecting the crystallite lattice development. In addition, by analogy with the calcite classification proposed in Frisia (2015), which was considered as a starting point for this specific subdivision, the deposition of the classified textures under increased hydrological stress (i.e. less regular dripping) was inferred, which may also have influenced the stable isotope fractionation of the precipitated calcite.

Calcite textures were thus classified every millimetre corresponding to the samples drilled for stable isotope analyses (Fig. 4.8).

4.3.5 Statistical analyses used for comparing petrography and geochemical signals in stalagmites BS14 and BS15

Each petrography class was examined on the basis of calcite stable isotope and trace element composition to investigate the possible presence of geochemical signatures. In order to test whether isotopic variations are associated with petrographic changes, the isotope data were ranked and a Kruskal-Wallis test was performed. Indeed, this test is a non-parametric method that is used to determine whether the analysed samples (in this case the $\delta^{13}\text{C}$ and $\delta^{18}\text{O}$ grouped according to the classified petrography classes) belong to the same distribution (Kruskal and Wallis, 1952).

An isotope-fabric plot (IsoFab) was built according to the method described by Frisia (2015), calculating the average $\delta^{13}\text{C}$ and $\delta^{18}\text{O}$ values for each fabric and the associated standard deviations. In order to investigate the statistical significance of isotopic differences/similarities between the petrography groups, multiple comparisons using the Bonferroni correction were performed (e.g., Dunn, 1961) using an SPSS IBM software ®. Finally, to further investigate the presence of geochemical signatures in the classified petrography groups, discriminant analyses were performed using SPSS IBM software ®, considering first the $\delta^{13}\text{C}$ and $\delta^{18}\text{O}$ composition of petrography classes in stalagmites BS14 and BS15, then $\delta^{13}\text{C}$, $\delta^{18}\text{O}$, Sr, and Mg composition (e.g., Green et al., 2008). Indeed, this particular multivariate analysis allows for the attribution of single individuals to

different groups according to chosen variables. These variables (i.e. Mg, Sr, $\delta^{13}\text{C}$ and $\delta^{18}\text{O}$) were used to construct canonical discriminant functions as a function of which individuals were plotted.

4.3.6 Analyses applied specifically to the black layer

In order to understand the nature and origin of a black layer identified close to the top of the four stalagmites sampled in Mračna Pećina cave, further analyses were carried out: in particular, observations with a fluorescence microscope, micro-Raman spectroscopy analyses, Fourier transform infrared spectroscopy (FTIR) analyses and scanning electron microscope (SEM) analyses. Since the dark layer is more evident and thick in stalagmites BS15 and BS14, only these two samples were chosen for further analyses.

4.3.6.1 Fluorescence microscope

Fluorescence microscopy enables the detection of organic matter in the analysed sample. The instrument is provided with an illumination system able to illuminate the sample with a light of a specific wavelength. The organic matter absorbs the light, which causes its excitation and the subsequent emission of light of longer wavelength. A spectral emission filter is used to separate the light emitted by the sample allowing for its detection. These systems provide qualitative images of the analysed samples in which colour intensities are indicative of the presence of organic matter. Thin sections of stalagmites BS14 and BS15 were observed with an Olympus BX51P polarizing microscope. The fluorescence was observed using a 50 Watt tungsten light source which is filtered by two cubes which enable the observation of UV radiation (excitation filter: 330-335 nm; emission filter 420 nm). Pictures were taken with an Olympus UC30 integrated camera. These observations were carried out in the B. Bagolini laboratory at the University of Trento.

4.3.6.2 Micro-Raman spectroscopy analyses

The Raman technology is a spectroscopic technique that allows for the identification of the molecules of the analysed material through the detection of molecular vibrations and/or rotations. This technique depends on changes in the molecules polarizability.

A monochromatic laser is used, causing excitation in the system. The electromagnetic scattered radiation is collected with a lens and sent to a monochromator. The Rayleigh scattering (or elastic scattering) is filtered, allowing for the separation of the Raman scattering (or inelastic scattering) that is dispersed to a detector, measuring the relative frequencies at which the analysed sample scatters radiations. The micro-Raman utilises the Raman technology associated with an optic microscope. A Horiba JobinYvon J64000 was used, coupled with a reflected light microscope. The

black layer in stalagmite BS15 thin section has been analysed in the laboratories of the University of Grenoble Alpes using a laser pulse intensity of 0.5 mW and a microscope magnification of 50x.

4.3.6.3 Fourier Transform Infrared Spectroscopy (FTIR)

FTIR spectroscopy is a vibrational spectroscopic technique that allows for the identification of molecular composition of a material through the restitution of an infrared spectrum of absorption of the analysed sample, measuring the absolute frequencies at which a sample absorbs radiations. This technique relies on the direct absorption of light as a result of transitions between vibrational states (Ali et al., 2013). While the Raman spectroscopy is stronger in detecting symmetric electron rich moieties, the FTIR tends to perform better in the detection of asymmetric polar moieties and is less sensitive to the presence of organic matter (Ali et al., 2013). Thus, these two techniques can be considered complementary.

Two “blisters” were realised using calcite powder samples drilled in the black layer in stalagmites BS14 and BS15 (Fig. 4.9) and analysed at the University of Savoie Mont Blanc.

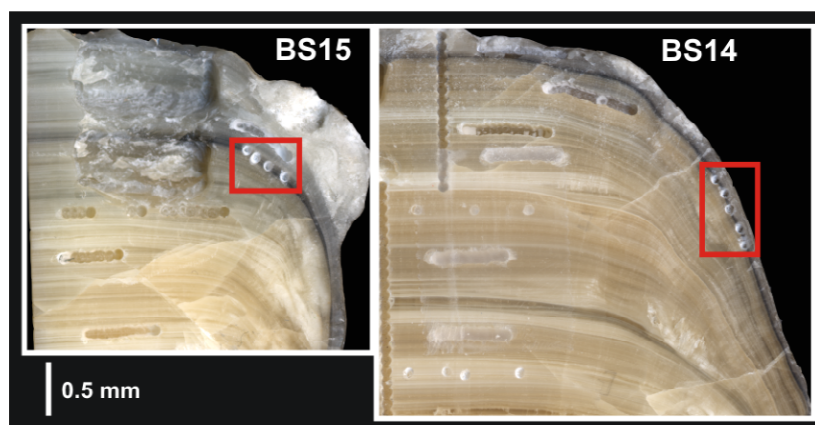


Fig. 4.9 – Red squares indicate the position where powder samples have been drilled along the black layer in stalagmites BS14 and B15.

4.3.6.4 Scanning Electron Microscope (SEM) analyses

The scanning electron microscope allows to carry out morphological and chemical analyses of samples using a focused beam of electrons. These electrons interact with the sample atoms whose excitation produces secondary electrons that are detected by the instrument. This signal contains information on both the morphology and the chemical composition of the analysed material.

A Stereoscan 440 was used at the University of Savoie Mont Blanc (Le Bourget du Lac, France) to observe and analyse both powder and solid samples. The leftover powders that had been previously used for FTIR analyses from stalagmites BS14 and BS15 were used (Fig. 4.9). In addition a further powder sample was drilled on the surface of stalagmite BS14, where the black layer reaches the surface (Fig. 4.10).



The slab cut from stalagmite BS15 and used for trace element analyses has also been used for SEM observations. None of the analysed samples was metalised not to compromise the original chemical composition. A copper tape was used to enhance electron reflectivity (Fig. 4.11).

Fig. 4.10 – The red square indicates the area on the surface of BS14 where one of the powder samples of the black layer was drilled.

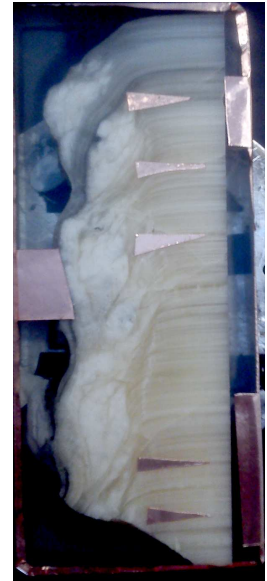


Fig. 4.11 – Copper tape on BS15 slab.

V. RESULTS

5.1 Monitoring data: cave dynamics and precipitation stable isotope composition

5.1.1 Cave dynamics

One year of monitoring data is available (May 2015-July 2016), providing insights on the cave hydrologic pattern in relation to precipitation. The data highlight the presence of strong seasonality affecting the monitored drip sites. In summer and at the beginning of autumn, although precipitation occurs, the cave is relatively dry with slow dripping at D1 (7 drops/hour in October) and almost no dripping at D2 (Fig. 5.1).

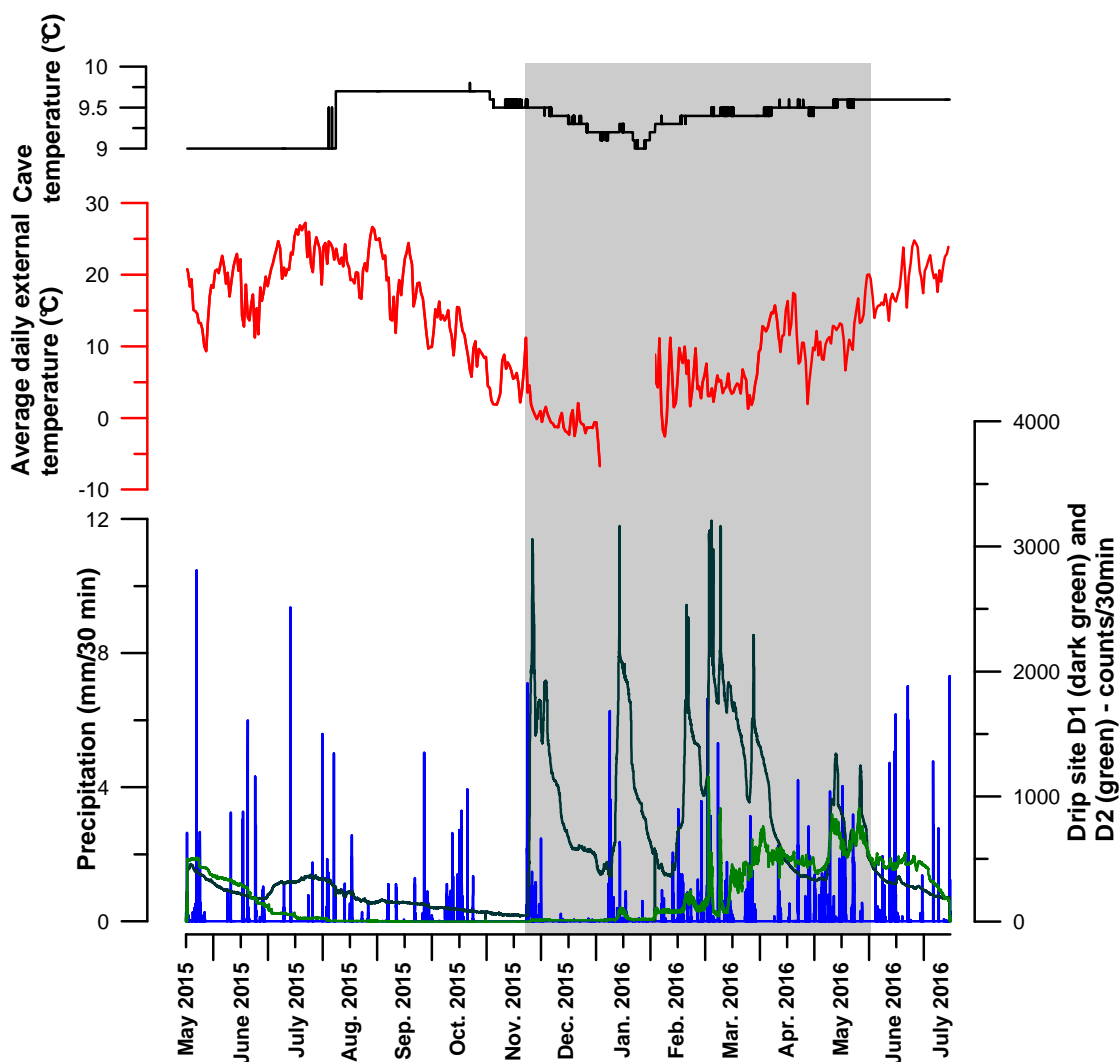


Fig. 5.1 – Monitoring results between May 2015 and the beginning of July 2016. The blue line represents precipitation recorded with a Driptych Pluvimate © (mm/30min). The dark green and the green lines represent, respectively, drip sites D1 and D2 (counts/30min). The red line represents external temperatures (°C). The black line on top represents cave temperature (°C). The grey box indicates the period of the year with stronger dripping.

In late autumn, drip site D1 is abruptly reactivated showing strong responses to rainfall events. Drip site D2, which generally shows slower dripping, is reactivated only by winter precipitation, in February, as precipitation events become more frequent. Drip sites show increased reactivity to precipitation in late autumn, winter and spring, when temperature is low (average daily temperature of 1.5 ± 6.6 °C and 7.8 ± 4.3 °C between, respectively, November-December and February-May) and precipitation more abundant. The dry period recorded in Mračna Pečina Cave is concomitant with the highest external temperature (average daily temperature for the period May-October 2015: 18.4 ± 5.1 °C). External temperature data are not available for January 2016 because the logger was accidentally removed.

Cave temperature was measured close to drip site 1, in the area where the broken stalagmites were collected and it appears relatively stable. Between May and July 2015, the data logger was inadequately set to measure temperature with a resolution of 0.5°C, and temperature did not vary by

	Date	pH	water temperature	SEC (µS/cm)
D1	17-05-2015	7.67	9.6	478
D2		8.1	10.5	582
G1		8.01	10.3	481
G2		Dry	Dry	Dry
G3		7.89	13.7	681
D1	07-08-2015	7.13	11.6	455
D2		Dry	Dry	Dry
G1		7.27	10.4	558
G2		Dry	Dry	Dry
G3		Dry	Dry	Dry
D1	29-10-2015	7.28	11.5	470
D2		Dry	Dry	Dry
G1		7.28	10.2	693
G2		Dry	Dry	Dry
G3		7.08	12.9	410
D1	31-01-2016	8.02	9.1	469
D2		8.38	10.9	n.m.
G1		8.13	9.4	497
G2		Dry	Dry	Dry
G3		8.15	11	588
D1	09-04-2016	n.m	n.m	n.m
D2		n.m	n.m	n.m
G1		n.m	n.m	n.m
G2		n.m	n.m	n.m
G3		n.m	n.m	n.m
D1	12/07/2016	n.m	n.m	n.m
D2		n.m	n.m	n.m
G1		n.m	n.m	n.m
G2		n.m	n.m	n.m
G3		n.m	n.m	n.m

Tab. 5.1 – pH, water temperature (°C) and specific electrical conductance (SEC) of monitored drip sites. N.m = not measured. D1 and D2: drip sites monitored with a stalagmite; G1, G2 and G3: drip sites where a glass tablet was positioned for growth rate monitoring.

more than this range, around 9°C (Fig. 5.1). After July 2015 temperature was measured with a resolution of 0.1°C. From August to October, cave temperature remained stable at 9.7 ± 0.1 °C and then it started decreasing, down to a minimum of 9.0°C in January 2016. Temperatures then progressively increased again, to reach 9.6°C in May 2016 and remaining stable in the following monitored months (Fig. 5.1). So the max T° amplitude measured in the cave over a year is 0.8°C.

pH values of dripping water show variations in the range of 7.08 - 8.38 depending on the sampling site and period of sampling (Tab. 5.1). In general, drip site D1 showed the lowest average pH among the measured drip sites. Considering the timing of the analyses, a clear difference in pH has been observed through the year. Relatively low values were detected in May, followed by the lowest pH values recorded in August and October associated with the highest conductivity at drip site G1 and D1

(Tab. 5.1). The highest pH values were observed in January.

Glass tablet G2 was left in situ for the whole period of monitoring (May 2015-July 2016) showing a growth rate of about 4 mm/year. Glass tablet positioned at site G1, close to the area where the stalagmite were found, shows a period of relatively high deposition (about 0.8 mm/year) between May and August 2015 followed by an extremely low if not null deposition rate between August and October 2015 (about 0.09 mm/year), while the growth rate measured between January and the beginning of July is about 0.7 mm/year. Between January 2016 and April 2016 the measured growth rate at G3 site is about 2.2 mm/year, followed by a higher growth rate of about 3.2 mm/year between April and the beginning of July 2016. The observed high growth rate may be related to a flowstone type calcite deposition occurring at the monitoring points.

5.1.2 Precipitation and drip water stable isotope composition

Owing to problems during water sample shipping, stable isotope results of both drip water and rain water are available only from September 2015 to March 2016 (Tab. 5.2; Fig. 5.2).

Rainfall sample	$\delta^{18}\text{O}$	δD	Drip water sample	$\delta^{18}\text{O}$	δD
S14 (10/09/2015)	-6.87	-49.9	D1 (29/10/2015)	-9.37	-64.6
S15 (20/09/2015)	-5.87	-31.0	G1 (29/10/2015)	-9.36	-64.9
S16 (27/09/2015)	-11.17	-80.6	G3 (29/10/2015)	-10.11	-70.0
S17 (10/10/2015)	-11.31	-81.2	D1 (31/1/2016)	-9.43	-64.4
S18 (17/10/2015)	-4.75	.19.7	D2 (31/1/2015)	-9.16	-62.2
S19 (21/11/2015)	-8.60	-53.0	G1 (31/1/2016)	-9.43	-64.7
S20 (25/11/2015)	-18.05	-133.1	G3 (31/1/2016)	-10.24	-71.1
S21 (2/1/2016)	-13.58	-95.4	D1 (9/4/2016)	-9.4	-63
S22 (16/01/2016)	-20.41	-156.1	D2 (9/4/2016)	-9.0	-61.3
S23 (4/2/2016)	-13.02	-96.5	G1 (9/4/2016)	-9.2	-61.5
S24 (15/2/2016)	-7.45	-59.0	G3 (9/4/2016)	-9.9	-66.9
S25 (26/2/2016)	-5.13	-62.2	D1 (12/7/2016)	-9.4	-62.3
S26 (29/2/2016)	-0.72	-9.8	D2 (12/4/2016)	-9.5	-64.2
S27 (7/3/2016)	-7.14	-53.4	G1 (12/7/2016)	-9.6	-63.6
S28 (21/3/2016)	-9.93	-65.2	G3 (12/7/2016)	-9.80	-66.6
S30 (14/4/2016)	-3.0	-14.2			
S31 (19/4/2016)	-5.8	-35.1			
S32 (24/4/2016)	-7.5	-57.5			
S34 (28/4/2016)	-5.4	-34.5			
S35 (3/5/2016)	-7.1	-47.1			
S36 (8/5/2016)	-4.9	-22.8			
S37 (12/5/2016)	-5.7	-34.0			
S38 (1/6/2016)	-1.6	-18.6			
S39 (6/6/2016)	-8.1	-55.3			

Tab. 5.2 – Stable isotope results of precipitation in Sarajevo (labelled with an S) and drip water from Mračna Pećina Cave (G and D samples). Monitored drip sites are indicated in Fig. 4.1 in Chapter 4).

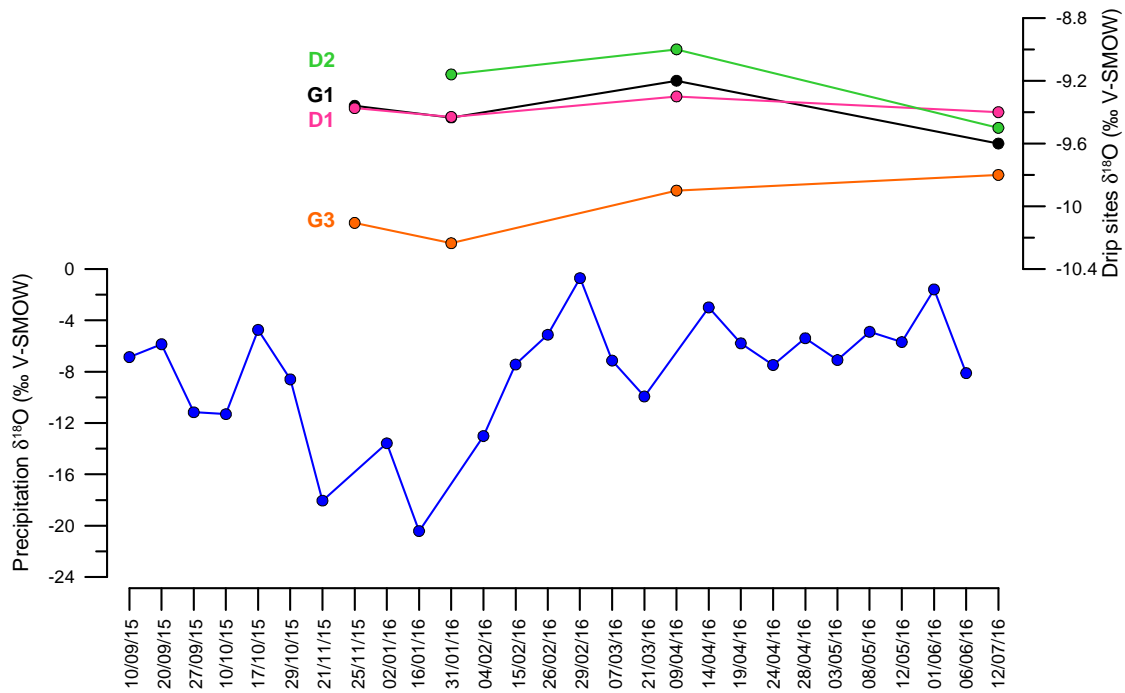


Fig. 5.2 – $\delta^{18}\text{O}$ composition of rainfall sampled in Sarajevo and drip sites D1, D2, G1 and G3 (see Tab. 5.2).

These data, although sparse, show similar isotopic values measured at sites D1 and G1 and relatively lower values at site G3 (Tab. 5.2; sampling location in Fig. 4.1, Paragraph 4.2.1).

Precipitation stable oxygen isotope ratios fluctuate between the highest values of -0.72‰ , measured in a precipitation event occurred on 29 February 2016, and the lowest value of -20.41‰ measured in a precipitation event occurred on 16 January 2016. Considering the general trend, the highest measured $\delta^{18}\text{O}$ ratios are related to precipitation occurring in late spring/early summer (April to June: $\delta^{18}\text{O} = -5.46 \pm 2.10\text{‰}$) and the lowest ones to winter precipitation (November to February: $\delta^{18}\text{O} = -10.87 \pm 6.63\text{‰}$). However, some intra-seasonal variability related to the isotopic signature carried by single precipitation events is visible. Drip water analyses show fairly constant values. Drip sites D1 and G1, which are located in the same gallery, present similar isotopic values (average $\delta^{18}\text{O}$, respectively, $-9.38 \pm 0.06\text{‰}$ and $-9.40 \pm 0.17\text{‰}$), slightly enriched if compared to the G3 site (average $\delta^{18}\text{O}$: $-10.01 \pm 0.20\text{‰}$), located further away from the cave entrance (Fig. 4.1 in section 4.1). Drip site G2, which is located close to monitoring site G3, present the highest isotopic (average $\delta^{18}\text{O}$: $-9.22 \pm 0.26\text{‰}$).

5.1.3 Air mass back trajectories of daily precipitation in Sarajevo

Back trajectories performed on rainy days in 2015 and 2016 highlighted a preponderance of precipitation events originating in the Atlantic Ocean. However, different air mass tracks have been identified. For each day in which precipitation occurred in Sarajevo, the three trajectories calculated at different heights (850, 700 and 500 hPa) are indicated in the plots with different colours (Fig.

5.3). When the three trajectories follow approximately the same path, shearing instabilities can be considered irrelevant and the calculated back trajectory is reliable (cf. Baldini et al., 2010). This occurs in the majority of the calculated trajectories (98 out of 163 back trajectories). Conversely, when air mass movement reconstructions show different trajectories at different heights, shearing instabilities may have occurred and the reconstructions are less accurate. This is mainly found during spring and autumn months. While in winter air mass tracks are mainly coming from N and NW crossing over the European continent, in summer the main trajectories of air masses coming from the Atlantic Ocean are slightly shifted southwards (Fig. 5.3). The westerlies circulation that characterises the European continent thus dominates the main storm paths. Trajectories of these moisture-bearing air masses originating in the Atlantic Ocean can be further modified over the Mediterranean basin developing complex patterns resulting in SW, S and NE paths (Fig. 5.3). These have been identified mainly in spring, summer and autumn. Also rarer storm paths involving air masses from eastern and north-eastern Europe have been identified in spring and autumn.

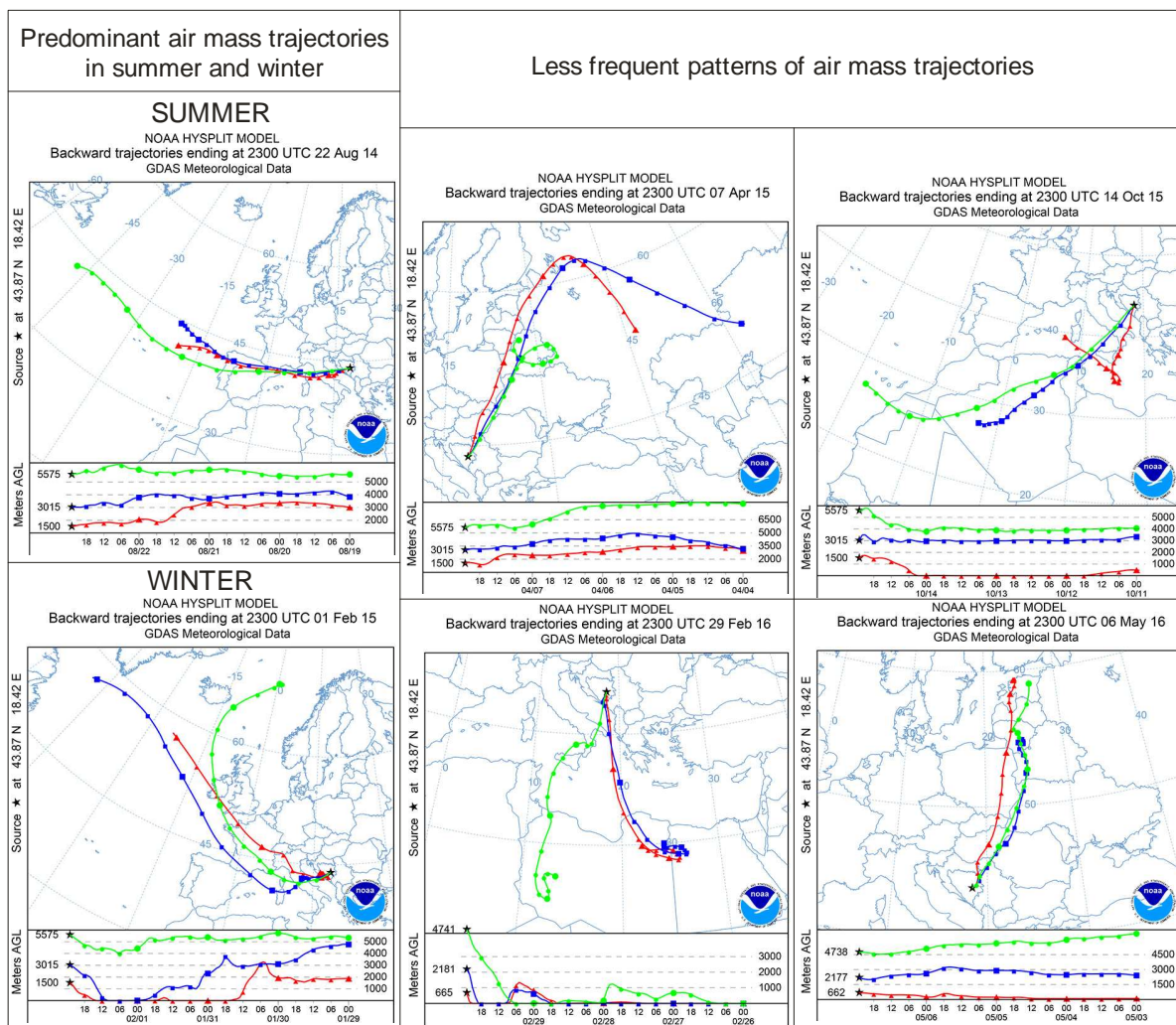


Fig. 5.3 – Example of backtrajectories performed on rainy days in Sarajevo showing the predominant patterns of winter and summer air mass trajectories (left) and the different and less frequent air mass trajectories mainly found in spring, autumn and summer (right).

5.2 Petrography

The polished sections of the studied stalagmites appear relatively compact and remarkable differences in calcite colour, textures and impurity content have been identified.

A detailed description of the observed textures follows.

5.2.1 Calcite textures in stalagmite G5

Stalagmite **G5** textures have only been observed on its polished surface since thin sections were not realised for this sample in order to preserve the stalagmite for further studies. The polished surface shows compact, greyish and translucent calcite made of columnar crystals elongated in the same direction as the stalagmite growth axis. The compactness and pale colour of the calcite suggest low content of impurities. Lamination is not or barely visible. Six surfaces interrupting the crystals continuity were identified on the polished section and are possibly related to growth interruptions. Two of them (86 and 272 mm from the top, surfaces 5 and 6 in Plate 1) present a sharp interruption of crystal growth associated with a diminished stalagmite diameter and followed by a widening above the surface. Conversely, the surfaces identified at 69, 55, 20 and 14 mm from the top are less obvious and could be linked to shorter growth interruptions (Plate 1).

5.2.2 Calcite textures in stalagmite BS8

The polished section of stalagmite **BS8** appears grey and translucent but less compact than G5. Relatively large pores are distributed along the whole length of the sample; however the texture in the lower half (from 51 mm from the top to the bottom) appears less compact than in the upper half. This stalagmite portion presents a lighter colour and frequent vertically orientated porosity (Plate 2). Faint lamination is visible in the more compact younger part. The more porous portion below 51 mm from the top presents a more evident but irregular lamination. On the stalagmite polished section, seven surfaces presenting sharp boundaries with the above calcite crystals were identified at 130, 123, 91, 51, 35, 21 and 9 mm from the top. Two of them (the ones at 51 and 21 mm from the top) display a detrital coating suggesting prolonged growth interruptions. A further surface at 7 mm from the top is instead marked by a sharp dark coating. All these sharp surfaces have also been identified under the petrographic microscope, where they correspond to crystal growth interruptions.

In thin sections, the calcite is made of composite crystals elongated according to the stalagmite growth axis with sharp boundaries and uniform extinction (Fig. 5.4). These crystals present the alternation of compact stacking of crystallites and a fabric characterised by linear and vertically orientated inter-crystalline porosity. These two textures can be referred to as **compact columnar**

and **open columnar calcite** (sensu Frisia et al., 2000; Couchoud, 2006; Frisia and Borsato 2010; Frisia, 2015). Their alternation is responsible for the faint lamination observed in the polished section of the stalagmite. The sharp boundaries between the composite crystals together with calcite compactness and colour suggest a negligible content in colloids. The presence of open columnar calcite is predominant from 51 mm from the top until the bottom of the stalagmite.

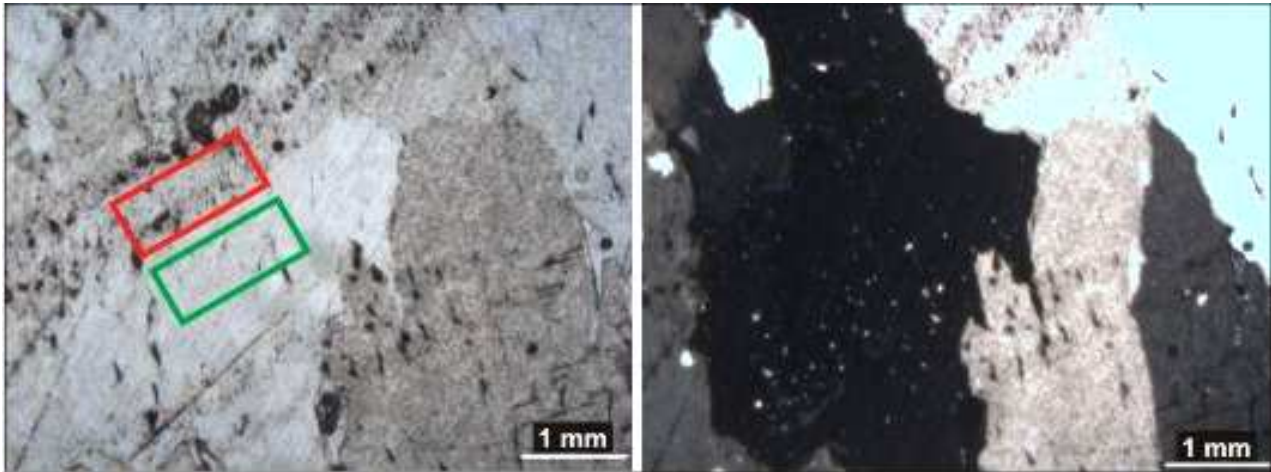


Fig. 5.4 – Image of stalagmite BS8 thin section under natural (right) and polarised light (left). Sharp boundaries between composite crystals are evident in the image on the right. The red and the green rectangles in the image on the left indicate, respectively, open and compact columnar portions.

5.2.3 Calcite textures in stalagmite BS9

Stalagmite **BS9** polished section have a different aspect from the previously described samples (Plate 3): its calcite alternates yellowish and compact portions with whitish and more porous intervals. The lower part of the stalagmite, from 93 mm from the top until the bottom, is milky and opaque. A dark interval appears between 16 and 13 mm from the top. Lamination is faint in the compact portions and wavy and irregular in the whitish and porous ones. Two relatively sharp surfaces are visible on the polished section. The first one, at 77 mm from the top, is associated with a shift of the stalagmite growth axis; the second one, identified at 62 mm from the top, is thick and sharp and is interrupting crystal growth. These two surfaces are also recognisable in thin sections (Plate 3). Another sharp surface has been identified in the dark interval cited above, similar to the one detected in stalagmite BS8.

Calcite texture in thin section appears less regular than in the previous sample. The milky portion of the stalagmite (from 93 mm from the top to the bottom) is characterised by branching crystals presenting $60^{\circ}/210^{\circ}$ orientation. This texture was identified as **dendritic calcite** (Fig. 5.5). The rest of the stalagmite presents composite crystals with uniform extinctions and highly irregular and interfingered parts. These types of crystal boundaries, together with the yellowish colour of the calcite, suggest the presence of colloids and impurities. Since the crystallite size is not visible under

the optic microscope, this structure can be referred to as **columnar microcrystalline calcite** (Frisia et al., 2000). The whitish portions identified between 90 and 81 mm, 54 and 40 mm, 32 and 30 mm from the top and from 23 mm up to the top of the stalagmite present a significant and irregular porosity. In this portion, subtle transitions from the columnar microcrystalline to the dendritic fabrics are visible, showing a continuum between these textures.

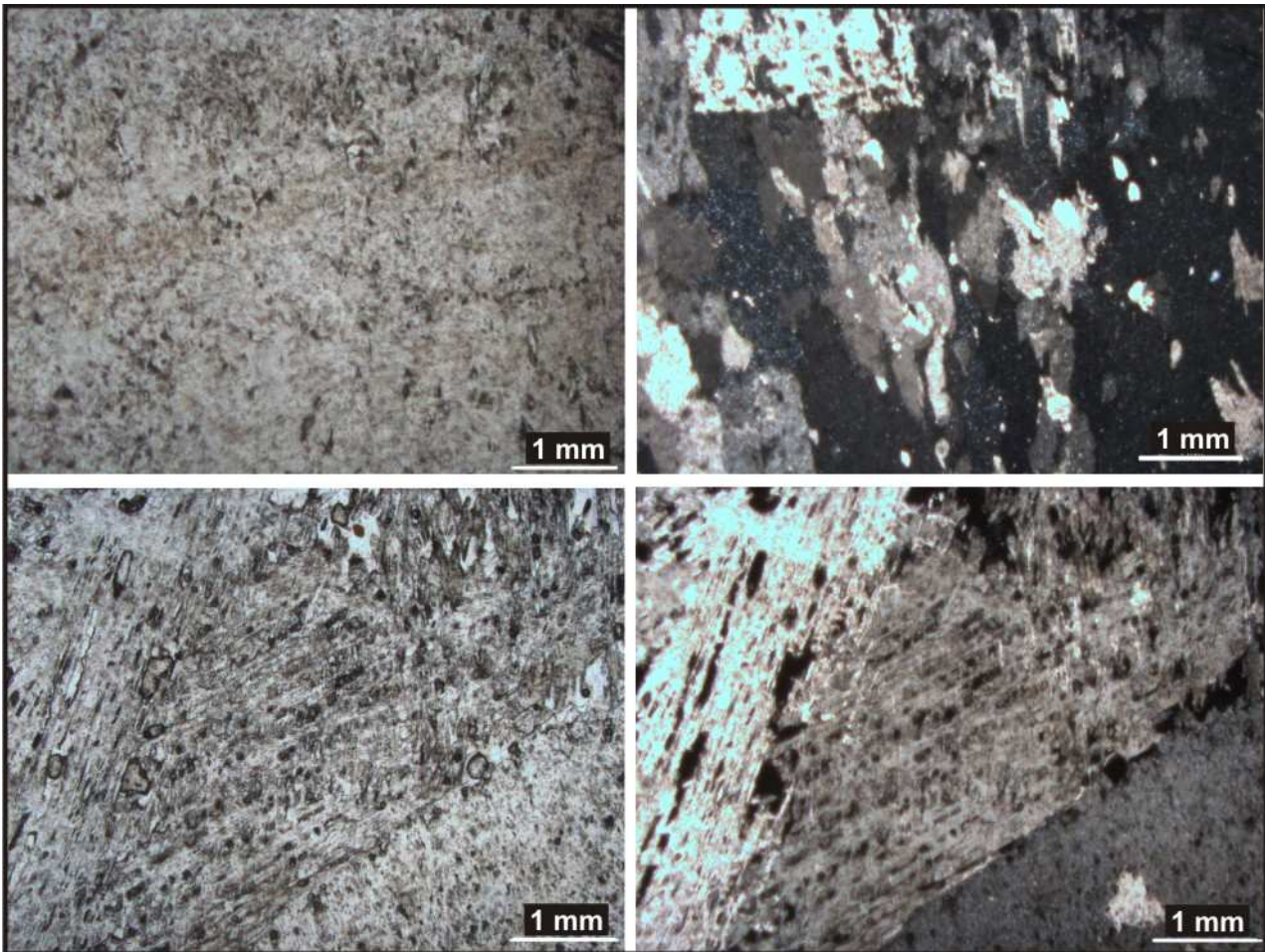


Fig. 5.5 – Image of stalagmite BS9 thin section under natural (left) and polarised light (right). The two upper images show the columnar microcrystalline calcite, while the lower two show dendritic calcite.

5.2.4 Classification of BS14 and BS15 textures for petrography micrologging

The polished sections of both **BS14** and **BS15** stalagmites show compact (especially in stalagmite BS15) and finely laminated calcite in the axial part and more porous and milky calcite on the flanks. On the polished sections the presence of composite columnar crystals (sensu Frisia et al., 2000; from 1 to 5 mm wide and from ~20 to 90 mm long) elongated along the growth direction can be distinguished (e.g. Fig. 5.6).

Two main “paleo” surfaces marking the temporary interruption of the stalagmite growth have been identified on the polished surface of stalagmite BS14 (at 15 and 25 mm from the top; 1 & 3 in Plate 4) and one in BS15 (at 18 mm from the top; surface 2 in Plate 4). These surfaces have been recognised also in thin section as sharp interruptions of crystal growth marked by visible crystal terminations associated with brown, dense surfaces coating crystal tips, especially in stalagmite BS14. Several other similar surfaces, presenting a sharp contact with the underlying laminae, are visible under the microscope only and possibly represent short-term hiatuses (e.g. a surface observed at 18 mm from the top in BS14 presents evidence of crystal-growth competition, demonstrating the presence of a growth interruption; surface 2 in Plate 4). In thin section, the textures observed on the polished stalagmite surfaces result mainly in large, columnar, microcrystalline, composite crystals, with the exception of dendritic calcite in a few areas. These composite crystals consist of aggregates stacked

with their *c*-axes oriented parallel to the vertical growth axis of the whole stalagmite, which may show mismatched stacking relative to the vertical growth direction in the upper portion of the stalagmite. The crystallites forming these composite crystals show optical continuity under polarised light. Relatively irregular vertical limits, which alternate with inter-fingered portions, characterise the composite crystals. This feature suggests subtle transitions to zones of higher proportion of impurities favouring the formation of crystal defects, resulting in high, intracrystalline microporosity (Frisia, 2015; Fig. 5.6). Brownish lamination related to periodic input of detrital/colloidal particulates is visible in both stalagmites (cf. Frisia et al., 2000).

The following detailed classification of fabrics from our samples is a subdivision of the columnar microcrystalline fabric, based on the observed porosity and composite crystal boundaries (Fig. 5.7):



Fig. 5.6 – Microphotographs of composite crystals identified in stalagmite BS15 thin section.

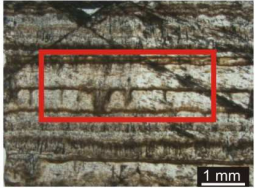
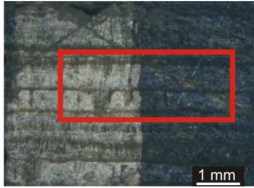
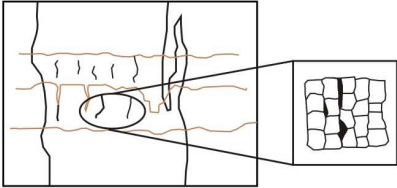
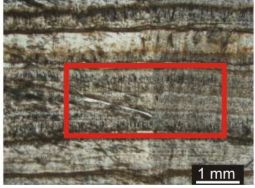
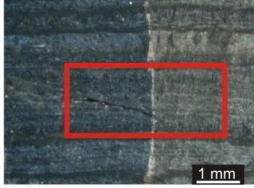
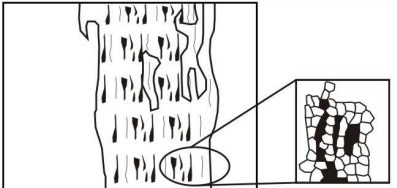
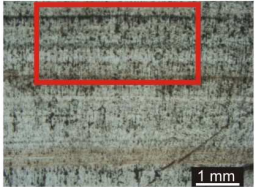
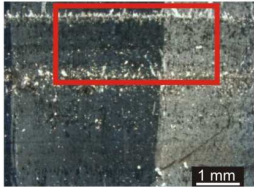
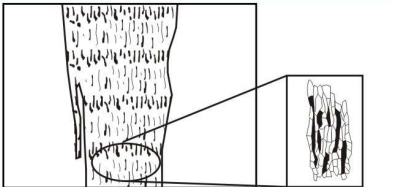
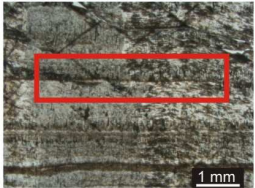
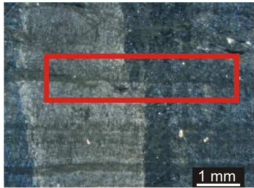
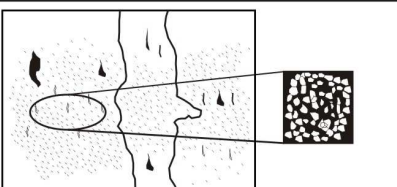
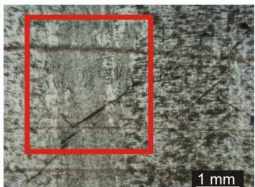

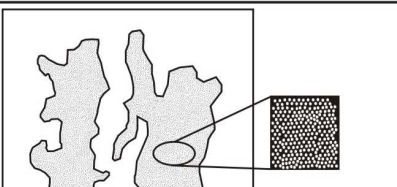
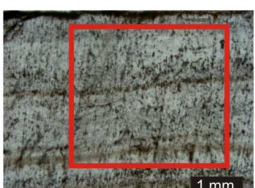

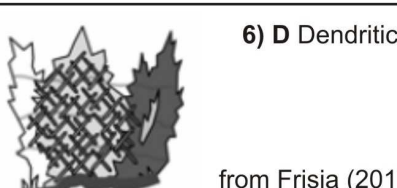
Thin section – Plane polarised light	Thin section – Cross Polarised light	Scheme of crystallites arrangements (left) Zoom-in inferred crystallite arrangements (right)	Sub-patterns of <i>columnar microcrystalline calcite (cm)</i>
a) 			1) Ccm “Compact”
b) 			2) Ocm “Open”
c) 			3) Ecm “Elongated”
d) 			4) Pcm “Porous”
e) 			5) SScm “Stricte sensu”
f) 			6) D Dendritic from Frisia (2015)

Fig. 5.7 – Fabric subdivision and classification (normal and polarised light) modified from Frisia (2015). The white bar on the picture corresponds to 1 mm. The red squares indicate the fabric classified in the columns on the right. The number in the second column corresponds to the value associated with each fabric in the micrologging curves.

1) Highly compact and translucent laminae consisting of welded crystallites, suggesting negligible presence of particulate and/or foreign ions that would create lattice deformation or occlude growth sites. This fabric subtype has here been classified as **compact columnar microcrystalline calcite (Ccm, Fig. 5.7a)**. Laminae formed by this fabric are bound by “wavy”

brownish surfaces, corresponding to flattened calcite crystal terminations and to cavities in the below compact carbonate lamina (Fig. 5.8).

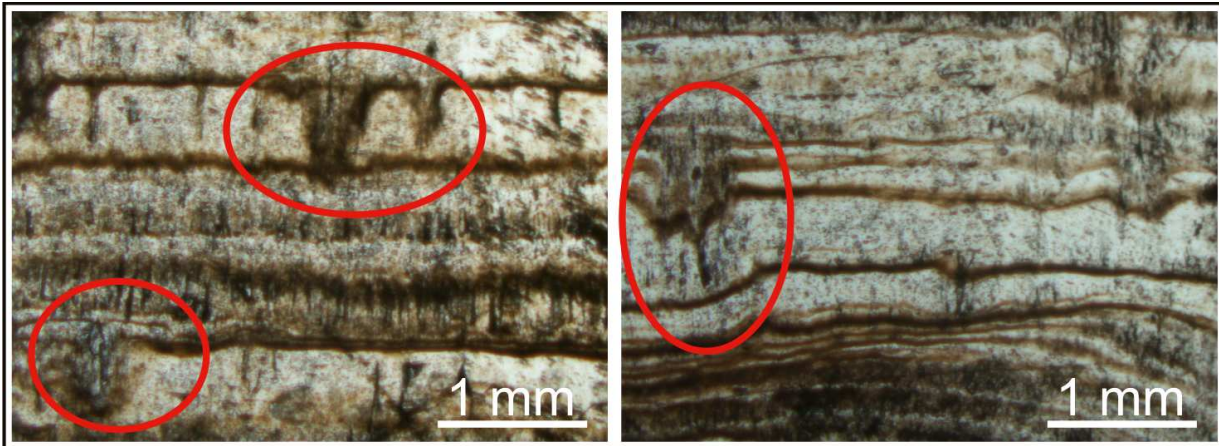


Fig. 5.8 - Thin section images of stalagmite BS15. Red circles indicate Ccm laminae presenting a brownish coating and evident signals of dissolution of the underlying calcite.

2) Some groups of laminae differentiate from the previous fabric (Ccm) by the occurrence of linear intercrystalline porosity. The boundaries between the composite crystals are irregular, suggesting that foreign ions or particulates occluded growth sites. Overall, the laminae appear milkier than in Ccm, and, under the optical microscope, show the presence of colloid-rich brown laminae with similar features as in Ccm. This fabric subtype has been classified as **open columnar microcrystalline calcite (Ocm, Fig. 5.7b)**.

3) Another fabric, observed only in the younger portion of stalagmite BS14, is characterised by elongated aggregates of crystallites (Fig. 5.7c). The composite crystal boundaries range from straight to inter-fingered. This is possibly related to a different content in particulate. This fabric is very similar to the elongated columnar calcite (sensu Frisia, 2015), which occurs under relatively high (> 0.3) Mg/Ca ratio of parent drip water associated with relatively fast dripping; when this fabric is associated with micrite and lateral overgrowth, diagenesis may have occurred (Frisia, 2015). However, the elongated appearance in this case is given by the succession of vertically oriented pores, which, in turn, are characterised by irregular boundaries preventing the identification of size and geometry of single crystallites. This suggests the presence of foreign particles favouring the formation of crystal defects, which are reflected in the observed irregular shapes (Frisia, 2015). Thus, this fabric has been referred to as **elongated microcrystalline calcite (Ecm; Fig. 5.7c)**.

4) Some sets of laminae consist of microcrystalline fabric, crossed by narrow, vertically oriented linear porosities and composite crystals with irregular boundaries similar to those illustrated by Frisia et al. (2000). Thus, the fabric has been classified as **porous microcrystalline**

calcite (Pcm; Fig. 5.7d). It differentiates from Ocm by the presence of a less regular intercrystalline linear porosity and a higher intracrystalline porosity inferred from the more irregular boundaries of the composite crystals. As for Ocm, some intervals attributed to the porous microcrystalline subtype contain brownish laminae, testifying the input of colloidal particulates, which, in this specific fabric, must have efficiently occluded growth sites.

5) The last columnar microcrystalline subtype identified in the Bosnian stalagmites is most common in the younger portion of BS15, and rare in BS14. The composite crystals show irregular boundaries more pronounced than in Pcm, but absent, or rare, elongated porosities. This fabric has thus been classified as *stricto sensu* **microcrystalline calcite (SScm; Fig. 5.7e).**

6) The only non-columnar fabric identified in the stalagmites is **dendritic (D)**, as described in Frisia et al. (2000), Couchoud (2006), Banks et al. (2010) and Frisia (2015). It can be observed on the flanks of both stalagmites and in the upper part of BS14 (Plate 4; Fig. 5.7f). The dendritic fabric is characterised by crystals that are not elongated along the growth axis of the stalagmites, and the composite crystals form branching assemblages, with a 60° angle.

The brownish lamination cited above, which is believed to be related to periodic input of colloidal/detrital particulate, has not been considered for this classification, but has been treated separately, assigning the value 0 to the pattern lacking the brownish lamination and the value 1 to the laminated one. This feature and the fabric subtypes are then represented as a function of distance from the stalagmite top, in profiles that can be compared with the geochemical data to discuss hydrological changes (Fig. 5.9). The realization of a petrography microlog has not been possible for stalagmites BS8 and BS9. The lack of a regular lamination and the stalagmite portion comprised in the thin sections (which did not contain the central growth axis), prevented an accurate and precise association between the stable isotope profiles and the petrographic changes.

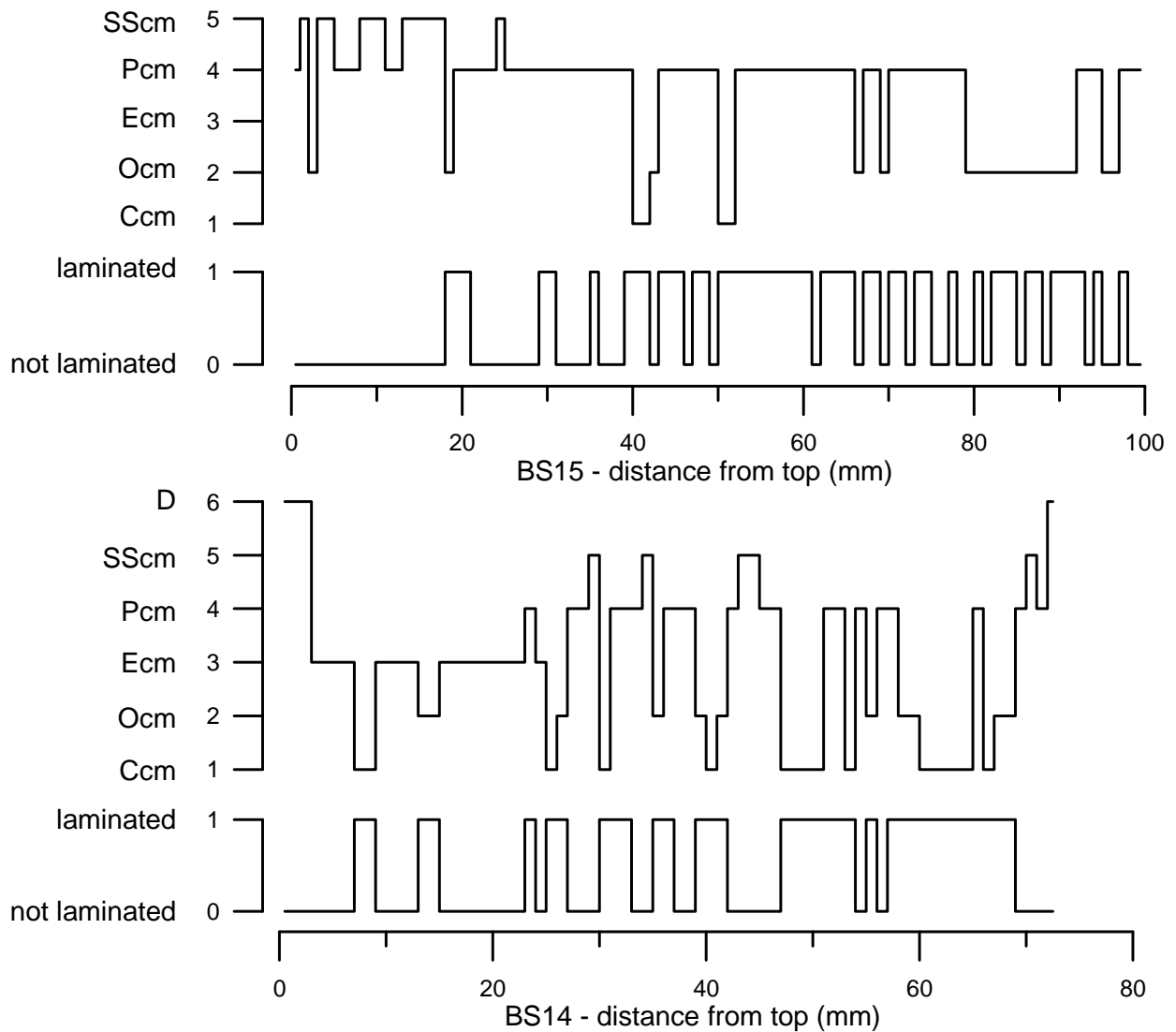


Fig. 5.9 – Petrography curve and lamination curve for stalagmites BS14 and BS15.

5.3 Ages of the bosnian stalagmites

According to the U-Th dating results, BS8, BS9, BS14 and BS15 stalagmites cover a period spanning from Early to Late Holocene (Tab. 5.3-5.4). All samples present low U content comprised between 53 and 2 ppb and generally low $^{230}\text{Th}/^{232}\text{Th}$ (between 0.4 and 1024.9) resulting in relatively large age errors. A detailed description of dating results for each stalagmite follows.

5.3.1 Stalagmite G5

Dating samples from stalagmites G5 present U concentrations between 2 and 28 ppb and $^{230}\text{Th}/^{232}\text{Th}$ ratios between 31.2 and 1024.9 in its Holocene portion. Raw ages were corrected using an initial $^{230}\text{Th}/^{232}\text{Th}$ of 1.50 ± 1.50 .

This sample started growing at about 73 ± 1.8 ka. A hiatus identified at 86 mm from the top was dated between about 12.5 ± 0.9 ka and 9.5 ± 0.3 ka. Thus, only the portion above the identified hiatus was considered for this study since it grew during the Holocene. In the studied portion of G5, at 14, 20, 55 and 69 mm from the top, four possible short growth interruptions were identified, which occurred, respectively, just after and before 7.0 ± 0.3 ka, before 8.6 ± 0.3 ka and before 9.1 ± 0.5 ka (Fig. 5.10).

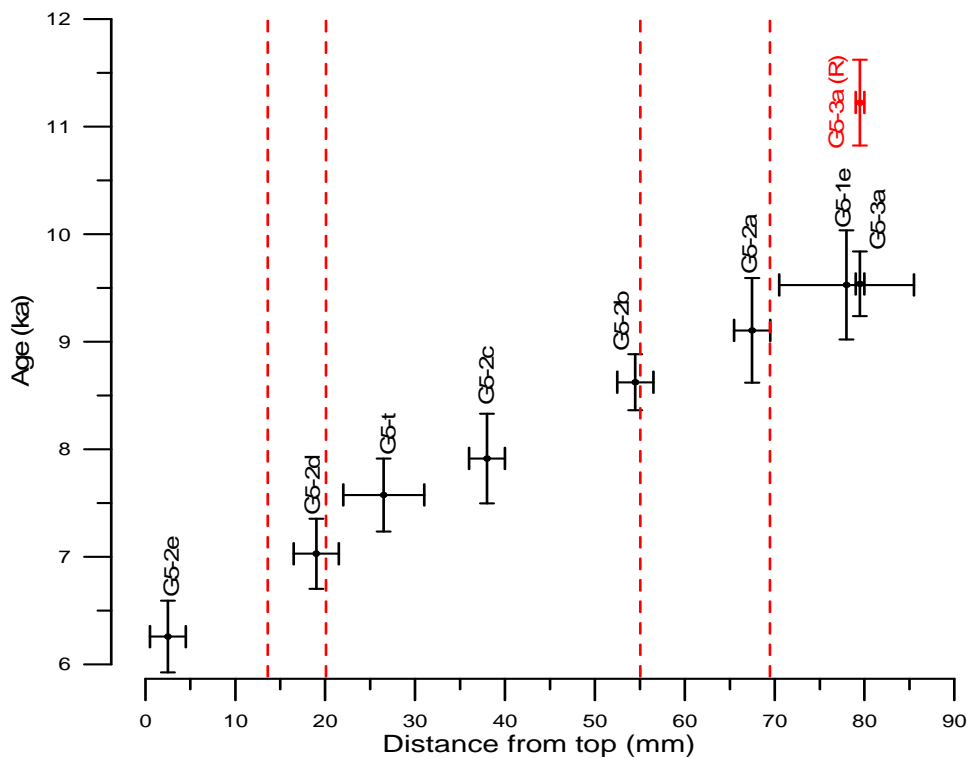


Fig. 5.10 – U-Th ages for stalagmite G5. Results are represented in relation to their distance from the stalagmite top. Black and red vertical lines represent age uncertainty; black and red horizontal lines indicate the width of the dated sample. One result which is not in stratigraphic order (i.e. younger above, older below) is indicated in red. Red dotted lines represent the identified growth interruption.

5.3.2 Stalagmite BS8

Dating samples from stalagmites BS8 present U concentrations between 3 and 44 ppb and $^{230}\text{Th}/^{232}\text{Th}$ ratios between 0.6 and 76.2. Raw ages were corrected using an initial $^{230}\text{Th}/^{232}\text{Th}$ of 0.30 ± 0.25 (tab. 5.3).

BS8 started growing at $\sim 12.1 \pm 0.4$ ka and stopped definitively at $\sim 0.7 \pm 0.2$ ka. Two major hiatuses were identified at 50.5 and 91 mm from the top and occurred between $\sim 5.3 \pm 0.3$ and 7.5 ± 0.4 ka and between $\sim 8.0 \pm 0.3$ and 8.9 ± 0.4 ka. Minor hiatuses were identified at 9, 21, 35, 123 and 129 mm from the top which occurred, respectively, after $\sim 1.8 \pm 0.2$ ka, 3.9 ± 0.2 ka, 5.1 ± 0.3 ka and

between $\sim 9.9 \pm 0.4$ and 10.3 ± 0.4 ka (Fig. 5.11). According to dating results, the black layer found at 7 mm from the top was deposited between $\sim 1.3 \pm 0.2$ and 1.8 ± 0.2 ka.

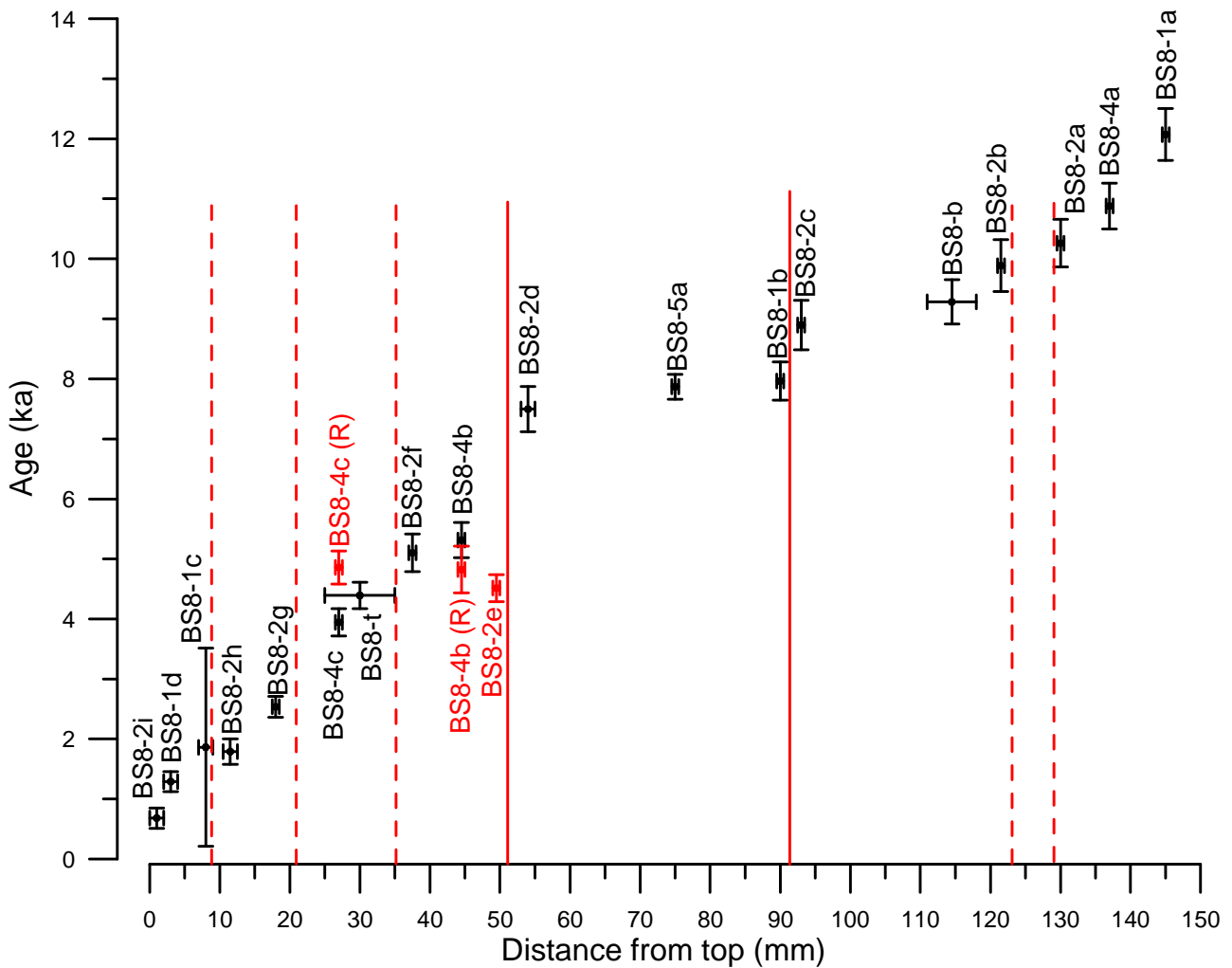


Fig. 5.11 – U-Th ages for stalagmite BS8. Results are represented in relation to their distance from the stalagmite top. Black and red vertical lines represent age uncertainty; black and red horizontal lines indicate the width of the dated sample. Results which are not in stratigraphic order (i.e. younger above, older below) are indicated in red. Red vertical lines represent the two major hiatuses; red dotted vertical lines represent the minor growth interruptions.

5.3.3 Stalagmite BS9

Dating samples from stalagmites BS9 present U concentrations between 22 and 42 ppb and $^{230}\text{Th}/^{232}\text{Th}$ ratios between 0.7 and 9.2. Raw ages have been corrected using an initial $^{230}\text{Th}/^{232}\text{Th}$ of 0.45 ± 0.30 (tab. 5.4).

Only the portion above the dendritic calcite identified in stalagmites BS9 was studied. This portion started growing at about 5.1 ± 0.4 ka, followed by a hiatus at 77 mm from the top, whose duration was not identified. Unfortunately, U-Th ages close to the hiatus identified at 62 mm from the top were affected by large age errors due to the high detrital Th content, preventing its identification.

However, it can be stated that the stalagmite stopped growing after about 4.5 ± 0.3 ka and started again at $\sim 2.3 \pm 0.2$ ka until $\sim 1.1 \pm 0.3$ ka (Fig. 5.12). According to dating results, the dark interval identified between 16 and 13 mm from the top was deposited at $\sim 1.0 \pm 0.3$ ka.

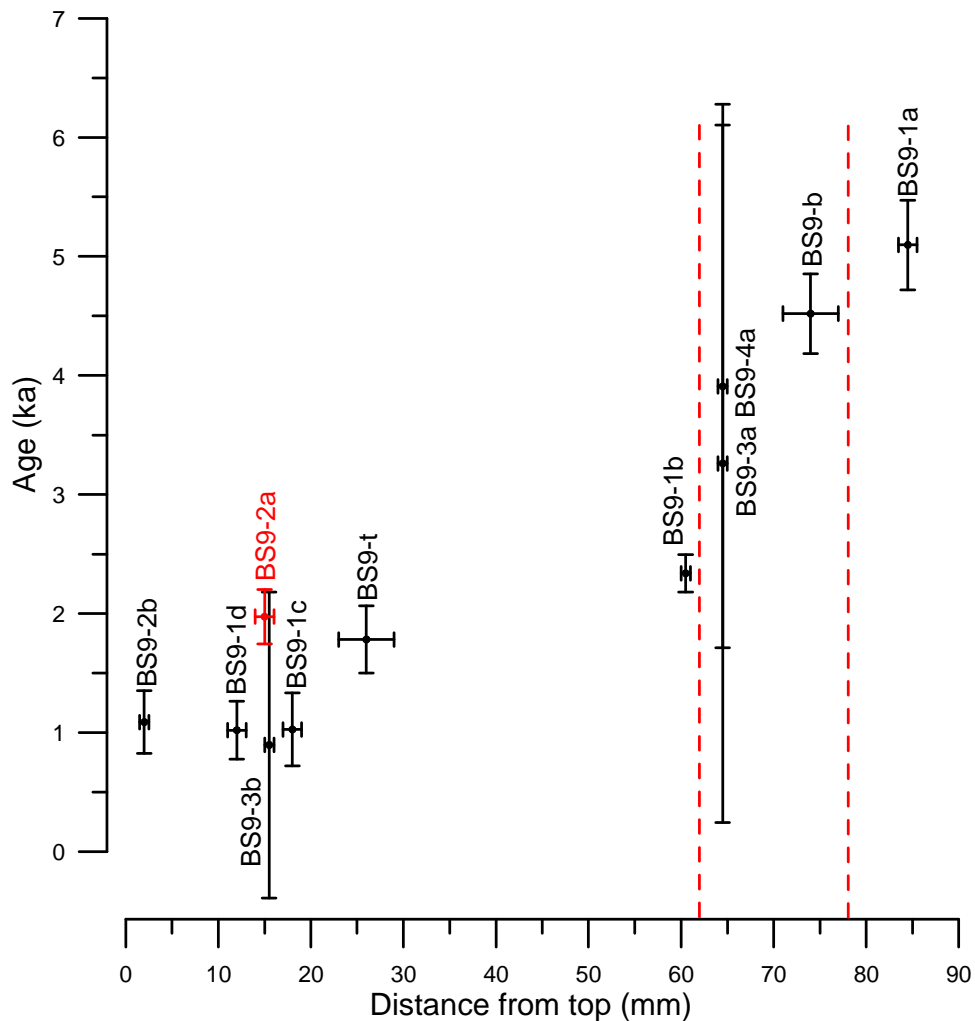


Fig. 5.12 – U-Th ages for stalagmite BS9. Results are represented in relation to their distance from the stalagmite top. Black and red vertical lines represent age uncertainty; black and red horizontal lines indicate the width of the dated sample. Results which are not in stratigraphic order (i.e. younger above, older below) are indicated in red. Red dotted vertical line represents the identified growth interruption.

5.3.4 Stalagmite BS14

Dating samples from stalagmites BS14 present U concentrations between 21 and 52 ppb and $^{230}\text{Th}/^{232}\text{Th}$ ratios between 0.4 and 128.8. Raw ages were corrected using an initial $^{230}\text{Th}/^{232}\text{Th}$ of 0.30 ± 0.20 (tab. 5.5).

This stalagmite started growing at $\sim 6.1 \pm 0.6$ ka (Fig. 5.13). Its top age is not precisely known due to the unreliability of the dating results in this portion (cf. Chapter 6.2).

The two most evident growth interruptions identified in thin sections at 15 and 25 mm from the top occurred, approximately, between $\sim 2.8 \pm 0.2$ and 2.3 ± 0.3 ka and between $\sim 4.4 \pm 0.4$ and 4.0 ± 0.4 ka (Fig. 5.13).

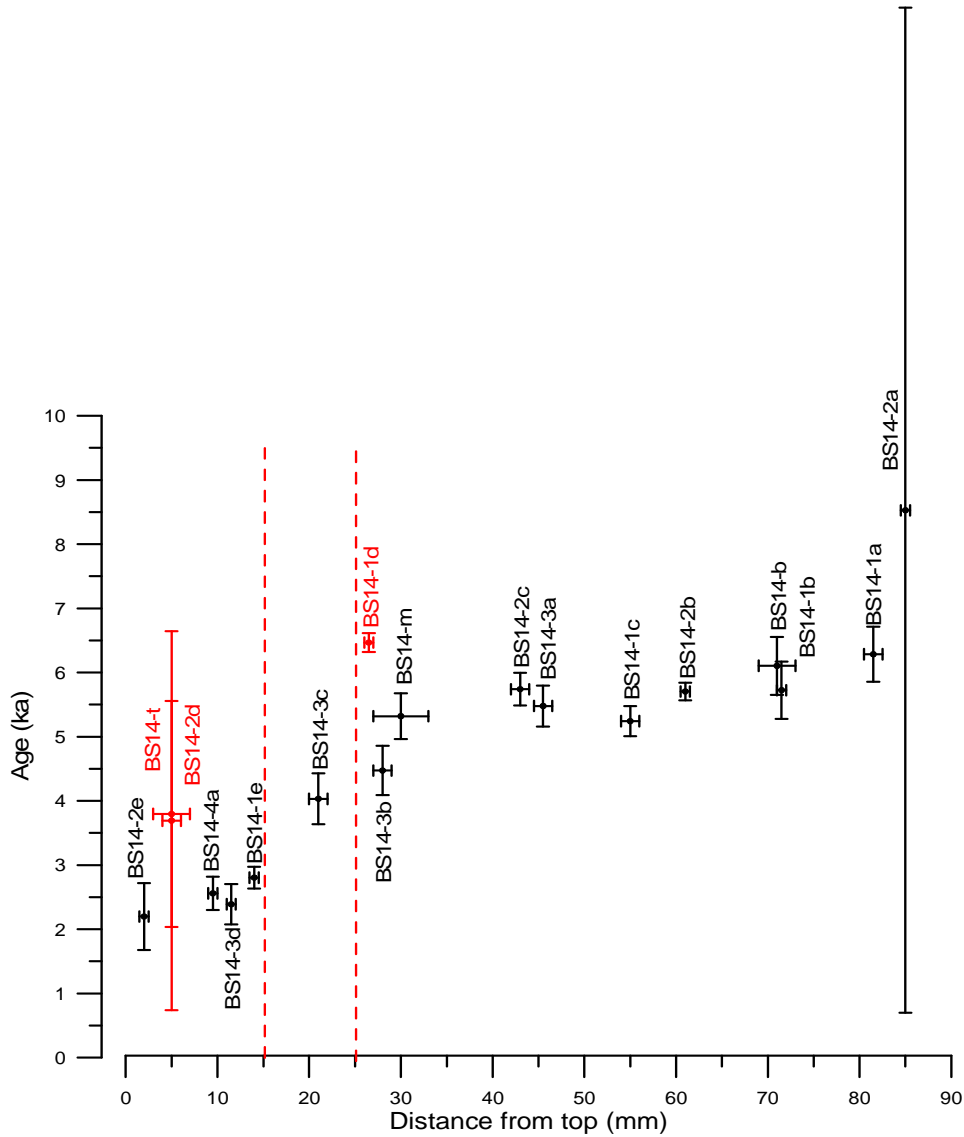


Fig. 5.13 – U-Th ages for stalagmite BS14. Results are represented in relation to their distance from the stalagmite top. Black and red vertical lines represent age uncertainty; black and red horizontal lines indicate the width of the dated sample. Results which are not in stratigraphic order (i.e. younger above, older below) are indicated in red. Red dotted vertical lines represent the identified growth interruptions.

5.3.5 Stalagmite BS15

Dating samples from stalagmite BS15 present U concentrations between 27 and 42 ppb and $^{230}\text{Th}/^{232}\text{Th}$ ratios between 41.3 and 1.0. Raw ages have been corrected using an initial $^{230}\text{Th}/^{232}\text{Th}$ of 0.65 ± 0.19 (tab. 5.5).

This stalagmite started growing at $\sim 4.3 \pm 0.4$ ka and stopped after 0.9 ± 0.1 ka (Fig. 5.14). A possible growth interruption is found at 18 mm from the top and occurred between about 1.9 ± 0.1 and 1.5 ± 0.2 ka.

The dark layer similar to the one found close to the top of the other stalagmites samples in Mračna Pečina Cave, which was found at 10 mm from the top, was deposited at $\sim 1.1 \pm 0.3$ ka.

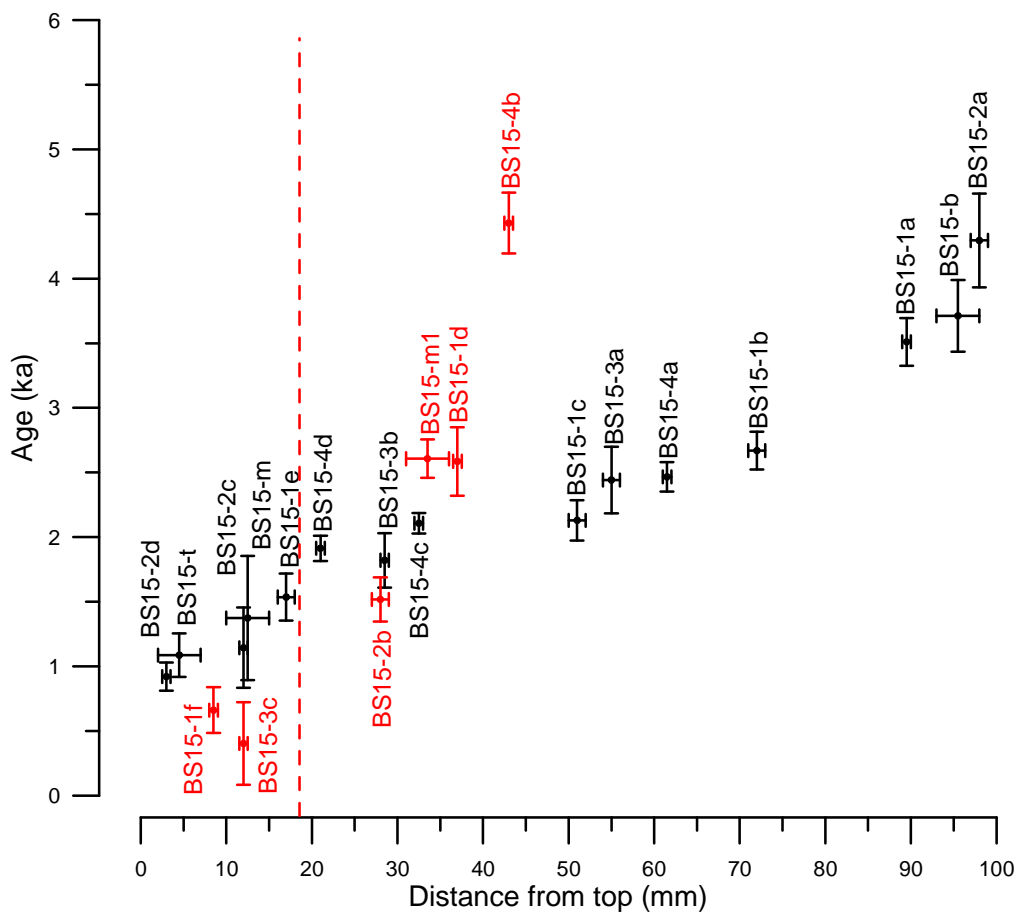


Fig. 5.14 – U-Th ages for stalagmite BS15. Results are represented in relation to their distance from the stalagmite top. Black and red vertical lines represent age uncertainty; black and red horizontal lines indicate the width of the dated sample. Results which are not in stratigraphic order (i.e. younger above, older below) are indicated in red. The red dotted vertical line represents the identified growth interruption.

Sample ID	Mass (g)	²³⁸ U (ng/g)	2σ	Depth (mm from top)	(²³⁰ Th/ ²³⁸ U) _A	2σ	(²³⁴ U/ ²³⁸ U) _A	2σ	Uncorrected Age (ka)	2σ	(²³² Th/ ²³⁸ U) _A	2σ	(²³⁰ Th/ ²³² Th) _i	(²³⁰ Th/ ²³² Th) _A	Corrected age (ka)	2σ
BS8-2i	0.0374	32.55	2.44	1 ± 1	0.0137	0.0008	1.7151	0.0118	0.874	0.051	0.010114	0.000067	0.30 ± 0.25	1.35	0.681	0.169
BS8-1d	0.1319	35.33	2.65	3 ± 1	0.0208	0.0026	1.7293	0.0065	1.318	0.166	0.001614	0.000044	0.30 ± 0.25	12.89	1.289	0.167
BS8-1c	0.0416	18.98	1.43	8 ± 1	0.0590	0.0059	1.7320	0.0063	3.772	0.383	0.100471	0.000230	0.30 ± 0.25	0.59	1.862	1.649
BS8-2h	0.0380	39.34	2.98	11.5 ± 1	0.0296	0.0033	1.7698	0.0228	1.837	0.208	0.002654	0.000049	0.30 ± 0.25	11.14	1.788	0.211
BS8-2g	0.0431	39.34	2.98	18 ± 0.5	0.0407	0.0026	1.7271	0.0166	2.597	0.169	0.003226	0.000063	0.30 ± 0.25	12.62	2.535	0.177
BS8-4c	0.0222	3.70	0.28	27 ± 0.5	0.0626	0.0035	1.7451	0.0101	3.973	0.227	0.001639	0.000036	0.30 ± 0.25	38.21	3.944	0.228
BS8-4c (R)	0.0191	3.39	0.26	27 ± 0.5	0.0766	0.0042	1.7392	0.0098	4.897	0.275	0.002174	0.000053	0.30 ± 0.25	35.25	4.857	0.277
BS8-t	0.0305	37.53	2.82	30 ± 5	0.0696	0.0033	1.7403	0.0083	4.439	0.214	0.002557	0.000065	0.30 ± 0.25	27.23	4.391	0.220
BS8-2f	0.0347	35.46	2.70	37.5 ± 0.5	0.0804	0.0046	1.7308	0.0250	5.171	0.310	0.003760	0.000072	0.30 ± 0.25	21.38	5.101	0.316
BS8-4b	0.0264	2.63	0.20	44.5 ± 0.5	0.0836	0.0043	1.7292	0.0171	5.385	0.287	0.003906	0.000064	0.30 ± 0.25	21.41	5.314	0.292
BS8-4b (R)	0.0202	2.81	0.21	44.5 ± 0.5	0.0766	0.0059	1.7464	0.0125	4.877	0.383	0.002947	0.000089	0.30 ± 0.25	25.99	4.822	0.288
BS8-2e	0.0344	43.73	3.33	49.5 ± 0.5	0.0725	0.0030	1.7441	0.0270	4.395	0.270	0.005647	0.000088	0.30 ± 0.25	12.84	4.512	0.224
BS8-2d	0.0395	24.44	1.85	54 ± 1	0.1186	0.0055	1.7643	0.0213	7.551	0.372	0.003189	0.000076	0.30 ± 0.25	37.20	7.496	0.377
BS8-5a	0.0485	31.87	2.39	75 ± 0.5	0.1266	0.0031	1.7997	0.0085	7.913	0.205	0.002465	0.000019	0.30 ± 0.25	51.34	7.870	0.206
BS8-1b	0.0399	32.67	2.45	90 ± 0.5	0.1288	0.0047	1.7963	0.0091	8.072	0.307	0.006030	0.000067	0.30 ± 0.25	21.37	7.963	0.320
BS8-2c	0.0416	28.18	2.13	93 ± 0.5	0.1434	0.0060	1.8136	0.0271	8.930	0.411	0.001882	0.000062	0.30 ± 0.25	76.19	8.897	0.412
BS8-b	0.0327	29.85	2.25	114.5 ± 3.5	0.1500	0.0054	1.8049	0.0096	9.402	0.354	0.006837	0.000156	0.30 ± 0.25	21.94	9.282	0.369
BS8-2b	0.0400	34.23	2.60	121.5 ± 0.5	0.1594	0.0064	1.8164	0.0183	9.950	0.427	0.003571	0.000087	0.30 ± 0.25	44.63	9.887	0.432
BS8-2a	0.0397	27.10	2.04	130 ± 0.5	0.1615	0.0057	1.7749	0.0158	10.335	0.392	0.003992	0.000067	0.30 ± 0.25	40.47	10.260	0.398
BS8-4a	0.0262	2.99	0.23	137 ± 0.5	0.1725	0.0075	1.7845	0.0085	11.008	0.503	0.008382	0.000156	0.30 ± 0.25	20.58	10.881	0.383
BS8-1a	0.0423	25.62	1.92	145 ± 0.5	0.1904	0.0055	1.7693	0.0096	12.318	0.381	0.013430	0.000068	0.30 ± 0.25	14.18	12.073	0.432

Tab. 5.3 – U-Th results for stalagmite BS8. The ages that are not in stratigraphic order and that were not used in age models are indicated in red.

Sample ID	Mass (g)	²³⁸ U (ng/g)	2σ	Depth (mm from top)	(²³⁰ Th/ ²³⁸ U) _A	2σ	(²³⁴ U/ ²³⁸ U) _A	2σ	Uncorrected age	2σ	(²³² Th/ ²³⁸ U) _A	2σ	(²³⁰ Th/ ²³² Th) _i	(²³⁰ Th/ ²³² Th) _A	Corrected age	2σ
BS9-2b	0.0511	26.48	1.99	2 ± 0.5	0.0187	0.0021	1.4640	0.0067	1.401	0.160	0.009348	0.000209	0.45 ± 0.30	2.00	1.088	0.264
BS9-1d	0.0349	27.51	2.07	12 ± 1	0.0168	0.0022	1.4369	0.0071	1.281	0.169	0.007672	0.000046	0.45 ± 0.30	2.19	1.020	0.244
BS9-2a	0.0438	34.45	2.59	15 ± 1	0.0292	0.0021	1.4503	0.0064	2.216	0.161	0.007155	0.000093	0.45 ± 0.30	4.09	1.974	0.229
BS9-3b	0.0433	31.70	2.39	15.5 ± 0.5	0.0360	0.0030	1.4331	0.0127	2.771	0.235	0.054309	0.000604	0.45 ± 0.30	0.66	0.896	1.285
BS9-1c	0.0412	30.81	2.35	18 ± 1	0.0172	0.0032	1.4490	0.0155	1.301	0.244	0.008166	0.000046	0.45 ± 0.30	2.10	1.026	0.307
BS9-t	0.0350	41.53	3.12	26 ± 3	0.0277	0.0017	1.4132	0.0066	2.157	0.134	0.010790	0.000170	0.45 ± 0.30	2.56	1.782	0.283
BS9-1b	0.0644	27.80	2.09	60.5 ± 0.5	0.0308	0.0015	1.3644	0.0085	2.488	0.124	0.004173	0.000029	0.45 ± 0.30	7.37	2.338	0.158
BS9-4a	0.0428	21.69	1.63	64.5 ± 0.5	0.0927	0.0047	1.3611	0.0044	7.669	0.402	0.120132	0.000552	0.45 ± 0.30	0.77	3.261	3.018
BS9-3a	0.0428	25.94	1.97	64.5 ± 0.5	0.0838	0.0029	1.3231	0.0168	7.117	0.272	0.085548	0.001314	0.45 ± 0.30	0.98	3.908	2.195
BS9-b	0.0404	35.48	2.66	74 ± 3	0.0611	0.0019	1.3715	0.0064	4.959	0.159	0.012339	0.000175	0.45 ± 0.30	4.95	4.519	0.334
BS9-1a	0.0348	30.45	2.29	84.5 ± 1	0.0643	0.0039	1.3400	0.0070	5.352	0.334	0.006957	0.000041	0.45 ± 0.30	9.25	5.097	0.376
G5-2e	0.0510	17.98	1.36	2.5 +/- 2	0.1059	0.0047	1.8523	0.0226	6.395	0.302	0.001551	0.000065	1.50 ± 1.50	68.26	6.257	0.333
G5-2d	0.0542	26.32	2.00	19 ± 2.5	0.1165	0.0048	1.8453	0.0291	7.077	0.322	0.000578	0.000045	1.50 ± 1.50	201.77	7.028	0.326
G5-t	0.0452	27.94	2.10	26.5 ± 4.5	0.1288	0.0053	1.8881	0.0069	7.645	0.317	0.001075	0.000025	1.50 ± 1.50	119.83	7.574	0.340
G5-2c	0.0513	28.25	2.13	38 ± 2	0.1337	0.0066	1.8956	0.0196	7.933	0.410	0.000221	0.000034	1.50 ± 1.50	604.93	7.913	0.416
G5-2b	0.0482	23.19	1.76	54.5 ± 2	0.1514	0.0039	1.9746	0.0266	8.646	0.259	0.000285	0.000059	1.50 ± 1.50	531.60	8.622	0.261
G5-2a	0.0543	23.15	1.77	67.5 ± 2	0.1597	0.0079	1.9788	0.0286	9.117	0.488	0.000156	0.000053	1.50 ± 1.50	1024.94	9.104	0.487
G5-1e	0.1297	25.95	1.95	78 ± 7.5	0.1750	0.0037	1.9896	0.0059	9.940	0.215	0.005603	0.000070	1.50 ± 1.50	31.23	9.527	0.507
G5-3a	0.03599	1.72	0.13	79.5 ± 0.5	0.1691	0.0046	1.9825	0.0104	9.654	0.277	0.001454	0.000066	1.50 ± 1.50	116.28	9.537	0.301
G5-3a (R)	0.02806	1.62	0.12	79.5 ± 0.5	0.1987	0.0064	2.0030	0.0149	11.298	0.390	0.000938	0.000049	1.50 ± 1.50	211.89	11.223	0.398

Tab. 5.4 - U-Th results for stalagmites BS9 and G5. The ages that are not in stratigraphic order and that were not used in age models are indicated in red.

Sample ID	Mass (g)	²³⁸ U (ng/g)	2σ	Depth (mm from top)	(²³⁰ Th/ ²³⁸ U) _A	2σ	(²³⁴ U/ ²³⁸ U) _A	2σ	Uncorrected age	2σ	(²³² Th/ ²³⁸ U) _A	2σ	(²³⁰ Th/ ²³² Th) _i	(²³⁰ Th/ ²³² Th) _A	Corrected age	2σ
BS14-2e	0.0438	21.36	1.60	2 ± 0.5	0.0395	0.00356	1.4754	0.0058	2.956	0.274	0.04263	0.00126	0.30 ± 0.20	0.93	2.011	0.690
BS14-t	0.0395	32.99	2.40	5 ± 2	0.0854	0.00287	1.4275	0.0066	6.708	0.237	0.15734	0.00422	0.30 ± 0.20	0.54	3.039	2.478
BS14-2d	0.0445	27.49	2.06	5 ± 1	0.1090	0.00452	1.4349	0.0048	8.582	0.368	0.26325	0.00553	0.30 ± 0.20	0.41	2.401	4.251
BS14-4a	0.0526	29.71	2.23	9.5 ± 0.5	0.0375	0.00109	1.3913	0.0067	2.976	0.089	0.02214	0.00008	0.30 ± 0.20	1.69	2.454	0.363
BS14-3d	0.0404	29.84	2.26	11.5 ± 0.5	0.0333	0.00343	1.3838	0.0139	2.653	0.276	0.01386	0.00023	0.30 ± 0.20	2.40	2.327	0.349
BS14-1e	0.0430	35.86	2.69	14 ± 0.5	0.0369	0.00198	1.3999	0.0072	2.909	0.160	0.00564	0.00004	0.30 ± 0.20	6.55	2.779	0.184
BS14-3c	0.0401	27.84	2.11	21 ± 1	0.0534	0.00483	1.4141	0.0170	4.191	0.387	0.00856	0.00013	0.30 ± 0.20	6.23	3.995	0.413
BS14-1d	0.0470	37.29	2.80	26.5 ± 0.5	0.0822	0.00166	1.4110	0.0061	6.528	0.142	0.00329	0.00002	0.30 ± 0.20	24.98	6.451	0.153
BS14-3b	0.0405	29.32	2.22	28 ± 1	0.0575	0.00439	1.3738	0.0188	4.653	0.367	0.00947	0.00023	0.30 ± 0.20	6.07	4.432	0.398
BS14-m	0.0309	34.01	2.55	30 ± 2	0.0682	0.00426	1.3996	0.0049	5.436	0.353	0.00622	0.00015	0.30 ± 0.20	10.96	5.292	0.363
BS14-2c	0.0427	38.54	2.89	43 ± 1	0.0723	0.00303	1.3832	0.0052	5.841	0.250	0.00534	0.00012	0.30 ± 0.20	13.52	5.717	0.265
BS14-3a	0.0406	38.66	2.94	45.5 ± 1	0.0681	0.00372	1.3737	0.0189	5.534	0.318	0.00289	0.00005	0.30 ± 0.20	23.60	5.462	0.322
BS14-1c	0.0483	34.59	2.60	55 ± 1	0.0649	0.00282	1.3724	0.0076	5.271	0.234	0.00151	0.00002	0.30 ± 0.20	42.99	5.235	0.235
BS14-2b	0.0473	41.47	3.11	62 ± 0.5	0.0698	0.00163	1.3641	0.0054	5.715	0.136	0.00054	0.00002	0.30 ± 0.20	128.76	5.703	0.137
BS14-b	0.0389	45.32	3.40	71 ± 2	0.0823	0.00271	1.3635	0.0053	6.771	0.229	0.03469	0.00060	0.30 ± 0.20	2.37	5.943	0.609
BS14-1b	0.0417	40.60	3.05	71.5 ± 0.5	0.0779	0.00242	1.3644	0.0057	6.396	0.205	0.03499	0.00015	0.30 ± 0.20	2.23	5.556	0.596
BS14-1a	0.0418	34.47	2.59	80.5 ± 1	0.0814	0.00222	1.3174	0.0064	6.939	0.196	0.03285	0.00019	0.30 ± 0.20	2.48	6.121	0.578
BS14-2a	0.0473	51.82	3.89	85 ± 0.5	0.2228	0.00518	1.2564	0.0046	21.145	0.548	0.57385	0.00193	0.30 ± 0.20	0.39	5.105	11.607

Tab. 5.5 - U-Th results for stalagmites BS14. The ages that are not in stratigraphic order and that were not used in age models are indicated in red.

Sample ID	Mass (g)	²³⁸ U (ng/g)	2σ	Depth (mm from top)	(²³⁰ Th/ ²³⁸ U) _A	2σ	(²³⁴ U/ ²³⁸ U) _A	2σ	Uncorrected age (ka)	2σ	(²³² Th/ ²³⁸ U) _A	2σ	(²³⁰ Th/ ²³² Th) _i	(²³⁰ Th/ ²³² Th) _A	Corrected age (ka)	2σ
BS15-2d	0.0486	29.67	2.23	3 ± 0.5	0.0143	0.00136	1.5043	0.0064	1.041	0.103	0.00257	0.00007	0.65 ± 0.19	5.58	0.920	0.109
BS15-t	0.0341	32.06	2.41	4.5 ± 2	0.0173	0.00221	1.5130	0.0074	1.254	0.161	0.00355	0.00009	0.65 ± 0.19	4.86	1.087	0.168
BS15-1f	0.0460	29.84	2.24	8.5 ± 0.5	0.0123	0.00221	1.4902	0.0074	0.904	0.163	0.00509	0.00002	0.65 ± 0.19	2.42	0.661	0.177
BS15-3c	0.0354	26.75	2.03	12 ± 0.5	0.0169	0.00285	1.5087	0.0215	1.235	0.205	0.01768	0.00025	0.65 ± 0.19	0.96	0.403	0.320
BS15-2c	0.0452	34.16	2.56	12.0 ± 0.5	0.0277	0.00179	1.4600	0.0056	2.087	0.137	0.01937	0.00041	0.65 ± 0.19	1.43	1.144	0.311
BS15-m	0.0339	35.21	2.65	12.5 ± 2	0.0380	0.00246	1.4648	0.0087	2.862	0.191	0.03060	0.00083	0.65 ± 0.19	1.24	1.374	0.481
BS15-1e	0.0315	31.81	2.39	17 ± 1	0.0243	0.00213	1.4608	0.0063	1.828	0.159	0.00601	0.00009	0.65 ± 0.19	4.03	1.536	0.181
BS15-4d	0.0491	28.11	2.11	21 ± 0.5	0.0272	0.00112	1.4391	0.0037	2.079	0.085	0.00338	0.00002	0.65 ± 0.19	8.06	1.913	0.097
BS15-1d	0.0443	34.27	2.58	28 ± 1	0.0233	0.00185	1.4168	0.0080	1.806	0.149	0.00579	0.00005	0.65 ± 0.19	4.03	1.517	0.171
BS15-3b	0.0410	32.83	2.51	28.5 ± 0.5	0.0271	0.00240	1.4083	0.0216	2.118	0.192	0.00591	0.00011	0.65 ± 0.19	4.58	1.821	0.210
BS15-4c	0.0517	29.86	2.24	32.5 ± 0.5	0.0281	0.00100	1.4308	0.0056	2.161	0.078	0.00109	0.00001	0.65 ± 0.19	25.74	2.107	0.080
BS15-m1	0.0394	33.93	2.55	33.5 ± 2	0.0369	0.00174	1.4369	0.0070	2.834	0.133	0.00461	0.00011	0.65 ± 0.19	8.02	2.606	0.148
BS15-2b	0.0429	31.23	2.34	37 ± 0.5	0.0347	0.00329	1.4070	0.0069	2.719	0.262	0.00267	0.00005	0.65 ± 0.19	12.99	2.586	0.264
BS15-4b	0.0526	26.64	2.00	43 ± 0.5	0.0599	0.00251	1.3834	0.0043	4.825	0.206	0.00774	0.00002	0.65 ± 0.19	7.76	4.429	0.235
BS15-1c	0.0423	38.03	2.86	51 ± 1	0.0276	0.00186	1.3770	0.0057	2.206	0.154	0.00149	0.00002	0.65 ± 0.19	18.43	2.130	0.156
BS15-3a	0.0396	34.91	2.66	55 ± 1	0.0310	0.00306	1.3623	0.0231	2.508	0.257	0.00126	0.00006	0.65 ± 0.19	24.57	2.442	0.258
BS15-4a	0.0603	28.35	2.13	61.5 ± 0.5	0.0347	0.00091	1.3872	0.0056	2.759	0.073	0.00575	0.00003	0.65 ± 0.19	6.04	2.466	0.113
BS15-1b	0.0388	34.55	2.60	72 ± 1	0.0363	0.00173	1.4024	0.0060	2.856	0.136	0.00371	0.00002	0.65 ± 0.19	9.77	2.669	0.147
BS15-1a	0.0494	32.97	2.48	89.5 ± 0.5	0.0488	0.00186	1.4016	0.0060	3.859	0.154	0.00689	0.00004	0.65 ± 0.19	7.07	3.511	0.185
BS15-b	0.0315	41.67	3.13	95.5 ± 2	0.0486	0.00347	1.4280	0.0055	3.769	0.275	0.00118	0.00003	0.65 ± 0.19	41.31	3.712	0.277
BS15-2a	0.0392	26.87	2.02	98 ± 1	0.0576	0.00454	1.4226	0.0054	4.498	0.357	0.00409	0.00011	0.65 ± 0.19	14.10	4.295	0.362

Tab. 5.6 - U-Th results for stalagmites BS15. The ages that are not in stratigraphic order and that were not used in age models are indicated in red.

5.4 Stable oxygen and carbon isotope composition

5.4.1 $\delta^{13}\text{C}$ and $\delta^{18}\text{O}$ variability along the growth axis of the studied stalagmites

BS8, BS9, BS14 and BS15 stalagmites present $\delta^{18}\text{O}$ ratios dispersed in the same range of values (BS8 $\delta^{18}\text{O}$ mean value: -8.5 ± 0.3 ‰; BS9 $\delta^{18}\text{O}$ mean value: -8.86 ± 0.87 ‰; BS14 $\delta^{18}\text{O}$ mean value: -7.98 ± 0.37 ‰; BS15 $\delta^{18}\text{O}$ mean value: -8.12 ± 0.28 ‰; Fig. 5.15); stalagmite G5 displays slightly lighter $\delta^{18}\text{O}$ ratios (-8.84 ± 0.3 ‰; Fig. 5.15).

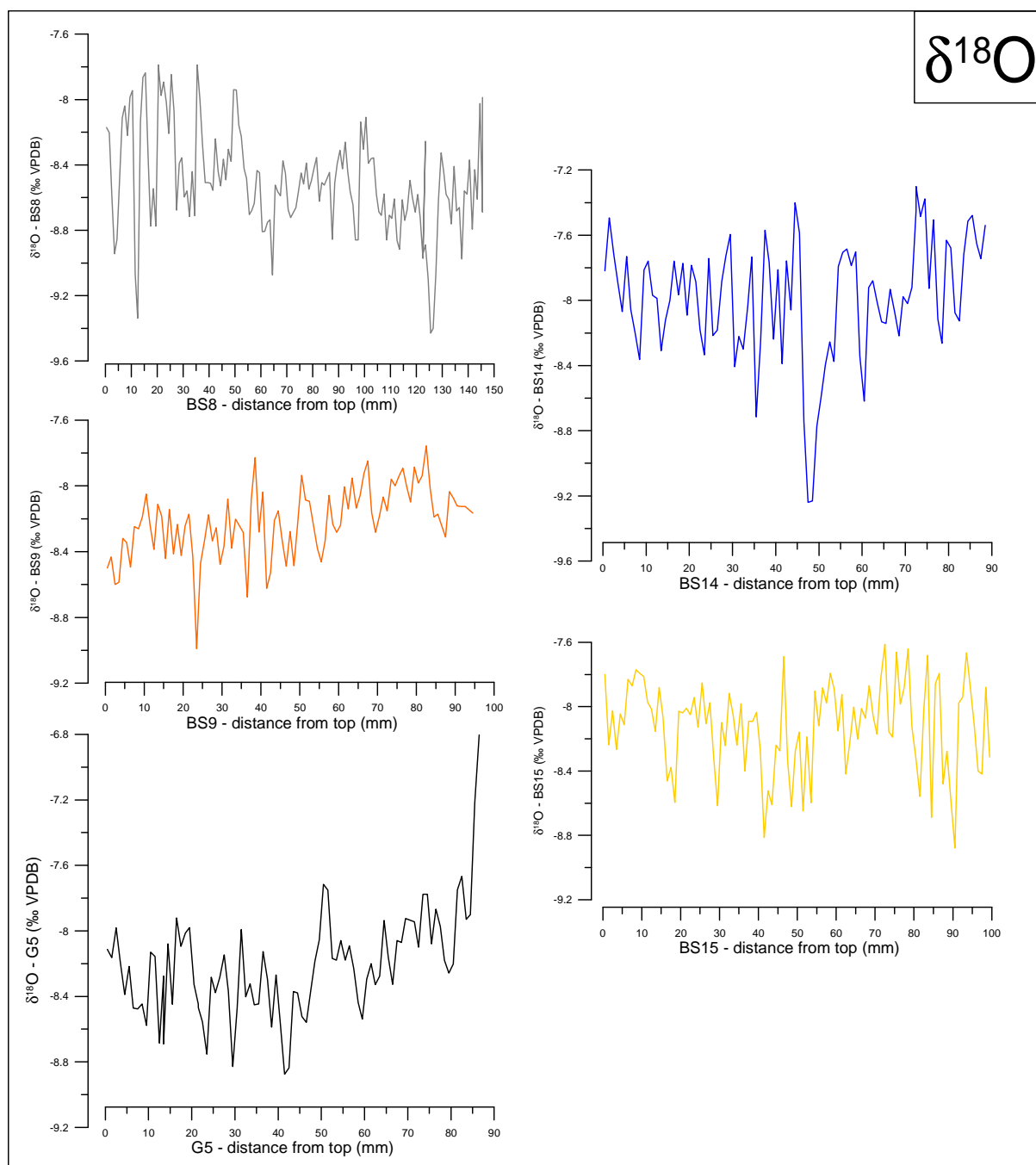


Fig. 5.15 – Oxygen stable isotope ratio along the growth axis of stalagmites BS8, BS9, BS14, BS15 and G5.

$\delta^{13}\text{C}$ values present bigger differences among the analysed samples. In particular, on the basis of $\delta^{13}\text{C}$ results, stalagmite BS8 can be divided into two portions: one from the bottom up to 51 mm from the top, presenting an average $\delta^{13}\text{C}$ ratio of $-5.06 \pm 0.25 \text{ ‰}$, the second from 51 mm depth until the top, presenting a lower average $\delta^{13}\text{C}$ ratio ($-8.96 \pm 0.48 \text{ ‰}$). Stalagmite BS9 presents higher values in the bottom portion ($-7.18 \pm 1.27 \text{ ‰}$ below 80 mm from the top) and then stabilises around $-9.14 \pm 0.30 \text{ ‰}$ with weak trend towards higher values at the stalagmite top (Fig. 5.16). The BS14 record does not present any trend, but is characterised by large fluctuation of $\delta^{13}\text{C}$ ratios ($\delta^{13}\text{C}$ mean value: $-8.42 \pm 1.01 \text{ ‰}$). BS15 $\delta^{13}\text{C}$ ratios have smaller fluctuations than BS14 ones ($-9.42 \pm 0.39 \text{ ‰}$). These values present a long-term trend towards ^{13}C enriched values which steepen from 40 mm depth to the top (Fig. 5.16). Stalagmite G5 $\delta^{13}\text{C}$ values are dispersed around $-8.21 \pm 0.32 \text{ ‰}$.

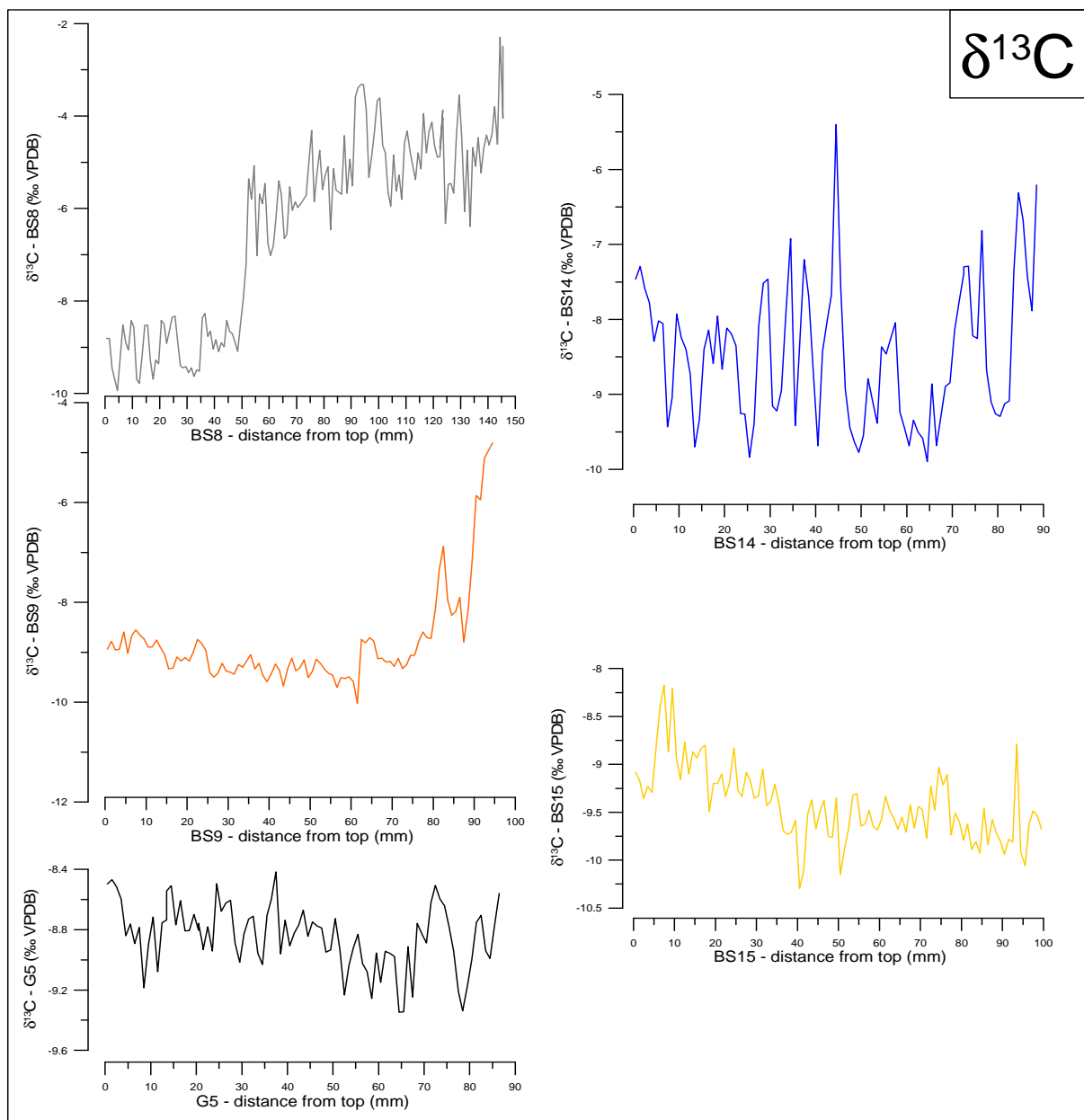


Fig. 5.16 – Stable carbon isotope variation along the growth axis of stalagmites BS8, BS9, BS14, BS15 and G5.

5.4.2 Tests for fractionation conditions during calcite precipitation

Stable oxygen and carbon isotope fluctuations show a relatively good correlation in stalagmite BS14 ($R^2 = 0.44$) and in the upper portion (above the hiatus at 51 mm from the top) of stalagmite BS8 ($R^2 = 0.67$), suggesting that calcite precipitation likely occurred under disequilibrium conditions (cf. Hendy, 1971; Fig. 5.17). In stalagmites BS9, BS15 and G5, and in the lower portion of stalagmite BS8 stable oxygen and carbon isotope values show no correlation (R^2 respectively 0.19, 0.10, 0.14 and 0.1), suggesting that precipitation possibly occurred closer to isotopic equilibrium (although equilibrium conditions are unlikely in most cave environments; e.g. Mickler et al., 2006 and references therein).

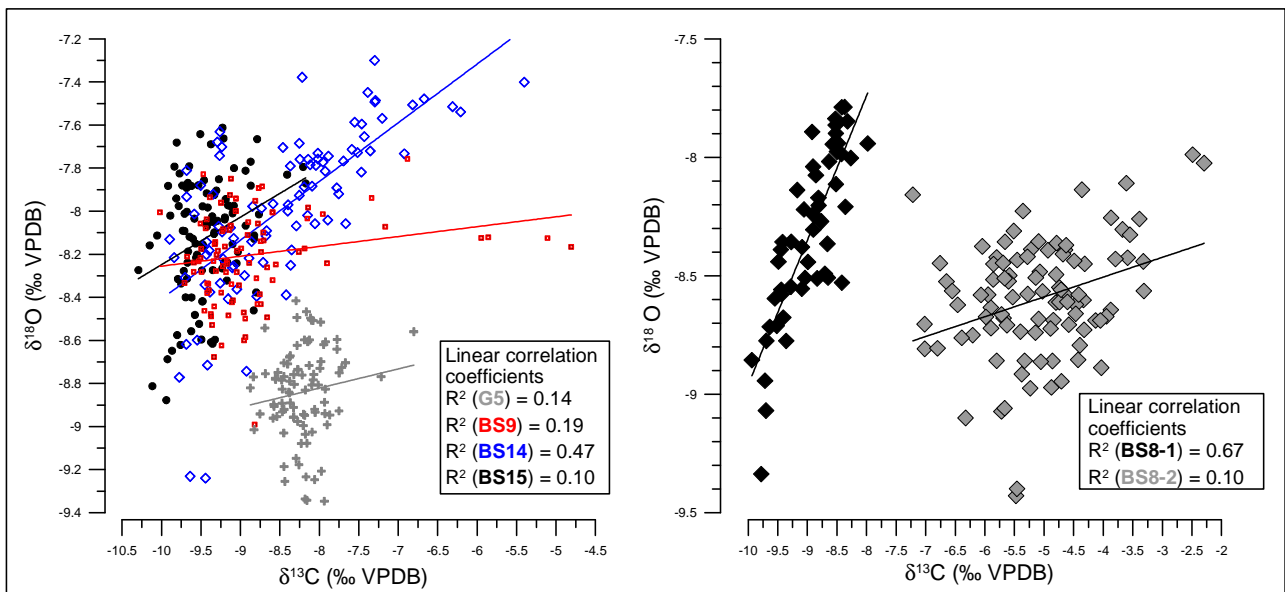


Fig. 5.17 – $\delta^{13}\text{C}$ - $\delta^{18}\text{O}$ diagrams. Left: stalagmites G5, BS9, BS14 and BS15. Right: data restricted to the part above above 51 mm from the top (black rhombohedra; BS8 - 1) and below 51 mm from the top (grey rhombohedra; BS8-2) in stalagmite BS8.

To support this first inference, the Hendy test (1971) was performed on a few laminae:

- **BS14** stalagmite:

The samples along the lamina at 59 mm from the top (H3 in Fig. 5.18) show a lateral enrichment of 0.86‰ for $\delta^{13}\text{C}$ and of 0.51‰ for $\delta^{18}\text{O}$, suggesting significant disequilibrium fractionation. The two laminae sampled at 31.5 and 16.5 mm from the top (H2 and H1 in Fig. 5.18) show a smaller lateral variation in stable isotope values (respectively 0.32‰ and 0.13‰ for $\delta^{13}\text{C}$ and 0.17‰ and 0.26‰ for $\delta^{18}\text{O}$) pointing to a lower degree of disequilibrium fractionation in this portion.

- **BS15** stalagmite:

Variations along the laminae at 79 mm and 32.5 mm from the top are comparable (respectively 0.20‰ and 0.16‰ for $\delta^{13}\text{C}$ and 0.17‰ and 0.26‰ for $\delta^{18}\text{O}$; H3 and H2 in Fig. 5.18). Samples from

the lamina at 8 mm from the top show stronger fluctuations for $\delta^{13}\text{C}$ values (range of 0.62‰; H1 in Fig. 5.18) while $\delta^{18}\text{O}$ values are more stable (range of 0.18‰), suggesting the possible occurrence of prolonged CO_2 exchange with the cave air related to long residence time of a thin film of fluid at the growing stalagmite surface in this portion of the stalagmite (Dreybrodt & Scholz, 2011; Hansen et al., 2013).

- **BS8** stalagmite:

Laminae sampled at 56.5 and 99 mm from the top of stalagmite BS8 present a strong variation in $\delta^{13}\text{C}$ values (H2 and H3, respectively 1.15 and 1.92‰) but $\delta^{18}\text{O}$ does not vary much (0.18 and 0.38‰). It suggests its growth under a thin film of fluid of water and prolonged CO_2 exchange with the cave air. Samples from lamina at 26.5 mm from the top show lower variations in $\delta^{13}\text{C}$ ($\delta^{13}\text{C}$ amplitude: 0.2‰; $\delta^{18}\text{O}$ amplitude: 0.32 ‰).

sample	Depth from top	$\delta^{13}\text{C}$ (‰)	$\delta^{18}\text{O}$ (‰)	Sample	Depth from top	$\delta^{13}\text{C}$ (‰)	$\delta^{18}\text{O}$ (‰)	sample	Depth from top	$\delta^{13}\text{C}$ (‰)	$\delta^{18}\text{O}$ (‰)
BS15-h1a1	8 mm	-7.49	-7.51	BS14-H1a1	16.5 mm	-7.86	-7.96	BS8-H1a	26.5 mm	-8.60	-7.89
BS15h1b		-7.91	-7.60	BS14- H1a		-7.83	-7.92	BS8-H1b		-8.80	-8.04
BS15-h1c		-7.99	-7.62	BS14- H1b		-7.79	-7.77	BS8-H1-c		-8.80	-8.06
BS15-h1d		-8.05	-7.67	BS14- H1c		-7.74	-7.83	BS8-H1d		-8.70	-8.03
BS15-h1e		-8.11	-7.69	BS14- H1d		-7.83	-7.86	BS8-H1e		-8.79	-8.21
BS15-h1f		-8.03	-7.67	BS14- H1e		-7.83	-7.70				
BS15-H2a1	32.5 mm	-9.15	-7.49	BS14-H2a1	31.5 mm	-9.07	-8.41	BS8-H2a	56.5 mm	-5.83	-9.15
BS15-H2a		-9.23	-7.58	BS14-H2a		-9.12	-8.34	BS8-H2b		-4.71	-8.97
BS15-H2b		-9.25	-7.56	BS14-H2b		-8.92	-8.30	BS8-H2c		-5.36	-8.97
BS15-H2c2		-9.31	-7.63	BS14-H2c		-8.88	-8.47	BS8-H2d		-4.68	-8.99
BS15-H2d		-9.30	-7.75	BS14-H2d1		-8.82	-8.43				
BS15-H2e		-9.31	-7.68	BS14- H2e		-8.80	-8.34				
BS15-H3a1	79 mm	-9.30	-7.67	BS14-H3a	59 mm	-8.57	-7.16	BS8-H3a	99 mm	-4.38	-8.68
BS15- H3a		-9.31	-7.51	BS14-H3b		-9.10	-7.40	BS8-H3b		-3.76	-8.61
BS15- H3b		-9.41	-7.51	BS14-H3c		-9.17	-7.62	BS8-H3b1		-3.68	-8.66
BS15- H3c		-9.36	-7.52	BS14-H3d		-9.32	-7.59	BS8-H3c1		-2.46	-8.30
BS15- H3d		-9.42	-7.68	BS14-H3e		-9.25	-7.42	BS8-H3d		-3.92	-8.36
BS15- H3e		-9.22	-7.54	BS14-H3f		-8.46	-7.11	BS8-H3e		-3.98	-8.54
BS15- H3f	-9.32	-7.59									

Tab. 5.7 – Oxygen and carbon stable isotope variation along single laminae of BS8, BS14 and BS15 stalagmites.

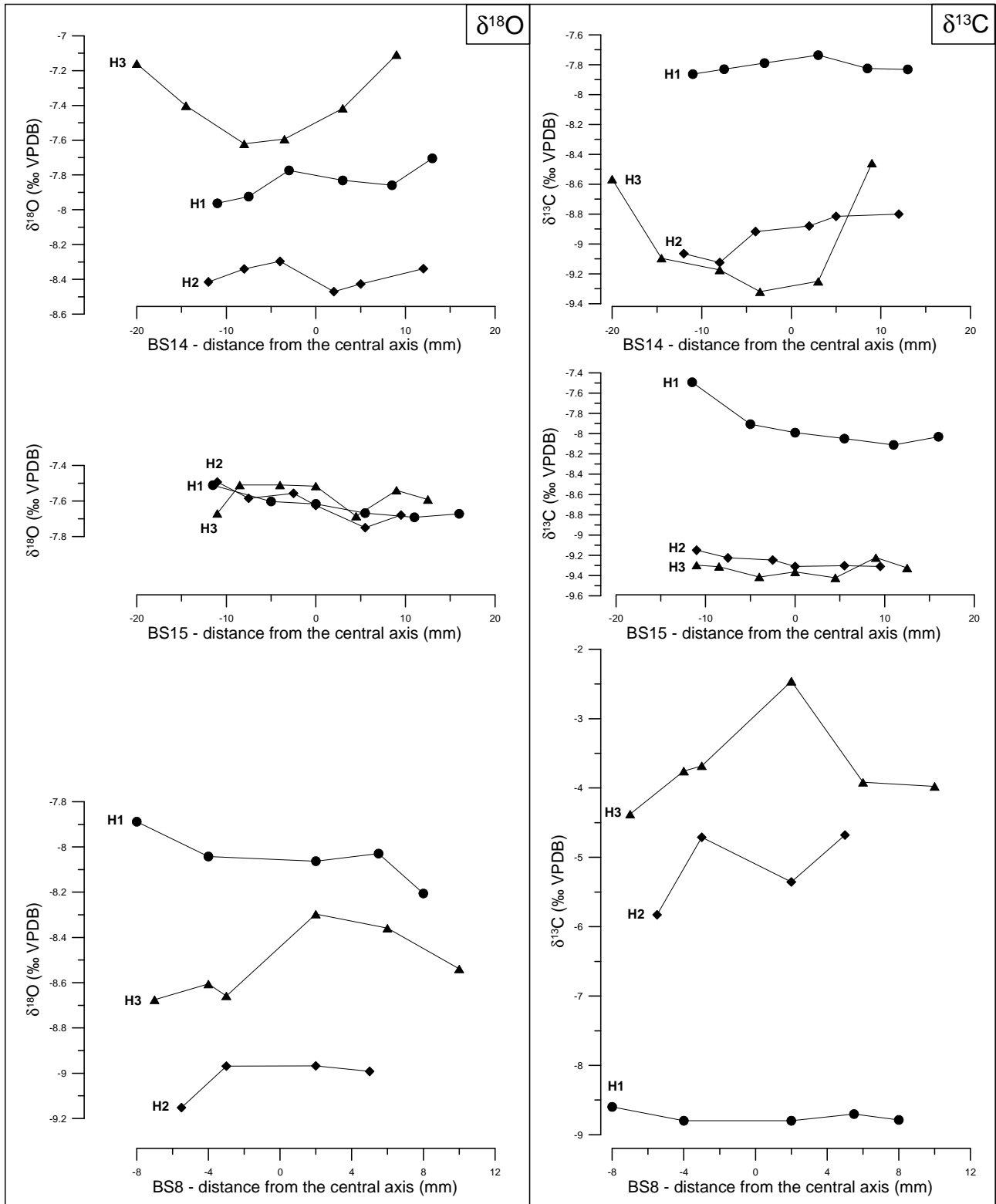


Fig. 5.18 – Hendy test results for stalagmites BS8, BS14 and BS15. H1, H2 and H3 were sampled, respectively, at 26.5, 56.5 and 99 mm from the top in BS8, 16.5, 31.5 and 59.0 mm from the top in BS14 and 8.0, 32.5 and 79.0 mm from the top in BS15. Values are reported in Tab. 5.7.

5.5 Trace element concentration in stalagmite BS15

Trace elements were analysed by laser ablation only in stalagmite BS15. The results show a relatively weak variability along the stalagmite profile.

In order to highlight the main trends, moving average filters have been applied. Progressively wider windows (5, 11, 21 and 31 points) were used to test the reliability of the method in keeping the general trends; results obtained after smoothing the values on the base of 31 points were chosen for data representation. In order to uniform the observation scale of the analysed proxy (i.e. stable isotopes and petrography) an average value for each millimetre corresponding to the stable isotope profiles was calculated (Fig. 5.19); the so obtained trace element profiles were considered for further considerations.

Correlation coefficients were calculated between each analysed element in order to support graphic observations (Tab. 5.8). Among divalent cations (Sr, Ba, and Mg), the results show a strong covariation between Sr and Ba, and an antiphase trend between Mg and both Sr and Ba. The trivalent cation Y, the metals Cu and Zn, and the electronegative element P are linked by positive correlations, resulting in common trends. These elements are characterised by strong adsorption behaviour in soils, compared to the solution preference of the divalent cations like Sr and Mg (Borsato et al., 2007 and reference therein). No correlation is found between Mg and P. However, from the observation of their profiles, it is possible to distinguish a trend towards higher values from about 40 mm from the top (Fig. 5.19). The Mn signal shows little variability and has a long-term trend towards slightly higher values until 28 mm from the top, when it starts decreasing again. Considering Th, even if its concentration is just above the instrument detection limit, it shows a higher frequency of spikes in the upper part of the stalagmite starting ca. 48 mm from its top (Fig. 5.19).

Trace elements	Mg	P	Mn	Cu	Zn	Sr	Y	Ba	Th
LOD	0.021	1.2	0.16	0.014	0.025	0.0021	-	0.00067	
CORRELATION COEFFICIENT									
Mg p value		0.06 0.54	0.29 4E-3	-0.01 0.89	0.02 0.81	-0.62 1.2E-11	-0.25 0.01	-0.48 5.17E-7	0.13 0.22
P p value	0.06 0.54		-0.46 1.3E-6	0.41 2.1E-5	0.74 1.5E-18	-0.58 3.9 E-10	0.85 3.3E-28	-0.29 3.5E-3	-0.11 0.22
Mn p value	0.29 4E-3	0.46 1.3E-6		-0.62 0.55	-0.36 2.9E-4	0.20 4.9E-2	-0.57 7.5E-10	0.28 4.6E-3	0.28 4.8E-3
Cu p value	-0.01 0.89	0.41 2.1E-5	-0.62 0.55		0.61 2.6E-11	-0.11 0.28	0.46 2.2E-6	0.02 0.87	0.15 0.14
Zn p value	0.02 0.81	0.74 1.5E-18	-0.36 2.9E-4	0.61 2.6E-11		-0.33 7.8E-4	0.77 6E-21	-0.13 0.21	-0.02 0.88
Sr p value	-0.62 1.2E-11	-0.58 3.9 E-10	0.20 4.9E-2	0.11 0.28	-0.33 7.8E-4		-0.29 3E-3	0.82 5.9E-25	-0.04 0.72
Y p value	-0.25 0.01	0.85 3.3E-28	-0.57 7.5E-10	0.46 2.2E-6	0.77 6E-21	-0.29 3E-3		-0.06 0.57	-0.09 0.37
Ba p value	-0.48 5.17E-7	-0.29 3.5E-3	0.28 4.6E-3	0.02 0.87	-0.13 0.21	0.82 5.9E-25	-0.06 0.57		-0.01 0.95
δ¹³C p value	0.72 9.8E-17	0.14 0.16	0.31 2E-3	-0.08 0.44	-0.08 0.41	-0.55 3.3E-9	-0.20 0.03	-0.44 4.5E-6	0.02 0.86

Tab. 5.8 - Trace elements analysed in stalagmite BS15 by laser ablation. LOD = instrument detection limit (ppm). Correlation coefficients (r) have been calculated among the data series obtained calculating the average trace element content every millimetre corresponding to the stable isotope profile. Statistically significant correlations are indicated in bold.

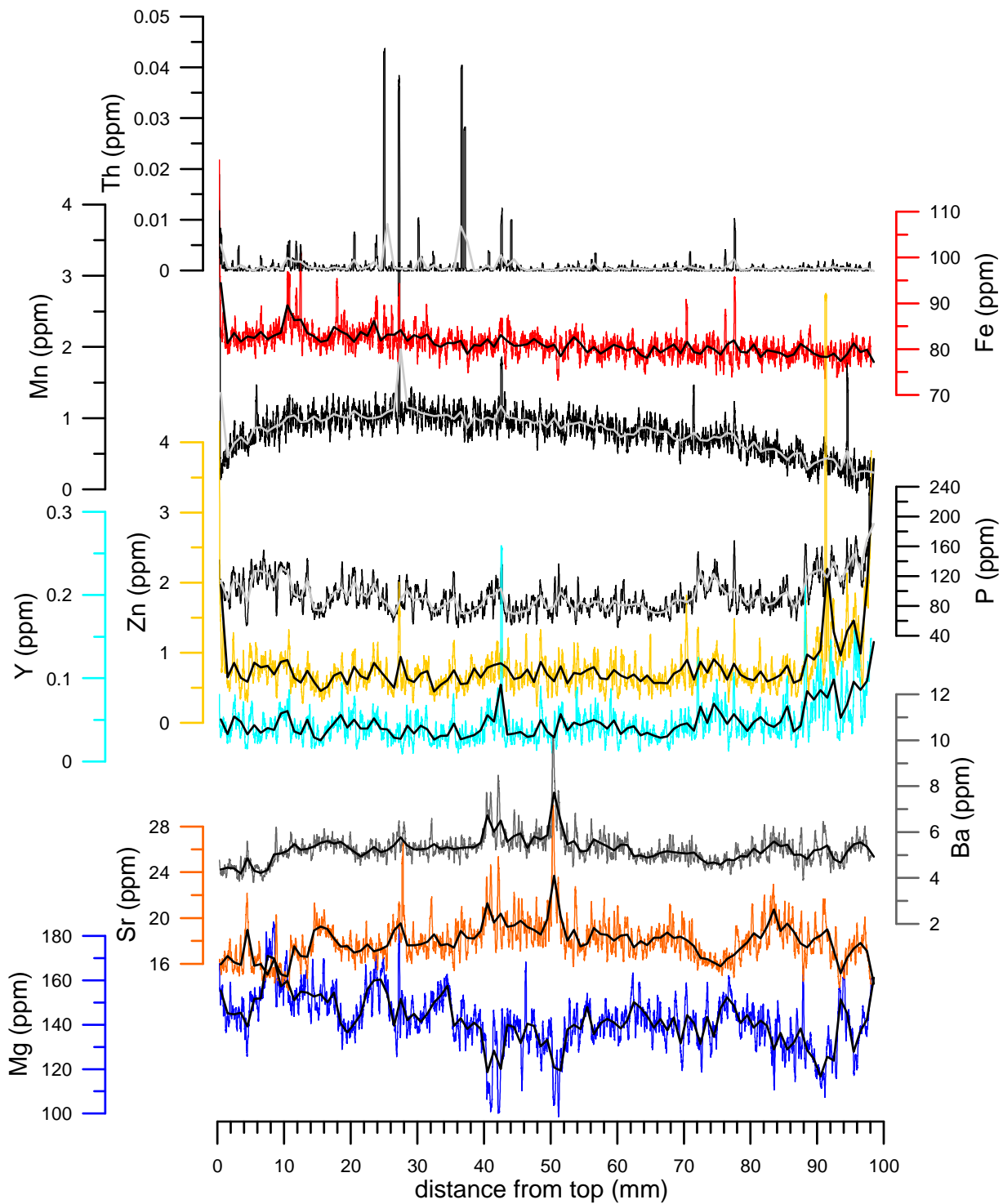


Fig. 5.19 – Trace element concentrations in stalagmite BS15 expressed as 31-point moving averages (coloured lines) and millimetric averages (black and grey bold lines). Results are expressed in ppm.

5.6 Statistical approach used to couple petrography and geochemical signals in stalagmites BS14 and BS15

The classified petrography groups have been compared with oxygen and carbon stable isotope and trace element composition in order to look for the eventual presence of a geochemical signature characterising the classified textures (cf. Paragraph 4.3.5). According to the chosen statistical approach, these petrography groups present a different and specific $\delta^{13}\text{C}$ and $\delta^{18}\text{O}$ composition (Kruskal-Wallis test; Tab. 5.9).

Kruskal-Wallis test	H	Hcrit. (0.05)	Petrography groups sample size
BS14 $\delta^{18}\text{O}$	23.20	11.07	1) Ccm n=16
			2) Ocm n=11
$\delta^{13}\text{C}$	51.69	11.07	3) Ecm n=17
			4) Pcm n=20
			5)SScm n=5
			6) D n=4
BS15 $\delta^{18}\text{O}$	10.01	9.49	1) Ccm n=4
			2) Ocm n=20
$\delta^{13}\text{C}$	43.84	9.49	4) Ecm n=64
			5)SScm n=12

Tab. 5.9 - Results from Kruskal-Wallis test performed among fabric groups according to $\delta^{18}\text{O}$ and $\delta^{13}\text{C}$ in stalagmites BS14 and BS15. The null hypothesis is the presence of similar isotopic composition in the considered petrography groups. H is a calculated value; Hcrit. is a value found on the Kruskal-Wallis tables. When $H > H_{crit.}$ the null hypothesis must be rejected with a 95 % confidence level.

In particular, the IsoFab plot highlighted progressively higher isotopic values from Ccm to D (Fig. 5.20). Multiple tests associated with the Bonferroni correction show that the $\delta^{13}\text{C}$ values for each recognised fabric in BS15 are statistically different with at least 95% confidence level, with the exception of Ccm and Ocm for which the confidence stays a bit lower (92.4%). In BS14 the groups are less defined: while Ccm and Ocm cannot be considered statistically different, they differ from all the remaining groups. The same can be stated for the couples Cem - Pcm and SScm – D (Tab. 5.10 and Fig. 5.20). On the contrary, the petrography groups are less according to $\delta^{18}\text{O}$ composition. In stalagmite BS15, Ccm presents $\delta^{18}\text{O}$ values statistically different from Pcm (97.2 % confidence level) and SScm (93.5 % confidence level) but comparable values with Ocm, which in turns can be considered separated from Pcm group, but not from SScm, which presents more sparse isotopic values. Pcm and SScm petrography groups present comparable $\delta^{18}\text{O}$ values (Tab. 5.10). Petrography classes in stalagmite BS14 have a better-defined $\delta^{18}\text{O}$ signature than in BS15. In this

(BS14) stalagmite Ccm and Ocm have similar $\delta^{18}\text{O}$ values, but at the same time Ccm isotopic signature can be considered different from all the other groups. $\delta^{18}\text{O}$ values of Ocm group can be considered statistically different from D only, while the remaining groups present comparable $\delta^{18}\text{O}$ values (Tab. 5.10; Fig. 5.20).

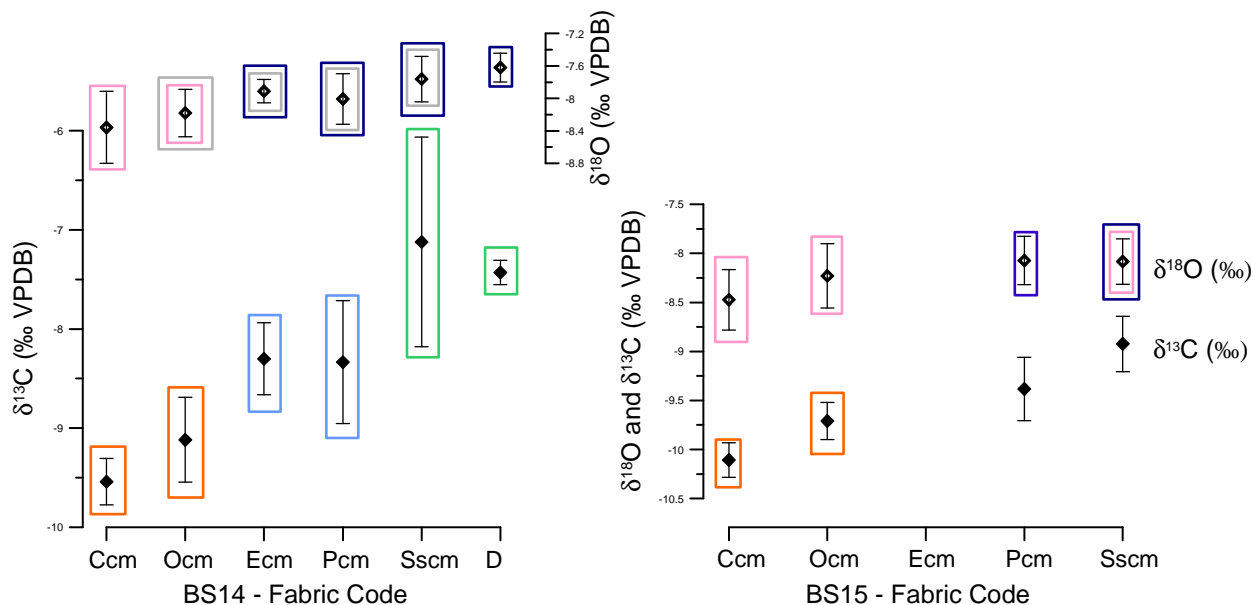


Fig. 5.20 - Isotope-fabric plots for BS14 and BS15 stalagmites. For each fabric type, average $\delta^{13}\text{C}$ and $\delta^{18}\text{O}$ values are plotted with their standard deviation. Isotope compositions that cannot be considered statistically different (confidence level 0.05; Table 4) are indicated with rectangles of the same colour.

BS14	1) Ccm	2) Ocm	3) Ecm	4) Pcm	5) SScm	6) D
1) Ccm		$\delta^{18}\text{O}$: 1 $\delta^{13}\text{C}$: 0.514	$\delta^{18}\text{O}$: 0.001 $\delta^{13}\text{C}$: 1.3E-8	$\delta^{18}\text{O}$: 0.018 $\delta^{13}\text{C}$: 9.7E-10	$\delta^{18}\text{O}$: 0.005 $\delta^{13}\text{C}$: 8.5E-13	$\delta^{18}\text{O}$: 0.001 $\delta^{13}\text{C}$: 2.3E-9
2) Ocm	$\delta^{18}\text{O}$: 1 $\delta^{13}\text{C}$: 0.514		$\delta^{18}\text{O}$: 0.395 $\delta^{13}\text{C}$: 0.001	$\delta^{18}\text{O}$: 1 $\delta^{13}\text{C}$: 0.001	$\delta^{18}\text{O}$: 0.213 $\delta^{13}\text{C}$: 4E-9	$\delta^{18}\text{O}$: 0.040 $\delta^{13}\text{C}$: 3.2E-6
3) Ecm	$\delta^{18}\text{O}$: 0.01 $\delta^{13}\text{C}$: 1.3E-8	$\delta^{18}\text{O}$: 0.395 $\delta^{13}\text{C}$: 0.001		$\delta^{18}\text{O}$: 1 $\delta^{13}\text{C}$: 1	$\delta^{18}\text{O}$: 1 $\delta^{13}\text{C}$: 2.4E-4	$\delta^{18}\text{O}$: 1 $\delta^{13}\text{C}$: 0.039
4) Pcm	$\delta^{18}\text{O}$: 0.018 $\delta^{13}\text{C}$: 9.7E-10	$\delta^{18}\text{O}$: 1 $\delta^{13}\text{C}$: 0.001	$\delta^{18}\text{O}$: 1 $\delta^{13}\text{C}$: 1		$\delta^{18}\text{O}$: 1 $\delta^{13}\text{C}$: 1.1E-4	$\delta^{18}\text{O}$: 0.374 $\delta^{13}\text{C}$: 0.024
5) SScm	$\delta^{18}\text{O}$: 0.005 $\delta^{13}\text{C}$: 8.5E-13	$\delta^{18}\text{O}$: 0.213 $\delta^{13}\text{C}$: 4E-9	$\delta^{18}\text{O}$: 1 $\delta^{13}\text{C}$: 2.4E-4	$\delta^{18}\text{O}$: 1 $\delta^{13}\text{C}$: 1.1E-4		$\delta^{18}\text{O}$: 1 $\delta^{13}\text{C}$: 1
6) D	$\delta^{18}\text{O}$: 0.01 $\delta^{13}\text{C}$: 2.3E-9	$\delta^{18}\text{O}$: 0.040 $\delta^{13}\text{C}$: 3.2E-6	$\delta^{18}\text{O}$: 1 $\delta^{13}\text{C}$: 0.039	$\delta^{18}\text{O}$: 0.374 $\delta^{13}\text{C}$: 0.024	$\delta^{18}\text{O}$: 1 $\delta^{13}\text{C}$: 1	
BS15	1) Ccm	2) Ocm		4) Pcm	5) SScm	
1) Ccm		$\delta^{18}\text{O}$: 0.703 $\delta^{13}\text{C}$: 0.076		$\delta^{18}\text{O}$: 0.018 $\delta^{13}\text{C}$: 3.6E-5	$\delta^{18}\text{O}$: 0.065 $\delta^{13}\text{C}$: 2.3E-9	
2) Ocm	$\delta^{18}\text{O}$: 0.703 $\delta^{13}\text{C}$: 0.076			$\delta^{18}\text{O}$: 0.044 $\delta^{13}\text{C}$: 3.3E-4	$\delta^{18}\text{O}$: 0.517 $\delta^{13}\text{C}$: 6.9E-10	
4) Pcm	$\delta^{18}\text{O}$: 0.018 $\delta^{13}\text{C}$: 3.6E-5	$\delta^{18}\text{O}$: 0.044 $\delta^{13}\text{C}$: 3.3E-4			$\delta^{18}\text{O}$: 1 $\delta^{13}\text{C}$: 1.8E-5	
5) SScm	$\delta^{18}\text{O}$: 0.065 $\delta^{13}\text{C}$: 2.3E-9	$\delta^{18}\text{O}$: 0.517 $\delta^{13}\text{C}$: 6.9E-10		$\delta^{18}\text{O}$: 1 $\delta^{13}\text{C}$: 1.8E-5		

Tab. 5.10 - Bonferroni test results between petrography groups in stalagmites BS14 and BS15 for $\delta^{18}\text{O}$ and $\delta^{13}\text{C}$ ratios. Significance value is indicated for both isotopic ratios. Bold italic values indicate significantly different groups in terms of $\delta^{18}\text{O}$ and/or $\delta^{13}\text{C}$ composition (0.05 significance level).

Discriminant analyses were performed for both stalagmites using $\delta^{13}\text{C}$ and $\delta^{18}\text{O}$ to discriminate the petrography groups (Green et al., 2008; Fig. 5.21; Tab. 5.11).

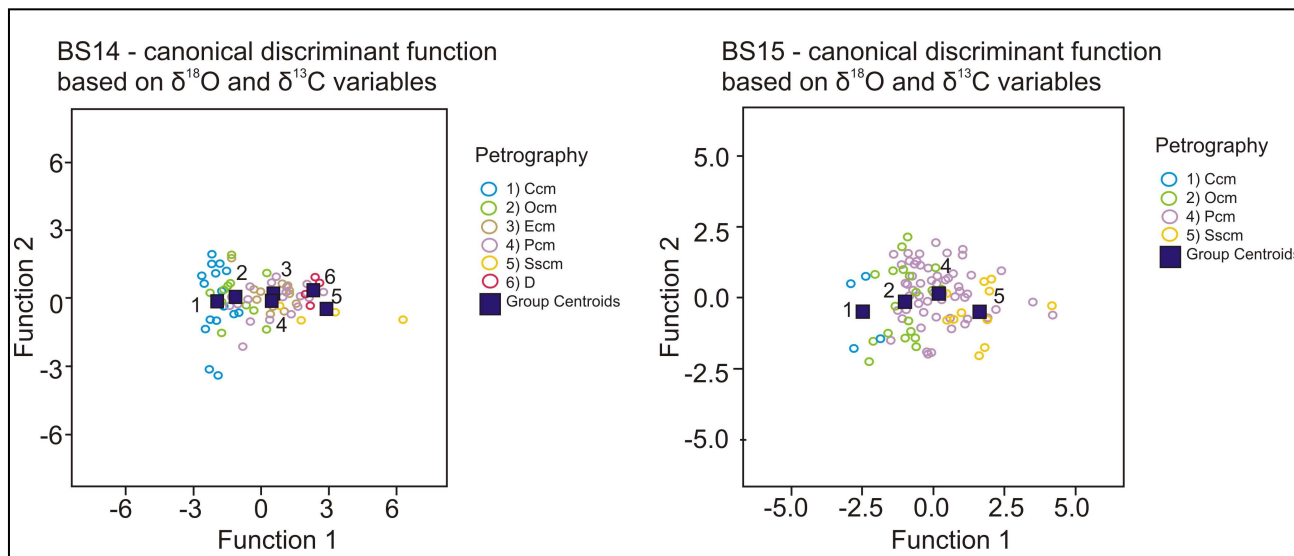


Fig. 5.21 – Discriminant function for the classified petrography groups using two variables ($\delta^{18}\text{O}$ and $\delta^{13}\text{C}$) for stalagmites BS14 (left) and BS15 (right). This representation shows that according the considered variables, 55% (BS15) and 46% (BS14) of petrography samples have been well discriminated.

2 variables	BS15 – predicted group membership						
Petrography	1	2	4	5	Total		
1) (counts)	4				4		
2) (counts)	4	12	4		20		
4) (counts)	1	22	29	12	64		
5) (counts)			2	10	12		
1) (%)	100%	0%	0%	0%	100%		
2) (%)	20%	60%	0%	0%	100%		
4) (%)	1.6%	34.4%	18.8%	18.8%	100%		
5) (%)	0%	0%	83.3%	83.3%	100%		
2 variables	BS14 – predicted group membership						
Petrography	1	2	3	4	5	6	Total
1) (counts)	9	4		2		1	16
2) (counts)	1	6	2			2	11
3) (counts)	1	2	8	2	4		17
4) (counts)	9	2	1	3	2	3	20
5) (counts)		1	1		2	1	5
6) (counts)					1	3	4
1) (%)	56.3%	25%	0%	12.5%	0%	6.3%	100%
2) (%)	9.1%	54.5%	18.2%	0%	0%	18.2%	100%
3) (%)	5.9%	11.8%	47.1%	11.8%	23.5%	0%	100%
4) (%)	45%	10%	5%	15%	10%	15%	100%
5) (%)	0%	20%	20%	0%	40%	20%	100%
6) (%)	0%	0%	0%	0%	25%	75%	100%

Tab. 5.11 – Discriminant analysis results for stalagmites BS14 and BS15. Petrography class have been discriminated according to their $\delta^{18}\text{O}$ and $\delta^{13}\text{C}$ composition. The predicted group membership indicate how many samples belonging to each classified petrography group are well classified and how many should belong to a different group according to their stable isotope composition. According to this analysis 55% and 46.6% of samples from stalagmites BS15 and BS14 are well classified.

According to this analysis, 55% and 46.6% of samples in BS15 and BS14 are well classified in terms of stable isotope composition. In particular, the graphic representation demonstrates the presence of a fabric–stable isotope relation, which associates progressively higher isotope ratios to the more porous and impurity-rich fabrics (Fig. 5.21).

A discriminant analysis was performed for stalagmite BS15, considering Mg and Sr content in addition to $\delta^{18}\text{O}$ and $\delta^{13}\text{C}$ values (Tab. 5.12; Fig. 5.22). It resulted in a good distinction of the different petrography groups (67.7% of samples well classified).

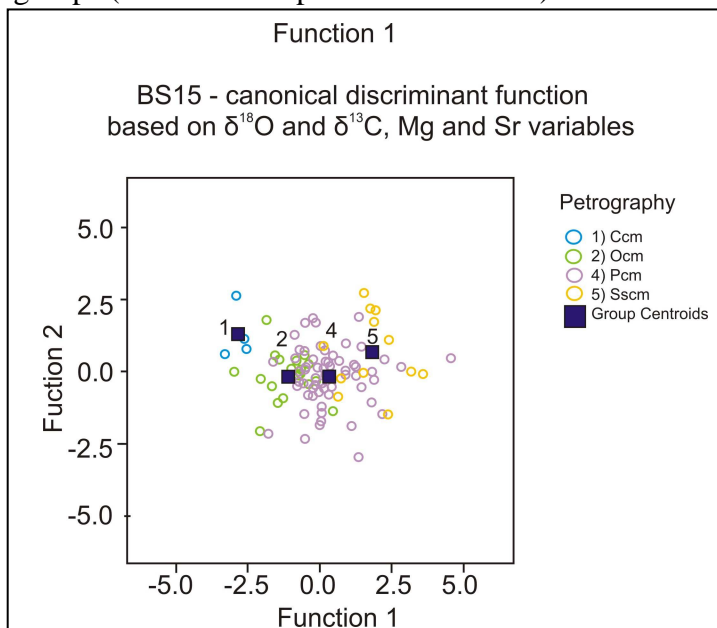


Fig. 5.22 – Discriminant function for the classified petrography groups using four variables ($\delta^{18}\text{O}$, $\delta^{13}\text{C}$, Mg and Sr) for stalagmite BS15. This representation shows that according the considered variables, 67.7% of samples are well discriminated.

4 variables	BS15 – predicted group membership				
Petrography	1	2	4	5	Total
1) (counts)	4				4
2) (counts)	2	15	3		20
4) (counts)		14	39	10	63
5) (counts)			3	9	12
1) (%)	100%	0%	0%	0%	100%
2) (%)	19%	75%	15%	0%	100%
4) (%)	0%	22.2%	61.9%	15.9%	100%
5) (%)	0%	0%	25%	75%	100%

Tab. 5.12 – Discriminant analysis results for stalagmite BS15. Petrography class have been discriminated according to their $\delta^{18}\text{O}$, $\delta^{13}\text{C}$, Sr and Mg composition. The predicted group membership indicates how many samples belonging to each classified petrography group are well classified and how many should belong to a different group according to their stable isotope composition. According to this analysis 67.7 % of samples from stalagmite BS15 are well classified.

5.7 The black layer

A sharp, dark surface was observed close to the top of all the stalagmites sampled in Mračna Pečina Cave (i.e. BS8, BS9, BA14 and BS15) and described in the previous paragraphs. In order to investigate the nature and origin of this layer several analyses were performed on BS14 and BS15 samples. Only these two stalagmites were chosen because they show a thicker and more marked dark layer, both on their polished surface and in thin sections, thus facilitating its examination.

5.7.1 Fluorescence microscopy

The observation of thin sections under a fluorescence optic microscope highlighted an alternation of more and less fluorescent laminae.

Since fluorescence is indicative of the presence of organic matter, this result confirms the organic nature of the brownish lamination identified in both BS14 and BS15 stalagmites.

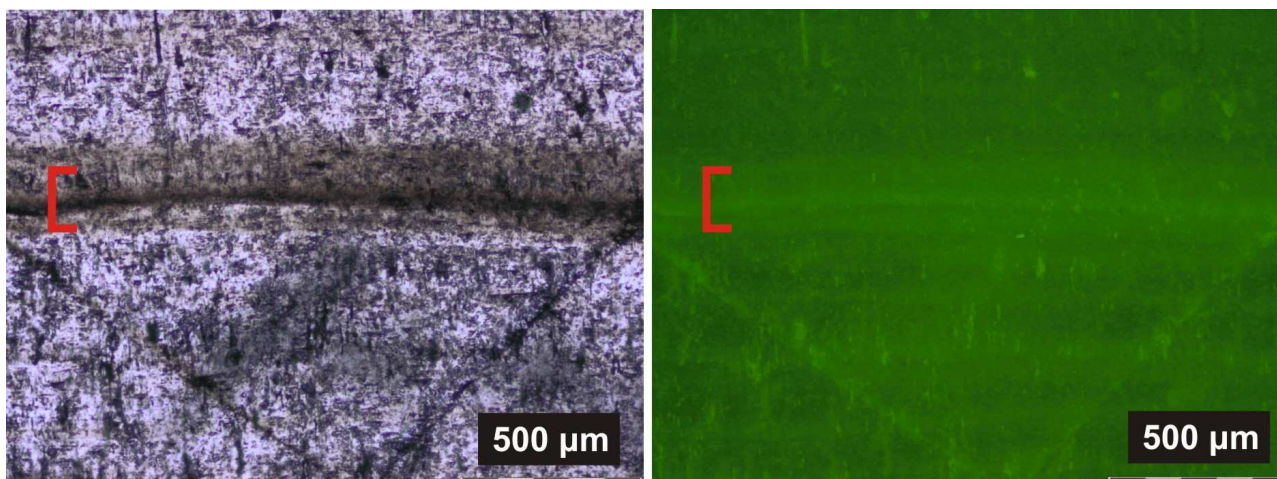


Fig. 5.23– Microphotographs of the black layer in BS15 stalagmite (10 mm from the top; red bracket). Left: natural light. Right: luminescence emitted under UV lamp excitation.

In stalagmite BS15 thin section, the lamina presenting the dark coating responded to fluorescence, suggesting organic matter/compounds as probable responsible of the dark layer (Fig. 5.23).

5.7.2 FTIR and micro-Raman results

FTIR analyses of the black layer in stalagmites BS14 and BS15 did not detect any other mineral phase than calcite (Fig. 5.24).

The infrared spectra show peaks in the same position. Two prominent peaks appear at 713 and 877 cm^{-1} wavelengths. A wide peak appears between 1380 and 1540 cm^{-1} and minor peaks appear at 1800, 2520, 2880 and 2990 cm^{-1} . Those identified peaks correspond to the calcite signal.

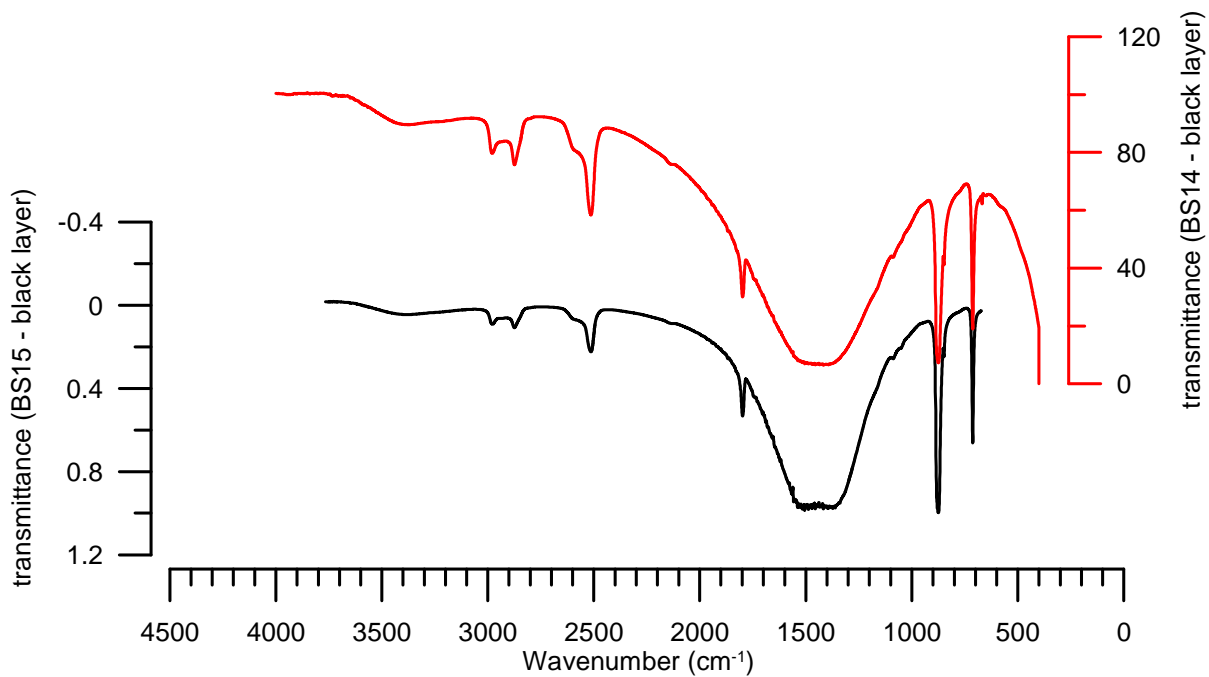


Fig. 5.24 – FTIR analyses of the black layer in both stalagmites BS15 (black) and BS14 (red).

Similar results were obtained with micro-Raman analyses. A predominant peak at 1086 and smaller peaks at 282, 712, 1436 and 1755 appear in stalagmite BS15, indicating only calcite (Fig. 5.25).

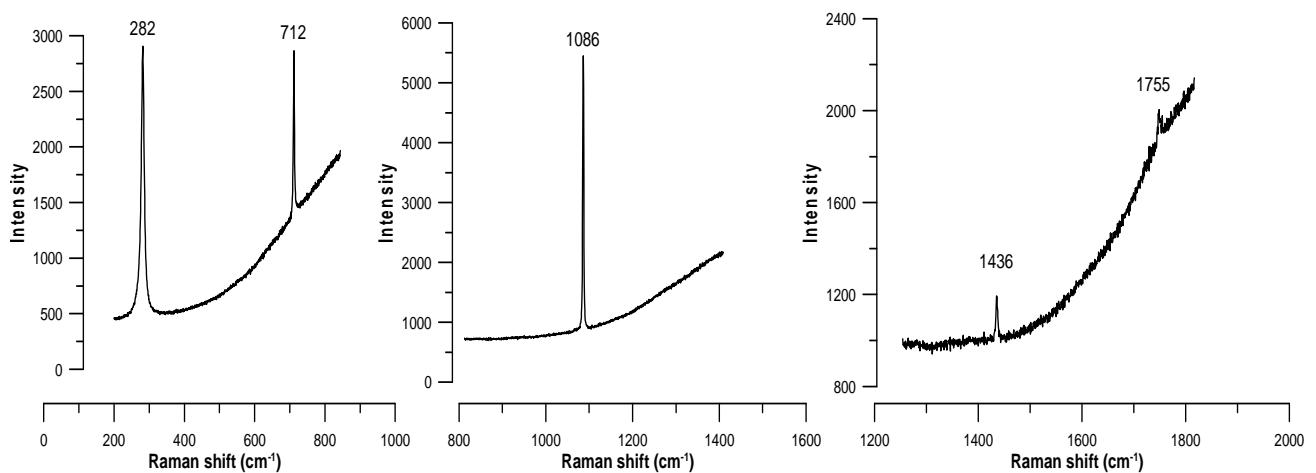


Fig. 5.25 – Analysis of the black layer in stalagmite BS15 by micro-raman.

5.7.3 SEM observations and analyses

SEM observations were performed on both the BS15 slab used for trace element analyses and in powder samples from stalagmites BS14 and BS15. Observations on the solid sample, made using both the secondary and backscattered detector, did not detect any foreign particle in the black layer. The chemical analyses identified the major presence of Ca, C and O, obviously associated with the calcite (Fig. 5.26), but no other compound potentially linked to the dark coloration was detected.

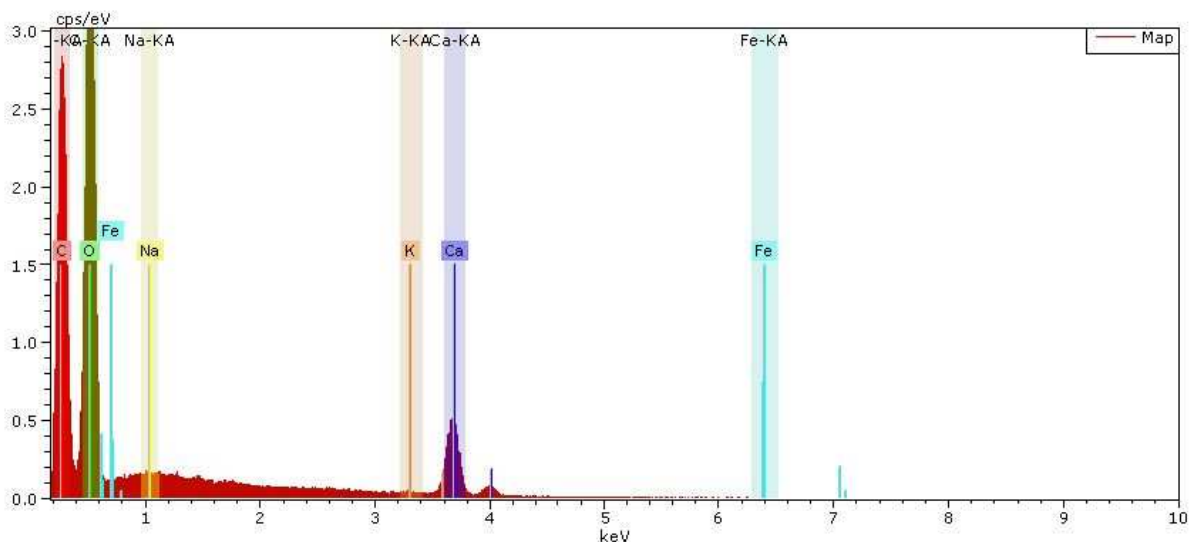


Fig. 5.26 - Chemical results by SEM analysis of the black layer in BS15 stalagmite.

In agreement with the analyses performed on the solid sample, SEM observations performed on non-metallised powder samples (the same samples used for FTIR analyses), did not show any other compound than calcite.

The images obtained with the secondary detector did not show any anomaly in the calcite fragments composing the powder (Fig. 5.27). The resulting chemical map shows, as expected, preponderance of calcium carbonate but no other mineral phase which might be responsible for the dark colour of the analysed layer (Fig. 5.28).

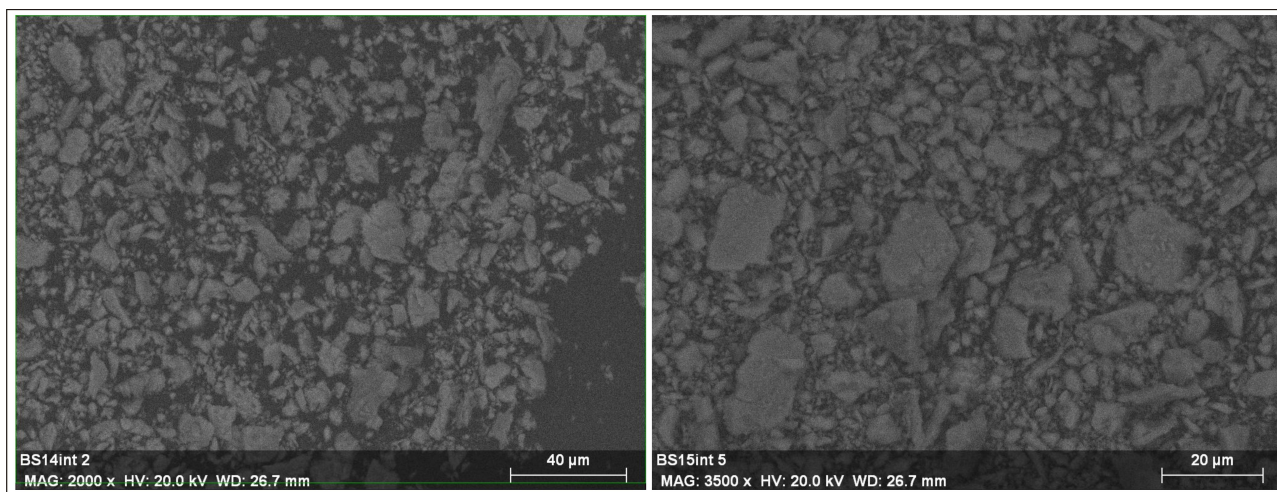
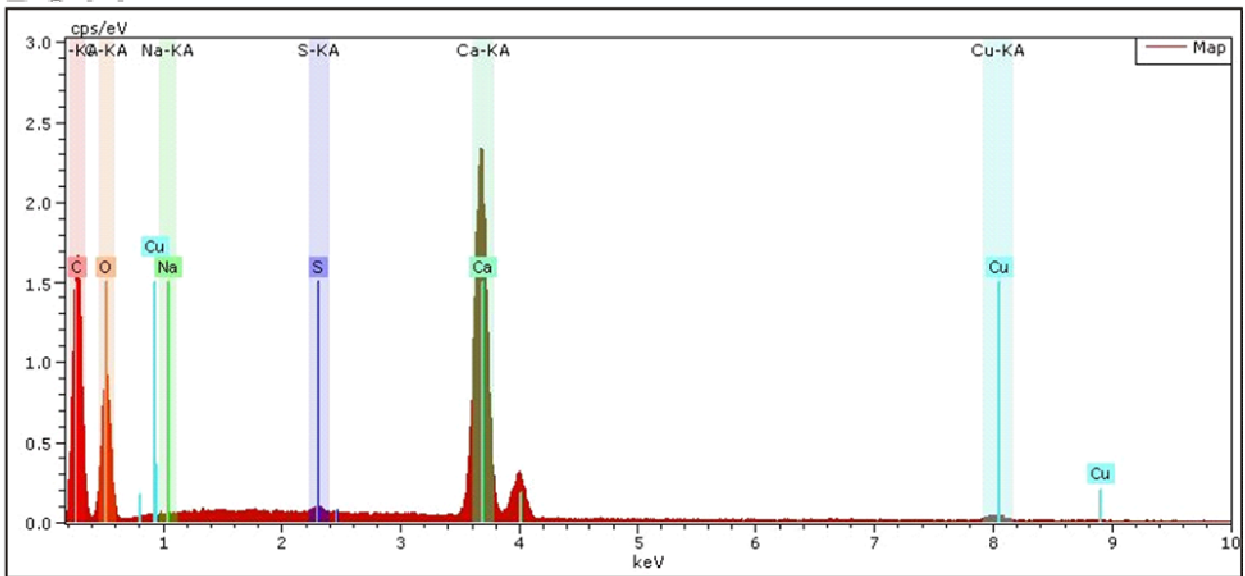


Fig. 5.27 - Picture obtained with the SEM secondary detector on powder from the black layer of stalagmites BS14 (left) and BS15 (right). The dark area between the grains is the substrate on which the powder was set.

BS14



BS15

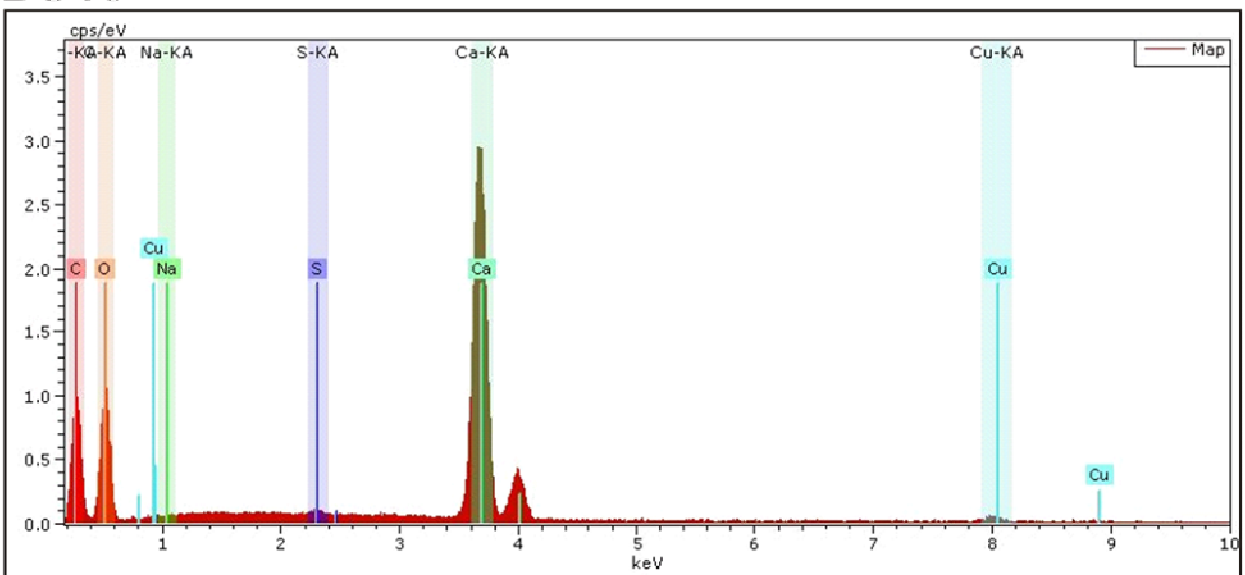


Fig. 5.28 – Results from chemical cartography performed on the black layer powder samples of stalagmites BS14 and BS15.

In stalagmite BS14, the black layer is found at the very top of the stalagmite. Another powder sample was taken from the stalagmite surface, aiming to sample a greater quantity of the investigated layer in order to increase the possibility of its identification (cf. Paragraph 4.3.6.4).

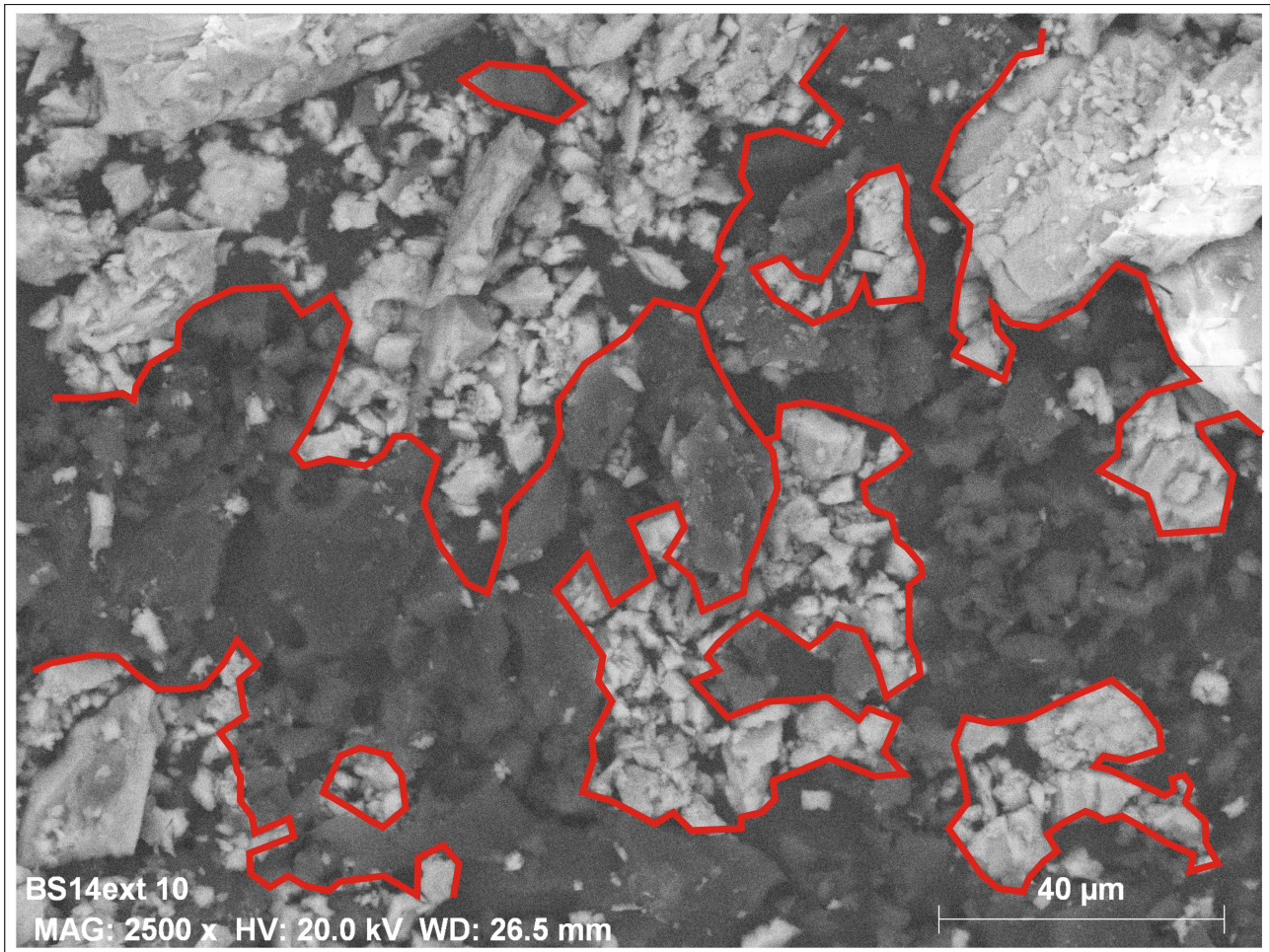


Fig. 5.29 – SEM image of BS14ext powder sample. Red lines delimitate groups of crystals covered by a dark coating.

This sample consisted of a coarser powder which was directly abraded on the layer surface. SEM observations provided different results from the ones performed on the powder samples taken on the stalagmite polished section perpendicularly to the targeted layer (cf. Paragraph 4.3.6.4).

A dark coating was visible on calcite fragments (Fig. 5.29). Chemical maps were made on two crystals with dark coating and two without (Fig. 5.30). The results show the major presence of C, Ca, O and Fe (Fig. 5.30). A Fe-hydroxide was detected (BS14ext4 in Fig. 5.30).

Chemical mapping was also performed on a sample portion presenting both “clean crystals” and dark coated fragments, focusing the analyses of the repartition of C and Ca elements among the different crystals (Fig. 5.31). This analysis clearly showed that the dark coating is mainly composed by C atoms, which are not associated with Ca atoms forming the calcite crystals.

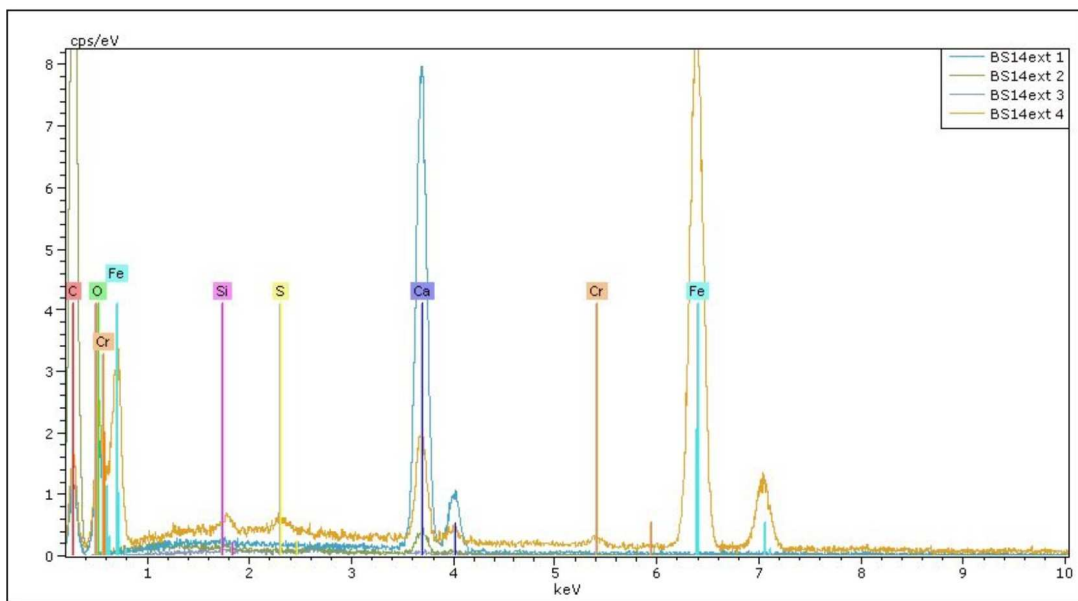
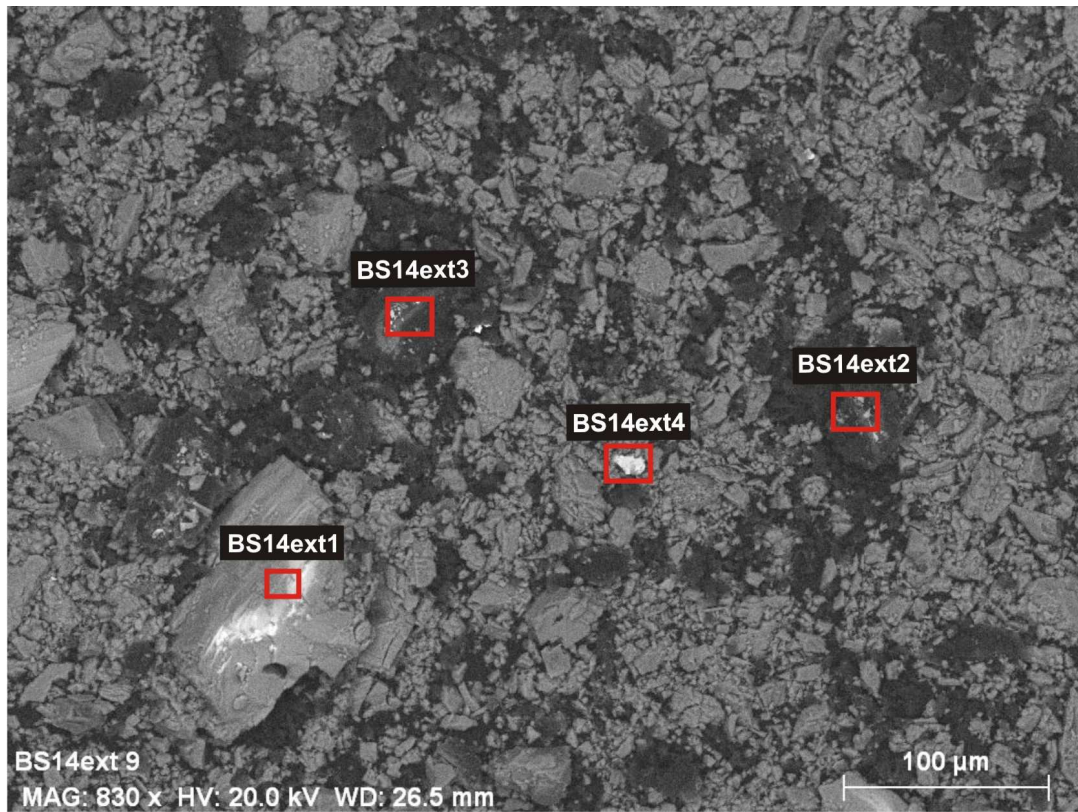


Fig. 5.30 Above: SEM image of BS14ext powder sample on which the points chosen for chemical mapping are indicated with red squares. Below: results of chemical mapping corresponding to the chosen points.

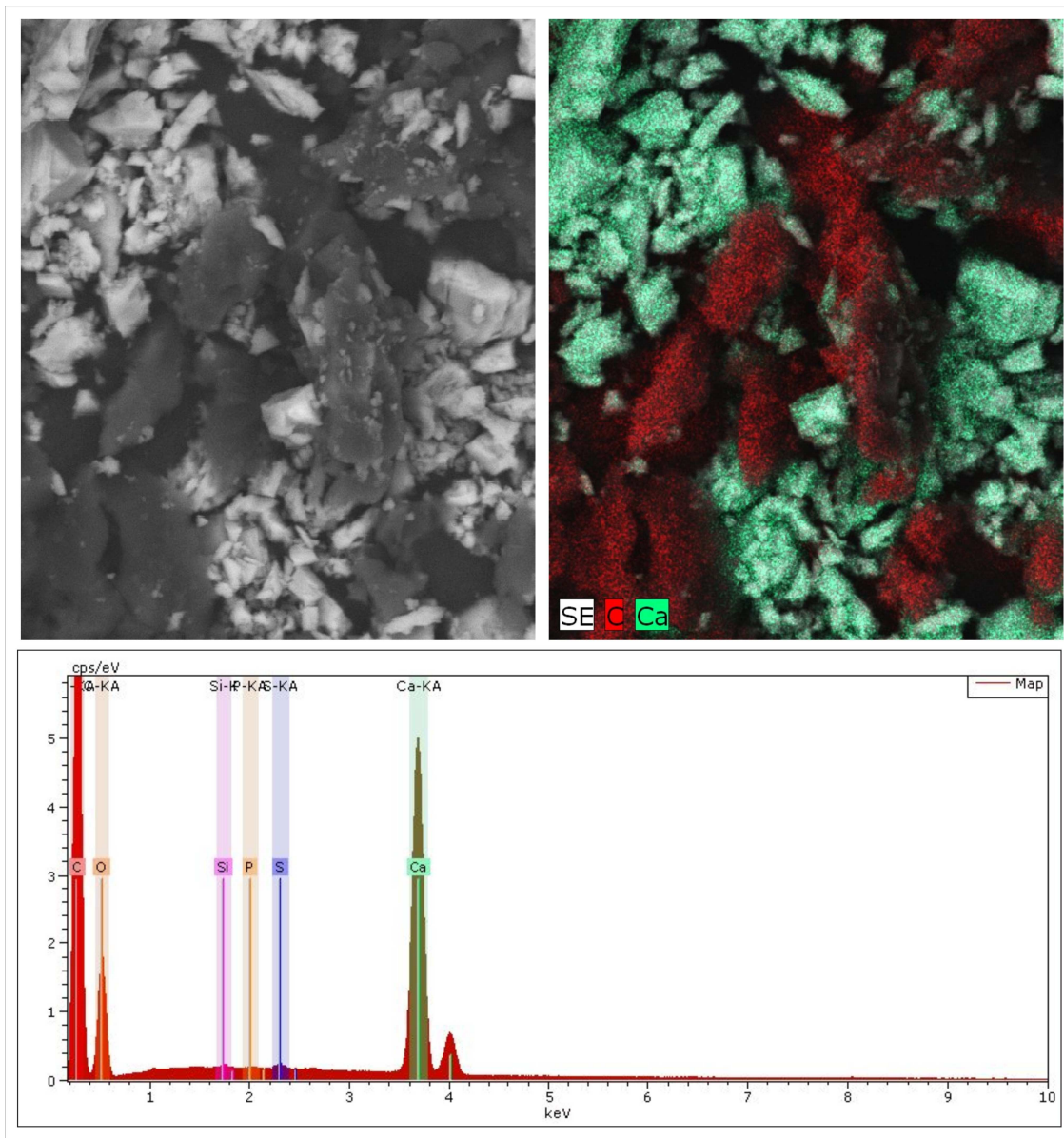


Fig. 5.31 – Above: SEM image of calcite coarse powder of the black layer; left: secondary detector picture; right: chemical mapping according to Ca and C concentration directly plotted on the analysed surfaces. Below: results of the chemical mapping showing the intensities of peaks corresponding to the detected elements.

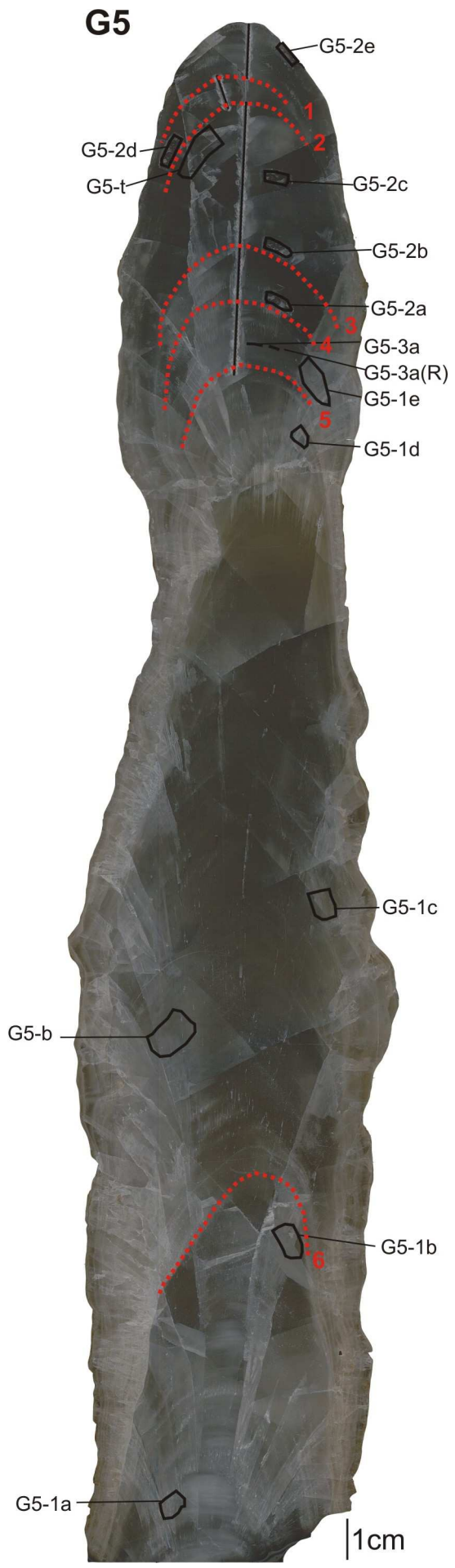


Plate 1 – Polished surface of stalagmite G5. Potential hiatuses are indicated in red. Black squares represent dated samples. The black line on the central growth axis in the top part represents the stable isotope profile.

BS8

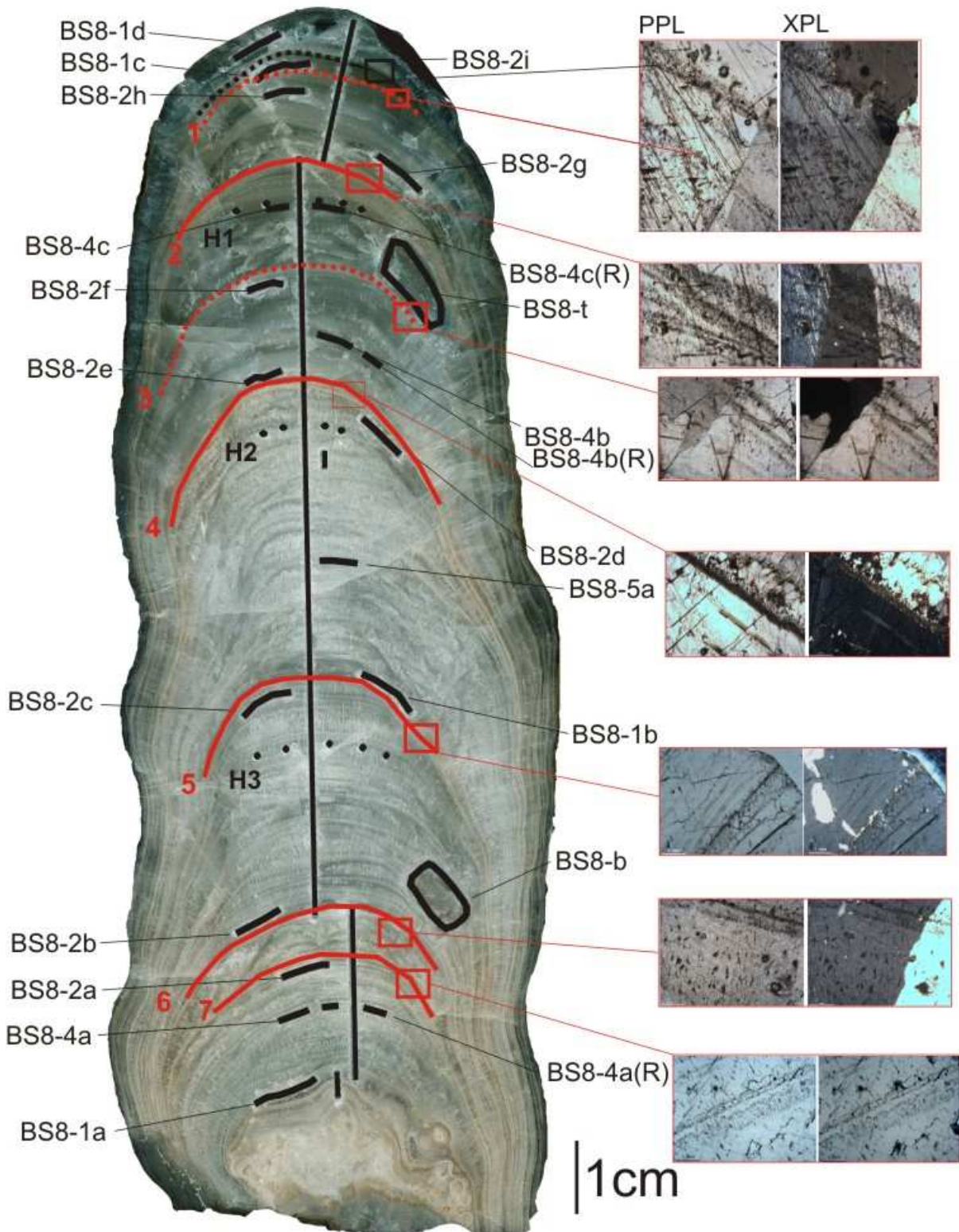


Plate 2 – Polished surface of stalagmite BS8. Potential hiatuses are indicated in red. Thin section images corresponding to these surfaces are reported on the right. Black squares represent dated samples. The black lines on the central growth axis represent the stable isotope profile. H1, H2 and H3 indicate the laminae on which the Hendy test was performed.

BS9

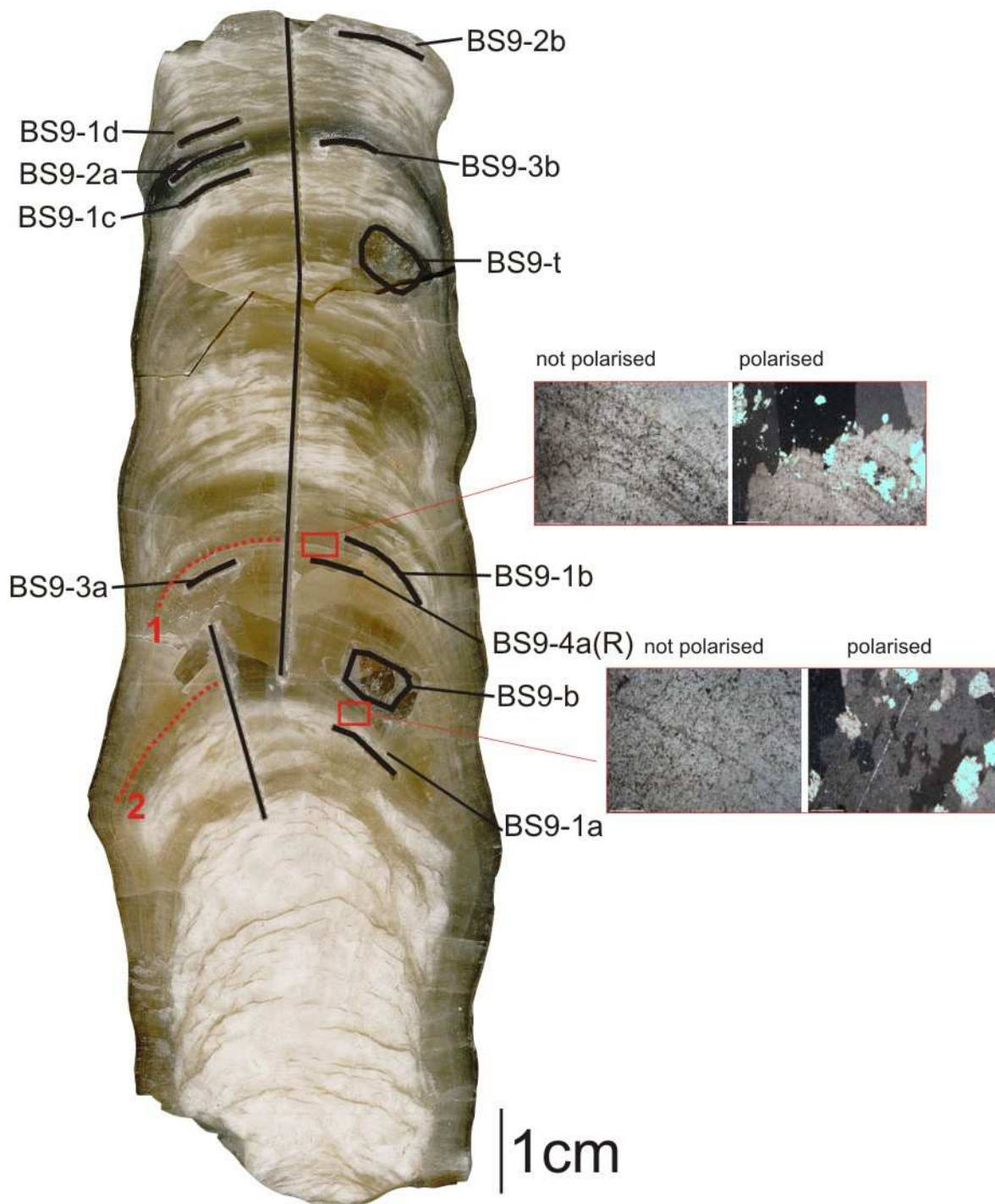
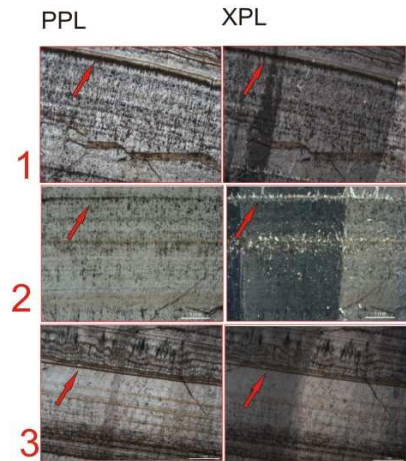
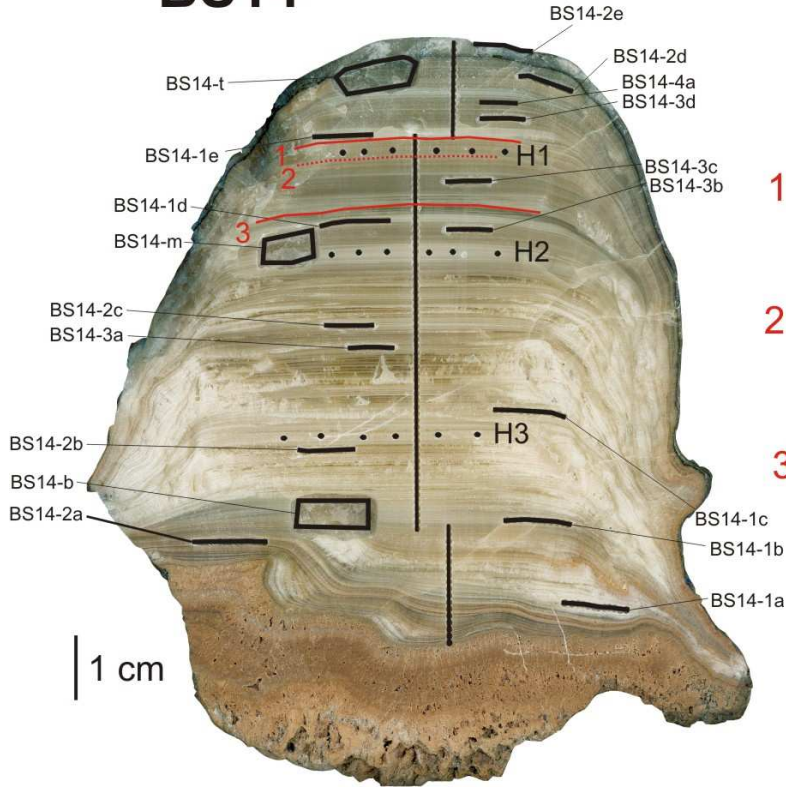


Plate 3 – Polished surface of stalagmite BS9. Potential hiatuses are indicated in red. Thin section images corresponding to these surfaces are reported on the right. Black squares represent dated samples. The black lines on the central growth axis represent the stable isotope profile.

BS14



BS15

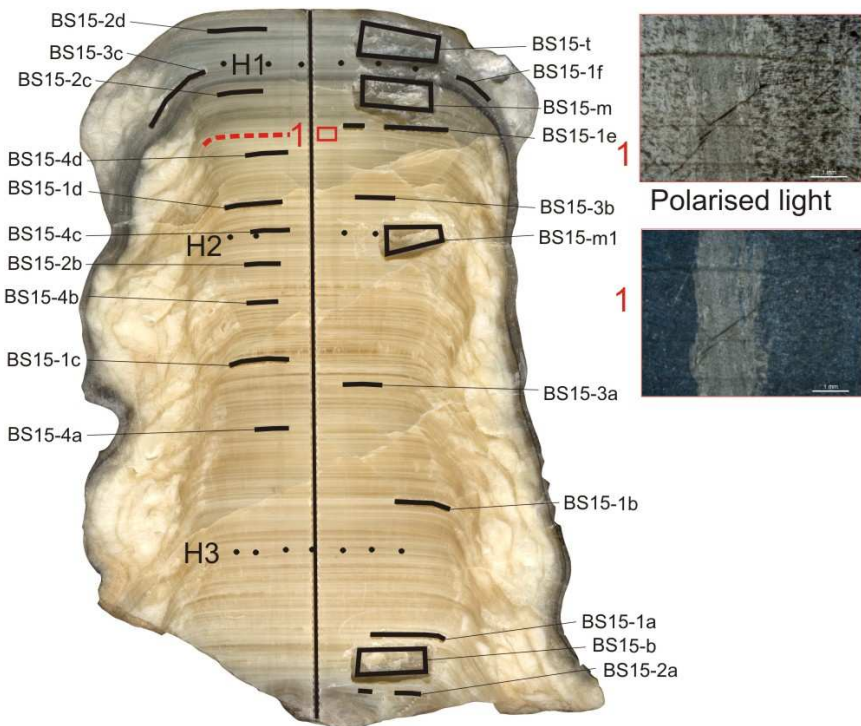


Plate 4 – Polished surface of stalagmites BS14 (above) and BS15 (below). Potential hiatuses are indicated in red. Thin section images corresponding to these surfaces are reported on the right. Black squares represent dated samples. The black lines on the central growth axis represent the stable isotope profile. H1, H2 and H3 indicate the laminae on which the Hendy test was performed.

VI. DISCUSSION

6.1 Processes behind the isotopic signal of precipitation and its transfer to the karst environment

6.1.1 Introduction

During the current inter-glacial period the modern atmospheric circulation pattern was established. Even if during these periods climate can be considered relatively stable in comparison to the glacial cycles, relatively small-scale fluctuations occurred in terms of both temperature and precipitation changes during the last ~11.000 years. In order to understand and interpret the climate information registered in Holocene speleothems, it is of great importance to understand the origin of the recorded proxy signals and the processes and dynamics of their transfer to the karst environment. Aiming to understand these processes for the Bosnian site, both monthly GNIP data (Global Network of Isotopes in Precipitation; 1980-2003; <http://www.iaea.org/water>; IAEA, 2015) of present-day precipitation in Zagreb and the sparse daily data from precipitation monitoring in Sarajevo sampled between September 2015 and July 2016 have been analysed and compared with Mračna Pećina Cave monitoring results.

6.1.2 Stable isotope composition of modern precipitation in Zagreb and their relation with atmospheric physical parameters

At the local scale, the parameters that can directly affect stable isotope composition of precipitation are temperature and rainfall amount. While stable isotope fractionation in precipitation is generally related to rainfall amount in tropical areas, in temperate climates at mid latitudes (like the Sarajevo region), it is mainly associated with variations in temperature (Vreča et al., 2006 and reference therein). In order to verify this trend and more deeply understand the role played by both temperature and precipitation amount in the Balkan Peninsula, GNIP monthly data from Zagreb have been analysed. Considering the few available isotopic data from precipitation monitoring (see Paragraph 5.1), the Zagreb site was chosen because it hosts the GNIP station closest to the Sarajevo region, providing a 23 years long record of monthly isotopic composition of precipitation together with monthly temperature and amount of precipitation. Zagreb is located 290 km NW from Sarajevo along an ideal line that runs parallel to the Adriatic coast. Both cities are located at similar distances from the Adriatic Sea (~140 km) and present similar precipitation and temperature patterns over the year (Fig. 6.1.1). In addition, they have a similar local meteoric water line, which is close to the global meteoric line calculated by Craig (1961) (Fig. 6.1.2). For these reasons, factors influencing stable isotope composition of precipitation in Zagreb have been considered representative also for the Sarajevo region.

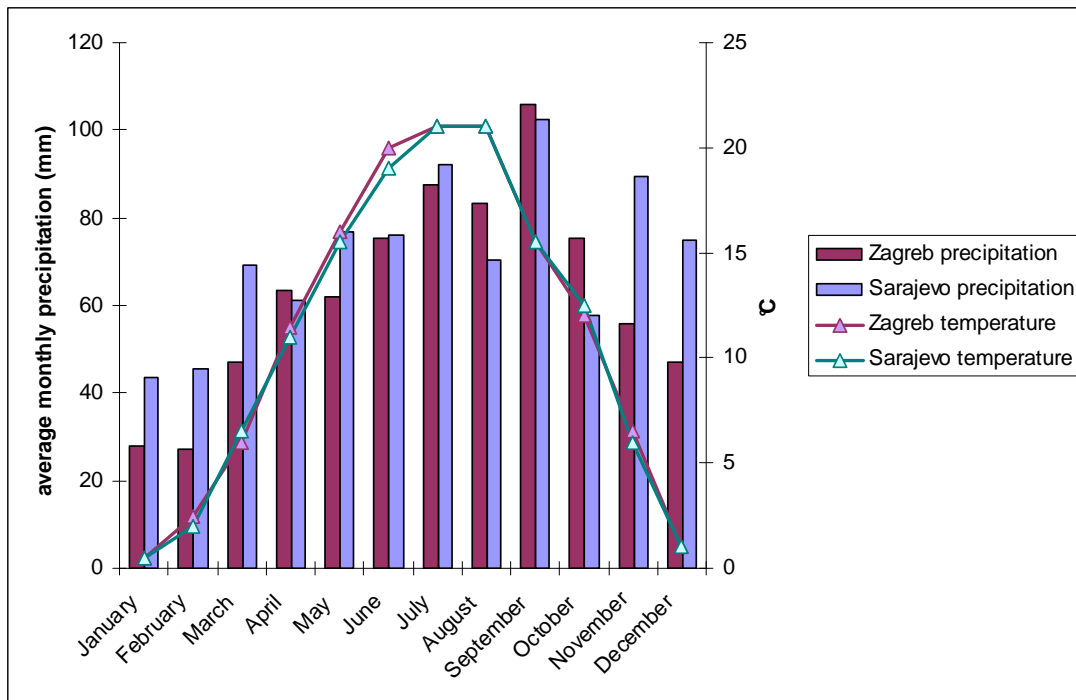


Fig. 6.1.1 – Average monthly precipitation and temperature in Sarajevo and Zagreb over the period 2000-2012 (data from www.worldweatheronline.com).

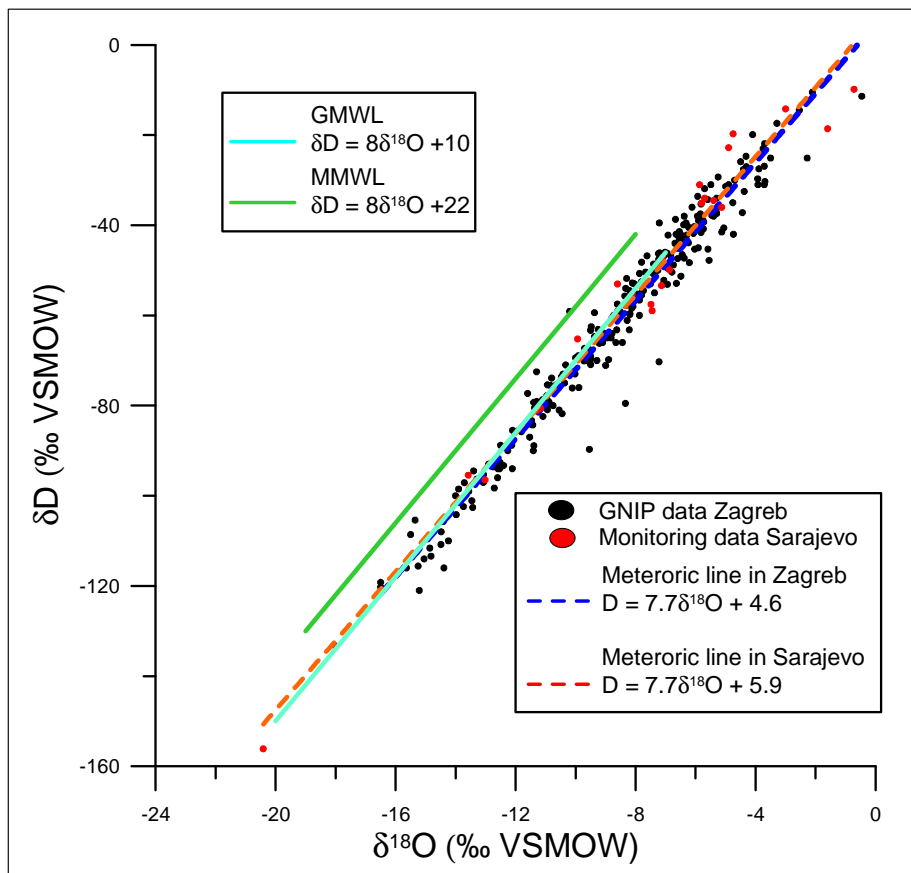


Fig. 6.1.2 - Comparison between Global Meteoric Water Lines (GMWL; Craig, 1961), Mediterranean Meteoric Water lines (MMWL; Gat and Carmi, 1970), Zagreb and Sarajevo local water lines.

The proximity between both the Zagreb and Sarajevo water lines and the GMWL suggests that no significant evaporation affects atmospheric moisture at these sites (Craig, 1961). The offset in $\delta^{18}\text{O}$ with the MMWL suggests that Mediterranean Sea is not the main moisture source.

Raw monthly precipitation and temperature data from Zagreb have been plotted against $\delta^{18}\text{O}$ ratios, showing a major dependence of the isotopic ratios on temperature rather than precipitation amount (r^2 respectively of 0.67 and 0.008; Fig. 6.1.3).

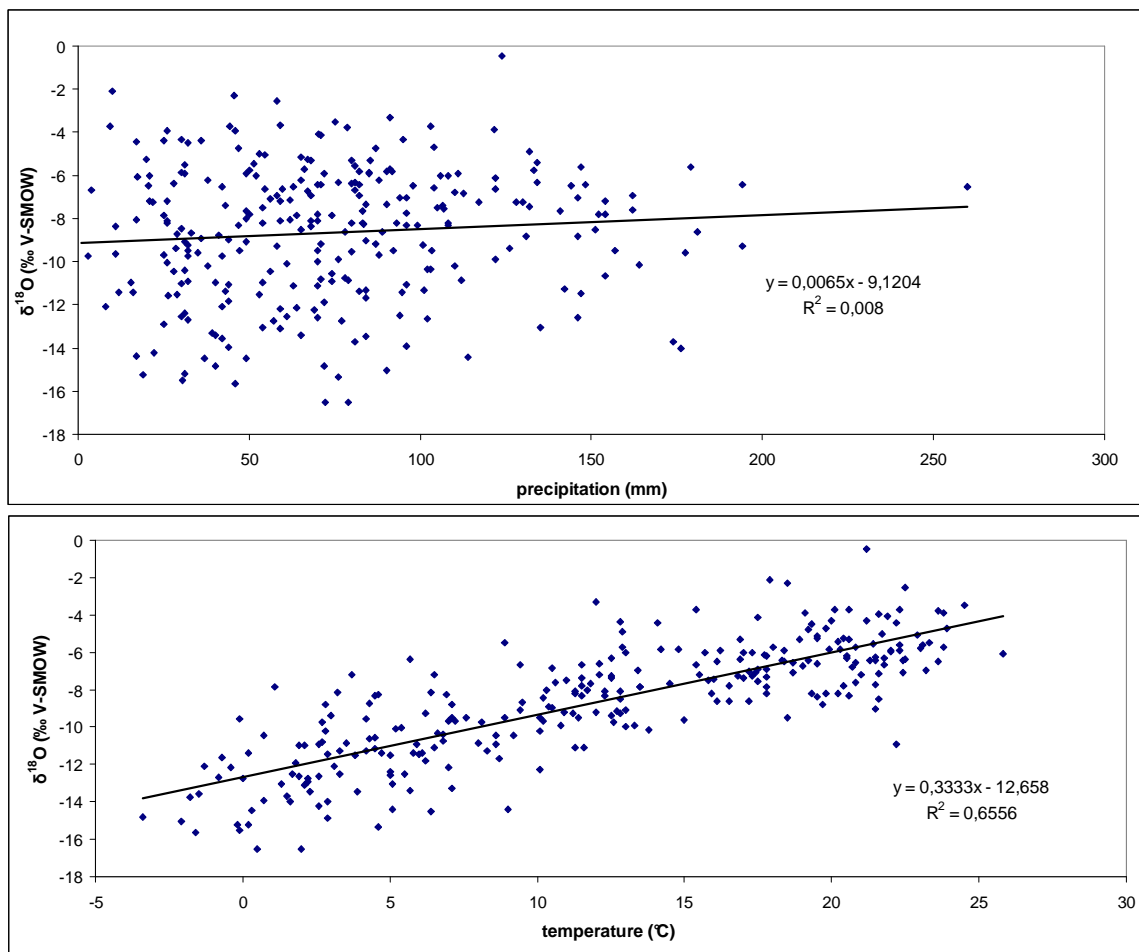


Fig. 6.1.3 – Average monthly $\delta^{18}\text{O}$ composition of precipitation in Zagreb plotted in function of precipitation (mm; above) and temperature ($^{\circ}\text{C}$; below).

The two variables appear bounded by a coefficient of $0.33\text{‰}/^{\circ}\text{C}$, in line with the temperature dependence of $\delta^{18}\text{O}$ observed by Vreča et al. (2006) in Croatia.

In order to deeper investigate these relationships, data were stratified, dividing the members of the population into homogeneous subgroups: data have thus been divided into temperature and precipitation classes corresponding, respectively, to an amplitude of 2°C and 20 mm. Weighed average $\delta^{18}\text{O}$ values have been calculated for each class. In this particular case, the creation of two series of classes (temperature and precipitation) allowed for a deeper investigation of the contribution of the two variables (temperature and precipitation) in modulating the $\delta^{18}\text{O}$

composition, highlighting the patterns of the analysed data. For each temperature class, a weighted $\delta^{18}\text{O}$ and temperature average value was calculated with respect to precipitation amount, allowing for the attribution of the right weight in relation to the amount of precipitation (i.e. average monthly data relative to wetter months weights more than values measured during drier months). This process highlighted the already detected strong positive relationship between $\delta^{18}\text{O}$ and temperature ($r^2 = 0.97$; Fig. 6.1.4).

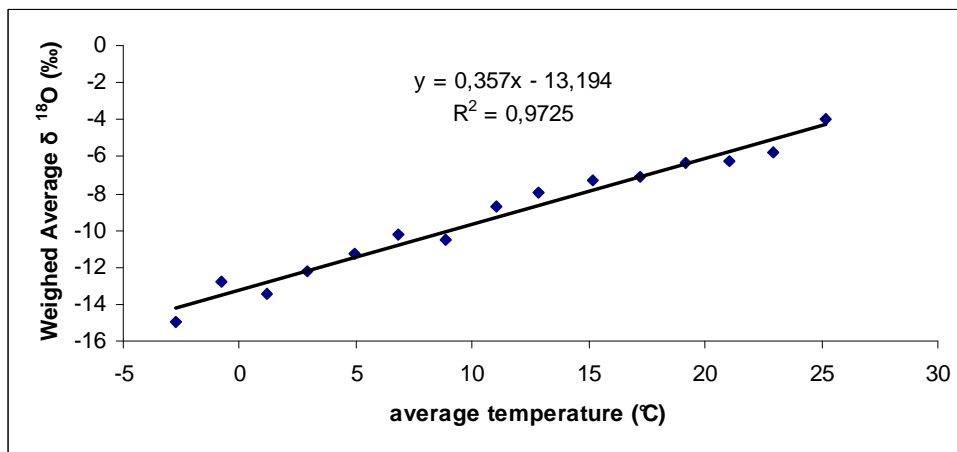


Fig. 6.1.4 Weighed average $\delta^{18}\text{O}$ for each temperature class plotted versus the average temperature for each class (GNIP data from Zagreb).

A similar procedure was repeated for the data series subdivided into precipitation classes. In this case average monthly precipitation and $\delta^{18}\text{O}$ composition were weighted in relation to temperature and plotted against the average amount of precipitation of each class. Any remarkable relation was found between $\delta^{18}\text{O}$ and precipitation amount, even if a weak trend toward lower $\delta^{18}\text{O}$ values with higher amount of precipitation is visible (Fig. 6.1.5), confirming the strongest influence played by temperature in modulating precipitation $\delta^{18}\text{O}$ ratios.

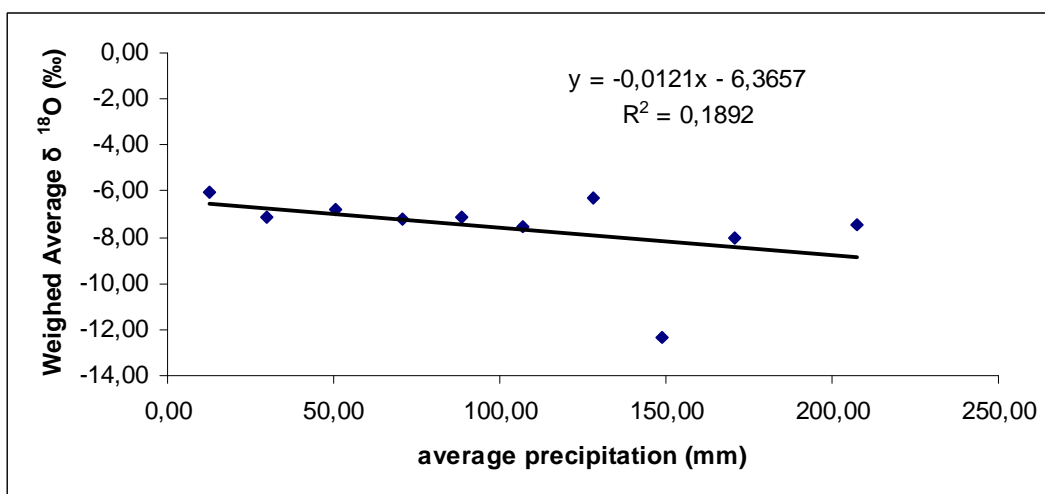


Fig. 6.1.5 Weighed average $\delta^{18}\text{O}$ for each precipitation class plotted versus the average precipitation for each class (GNIP data from Zagreb).

GNIP data from Zagreb were also compared with NAO indices (IAEA).

In order to reduce the noise and highlight potential common trends, moving averages on 15 and 25 points were performed. As expected, some resemblance appeared between $\delta^{18}\text{O}$ and temperature records (Fig. 6.1.6).

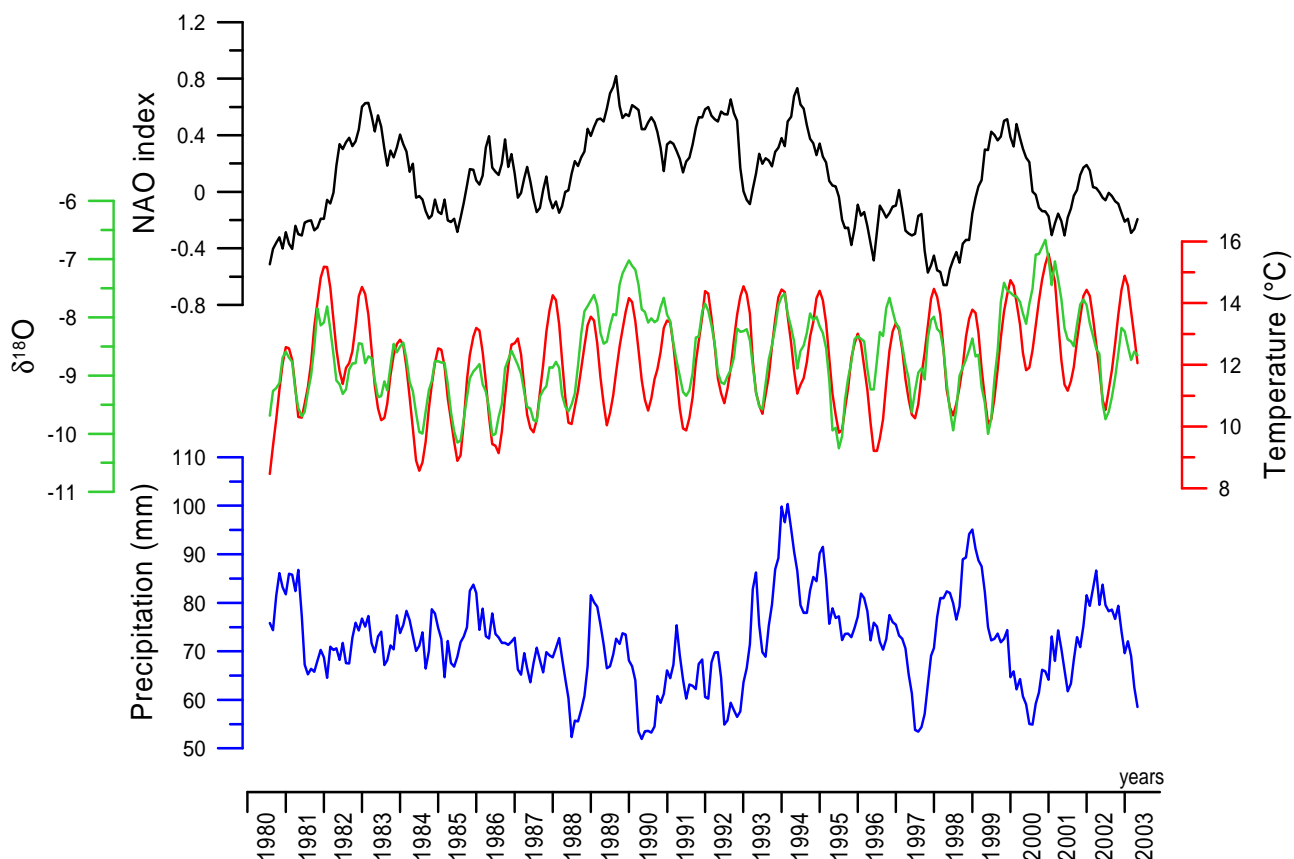


Fig. 6.1.6 – Comparison of smoothed data (moving averages on 15 points) of: monthly precipitation (blue curve), $\delta^{18}\text{O}$ (green curve), temperature (red curve), and the NAO index (black curve) for the Zagreb station.

Moving averages performed on 25 points still highlighted a close resemblance of $\delta^{18}\text{O}$ and temperature variations, whose long-term trend seems to follow the NAO index trend (Fig. 6.1.7).

Between about 1988 and 1991 a phase with relatively high precipitation $\delta^{18}\text{O}$ ratios occurred, which was not associated with marked higher average temperature. At the same time relatively dry conditions during a positive NAO phase were identified (Fig. 6.1.7). Under these conditions, low precipitation may have influenced precipitation oxygen stable isotope composition.

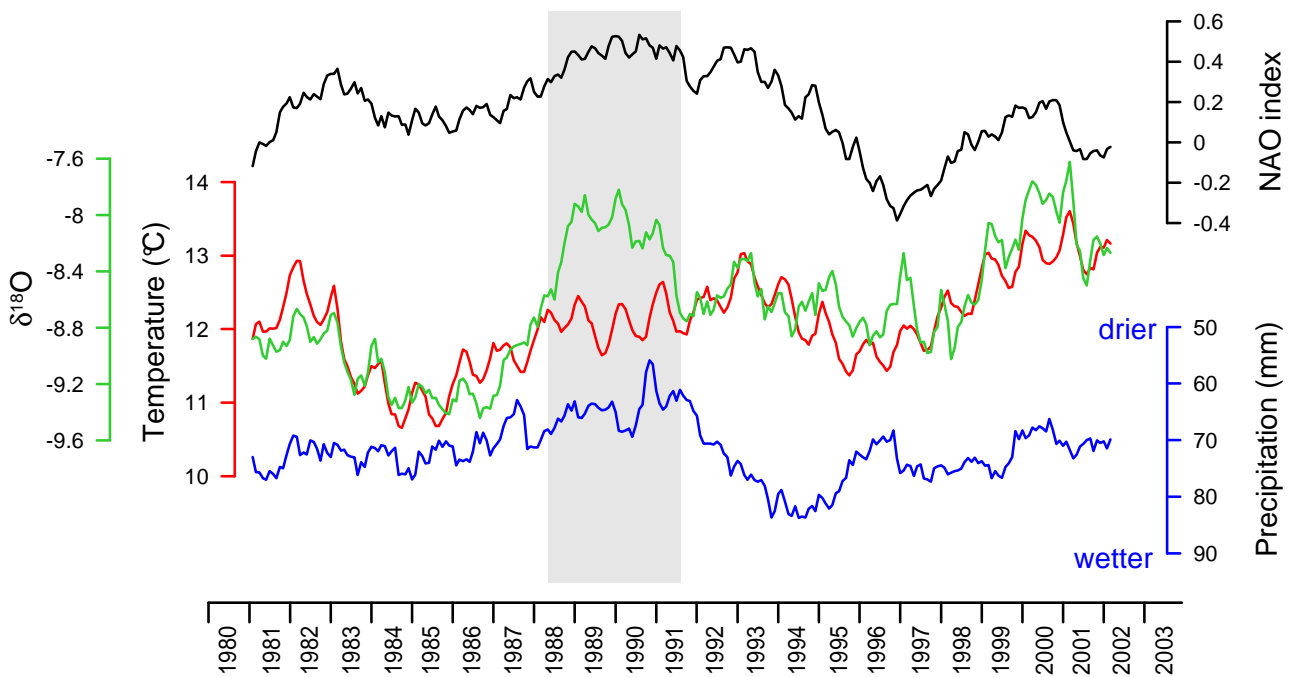


Fig. 6.1.7 – Data smoothing (moving averages on 25 points) of monthly precipitation (blue curve), $\delta^{18}\text{O}$ (green curve), temperature (red curve), and NAO index (black curve).

6.1.3 Present day atmospheric circulation in Sarajevo and its influence on the isotopic signal of precipitation

As described in the previous paragraph, precipitation $\delta^{18}\text{O}$ in the central Balkans is mainly related to changes in temperature that, on the long term, seems to be associated with the NAO trend. Precipitation amount has only a minor and very marginal influence in $\delta^{18}\text{O}$ fluctuations. In order to deeper investigate precipitation dynamics in the studied site, data related to sampled precipitation events in Sarajevo were examined.

Stable isotope composition of precipitation events was then compared with daily temperature (Fig. 6.1.8). A coefficient stronger than the one calculated from Zagreb GNIP data relates temperature variations and precipitation $\delta^{18}\text{O}$ ratios ($0.57\text{‰}/\text{°C}$; Fig. 6.1.8).

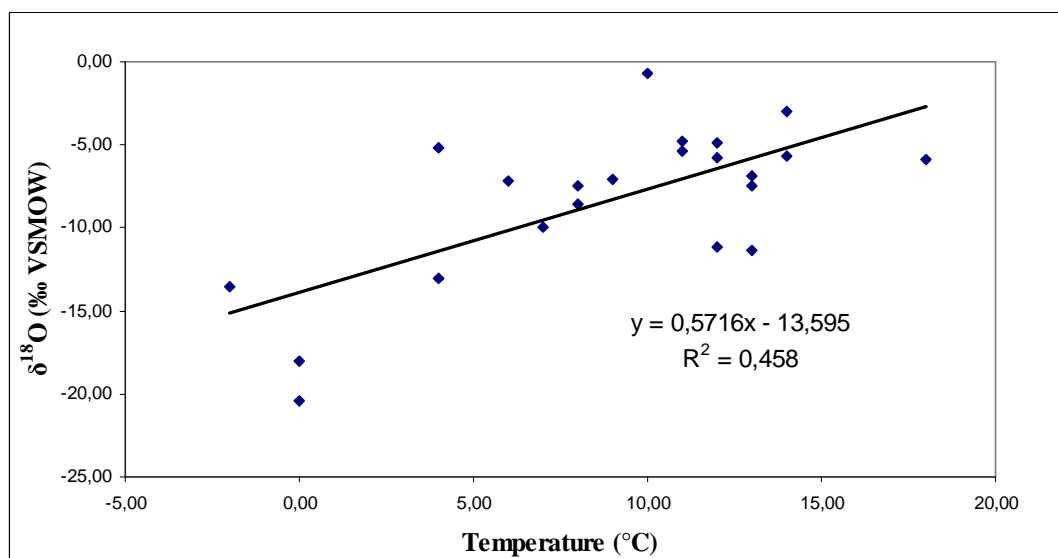


Fig. 6.1.8 – Relation between daily temperature (from www.wunderground.com) and $\delta^{18}\text{O}$ of sampled precipitation in Sarajevo.

Although the preponderant temperature dependence of precipitation $\delta^{18}\text{O}$ was demonstrated, it was noticed that other parameters, possibly related to atmospheric circulation, can play a marginal role in stable isotope variations. In order to better understand atmospheric dynamics at the studied site, air mass back trajectories were performed on rainy days in Sarajevo from January 2015 until July 2016 (Paragraphs 4.2.2 and 5.1.3). The results showed the presence of different storm tracks at both the seasonal and intra-seasonal scale. The trajectories of moisture-bearing air masses are of great importance in the understanding of the imprinted $\delta^{18}\text{O}$ signal. Indeed, the isotopic composition of the moisture source together with all the processes that occur during the movement of air masses (i.e. Rayleigh distillation and temperature at which condensation occurs) determines the final isotopic signatures of precipitation (cf. Paragraph 2.4.2.2).

In agreement with both the Zagreb and Sarajevo meteoric water line (Fig. 6.1.2), the general observed circulation patterns confirm the Atlantic Ocean as a possible major moisture source, as expected by the westerlies-dominated atmospheric circulation over Europe (e.g. Bisselick and Dolman, 2008). However, a possible increased contribution of moisture originating in the Mediterranean during the warmest seasons was observed (Paragraph 5.1.3).

Examining stable isotope composition of precipitation events, lighter $\delta^{18}\text{O}$ values were found during late autumn and winter (Fig. 6.1.9).

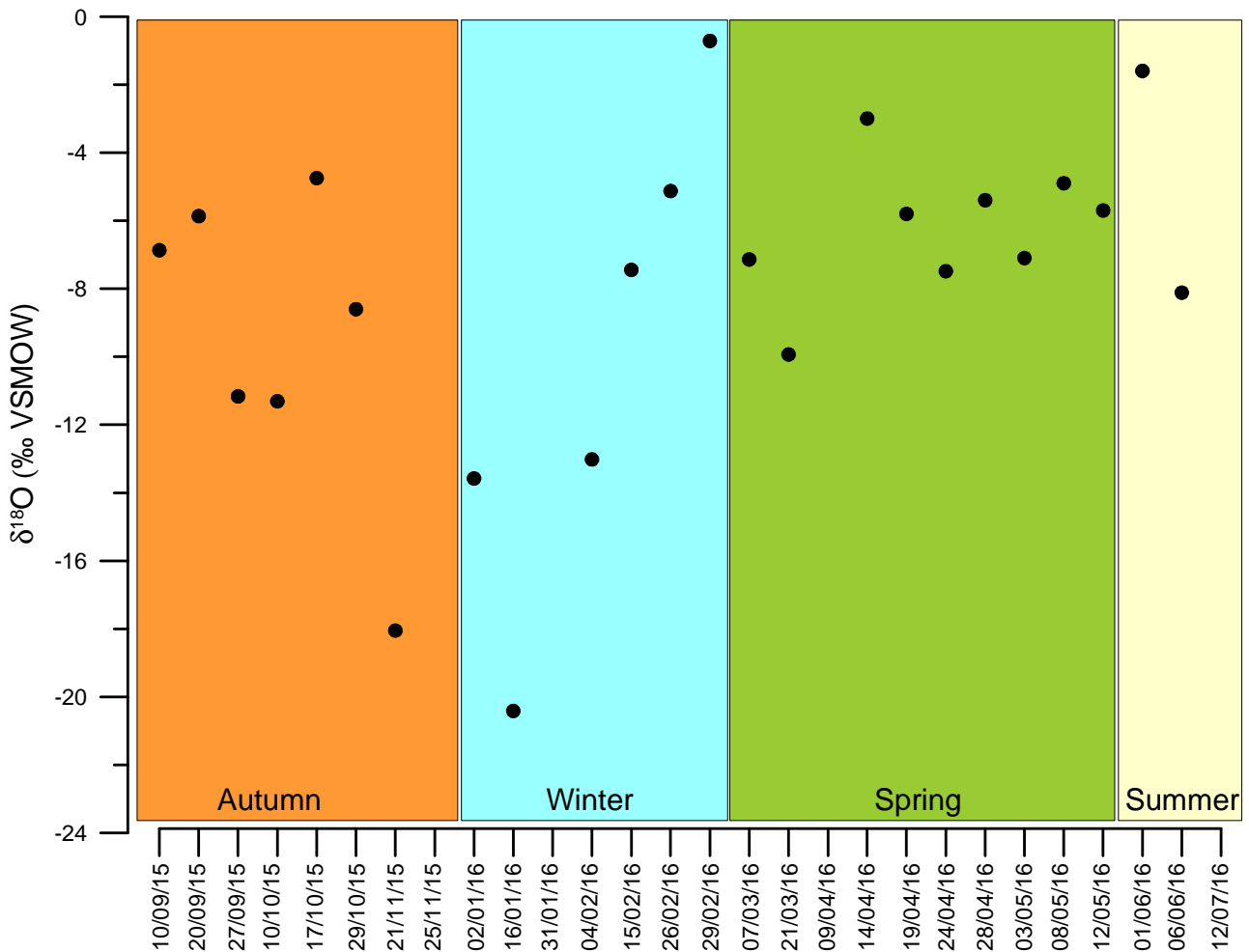


Fig. 6.1.9 – Black dots: $\delta^{18}\text{O}$ composition of sampled precipitation. The orange box corresponds to samples collected during the meteorological autumn (1st September – 30th November), the light blue box the ones collected during the meteorological winter (1st December – 28th February), the green one the samples collected during the meteorological spring (1st March – 31st May) and the light yellow one samples collected in summer (1st June – July).

This finding is in perfect agreement with the cold winter temperatures. However, some exceptions were found which consisted in late autumn and late winter precipitation characterised by respectively depleted and enriched values with respect to the seasonal trend. Considering daily temperature in Sarajevo it is still possible to find a correlation between these anomalies and temperature: the late November precipitation event presenting low $\delta^{18}\text{O}$ composition occurred at a temperature of 0°C, remarkably lower than the temperature average for that season (12.5 ± 3.3 °C); on the contrary, the late winter precipitation events presenting high $\delta^{18}\text{O}$ composition occurred at temperatures of 13°, 4° and 10°C, which are higher than the average temperature during the previous winter precipitation events (0.7 ± 3.1 °C) (Fig. 6.1.10).

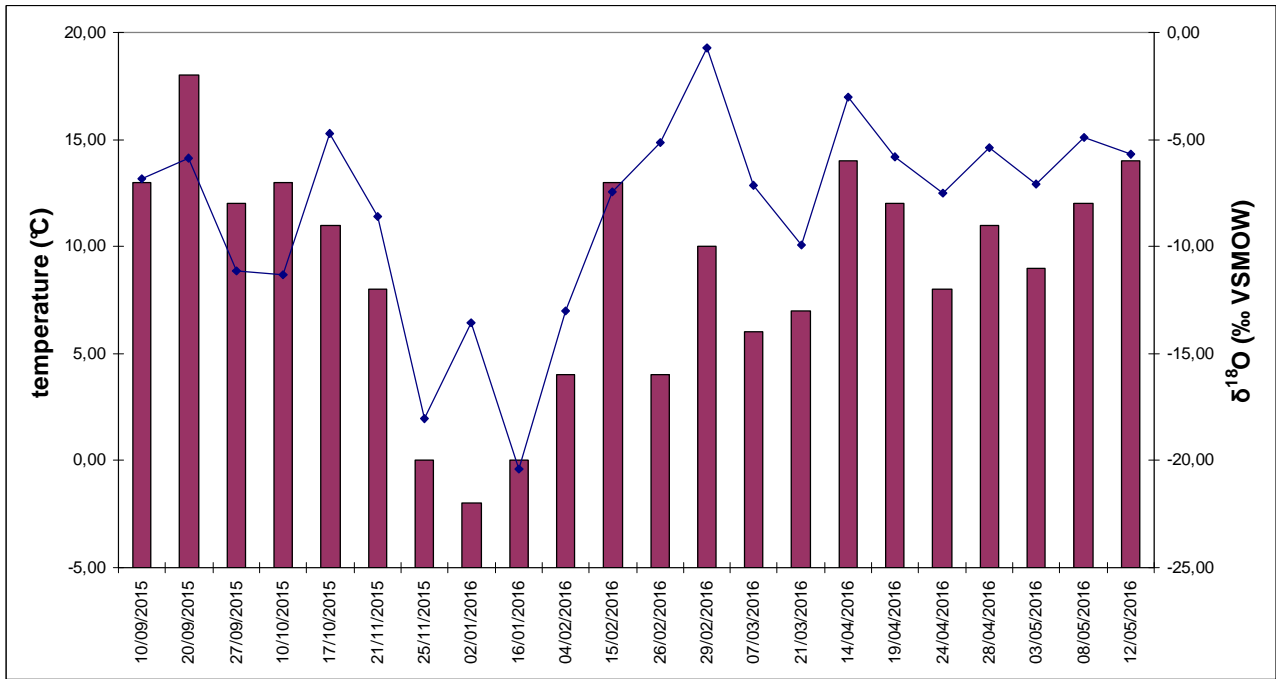


Fig. 6.1.10 – Daily temperature (purple squares) and $\delta^{18}\text{O}$ (blue points) in Sarajevo. Temperatures have been obtained from www.wuunderground.com

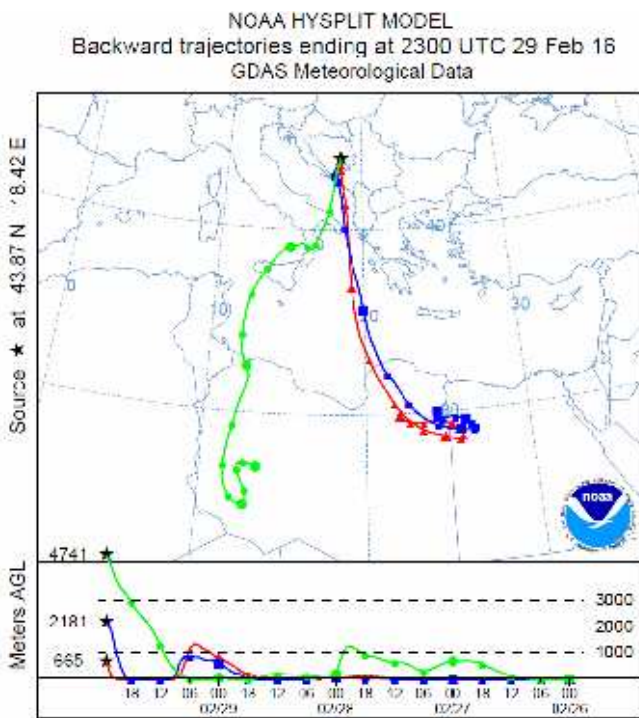


Fig. 6.1.11 – Backtrajectory analyses performed on February 29th, 2016.

Although the above described exceptions can be explained with temperature “anomalies” during these precipitation events, intra-seasonal circulation patterns may provide further details. An example is provided by the moisture-bearing air trajectory of precipitation occurred at the end of February 2016. The high $\delta^{18}\text{O}$ values of this precipitation event may be related to both relatively higher temperature and a southern air mass provenance (Fig. 6.1.11).

In conclusion, temperature appears to be the main factor influencing precipitation $\delta^{18}\text{O}$, but air mass trajectories can marginally trigger isotopic fluctuations intra-seasonally, smoothing or enhancing the temperature signal.

6.1.4 Cave hydrology and sensitivity to external changes

Cave monitoring covering the period spanning between May 2015 and July 2016 shows a good connection between cave hydrology and winter precipitation, especially at drip site D1 which presented peaks in dripping frequency after the most intense precipitation events during this season (Paragraph 5.1.1; Fig. 5.1). The potential infiltration calculated subtracting the potential evapotranspiration (PET, obtained using the Thornthwaite and Mather (1957) equation) from the average monthly precipitation (over the period 1992-2015) shows an extremely low infiltration during summer, due to the high temperature of this season, which is the responsible of the low-to-absent dripping recorded at both monitored drip sites. In addition, the available data highlighted a slightly longer, warm and dry season in 2015 compared to the previous 23-year period, which may have further contributed to the dripping dynamics (Fig. 6.1.12).

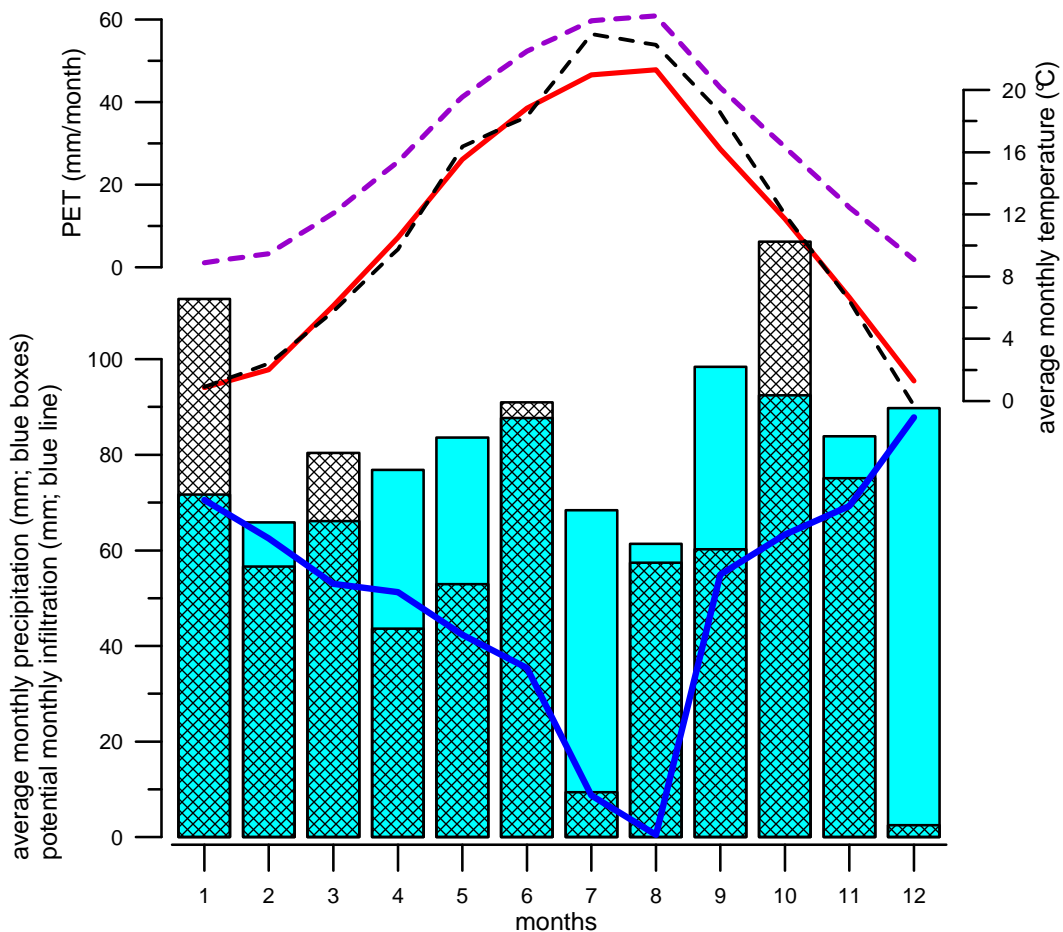


Fig. 6.1.12 – Average monthly temperature (red line: time interval 1992-2015; black dashed line: year 2015) and average monthly precipitation (blue boxes: time interval 1992-2015; black squared boxes: year 2015). The dashed purple line is the potential evapotranspiration (PET) calculated using average monthly temperature in the Thornthwaite and Mather (1957) equation; potential infiltration (blue line) was estimated as the difference between precipitation and PET. Data from the Sarajevo weather station, Federal Institute of Hydrometeorology (Bosnia and Herzegovina).

Thus, evapotranspiration is thought to have played an important role in summer hydrology and the presence of a strong seasonality of dripping is associated with the seasonality of effective rainfall. The different behaviour registered in drip site 2 (D2; Paragraph 5.1.1), which experienced a marked reactivation only in late January 2016 and almost no dripping between July 2015 and January 2016, is probably due to a different hydrologic behaviour possibly related to a thicker bedrock cover and/or flow paths with lower transmissivity, buffering the rainfall signal.

All monitored drip sites present relatively higher pH values in winter months if compared to summer and autumn measurements, when the most acidic drips have been detected (Fig. 6.1.13; Tab. 6.1.1). Lower pH values in summer and autumn are common in caves developed in Alpine environments and are compatible with lower cave ventilation during this season (e.g. Frisia et al., 2000; Spötl et al., 2005). These pH variations suggest the presence of higher calcite saturation indices during late summer and autumn, thus preventing and/or diminishing calcite precipitation during these seasons (Frisia et al., 2000). This is confirmed by the sparse growth rate data, which indicate calcite precipitation occurring mainly in winter, spring and early summer months at monitoring sites G1 and G3 (Paragraph 5.1.1).

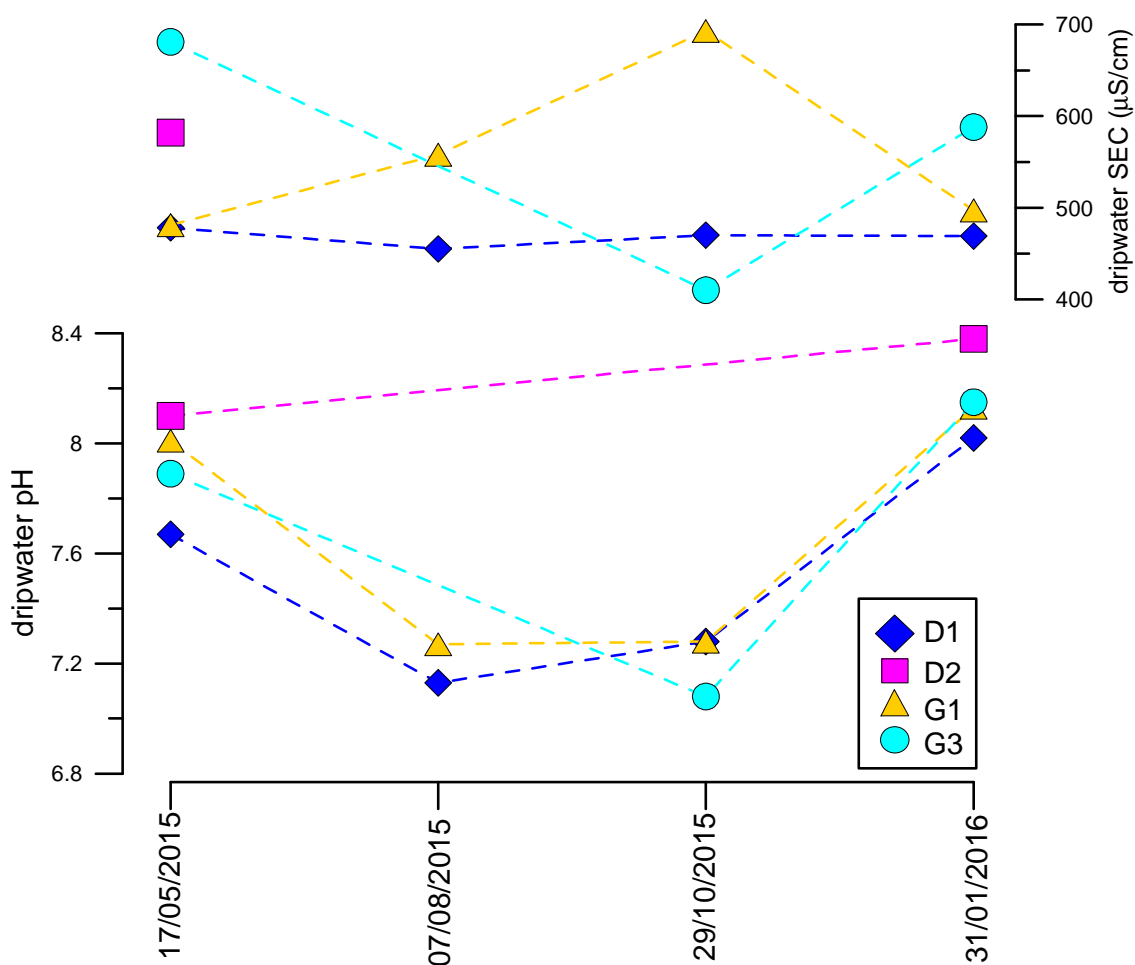


Fig. 6.1.13 – pH and specific electrical conductivity (SEC) measurements for drip sites D1, D2, G1 and G3 in Mračna Pečina Cave.

Conductivity measurements show instead different trends among the monitored drip sites. In particular, while D1 shows low variability, drip sites G1 and G3 present an opposite trend, with higher/lower values in summer/winter samples (Fig. 6.1.13). High conductivity at drip site G1 (October 2015) can be considered a consequence of the high measured pH, which allowed for a higher concentration of solute in the infiltrating water and higher calcite saturation index during a period of low cave ventilation (Smith et al., 2015). However, the drip water sample collected in July 2016 at this monitoring site has comparable low pH values with the one collected in October of the same year, but lower conductivity. This may be explained with higher ion concentration in drip water leached during vegetation dieback and/or lower prior calcite precipitation occurring in this season, even if further analyses would be necessary to corroborate these hypotheses. Increased ions in drip water during autumns are usually associated with colloids flushing during rapid infiltration events (Borsato et al., 2007 and reference therein). Unfortunately, a condition of high flow before the sampling of the 19th of October at drip site G1 cannot be verified. At the close monitoring site D1, relatively low and constant dripping was recorded at that time despite the recorded intense precipitation (Fig. 5.1; Paragraph 5.1.1).

Low electrical conductivity associated with high water pH at drip site G3 (October 2015) appears to contrast with the results described above at monitoring site G1. This monitoring site was chosen further away from the cave entrance close to drip site D2, which presented low to absent dripping from August 2015 until mid January 2016. The lower electrical conductivity may be explained with enhanced prior calcite precipitation at this site, thus lowering the solute content of drip water entering the cave (e.g. Fairchild et al., 2000).

Average $\delta^{18}\text{O}$ (‰ V-SMOW)	precipitation	D1	G1	D2	G3
All data Sept. 2015 – July 2016	-8.05 ± 4.70	-9.38 ± 0.06	-9.40 ± 0.17	-9.22 ± 0.26	-10.01 ± 0.20
Autumn and Winter	-9.76 ± 5.56	-9.40 ± 0.04	-9.40 ± 0.05		-10.17 ± 0.09
Winter	-10.87 ± 6.63	-9.43	-9.43	-9.16	-10.24
Spring and Summer	-6.02 ± 2.34	-9.35 ± 0.07	-9.40 ± 0.28	-9.25 ± 0.35	-9.85 ± 0.07

Tab. 6.1.1 – Average $\delta^{18}\text{O}$ composition of drip water samples collected between September 2015 and July 2016 and precipitation events collected in Sarajevo; average seasonal $\delta^{18}\text{O}$ composition of the collected water samples (autumn and winter – spring and summer); $\delta^{18}\text{O}$ composition of drip water in winter; average $\delta^{18}\text{O}$ composition of precipitation in winter.

Considering drip water stable isotope composition, drip sites D1 and G1 present similar isotopic values (Fig. 6.1.14). Their average $\delta^{18}\text{O}$ values, respectively -9.4 ± 0.17 and -9.38 ± 0.06 ‰, broadly correspond to the average $\delta^{18}\text{O}$ ratios of the sampled autumn and winter precipitation (-9.76 ± 5.56

‰), which is lower than the average $\delta^{18}\text{O}$ ratios of the sampled precipitation over the period September 2015 – June 2016 (-8.05 ± 4.70 ‰; Tab. 6.1.1). Cave temperature monitored in the area where the stalagmites were found, shows little variability during the year ($9.4 \pm 0.4^\circ\text{C}$; Paragraph 5.1.1): it is thus plausible to consider a possible temperature effect able to modify drip water $\delta^{18}\text{O}$ at the seasonal scale negligible. Drip site G3 displays slightly lower values (-10.01 ± 0.20 ‰). The slightly lower $\delta^{18}\text{O}$ values observed at drip site G3, may indicate a higher sensitivity of its feeding system to winter rainfall and/or spring snowmelt, which present a lighter isotopic signature (-10.87 ± 6.63 ‰; Tab. 6.1.13). If we look at the close monitoring site D2 (location in Fig. 4.2 in paragraph 4.2), we can see a reactivation of the site only during late winter and spring (Fig. 5.1; paragraph 5.1.1) but slightly higher drip water $\delta^{18}\text{O}$ composition. This delay with respect to site D1 may be due to the presence of an aquifer whose recharge occurs mainly during winter months, followed by strong evapotranspiration during the warm season (summer and early autumn). This different behaviour may be due to the presence of lower transmissivity and relatively lower sensitivity to precipitation events than the one feeding D1.

Although the data cover a limited period of time, a markedly stronger influence of autumn and winter precipitation in aquifer recharge can be inferred for all the monitored sites.

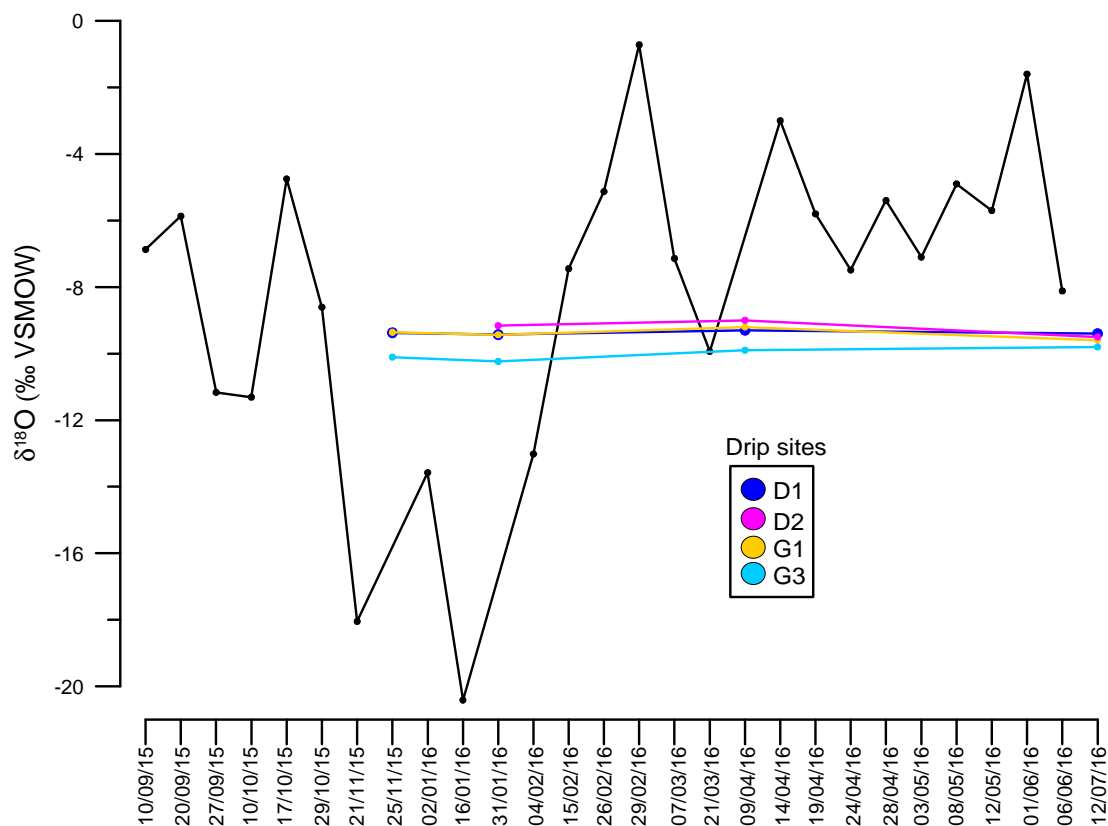


Fig. 6.1.14 – $\delta^{18}\text{O}$ composition of precipitation events sampled in Sarajevo (black dots and line) and of drip water collected at monitored drip sites D1 (blue), D2 (pink), G1 (yellow) and G3 (light blue) in Mračna Pećina cave,

6.1.5 Conclusions

The analyses and observations performed on present-day precipitation data show a major contribution of Atlantic moisture in precipitation of the Sarajevo area. Although the relation temperature- $\delta^{18}\text{O}$ is predominant, seasonal atmospheric circulation has a marginal influence on precipitation stable isotope composition. Monitoring of cave parameters showed a major reactivation of drip sites in response to winter and autumn precipitation. The reactivation of drip site D2 only in late winter and spring may be related to winter snowmelt and to a stronger sensitivity of aquifer recharge to winter precipitation. The few isotopic values of drip water show a major contribution of autumn and winter precipitation at all drip sites (especially G3). Dripwater from sites G1 and D1, located in the same area as the studied stalagmites, present similar isotopic values, which are close to the average autumn and winter precipitation $\delta^{18}\text{O}$ ratios. It is thus clear that both significant variation in average temperature and changes in seasonal precipitation can trigger drip water $\delta^{18}\text{O}$ fluctuation over time and can potentially be recorded in the speleothem calcite $\delta^{18}\text{O}$ ratios. If we consider the temperature-dependent fractionation between water and calcite precipitated under equilibrium conditions ($\sim -0.23\text{‰}/^\circ\text{C}$) acting in the opposite way as external temperature would do during the condensation process ($\sim 0.33\text{‰}/^\circ\text{C}$ according to Zagreb GNIP data and $\sim 0.57\text{‰}/^\circ\text{C}$ according to daily precipitation in Sarajevo), it is clear that only strong changes (at least a few degrees Celsius) in average temperature can be potentially recorded in stalagmites deposited in the studied cave. However such temperature changes are not realistic during the Holocene.

Even if temperature variations may have been recorded in the speleothem $\delta^{18}\text{O}$ profiles on the long-term scale (i.e. millennial), it is more reasonable to infer the major role of seasonal precipitation (i.e. proportion of winter and summer precipitation recharging the aquifer) in triggering Holocene stalagmite $\delta^{18}\text{O}$ variation in Mračna Pećina cave, at least at the decadal or multi-decadal time scale. In these terms, higher $\delta^{18}\text{O}$ values in stalagmites grown at or close to equilibrium conditions could be related to a stronger influence of summer precipitation in aquifer recharge, while lower $\delta^{18}\text{O}$ values could indicate a stronger contribution of winter precipitation, possibly with summer drought.

6.2 Age of the studied stalagmites

6.2.1 Introduction

Before discussing the geochemistry and petrography of the studied stalagmites, a Chapter about age modelling is developed. Age depth models were calculated from a Bayesian-Monte Carlo treatment of U-Th ages using a model developed by John Hellstrom (University of Melbourne, Australia). These have been used to interpolate the geochemical data and petrographic observations to allow for a paleoenvironmental/palaeoclimate interpretation.

The high concentration of detrital Th associated with the generally low U content was the main responsible for the large age uncertainties on radiometric ages. The $^{230}\text{Th}/^{232}\text{Th}$ activity ratios were extremely low for all the stalagmites (generally lower than 50) showing the presence of significant amount of detrital Th, with the exception of G5 (see tab. 5.3-5.6 in Chapter 5.3). These results made it necessary to introduce a correction of the obtained ages which was performed according to the stratigraphic approach described in Hellstrom (2006). Preliminary observations of thin sections did not allow for the identification of any obvious and pervasive diagenetic process affecting the studied stalagmites, thus suggesting the preservation of the original chemical signal and the potential reliability of the dating results. Indeed, radiometric ages can be considered reliable only when the system remains closed and there is no post depositional addition or removal of U and Th (Paragraph 2.4.2.1) However, despite the age corrections for detrital contamination, some ages from all stalagmites have been rejected by these models and were considered as possible outliers (red bold results in both tab. 5.3-5.6).

6.2.2 Age-depth model of stalagmite G5 and rejected ages

Stalagmite G5 started growing at ~75 ka. A hiatus identified at 86 mm from the top was dated between about 12.5 and 9.8 ka. Thus, only the portion above the identified hiatus was considered for this study since it grew during the Holocene. In the studied portion of this stalagmite, at 14, 20, 55 and 69 mm from the top (~6.8, 7.1, 8.7 and 9.2 ka according to the age model), four possible short growth interruptions were identified on the polished stalagmite section. These potential hiatuses were not considered in the age-depth model because the large age errors prevented their precise identification (Fig. 6.2.1). Only the U-Th age G5-3a(R) was rejected by the model since it was not in stratigraphic order, resulting younger than expected. Thin sections of this sample were not realised, thus it was not possible to examine the eventual presence of post depositional processes causing a not reliable U-Th result. However, since an extremely low quantity of powder

was used in the sample preparation (~28 mg) due to problems in sample preparation, this result was considered not reliable.

According to the calculated model, this sample showed a relatively regular growth with an average rate of ~0.02 mm/yr, from ~9.8 until 6.1 ka, with the exception of the period between ~7.7 and 7.1 ka when it decreased to ~0.01 mm/yr.

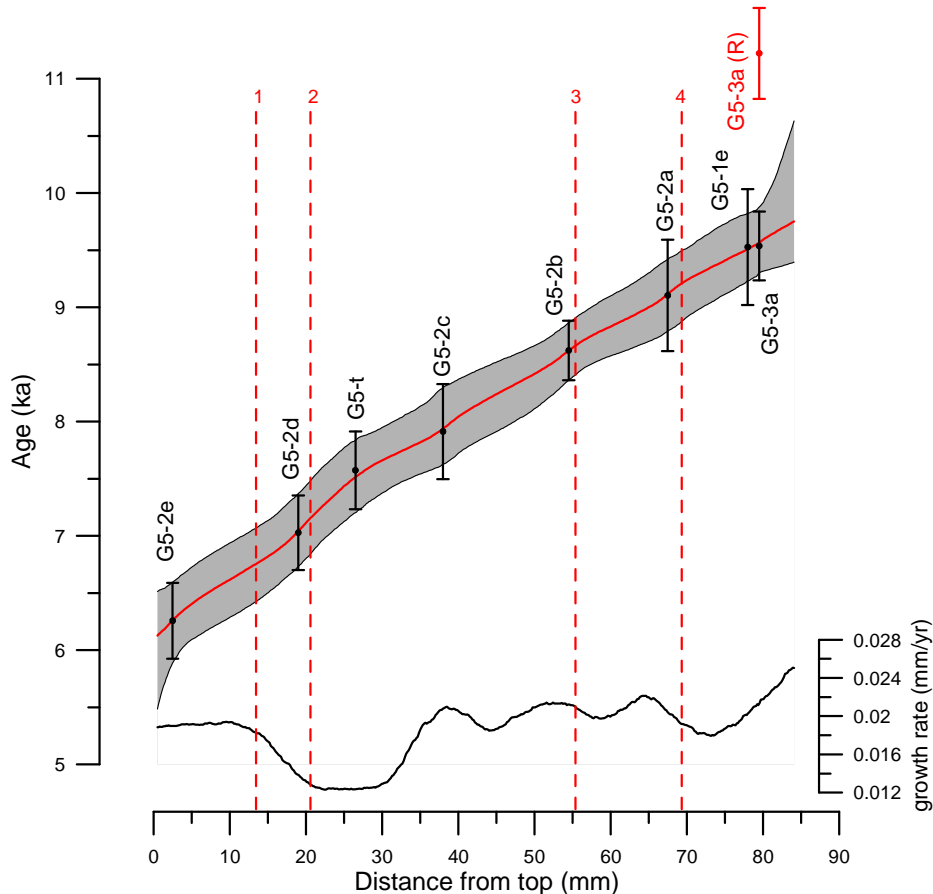


Fig. 6.2.1 – Age-depth model of stalagmite G5. Black vertical lines represent the U-Th results with their uncertainties used for the models calculation. The age rejected from the model is indicated in red. The red line indicates the values corresponding to the 50th percentile and corresponds to ages used for stable isotope interpolation. The grey shadow indicates the error affecting the model: the upper boundary corresponds to the 97th percentile values; the lower boundary corresponds to the 3rd percentile values. Vertical red dotted lines indicate the hiatuses not considered in the age-depth model. The curve at the bottom represents the growth rate (mm/yr) according to the age-depth model.

6.2.3 Age-depth model of stalagmite BS8 and rejected ages

BS8 started growing at ~12 ka with an average growth rate of ~0.01 mm/yr until ~10.4 ka. Then it slightly accelerated to 0.03 mm/yr until ~8.8 ka and stopped definitively at ~0.7 ka. Two major hiatuses were identified at 50.5 and 91 mm from top and considered in the age-depth model (Fig. 6.2.2). These two major hiatuses occurred, respectively, between ~5.8 and ~7.5 ka and ~7.9 and 8.8 ka. Between these two growth interruptions, the stalagmite grew with an average growth rate of

~0.16 mm/yr for about 100 years followed by a deposition rate of ~0.06 mm/yr. During the second half of the Holocene (from about 5.7 ka), the stalagmite slowed down to ~0.02 mm/yr until ~0.7 ka when it stopped growing (Fig. 6.2.2). Minor hiatuses were identified at 9, 21, 35, 123 and 130 mm from the top, occurring at ~1.7, 3.1, 4.8, 9.9 and 10.2 ka. As in the previous stalagmite, these hiatuses were not added to the age model because: 1) the model used for age-depth calculation requires more than 4 dates in order to run correctly; 2) the large age errors prevented their precise identification. In particular, since only three dates were available between 91 and 51 mm from the top, a linear function was used for the construction of an age-depth curve of this portion. According to the model, the black layer at 7 mm from the top has been dated between ~1.30 and 1.70 ka.

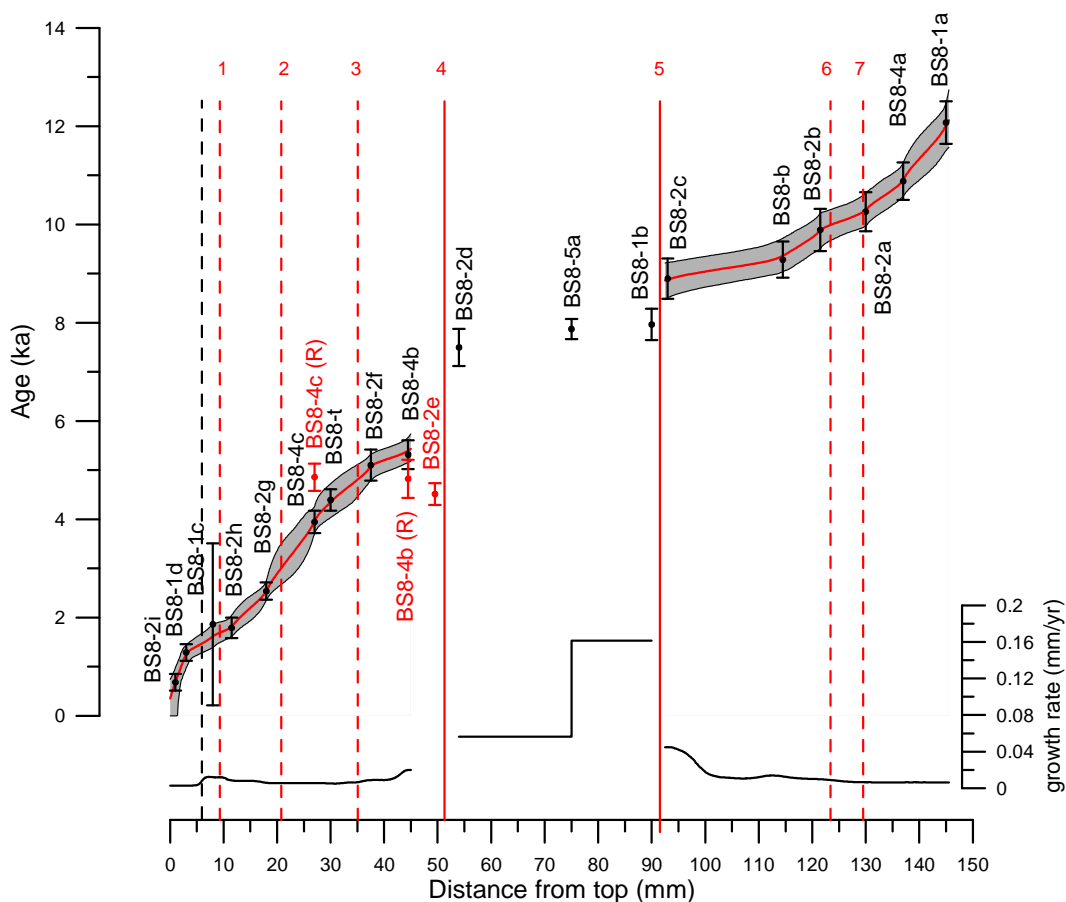


Fig. 6.2.2 – Age-depth model of stalagmite BS8. Black vertical lined represent the U-Th results with their uncertainties used for the models calculation. The age rejected from the model are indicated in red. The red line indicates the values corresponding to the 50th percentile and corresponds to the ages used for stable isotope interpolation. The grey shadow indicates the error affecting the model: the upper boundary corresponds to the 97th percentile values; the lower boundary corresponds to the 3rd percentile values. Between 51 and 90 mm from the top, the error on the model is not represented as its calculation was not possible due to the adoption of linear interpolation for the calculation of the age model in this portion. Red lines indicate the two major hiatuses considered in the age-depth model, while red dotted lines indicate minor hiatuses not considered in the model. The black dotted line indicates a dark layer found close to the stalagmite top. The curve at the bottom represents the growth rate (mm/yr) according to the age-depth model. Between the two major hiatuses (4 and 5) the growth rate was calculated using the U-Th ages.

In this stalagmite, 3 out of 21 dates were rejected since they were not in stratigraphic order according to the age-depth model based on the whole set of dating. In particular, sample BS8-2e was rejected as its age resulted younger than expected: according to petrography, evidence of possible diagenesis is visible at this sample location (Fig. 6.2.3).

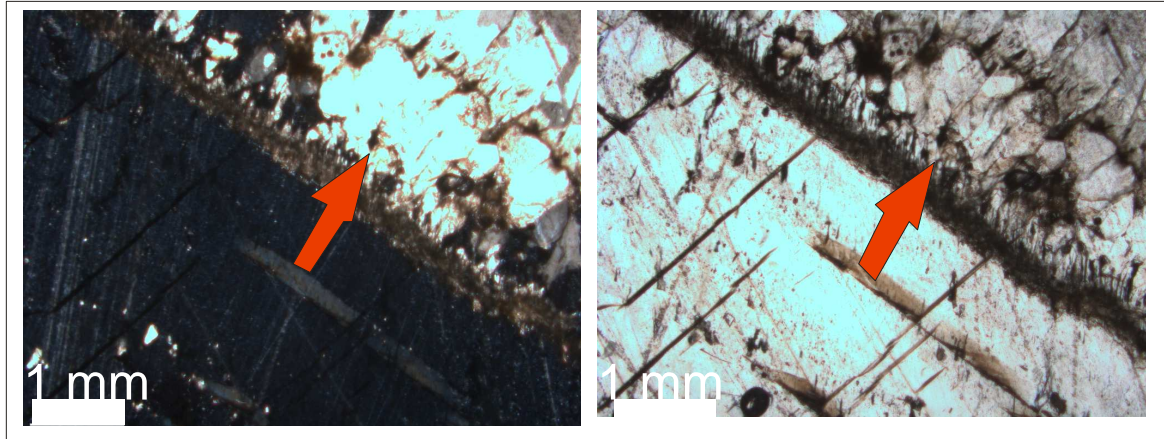


Fig. 6.2.3 – Thin section of BS8 corresponding to BS8-2e dating sample under normal (right) and polarised light (left). Red arrows indicate the portion above the hiatus where recrystallization might have occurred.

Ages BS8-4c (R) and BS8-4b (R) were analysed to try to improve the resolution of samples BS8-4c and BS8-4b. However the main problem regarding these results is related to the lack of replication among these two couples of samples (Fig. 6.2.2). The groups of laminae where they were sampled present various sizes of porosities clearly visible on the polished surface. Although there is no evidence of recrystallization occurring in these areas, the cryptic diagenesis described in Bajo et al. (2016) may be the responsible of the lack of replication. The BS8-4c (R) and BS8-4b (R) samples have been considered not reliable because they were sampled in a less compact area of the stalagmite and provided ages much older than other ages obtained from the same laminae.

6.2.4 Age-depth model of stalagmite BS9 and rejected ages

Only the portion above the dendritic calcite identified in stalagmites BS9 has been studied. This portion started growing at ~5.9 ka. The duration of the hiatus at 77 mm from the top was not determined due to the large age uncertainties of dating samples BS9-1a and BS9-b. Unfortunately, also U-Th ages close to the hiatus identified at 62 mm from the top were affected by large age errors due to the high detrital Th content, preventing the identification of its duration as well. Thus it was possible to calculate an age-depth model only for the portion above the hiatus identified between about 4.5 and 2.3 ka, while a linear function was used for the older part (Fig. 6.2.4). Even

if the precise timing of the above mentioned hiatus has not been resolved, it can be stated that the stalagmite stopped growing after about 4.5 ka and started again at about 2.3 ka with a growth rate of ~0.06 mm/yr until ~1.8 ka. Between 1.8 and 1.2 ka it slowed down to 0.02 mm/yr to accelerate again to 0.08 mm/yr during the last 200 years of growth. The stalagmite stopped growing at about 1 ka. According to the age-depth model, the dark interval identified between 16 and 13 mm from the top was deposited between 1.1 and 1.2 ka.

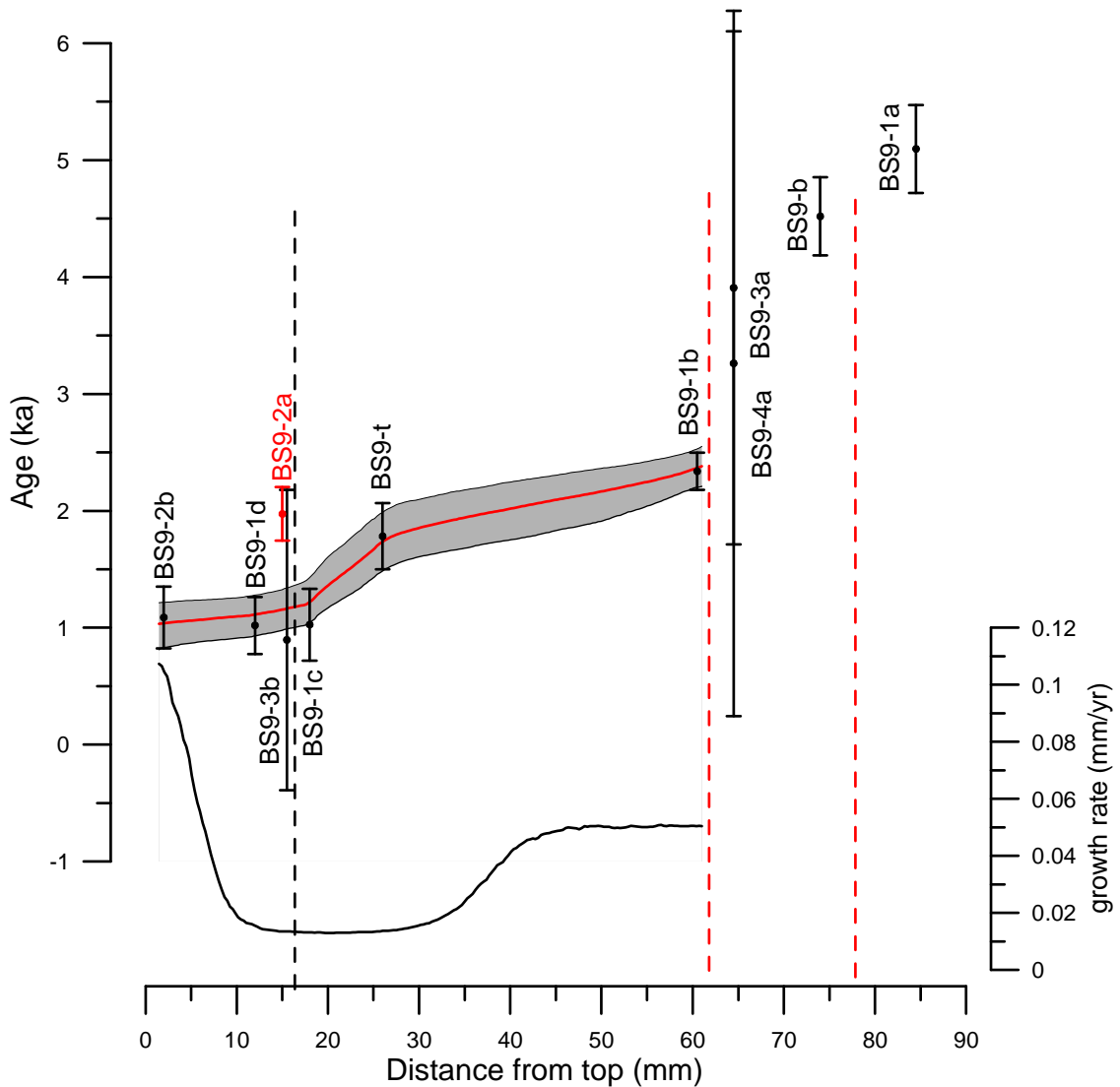


Fig. 6.2.4 – Age-depth model of stalagmite BS9. Black vertical lined represent the U-Th results with their uncertainties used for the models calculation. The age rejected from the model are indicated in red. The red line indicates the values corresponding to the 50th percentile and corresponds to the ages used for stable isotope interpolation. The grey shadow indicates the error affecting the model: the upper boundary corresponds to the 97th percentile values; the lower boundary corresponds to the 3rd percentile values. The red dotted line indicates a major hiatus. The black dotted line indicates a dark layer found close to the stalagmite top. The curve at the bottom represents the growth rate (mm/yr) according to the age-depth model.

For stalagmite BS9 only BS9-2e U-Th result was rejected in the age-depth model as it resulted older than expected according to its stratigraphic position (Fig. 6.2.4). This can be easily explained by extremely high detrital Th contamination that did not allow for an efficient age correction. This stronger contamination in comparison with other parts of the stalagmite can be explained by the incorporation of a dark layer, which is believed to be a soot layer (Chapter 6.5).

Finally, the large Th contamination leading to huge error bars on BS9-3a and BS9-4a ages can be explained by the occurrence of clayish laminae that were accidentally incorporated in the dating samples (Fig. 6.2.5).

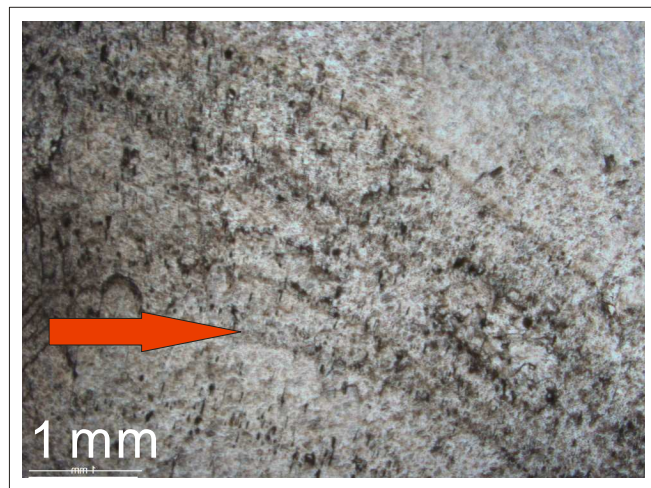


Fig. 6.2.5 – Thin section of stalagmite BS9 corresponding to the sampling position of samples BS9-3a and BS9-4a. The red arrow indicates a surface containing detrital material.

6.2.5 Age-depth model of stalagmite BS14 and rejected ages

BS14 started growing at ~6.4 ka and stopped during the late Holocene, after the deposition of a dark layer similar to the one observed in stalagmites BS8, BS9 and BS15. Unfortunately, its top age is uncertain due to the unreliability of the U-Th results in its younger portion. Indeed, in this sample, high porosity and initial phases of crystal cannibalisation are found above 25 cm from the top associated with the elongated columnar microcrystalline fabric (cf. Paragraph 5.2.4). These may have lead to U leaching and an opening of the system. Thus, ages of this portion must be considered with caution.

According to the age-depth model, this stalagmite started being deposited with a growth rate of ~0.04 mm/yr which slightly accelerated to 0.05 mm/yr at about 5.7 until ~5 ka. From this period onwards the stalagmite grew with a slower rate of approximately 0.01 mm/a (Fig. 6.2.6). The two most important growth interruptions identified in thin sections in BS14 occur between ~4.4 and 4.0 ka (25 mm) and between ~3.4 and 2.8 ka (15 mm). However the large age uncertainty affecting

the dating results, due to high detrital Th contamination, prevented estimating the precise duration of the hiatuses and allowed for the consideration of only the hiatus at 15 mm from the top in the age-depth model calculation (Fig. 5.13). According to the age model, the dark layer visible close to the top formed between about 1.6 and 2.5 ka.

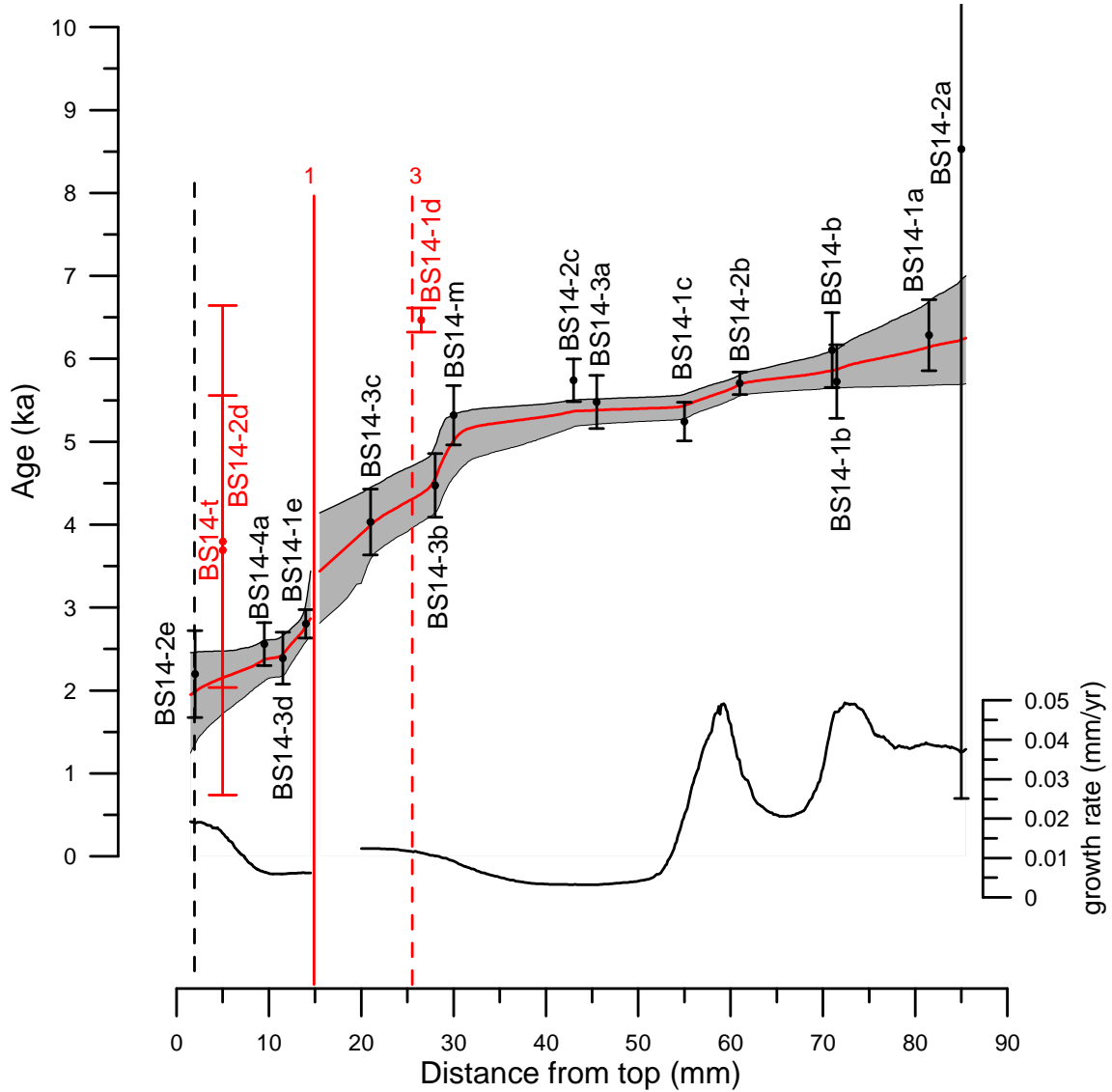


Fig. 6.2.6 – Age-depth model of stalagmite BS14. Black vertical lines represent the U-Th results with their uncertainties used for the models calculation. The age rejected from the model are indicated in red. The red line indicates the values corresponding to the 50th percentile and corresponds to the ages used for stable isotope interpolation. The grey shadow indicates the error affecting the model: the upper boundary corresponds to the 97th percentile values; the lower boundary corresponds to the 3rd percentile values. The red line indicates a hiatus considered in the age-depth model (surface 1 in plate 4, Chapter 5). The red dotted line indicates hiatus which was not considered in the age-depth model (surface 3 in Plate 4, Chapter 5). The black dotted line indicates a dark layer found close to the stalagmite top. The curve at the bottom represents the growth rate (mm/yr) according to the age-depth model.

Three ages from the upper portion of BS14 were rejected since they were affected by age inversions; two of them (BS14-t and BS14-2d; Fig. 6.2.6)

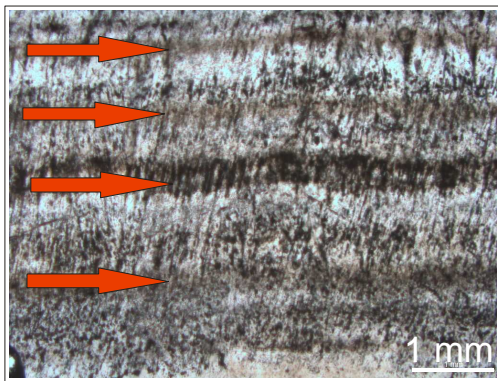


Fig. 6.2.7 – Thin section image corresponding to the area where samples BS14-t and BS14-3d were drilled. The red arrows indicate laminae possibly incorporating foreign particles.

were affected by large age errors due to high content of detrital contamination which can be explained with the accidental incorporation of laminae rich in foreign particles (Fig. 6.2.7). One major growth interruption is found between about 3.4 and 2.9 ka according to the age model (Surface 2 in Plate 4). However two more surfaces were recognised as possible growth interruptions and found at ~3.7 and 4.3 ka.

Unlike the samples described above, the 3rd rejected age from stalagmite BS14 (BS14-1d) resulted much older than expected for its stratigraphic position (Fig. 6.2.6). This

sample corresponds to a layer presenting a dense brown lamination ending at its base with a sharp crystal growth interruption (Fig. 6.2.8). The rejection of this age was based on the stratigraphic approach according to the U-Th results obtained in the younger and older portions of this stalagmite. This older-than-expected age may be the result of local opening of the system caused by U leaching related to small scale dissolution visible in thin section (Fig. 6.2.8, blue arrows). These dissolution phenomena could be related to the oxidation of the organic matter forming the brownish lamination (cf. Frisia, 1996).

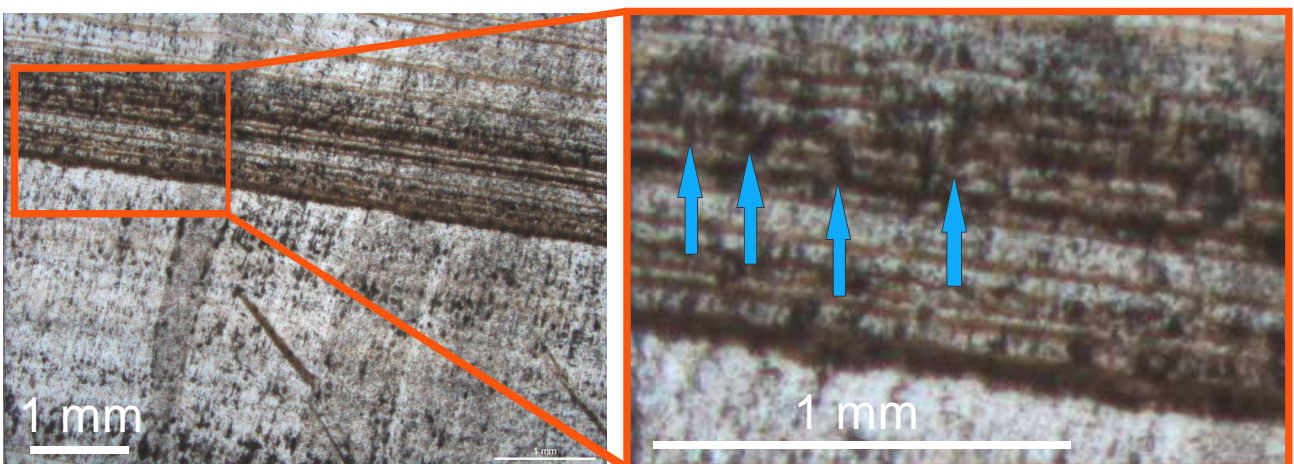


Fig. 6.2.8 – Petrography corresponding to sample BS14-1d (red arrow in the images on the left). The blue arrows on the right indicate possible small scale dissolution occurring where the brown laminae are present.

6.2.6 Age-depth model of stalagmite BS15 and rejected ages

Although 6 out of 21 U-Th ages have been rejected, as they were not coherent with the general stratigraphic order, the obtained model presents a lower uncertainty if compared the other stalagmites collected in Mračna Pećina Cave.

BS15 started growing ~4.3 ka with a rate of ~0.02 mm/yr until 2.7 ka, when it accelerated to 0.04 mm/yr until 2.2 ka. Between about 2.2 and 2.1 ka a fast growth was found (~0.12 mm/a). This fast growing period was followed by a decrease to 0.06 mm/a until 1.9 ka when a further decrease to 0.02 mm/yr occurred until the stalagmite stopped growing (~0.7 ka; Fig. 6.2.9).

A possible growth interruption is present at 18 mm from the top, corresponding to ~1.6 ka according to the age-depth model. The dark layer observed in all stalagmites near the top was dated between ~1 and 1.3 ka in BS15.

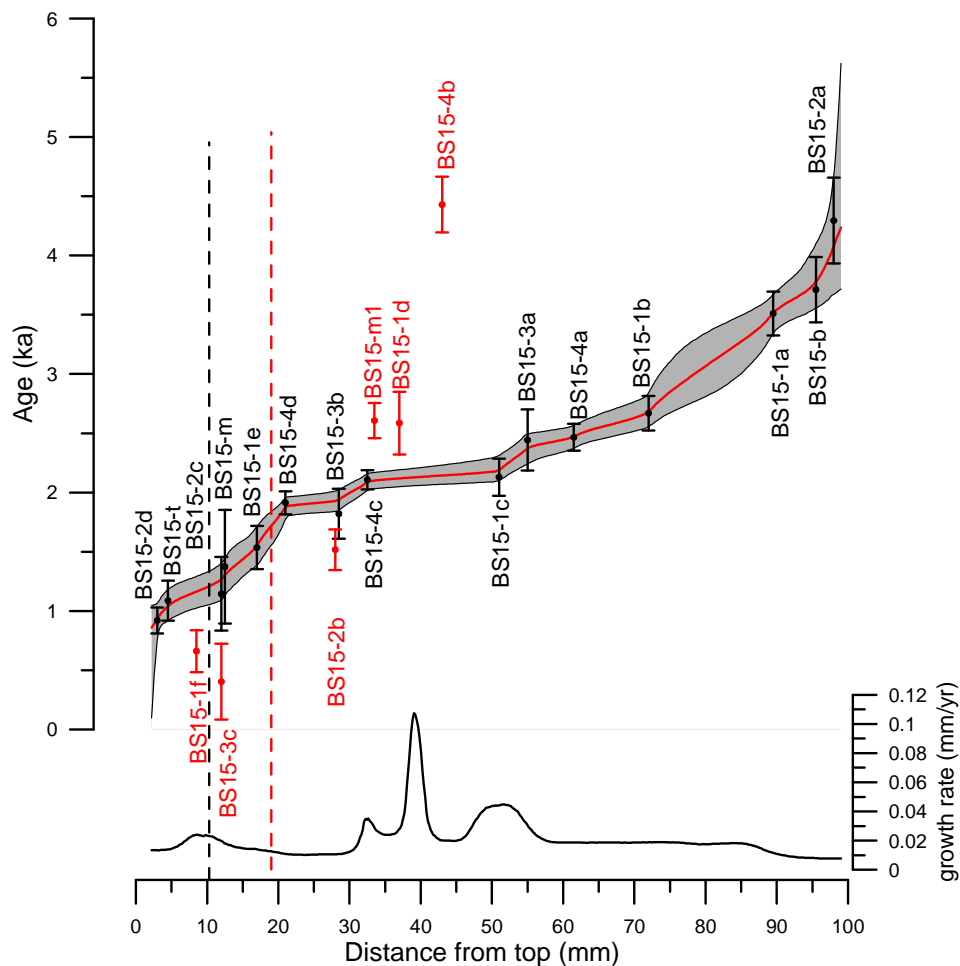


Fig. 6.2.9 – Age-depth model of stalagmite BS14. Black vertical lined represent the U-Th results with their uncertainties used for the models calculation. The age rejected from the model are indicated in red. The red line indicates the values corresponding to the 50th percentile and corresponds to the ages used for stable isotope interpolation. The grey shadow indicates the error affecting the model: the upper boundary corresponds to the 97th percentile values; the lower boundary corresponds to the 3rd percentile values. The black dotted line indicates a dark layer found close to the stalagmite top. The curve at the bottom represents the growth rate (mm/yr) according to the age-depth model.

In particular, samples BS15-1f, BS15-3c and BS15-1d resulted younger than expected according to their stratigraphic position. The rejection of the first two ages can be easily explained with the incorporation of some dendrite from the stalagmite flanks (Plate 4, Chapter 5): the presence of dendrite does not guarantee the maintenance of a closed system in this area explaining the unreliability of these ages. On the contrary, petrography observations where sample BS15-1d was taken did not show any clear feature that would indicate the opening of the system. However the presence of a fracture visible on the polished stalagmite surface may have caused capillary water infiltration causing cryptic diagenesis not visible at an observation through the optic microscope (e.g. Bajo et al., 2016). Dating results of samples BS15-m1, BS15-2b and BS15-4b have been rejected as they resulted older than expected according to their stratigraphic position. For these samples small-scale dissolution evidences similar to the ones observed in BS14 were identified as possible clues for U leaching (e.g. Fig. 6.2.8).

6.2.6 Comparison between stalagmite growth rates

Stalagmite formation is directly related to the amount of water discharge; calcite deposition rate depends on the degree of saturation of calcite in drip water, which is closely related to the difference between groundwater and cave air $p\text{CO}_2$ (e.g. Fairchild and Baker, 2012 and reference therein). In order to investigate the presence of eventual similarities in growth dynamics of the studied stalagmites, their growth rates have been compared (Fig. 6.2.10). Unfortunately, any remarkable similarity was identified. The detection of differences in the timing of growth rate changes may be both related to the uncertainties on the age models (which prevented the identification of small changes in growth rate) and to site-dependent variations in the feeding system of each speleothem.

However, considering stalagmites sampled in Mračna Pećina cave, it can be noted that 3 out of the 4 samples mainly grew during the second half of the Holocene, while stalagmite BS8 is the only one which started during the Early Holocene and recorded its fastest growing phase between about 8 and 7.5 ka. This may indicate that only after ~6 ka conditions more favourable to speleothem deposition were met in this cave.

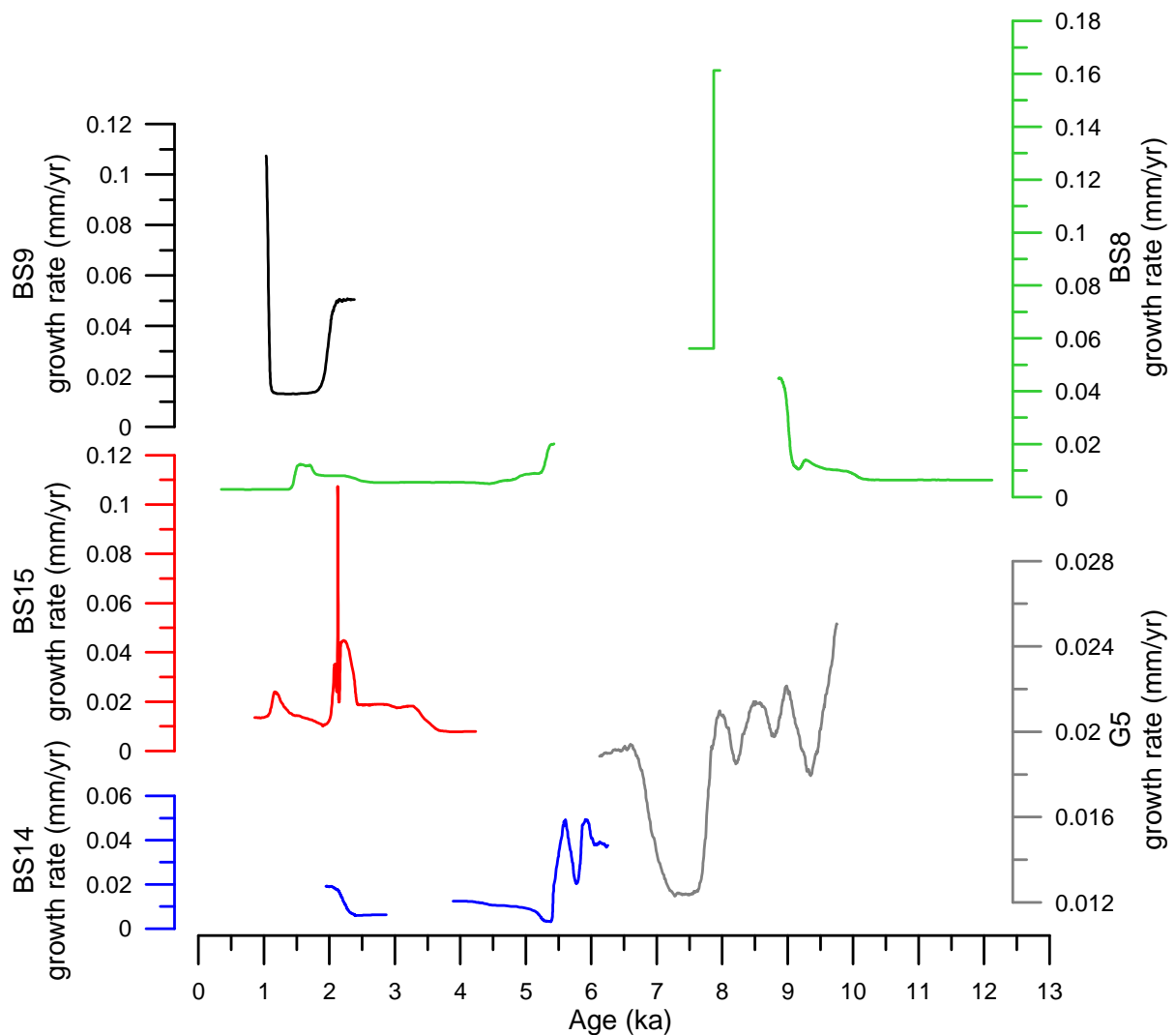


Fig. 6.2.10 – Growth rate (mm/yr) according to age-depth models for all the studied stalagmites.

6.2.7 Conclusions

Ages of the studied stalagmites were determined using the U-Th disequilibrium method. Unfortunately, the presence of strong detrital contamination during calcite deposition prevented the obtaining of precise U-Th ages. Some results have been considered not reliable on the basis of petrographic observations. Nevertheless, relatively reliable age-depth models were calculated using a model developed by John Hellstrom (University of Melbourne, Australia). However the presence of large age uncertainties due to both large U-Th age error bars and several growth interruptions of these samples must be taken into account when using these models to interpolate geochemical and petrographic observations for past climate and/or environment investigations.

6.3 Petrographical and geochemical changes in the Bosnian stalagmites

6.3.1 Introduction

Stalagmites are considered excellent continental materials for the study of past climate changes thanks to their formation in a relatively stable environment, protected from erosion and weathering processes, and thanks to the possibility of obtaining precise ages with the U-Th disequilibrium technique. Oxygen and carbon stable isotope ratios are the most commonly used climate and environmental proxies extracted from stalagmites (e.g. McDermott, 2004; Fairchild and Baker, 2012). The interpretation of the climate signal relies on the assumption that carbonate precipitation and stable isotope fractionation occurred under equilibrium conditions. This condition has been routinely validated with the Hendy test (1971). However, this test presents some limitations (e.g. Dorale et al., 2002; Spötl & Mangini, 2002; Couchoud, 2008; Dorale & Liu, 2009; Lachniet, 2009). In fact, there are cases in which stalagmites apparently affected by disequilibrium fractionation still preserve climate signals (e.g. Dorale & Liu, 2009; Lachniet, 2009). In addition, even stalagmites influenced by disequilibrium isotope fractionation, which occurs more frequently than previously believed, can indirectly provide information about climate and environmental changes as disequilibrium conditions can be triggered by factors related to climate (e.g. Hellstrom et al., 1998; Plagnes et al., 2002; Genty et al., 2006; Lachniet, 2009).

Further insights in the interpretation of the signals recorded by stalagmites can be provided by petrographic observations. The arrangement of calcite crystals in stalagmites changes under different hydrological conditions, chemistry of the feeding waters, outgassing and presence of impurities, providing additional information on the chemical and physical environment of formation and, thus, facilitating the interpretation of the stable isotope signal (e.g. Frisia et al., 2000; Couchoud, 2006; Frisia and Borsato, 2010; Matthey et al., 2010; Belli et al., 2013; Riechelmann et al., 2014; Frisia, 2015). According to Frisia (2015), the fabrics of speleothems are a useful, complementary tool to recognise the presence, and evaluate the intensity, of disequilibrium isotopic fractionation. Calcite fabrics and the $\delta^{13}\text{C}$ signal in particular can constrain interpretations because this isotopic ratio is more responsive to conditions associated with local soil CO_2 production and hydrology (e.g. Frisia, 2015). In particular, drip-rate variations influence the extent of time for degassing which can result in enrichment in ^{13}C (Dreybrodt, 1988; Usdowski & Hoefs, 1990).

The most recent and comprehensive speleothem calcite fabric classification has been proposed by Frisia (2015). It reports a methodology for fabric identification and for the sequential coding of fabrics, reflecting, in a hierarchic system, the conditions of precipitation: drip rate, supersaturation,

Mg/Ca ratio, and presence of impurities in the feeding waters. The coded fabrics can then be plotted in an age model, allowing comparison with the other geochemical time-series of the speleothem.

In this study, we examined five stalagmites picked up, already broken, in Mračna Pećina and Govještica caves (Bosnia and Herzegovina). A detailed petrographic study, coupled with stable isotope variations of these samples and trace element composition of one stalagmite, has allowed us to explore the possibility of extracting palaeoenvironmental signals from these samples, which otherwise would have been considered unsuitable for past climate reconstruction based on classic stable isotope studies. These samples are nevertheless potential natural archives for this region (the Dinarides), which has scarce palaeoclimate records so far.

6.3.2 Trace element variations in stalagmite BS15

The trace element composition of speleothems is related largely to hydrochemical processes in the unsaturated zone overlying the cave (i.e., Roberts et al., 1998; Huang & Fairchild, 2001; Fairchild et al., 2006; Borsato et al., 2007; Fairchild & Treble, 2009). Variations in calcite trace element concentration thus provide information on water-rock interaction, which relates to climate (Fairchild & Treble, 2009). In addition, the type and density of vegetation cover, which can be either related to climate or human activities, can influence trace element variation (Borsato et al., 2007). The understanding of the mechanisms responsible for their fluctuations in a given cave site is crucial for a correct interpretation of the trace element environmental significance.

Trace elements were analysed only in stalagmite BS15, since it was considered the most suitable sample for this analyses. In this sample, Sr and Mg concentrations show a negative correlation on a multi-annual scale (i.e. millimetre scale: $r = -0.615$; $p\text{-value} = 1.2\text{E-}11$; Fig. 6.3.1; Tab. 6.3.1). This opposed behaviour, also observed by Roberts et al. (1998) and Treble et al. (2013) would exclude the occurrence of prolonged and intense dry periods causing relevant phases of prior calcite precipitation (PCP) at least at a decadal time scale. This phenomenon, in fact, would be reflected in a positive correlation of both trace elements (Fairchild & Treble, 2009). Mucci and Morse (1990) demonstrated that temperature influences variations in Mg concentration. However, Mg concentration is also closely related to water residence time: drier conditions induce longer residence times and allow for selective leaching of Mg from soil or host rock, when the host rock is an Mg-bearing carbonate/metamorphic/igneous rock (Plummer, 1977; Fairchild et al., 2000). Sr can be instead related to calcite precipitation rate, where higher concentrations would indicate faster speleothem growth (Huang & Fairchild, 2001). The comparison of the Sr profile with the BS15

growth rate age model would confirm this pattern, with higher Sr content during period of fast growth (Fig. 6.3.1).

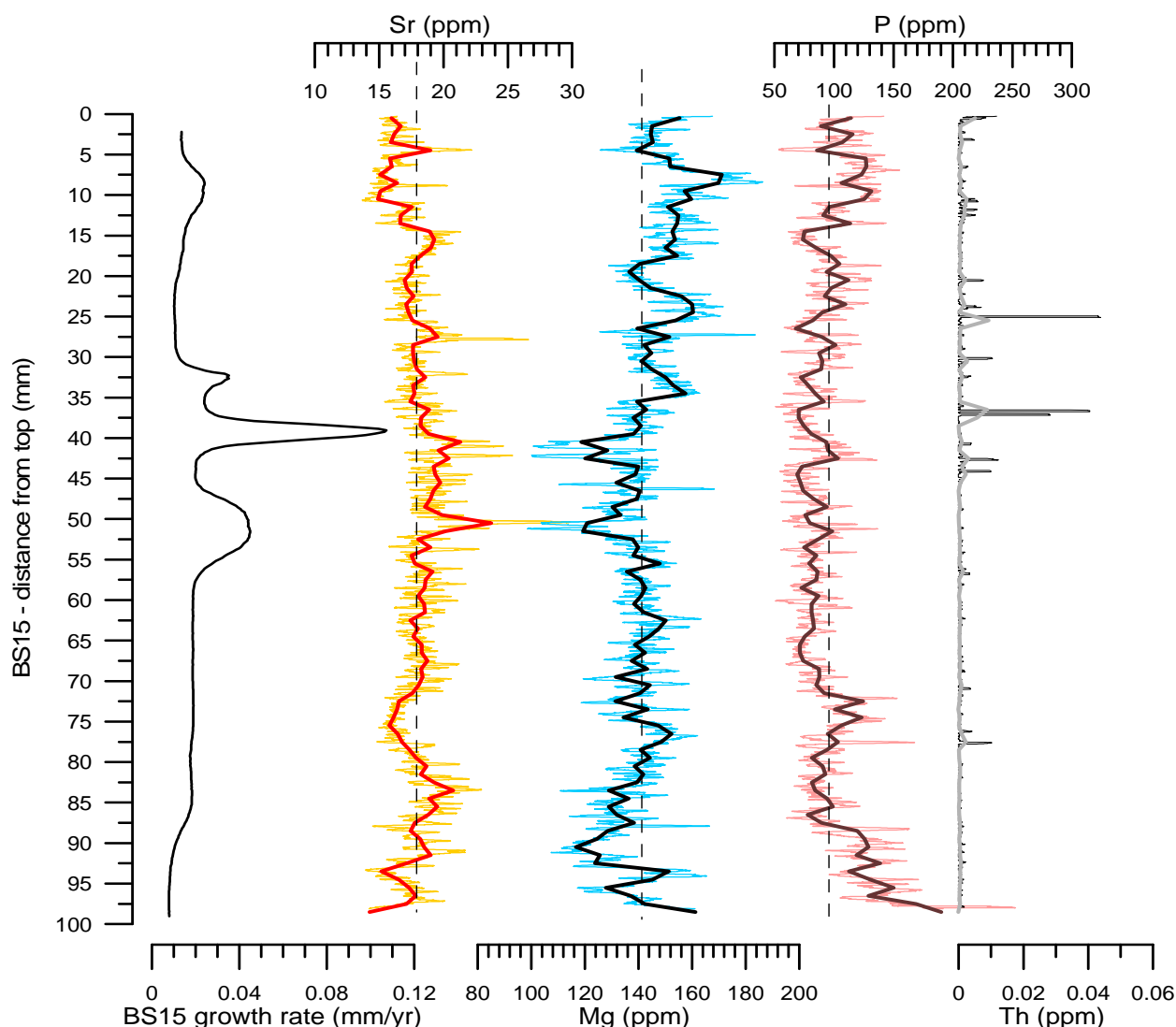


Fig. 6.3.1 – Comparison between Sr, Mg and P variation in BS15 and its growth rate (mm/yr) according to the calculated age-depth model. Trace elements profiles are represented as 31 points moving averages: yellow, blue, pink and black lines; average value calculated every millimetre corresponding to the stable isotope profiles: red, black, purple and grey bold lines. Vertical dotted lines in the trace element profiles represent the average trace element concentration value.

Thus, the antiphased variations of both elements in the studied stalagmite may be related to differential weathering of limestone and dolomite/Mg-bearing carbonate bedrock as the result of groundwater residence time (e.g. Huang et al., 2001). Their trends could then be explained as the result of hydrological processes: the alternation of relatively dry periods characterised by longer groundwater residence time and wetter ones, with a faster aquifer transmission and, possibly, higher growth rates (cf. Treble et al., 2013). P concentration in speleothems is commonly interpreted as being related to vegetation die-back or microbial mats (Huang et al., 2001; Treble et al., 2005;

Borsato et al., 2007; Fairchild and Treble, 2009). The mobility of P in soils is higher at pH between 4 and 6 (Giesler et al., 2005), conditions that usually occur in summer (Sartori et al., 2005). However, P is commonly re-adsorbed by the lower alkaline soil layer, maintaining its mobility only in presence of extremely rapid infiltration, as witnessed by its positive correlation with Y, Zn and Cu (e.g., Borsato et al., 2007). Given that plants consume P during their growing period, and that autumn is one of the wettest periods, its mobilisation should mainly occur during this season, when vegetation becomes dormant in temperate climates (Frisia, 2015 and reference therein). Autumnal organic matter flushing often results in a brownish coating at stalagmite tips that can act as a growth inhibitor. The hypothesis of autumnal flushing of P is further supported by its negative correlation with Sr ($r = -0.578$; p -value = $3.9E-10$, Tab. 6.3.1), since Sr is usually incorporated into stalagmite calcite lattice during period of high growth rate (Huang & Fairchild, 2001).

More frequent Th peaks are finally observed in the upper 40 mm of stalagmite BS15 (Fig. 6.3.1). Considering that Th has an extremely low solubility in water, its increase in this portion of the stalagmite is likely related to a higher detritus load in the parent drip water.

Trace elements	Mg	P	Mn	Cu	Zn	Sr	Y	Ba	Th
LOD	0.021	1.2	0.16	0.014	0.025	0.0021	-	0.00067	
CORRELATION COEFFICIENT									
Mg p value		0.062 0.541	0.286 0.004	-0.014 0.891	0.024 0.811	-0.615 1.2E-11	-0.253 0.012	-0.479 5.17E-7	0.125 0.218
P p value	0.062 0.541		-0.464 1.3E-6	0.413 2.1E-5	0.742 1.5E-18	-0.578 3.9 E-10	0.846 3.3E-28	-0.291 3.5E-3	-0.109 0.218
Mn p value	0.286 0.004	0.464 1.3E-6		-0.62 0.545	-0.356 2.9E-4	0.198 4.9E-2	-0.570 7.5E-10	0.282 4.6E-3	0.281 4.8E-3
Cu p value	-0.014 0.891	0.413 2.1E-5	-0.62 0.545		0.608 2.6E-11	-0.109 0.282	0.456 2.2E-6	0.016 0.873	0.150 0.138
Zn p value	0.024 0.811	0.742 1.5E-18	-0.356 2.9E-4	0.608 2.6E-11		-0.332 7.8E-4	0.774 6E-21	-0.126 0.214	-0.016 0.878
Sr p value	-0.615 1.2E-11	-0.578 3.9 E-10	4.9E-2	0.109 0.282	-0.332 7.8E-4		-0.296 0.003	0.817 5.9E-25	-0.036 0.72
Y p value	-0.253 0.012	0.846 3.3E-28	-0.570 7.5E-10	0.456 2.2E-6	0.774 6E-21	-0.296 0.003		-0.057 0.573	-0.090 0.374
Ba p value	-0.479 5.17E-7	-0.291 3.5E-3	0.282 4.6E-3	0.016 0.873	-0.126 0.214	0.817 5.9E-25	-0.057 0.573		-0.006 0.949
$\delta^{13}C$ p value	0.715 9.8E-17	0.142 0.160	0.310 0.002	-0.079 0.440	-0.083 0.411	-0.551 3.3E-9	-0.204 0.034	-0.443 4.5E-6	0.018 0.857

Tab. 6.3.1 – Trace elements analysed in stalagmite BS15 by laser ablation. LOD represents the instrument detection limit. Correlation coefficients (r) have been calculated among the data series obtained calculating the average trace element content every millimetre corresponding to the stable isotope profile. Statistically significant correlations are indicated in bold.

6.3.3 Stable isotope variability in the studied stalagmites. Reliability and significance of the recorded signals

Stable isotope composition ($\delta^{13}\text{C}$ and $\delta^{18}\text{O}$) of stalagmite calcite can provide information about past climate and environmental conditions, since it can reflect the stable isotope composition of parent drip water (cf. Chapter 2.2). However these values are influenced by several climate/environment – related factors. Even when a deep understanding of the dynamics behind the transfer of isotopic signals to the karst environment is present, the interpretation of stable isotope profiles of a given speleothem is not straightforward. Indeed, calcite deposition close to isotopic equilibrium is considered a prerequisite for the preservation of the parent drip water isotopic signal and the fulfilment of this condition must be tested. Finally even when calcite is deposited at non-equilibrium conditions, it still may be a source of information since disequilibrium itself may be induced by factors related to climate and/or environmental modification. In this Paragraph the preservation of palaeoenvironmental/palaeoclimate signals in the stable isotope profiles of the studied stalagmites is discussed.

6.3.3.1 Hendy test and replication test: disequilibrium or equilibrium fractionation?

According to Hendy (1971), if speleothem calcite is deposited close to equilibrium condition, then its $\delta^{18}\text{O}$ composition does not vary more than 0.5 ‰ along a growing lamina and there is no covariation between $\delta^{13}\text{C}$ and $\delta^{18}\text{O}$ both along its vertical axis and single laminae. However, several other authors recognised the role played by climate fluctuations in causing covariation of $\delta^{13}\text{C}$ and $\delta^{18}\text{O}$ (i.e. vegetation changes associated with climate changes; Cerling, 1984; Dorale et al., 1992; 1998).

Considering the $\delta^{13}\text{C}$ and $\delta^{18}\text{O}$ composition along the stalagmite growth axis, negligible covariation was found in BS15 and BS9, G5 and the older portion of stalagmite BS8 (i.e. below the hiatus at 51 mm from the top, where the calcite has a more porous textures than in the above portion), suggesting a possible deposition of calcite close to equilibrium conditions. In stalagmite BS15, the $\delta^{18}\text{O}$ profile is characterised by a decadal-centennial trend similar to the $\delta^{13}\text{C}$ one, in particular in its upper half. By considering the trace element fluctuations described earlier, the occurrence of PCP is excluded as a possible factor for such a long $\delta^{13}\text{C}$ and $\delta^{18}\text{O}$ covariation, thus this common trend may have been triggered by environmental factors. On the contrary, in stalagmite BS14 and in the younger portion of stalagmite BS8 (i.e. above the hiatus at 51 mm from the top) a more pronounced covariation of the two stable isotope ratios is observed (Fig. 6.3.2).

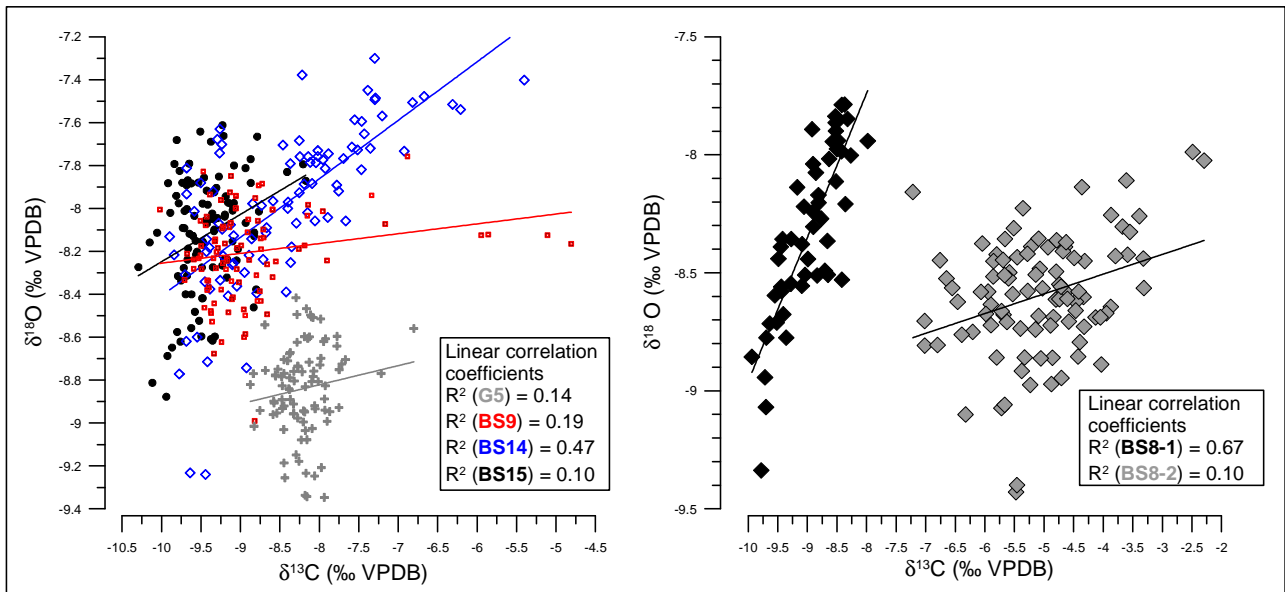


Fig. 6.3.2 – Left: linear correlation between $\delta^{13}\text{C}$ and $\delta^{18}\text{O}$ in stalagmites G5, BS9, BS14 and BS15; Right: linear correlation between $\delta^{13}\text{C}$ and $\delta^{18}\text{O}$ in stalagmite BS8, for its upper part (above 51 mm from the top; black rombohedra) and lower part (below 51 mm from the top; grey rombohedra).

In order to investigate the equilibrium/disequilibrium conditions of stalagmite calcite precipitation, the Hendy test was performed on three laminae in BS15, BS14 and BS8 (see Paragraphs 4.3.2 and 5.4.2). It indicates the presence of clear isotope fractionation on lamina H3 of stalagmite BS14, while the remaining laminae tested in BS14, BS15 and BS8 display lower stable isotope variations (Fig. 5.18, Paragraph 5.4.2). However, the asymmetric lateral enrichment of isotope composition observed in these laminae is also inconsistent with calcite precipitated under equilibrium conditions along a single lamina. Thus, it is likely that the thinness of single laminae did not allow a sufficient sampling resolution resulting in isotopic values biased by cross-contamination. Thus, disequilibrium conditions have been clearly identified only in lamina H3 of stalagmite BS14. Although isotopic fractionation cannot be evaluated with reliability by the Hendy test, a palaeo-environmental signal may still be recorded if disequilibrium fractionation (which results of environmental forcing) and environmental changes acted in the same direction on the isotopic ratios.

The relation between CO_2 dynamics and speleothem calcite stable isotope ratios has been widely investigated. It is known that CO_2 degassing in cave atmosphere is a fast process that is already completed when the water drop hits the stalagmite surface (Dreybrodt, 2011). However, when calcite starts precipitating, CO_2 is produced and released in the cave atmosphere. When this process occurs from a thin film of fluid, it causes ^{13}C and ^{18}O enrichment of the DIC (dissolved inorganic carbon) in the solution, while the increase of $\delta^{13}\text{C}$ is an irreversible process, $\delta^{18}\text{O}$ ratios can return to the equilibrium values through a slow isotope exchange with water in the hydration/dehydration

processes of CO₂ (Affek & Zaarur, 2014). However, this re-equilibration is an extremely slow process. Dreybrodt & Scholz (2011) and Hansen et al. (2013) demonstrated how the rate of outgassing is related to the thickness of the water film on speleothems, preventing complete $\delta^{18}\text{O}$ DIC re-equilibration in thin water films. Considering that the occurrence of disequilibrium conditions in DIC isotope ratios is recorded in the precipitating calcite, speleothems forming from thin films of fluid, which are the result of long drip intervals, may experience enriched $\delta^{13}\text{C}$ and $\delta^{18}\text{O}$ values (Mühlinghaus et al., 2007; Riechelmann et al., 2013; Caddeo et al., 2015). Thus, the large fluctuations of $\delta^{13}\text{C}$ and $\delta^{18}\text{O}$ observed in both stalagmites (especially BS14) suggest a probable influence of the water film thickness on both isotope ratios, with ^{13}C and ^{18}O enrichments during periods of low drip rates, reflecting more arid conditions.

In this context of slight disequilibrium conditions, higher $\delta^{18}\text{O}$ values associated with higher $\delta^{13}\text{C}$, may thus refer to periods of significantly lower drip rate, reflecting more arid conditions. Lower winter precipitation and/or a more important contribution to precipitation from $\delta^{18}\text{O}$ -enriched summer precipitation may have contributed to the higher speleothem $\delta^{18}\text{O}$ values. On the contrary, periods characterised by a more important contribution of depleted winter precipitation would be characterised by lower $\delta^{18}\text{O}$ values.

Finally, the stronger covariation bounding the two stable isotope ratios in BS14 and in the younger part of BS8 identified above may be related to a slower feeding system causing the speleothem growth under an extremely thin film of fluid affecting more deeply the $\delta^{18}\text{O}$ than in BS15. However, as explained above, in the studied stalagmites, the water film thickness is supposed to affect stable isotope ratios in the same direction as climate would, allowing for palaeoenvironmental signal preservation. Considering that four of the five samples were collected in the same area of the same cave and cover periods of time which overlaps, if their stable isotope profiles recorded palaeoenvironmental and/or palaeoclimate information, common $\delta^{13}\text{C}$ and $\delta^{18}\text{O}$ trends should be identifiable (cf. Dorale and Liu, 2009). Thus, all stable isotope records were compared to look for signal replication. Despite the large dating uncertainties, common trends were recognised among BS15 and BS9 during the late Holocene in both $\delta^{13}\text{C}$ and $\delta^{18}\text{O}$ profiles, suggesting both the reliability of the recorded signal and of the age model of these stalagmites (Fig. 6.3.3).

Common features have also been identified between BS15 and BS9 records and the younger part of stalagmite BS8. A slight offset in the age of the recorded events appears in stalagmite BS8, even if it still lies within age uncertainties of BS9 and BS15. The isotope signal recorded by BS8 presents a lower resolution if compared to BS9 and BS15 because of the presence of hiatuses not incorporated in the model. In addition, the large fluctuations affecting both $\delta^{18}\text{O}$ and $\delta^{13}\text{C}$ in the younger portion of BS8 suggest the presence of prolonged out-gassing related to calcite deposition under thin film of

fluids. The comparison of these records with BS14 does not show obvious correspondences, but only possible ones with slight timing offset (Fig. 6.3.4).

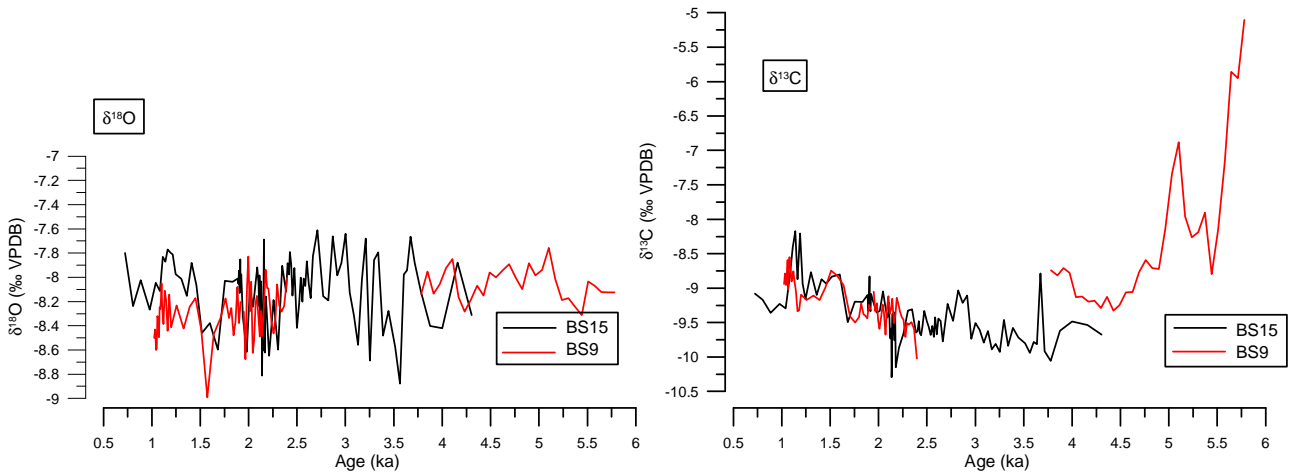


Fig. 6.3.3 – Comparison of $\delta^{18}\text{O}$ (left) and $\delta^{13}\text{C}$ (right) records in the two coeval stalagmites BS15 (black line) and BS9 (red line).

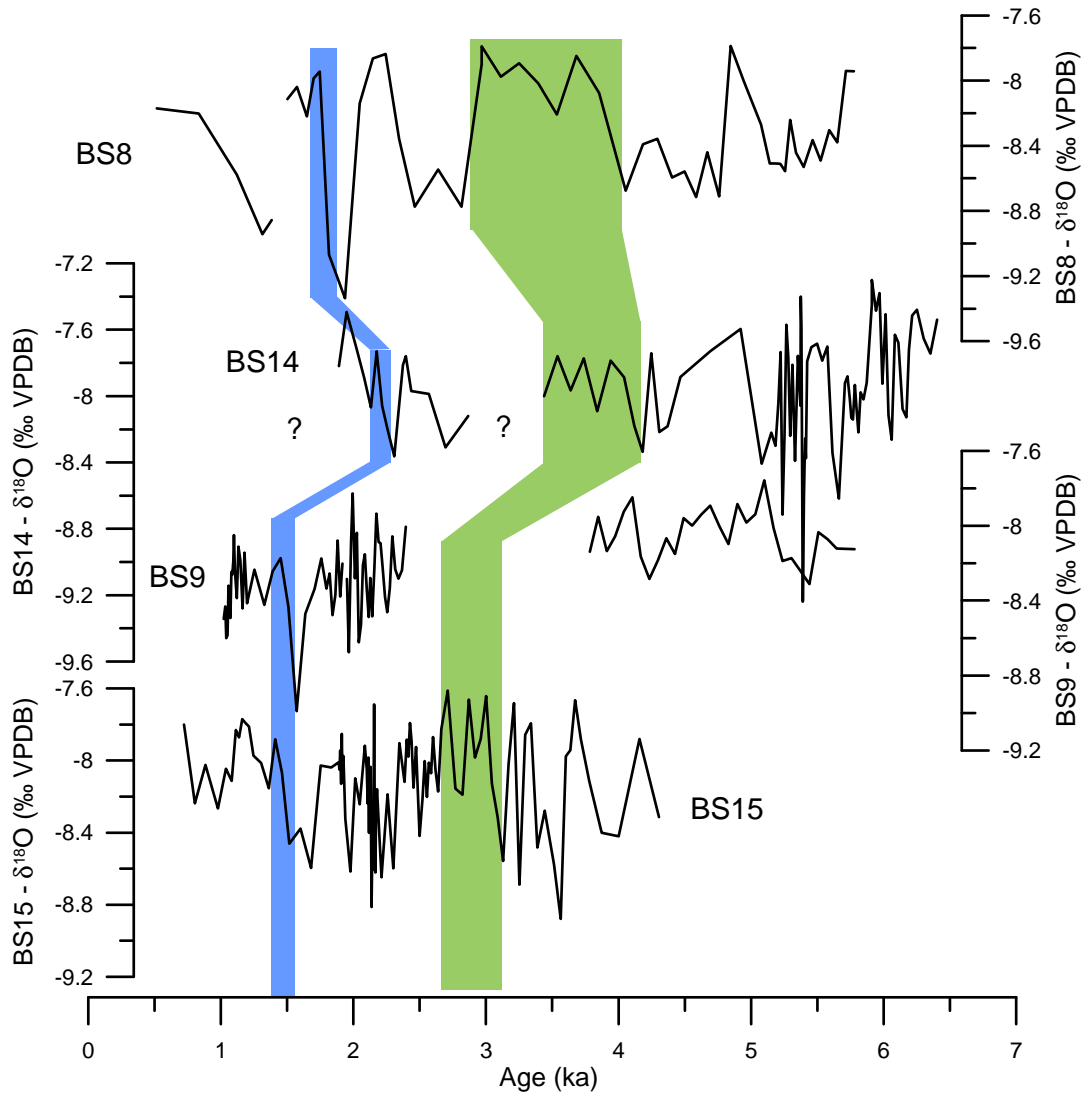


Fig. 6.3.4 – $\delta^{18}\text{O}$ mid-to-late Holocene time-series of stalagmites BS15, BS9, BS14 and BS8. The blue and green boxes shades indicate tentative correlations among the different records.

If we consider the first half of the Holocene, similar $\delta^{18}\text{O}$ values are recorded by both BS8 and G5 (Fig. 6.3.5). Common features are found in both $\delta^{18}\text{O}$ profiles despite the apparent timing offset, which stays within age model uncertainties.

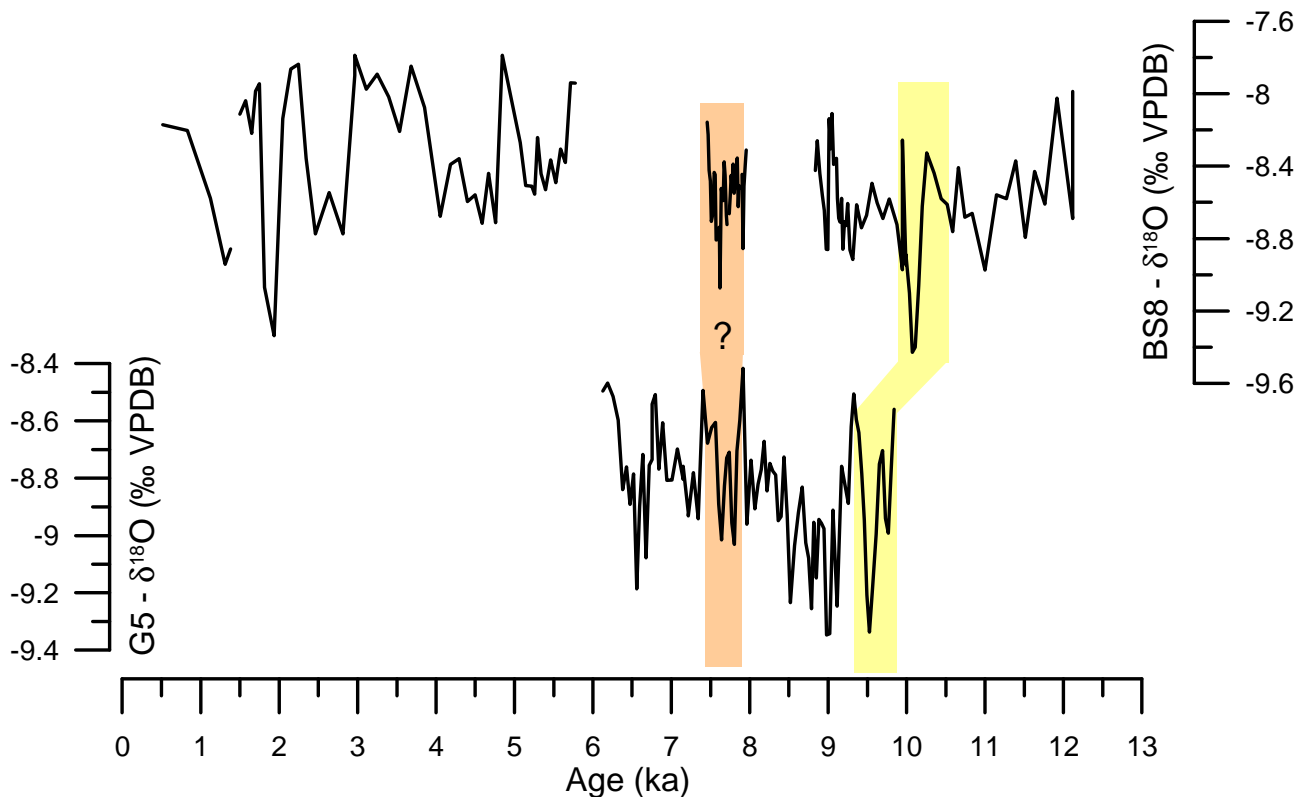


Fig. 6.3.5 – $\delta^{18}\text{O}$ profiles versus age of stalagmites BS8 and G5. Yellow and orange boxes indicate possible correlations among the two records during the first half of the Holocene.

The resemblance between $\delta^{18}\text{O}$ profiles of the studied stalagmites suggests that climate signals were preserved despite the likely occurrence of disequilibrium conditions during isotopic fractionation. However it is difficult to identify correspondences between profiles for short term fluctuations because of the age uncertainties on the age-depth models and the low sampling resolution. In addition, short term fluctuations are more likely to be influenced by site-specific processes. However, as discussed above, these processes are also related to the external environment, as they are influencing stable isotopes in the same direction, and this enables identifying environmental fluctuations.

6.3.3.2 Evidence from trace elements in stalagmite BS15 for stable isotope interpretation

In order to better interpret and understand the dynamics of stable isotope variations in Mračna Pećina stalagmites, BS15 trace element concentrations have been compared with its $\delta^{13}\text{C}$ and $\delta^{18}\text{O}$ profiles (Fig. 6.3.6). There is a strong ($r = 0.7$ $p < 0.0001$) positive correlation between $\delta^{13}\text{C}$ and Mg profiles in BS15. Considering the interpretation of Mg as related to precipitation patterns for the studied stalagmites (cf. Paragraph 6.3.2), the detected positive correlation allows considering $\delta^{13}\text{C}$ as a hydrological proxy.

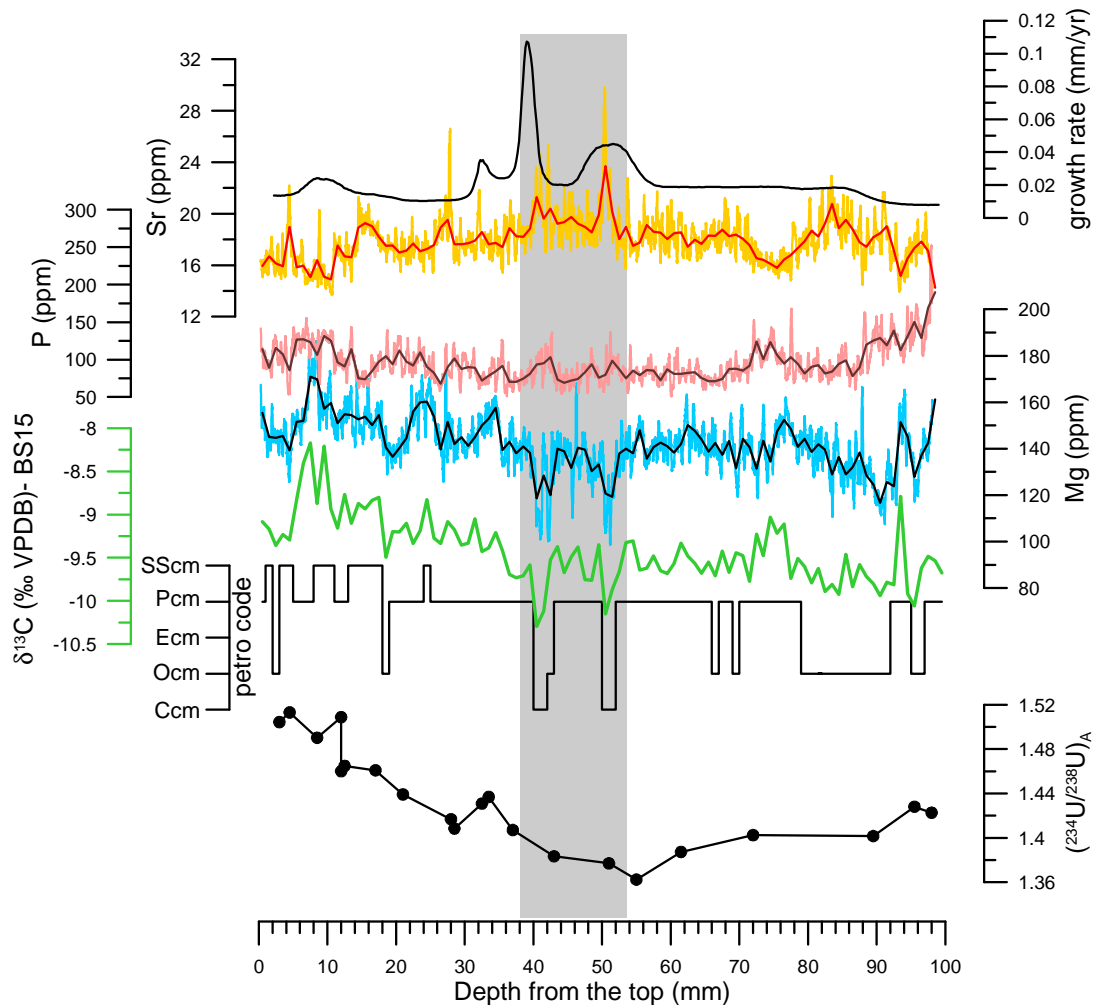


Fig. 6.3.6 – Growth rate (mm/yr), trace element concentrations (Sr, P, Mg: 31 points moving average and average calculated every millimetre in correspondence with the stable isotope profile) $\delta^{13}\text{C}$, calcite fabrics and $(^{234}\text{U}/^{238}\text{U})_A$ variations in stalagmite BS15. The grey box highlights a portion of higher growth rate corresponding to increased Sr content, lower $\delta^{13}\text{C}$ values, and decreased Mg content.

Mattey et al. (2010) noticed a correlation between $\delta^{13}\text{C}$ and Sr in a stalagmite sampled in a Gibraltar cave, interpreting the $\delta^{13}\text{C}$ signal as a proxy for cave air pCO_2 variations. They noticed a de-phasing between Sr and $\delta^{13}\text{C}$ at a sub-yearly scale and linked it to seasonal cave air circulation patterns. Namely, the seasonal temperature change drives cave air pCO_2 variations, favouring CO_2 degassing

from percolating waters in winter and driving higher calcite precipitation during this season rather than during the warmer months. Although this is a common process occurring at a sub-annual scale, it cannot be used to explain the negative correlation identified in stalagmite BS15 between Sr, Mg and, consequently, $\delta^{13}\text{C}$, since the latter has been analysed at a resolution (multi annual-decadal scale) not sufficient to disentangle a yearly signal. The negative correlation detected between Mg and Sr in our record closely links Mg to aquifer residence time and, consequently, hydrological changes (drier vs. wetter periods). Another factor that influences $\delta^{13}\text{C}$ ratios is the drip water interval: Mühlinghaus et al. (2007) showed ^{13}C enrichment associated with longer drip intervals and prolonged CO_2 out-gassing at stalagmite tips. Long drip intervals occurring during relatively dry periods could explain the correlation between $\delta^{13}\text{C}$ and Mg trend of stalagmite BS15. This interpretation is supported by the change in activity ratio of $(^{234}\text{U}/^{238}\text{U})_{\text{A}}$ that in some cases is dependent on the amount of precipitation (Hellstrom and McCulloch, 2000). This parameter shows a trend close to the $\delta^{13}\text{C}$ one (Fig. 6.3.6), which is reasonably related to precipitation: higher $\delta^{13}\text{C}$ and high Mg values are indicative of longer drip intervals and drier periods, while depleted values associated with lower concentrations of Mg are related to shorter drip intervals and wetter periods. In addition, the negative correlation between Sr and Mg and, consequently, $\delta^{13}\text{C}$, is consistent with this interpretation, since Sr can depend on growth rate (e.g. Huang et al., 2001), which is low in dry periods (less water) (Fig. 6.3.6).

6.3.4 Petrography variations and their relation to environmental changes

6.3.4.1 Chemical and physical parameters influencing fabric variation in stalagmites BS14 and BS15

The dimension of the crystallites forming the identified composite crystals has not been disentangled at the optical microscope level, suggesting the presence of extremely small calcite crystallites arranged in optical continuity within the crystal aggregates to which they belong. This general structure can be referred to as columnar microcrystalline (Frisia et al., 2000; Frisia & Borsato, 2010; Frisia 2015). According to Frisia (2015), this fabric can be found in temperate regions characterised by seasonal contrast in temperature, precipitation and vegetation activity. The presence of brown laminae, which is believed to be related to organic matter flushing following vegetation die-back (mainly during autumn at mid-latitudes, Frisia et al., 2000), suggests seasonal changes of water discharge. Although the Sarajevo area is not currently affected by a strong seasonality of precipitation, the significant seasonal temperature contrast must play an important

role on evapotranspiration, and thus water balance and year-round variations in drip rate, especially when summer periods are synchronous with relatively low precipitation (Fig. 6.3.7).

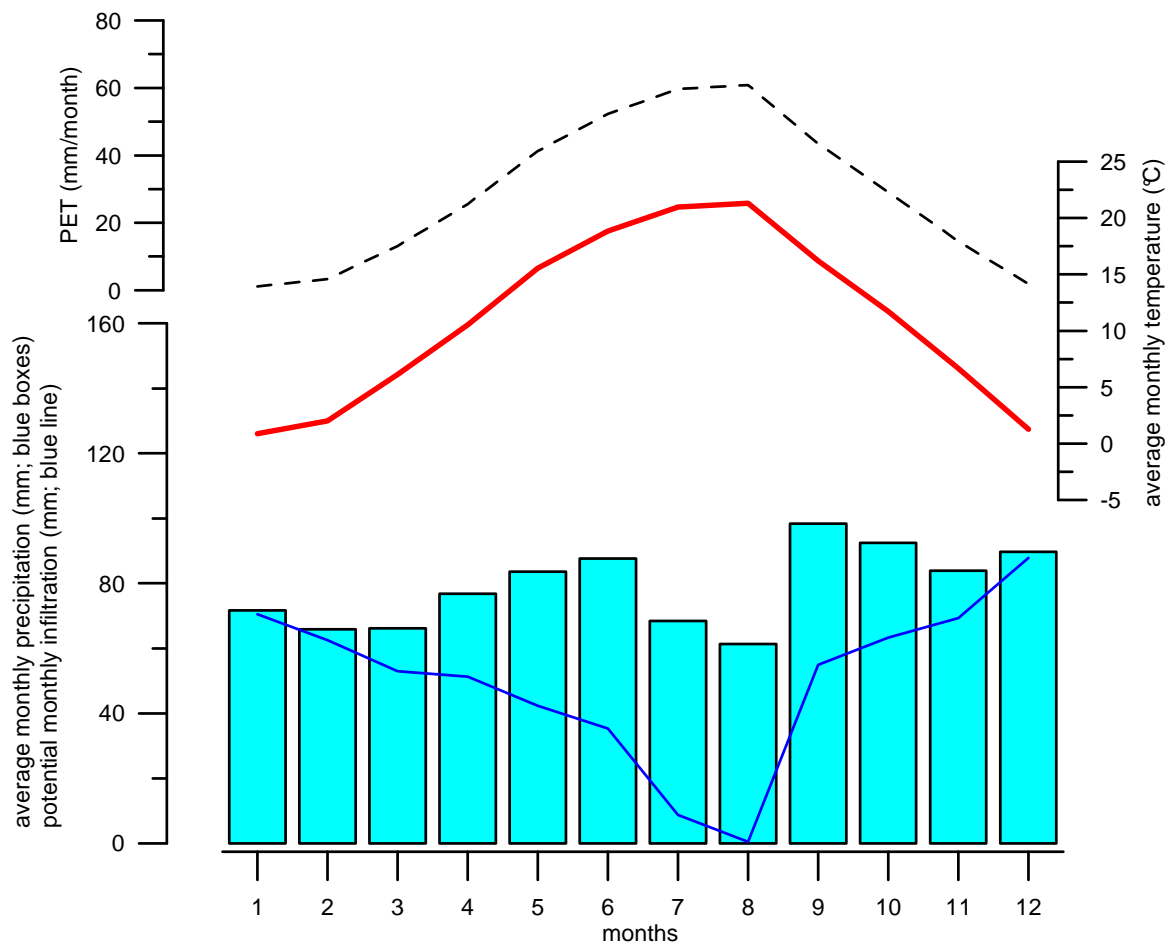


Fig. 6.3.7 – Average monthly precipitation (blue boxes: time interval 1992-2015); potential monthly infiltration (blue line); average monthly temperature (red line: time interval 1992-2015) and potential evapotranspiration (PET; black dotted line). PET was calculated using average monthly temperature in the Thornthwaite & Mather (1957) equation; potential infiltration was estimated as the difference between precipitation and PET. Data from the Sarajevo weather station, Federal Institute of Hydrometeorology (Bosnia and Herzegovina).

Present-day monitoring of drip sites in the area where the stalagmites were found shows a strong connection with the external environment (Fig. 5.1, Paragraph 5.1.1). In particular, higher discharge is found during late autumn to early spring precipitation, while low-to-absent dripping occurs in summer. Therefore, calcite fabric alternation is likely reflecting changes in drip water saturation and drip rate, which are related to environmental changes during the second half of the Holocene in the study area.

Stable isotope profiles and trace elements (stalagmite BS15) were compared with petrographic changes in order to better understand the factors involved in crystallite changes (Fig. 6.3.6 in the previous Paragraph and Fig. 6.3.8).

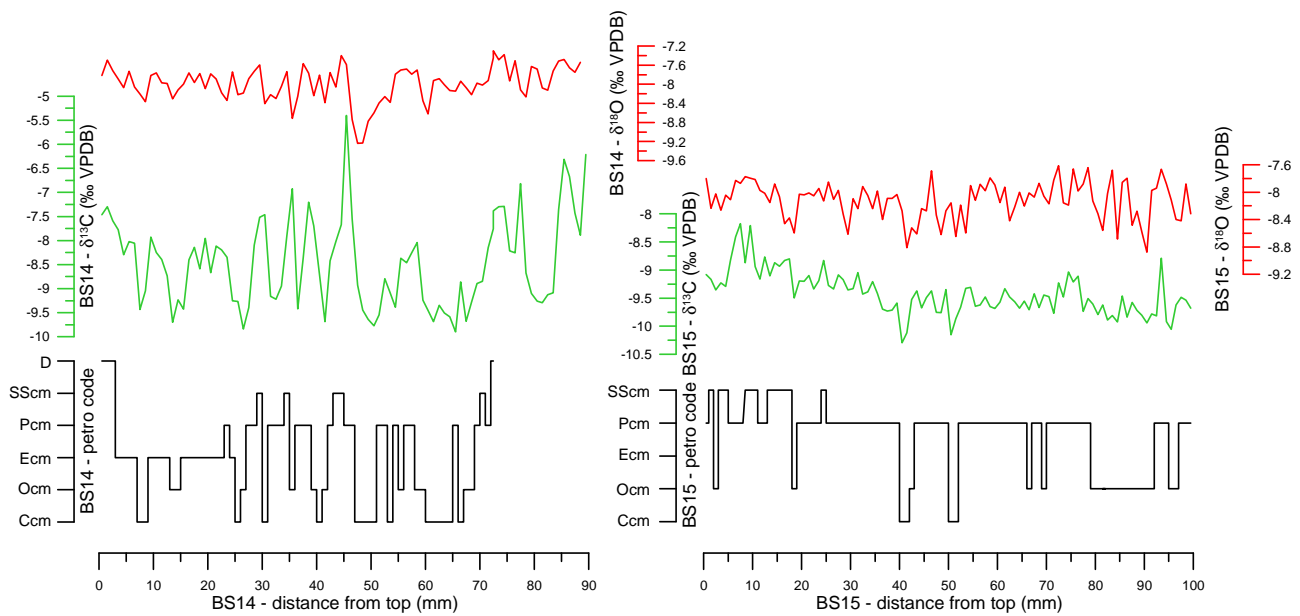


Fig. 6.3.8 – $\delta^{13}\text{C}$ and $\delta^{18}\text{O}$ profiles and micrologging curve for stalagmites BS14 (left) and BS15 (right).

Similar trends between fabric class variations and $\delta^{13}\text{C}$ has been found in both profiles, suggesting the presence of a common factor driving changes in both parameters (i.e. increased calcite porosity and calcite $\delta^{13}\text{C}$). Kruskal-Wallis and multiple tests associated with the Bonferroni correction and discriminant analyses confirmed the presence of a strong link between $\delta^{13}\text{C}$ and fabric sub-types which associates progressively higher isotope ratios with the more porous and impurity-rich fabrics (cf. Paragraph 5.6); a similar but markedly weaker trend affects the petrography classes $\delta^{18}\text{O}$ composition with progressively higher values from Ccm to Sscm and D (Fig. 6.3.9).

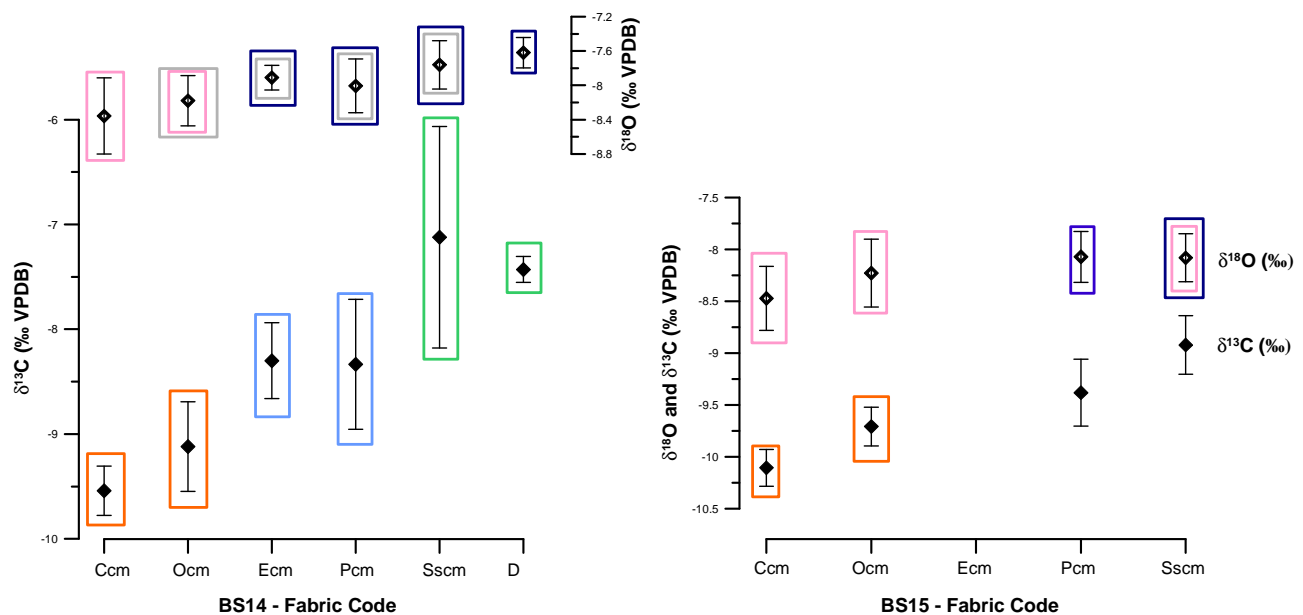


Fig. 6.3.9 – Isotope-fabric plots for BS14 and BS15 stalagmites. For each fabric type, average $\delta^{13}\text{C}$ and $\delta^{18}\text{O}$ values are plotted with their standard deviation. Isotope compositions which cannot be considered statistically different (confidence level 0.05) are indicated with rectangles of the same colour.

Considering the interpretation of $\delta^{13}\text{C}$ as a hydrologic proxy, the formation of a particular calcite texture under progressively increased hydrological stress is clear. Petrographic changes induced by variations in drip rate were first reported by Kendall & Broughton (1978), then subsequently by Frisia et al. (2000) and Frisia and Borsato (2010); Mühlinghaus et al. (2007) found that $\delta^{13}\text{C}$ values in speleothem calcite vary with the drip interval. However, this cannot be considered the sole factor triggering changes in calcite stable isotope composition.

The positive correlation between Mg and $\delta^{13}\text{C}$, and their negative correlation with Sr, in stalagmite BS15 suggests a possible trace element signature for each petrography class, which was highlighted by the discriminant analyses, performed using $\delta^{13}\text{C}$, $\delta^{18}\text{O}$, Mg, and Sr as variables (Fig. 5.22 in Paragraph 5.6). Riechelmann et al. (2014) described the role of Mg in triggering petrographic changes: the Mg content, which is related to hydrology, likely contributed to the fabric variations in the studied stalagmites contributing in the formation of crystallites presenting a higher density of defect sites.

Another factor that could influence calcite fabric and $\delta^{13}\text{C}$ changes is the mean annual temperature, which causes changes in the vegetation cover and, consequently, in soil CO_2 production. However, the studied stalagmites did not grow over periods long enough to experience significant temperature or climate-driven vegetation changes. Thus, it is more plausible to consider hydrological variations as the major factor triggering both $\delta^{13}\text{C}$ and fabric changes, while temperature seasonality could have played an indirect role in aquifer recharge after evapotranspiration. Over the long term, a marginal role of vegetation cover in influencing $\delta^{13}\text{C}$ ratios cannot be excluded, as these stable isotope variations are not fully explained by hydrological changes. In particular, in BS15 stalagmite, the uppermost 40 mm shows more numerous Th peaks, suggesting increased soil erosion possibly related to anthropic activities on the overlying plateau. The same portion does not display brown lamination, indicating the absence of flushing events. In conclusion, the cross comparison of the available data allowed for the understanding of the main driving factors involved in calcite texture development in the studied stalagmites. Indeed the fabrics classified in stalagmites BS14 and BS15 can be considered related to the thickness of the film fluid at the moment of their deposition and the Mg/Ca concentration of the parent solution, thus reflecting hydrology variations.

6.3.4.2 Palaeo-environmental information recorded by calcite fabrics

It was demonstrated that drip interval played a fundamental role in the type of calcite fabric of the studied stalagmites, and that the Mg concentration in drip water possibly influenced fabric development: a longer drip interval caused the calcite $\delta^{13}\text{C}$ ratios to increase, which corresponds to lower Sr and higher Mg concentration in stalagmite calcite, also resulting in higher defects and smaller-dimension of the calcite crystallites.

At the more detailed level, groups of laminae formed by **compact columnar microcrystalline (Ccm) calcite** are those characterised by the highest Sr and lowest Mg content. These laminae are separated by wavy brown surfaces, which show evidence of local dissolution of the underlying crystal tips and joints, suggesting flushing events carrying colloids. The presence of flattened calcite crystal terminations and cavities within the compact carbonate lamina below the brownish lamination suggest local (at stalagmite tip), organic-matter oxidation following flushing events (organic colloids from the soil zone), which created an acidic environment leading to very localized dissolution (Frisia, 1996). This pattern can be related to a wet season followed by a relatively dry period, before a strong infiltration event (in autumn) causing a massive flushing of organic matter. These conditions are found in Mediterranean-like climate, which is now present in the coastal area of the Balkans (Vreča et al., 2006).

The **open columnar microcrystalline fabric (Ocm)** is instead characterised by increased porosity, which suggests a less-regular crystallite stacking related to an increased amount of foreign particles/colloids. These particles may have caused higher crystal defects, possibly inducing a smaller crystallite size. Brown surfaces, where present, are less sharp than in the previous sub-pattern and contain less evidence of dissolution features, suggesting the occurrence of weaker infiltration events. If compared to the **Ccm** fabric, a slower growth rate can be inferred from the lower Sr content. The slightly higher Mg content suggests instead the presence of marginally drier conditions during its formation. The $\delta^{18}\text{O}$ values detected in the IsoFab plot between **Ocm** and **Ccm** are comparable and indicate the absence of strong differences in the water film on the tip of the stalagmites. However, slightly drier conditions may have translated into more irregular dripping, triggering the precipitation of this fabric.

The **elongated columnar microcrystalline (Ecm)** fabric has only been found in the younger portion of stalagmite BS14, followed by dendritic fabric at the very top of the stalagmite. Its formation possibly occurred under conditions similar to the ones that prevailed during deposition of elongated columnar calcite associated with the influence of impurities (Frisia, 2015). An increasing supply of foreign particles is thought to have caused the higher density of crystal defects, and thus the increased porosity. Its $\delta^{13}\text{C}$ and $\delta^{18}\text{O}$ values are higher when compared to **Ocm** and **Ccm**, suggesting its formation under thin films of fluid related to a generally drier climate.

The **porous columnar microcrystalline (Pcm)** calcite, observed in both stalagmites, coincides with higher $\delta^{13}\text{C}$ and $\delta^{18}\text{O}$ values when compared to the **Ocm**, but with similar values when compared to the **Ecm**. This fabric is also characterised by lower Sr and higher Mg content, indicating, respectively, slower growth rate and drier conditions. Increased summer temperature may have played a role together with increased aridity causing further irregularities in drip rate.

Finally, the *stricto sensu* **microcrystalline (SScm)** fabric and the **dendritic** fabric mainly occur, respectively, in the upper 18 mm of stalagmite BS15 and in the upper 3 mm of stalagmite BS14. The first is associated with higher $\delta^{13}\text{C}$ values but $\delta^{18}\text{O}$ values are comparable to those of **Pcm**. Brown laminae are faint or absent, suggesting the lack of major flushing events and/or lower soil and vegetation activity. The presence of **dendritic calcite** at the top of BS14, associated with isotopic values comparable to the SScm of the same stalagmite, would also indicate the presence of generally drier conditions (McDermott et al., 1999; Frisia, 2000). The presence of SScm in BS15 would also be in agreement with a less dense vegetation cover on the overlying plateau. In addition, a black layer preserved in both stalagmites close to their top is likely due to a soot coating. It indicates a likely human frequentation of the cave at this time, and thus settlements in the area.

6.3.4.3 Petrography variations in stalagmites BS8 and BS9

The high resolution petrography micrologging performed on BS14 and BS15 thin sections was not realised for stalagmites BS8 and BS9 and only a less detailed observation was done.

Both stalagmites present a candlestick shape, remarkably narrower than BS14 and BS15 samples. Since a stalagmite diameter is directly related to the drip rate and the height of ceiling (Gams, 1981), this narrower shape suggests their formation under slower dripping system and/or lower ceiling than the two samples examined in the previous paragraph.

- **Stalagmite BS9**

The part below 80 cm from the top is formed by dendritic calcite. The studied part of this stalagmite (i.e. above 80 mm from the top) is mainly formed by microcrystalline calcite, suggesting its formation under conditions of strong dripping seasonality and relatively low saturation (SI) (Frisia, 2015). The alternation of microcrystalline crystals and dendritic calcite along the growth axis suggests that in-cave parameters varied. In particular, according to Frisia et al. (2000), the presence of dendritic calcite in Holocene stalagmites may occur during periods of fast dripping alternating with prolonged droughts, with infiltrating water of low supersaturation (SIc between 0.2 and 0.4). In addition, as also noticed in other Holocene stalagmites containing this fabric (McDermott et al., 1999; Frisia et al., 2000), dendritic parts seem to have higher $\delta^{13}\text{C}$ than microcrystalline ones, while $\delta^{18}\text{O}$ does not present any fabric-related trend (Fig. 6.3.10). However, a general trend towards higher values in $\delta^{13}\text{C}$, which is not related to fabrics, is present. The possible presence of high hydrologic stress triggering the dendritic fabric without completely hampering the recording of the climate signal is inferred. The similarities between BS9 and BS15 stable isotope profiles further

support the reliability of the recorded signal in preserving environmental changes (Fig. 6.3.3 in Paragraph 6.3.3.1).

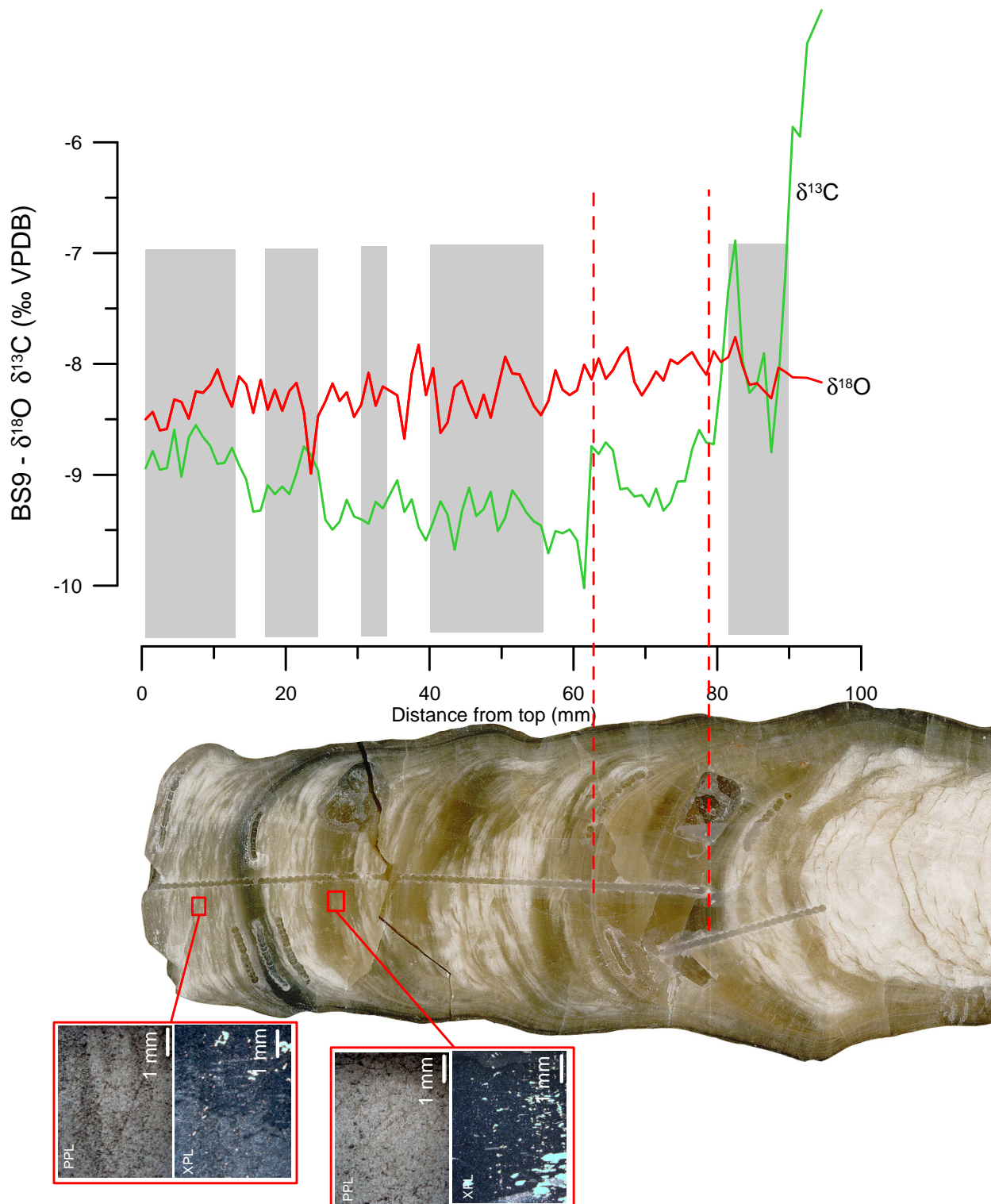


Fig. 6.3.10 – Stable isotope profiles compared with calcite fabrics in stalagmite BS9. Data are represented in relation to their distance from the stalagmite top (mm). The red dotted line indicates a hiatus. Grey boxes represent the parts of the growth axis made of dendritic calcite. At the bottom, microphotographs of thin sections (PPL and SPL light) represent examples of open-to-dendritic fabric (on the left) and microcrystalline fabric (on the right).

- **Stalagmite BS8**

It is mainly formed by compact columnar and open columnar calcite. The portion below the hiatus at 50 mm from the top, which corresponds to the early Holocene, is formed by a more open and porous calcite with higher $\delta^{13}\text{C}$ values than the late Holocene part (Fig. 6.3.10). According to Couchoud (2006) and Frisia (2015), the open columnar calcite occurs under more irregular and faster dripping than the compact columnar fabric. Although the younger portion of BS8 (above 51 mm from the top) is remarkably more compact, porosity is not completely absent and is the responsible for the faint lamination, which may reflect seasonal changes in cave ventilation and/or drip rate (e.g. Genty and Quinif, 1996; Boch et al., 2010; Matthey et al., 2008). A generally more regular and slower dripping is inferred for this younger portion of the stalagmite.

The observed higher $\delta^{13}\text{C}$ values in the more porous portion of the stalagmite (grey shade in Fig. 6.3.11), are not accompanied by any particular trend affecting the $\delta^{18}\text{O}$ ratios, which in turns present lower amplitude fluctuations in comparison to the younger portion (Fig. 6.3.11). Unfortunately Hendy test (Paragraph 6.3.3.1) did not allow demonstrating neither the presence nor the absence of equilibrium conditions in any of the sampled laminae. Thus, the occurrence of evaporation at the stalagmite tips during calcite deposition, which is known to cause isotopic disequilibrium, cannot be excluded. If we consider the stalagmite part comprised between 51 and 91 mm from the top, we found a markedly higher growth rate associated with a porous texture. High precipitation rate can be produced by both high drip rate associated with relatively high SIc (Saturation Index) and evaporation caused by strong cave ventilation (Deininger et al., 2012). Water SIc is driven by both soil pCO_2 , which allows for percolating water acidification favouring carbonate bedrock dissolution, and cave air pCO_2 influencing carbon dioxide degassing from water entering the chamber. However, the high $\delta^{13}\text{C}$ values recorded during the early to middle Holocene exclude a strong soil activity able to increase infiltrating water SIc, and rather suggest calcite deposition influenced by low cave air pCO_2 (cf. Boch et al., 2010). Thus it is reasonable to infer the deposition of the portion of BS8 stalagmite below the hiatus found at 50 mm from the top under conditions of high drip rate and/or stronger cave ventilation than in the younger portion. Stronger ventilation may have been triggered by both changes in seasonal temperature and variation of cave structure (e.g. occlusion of the natural entrance and/or cave passages able to modify cave air circulation). While the latter cannot be excluded *a priori*, the alternation of thick, porous and whitish laminae with thin, compact and greyish ones suggests the presence of a stronger seasonality of temperature and/or precipitation during the growth of the first half of stalagmite BS8.

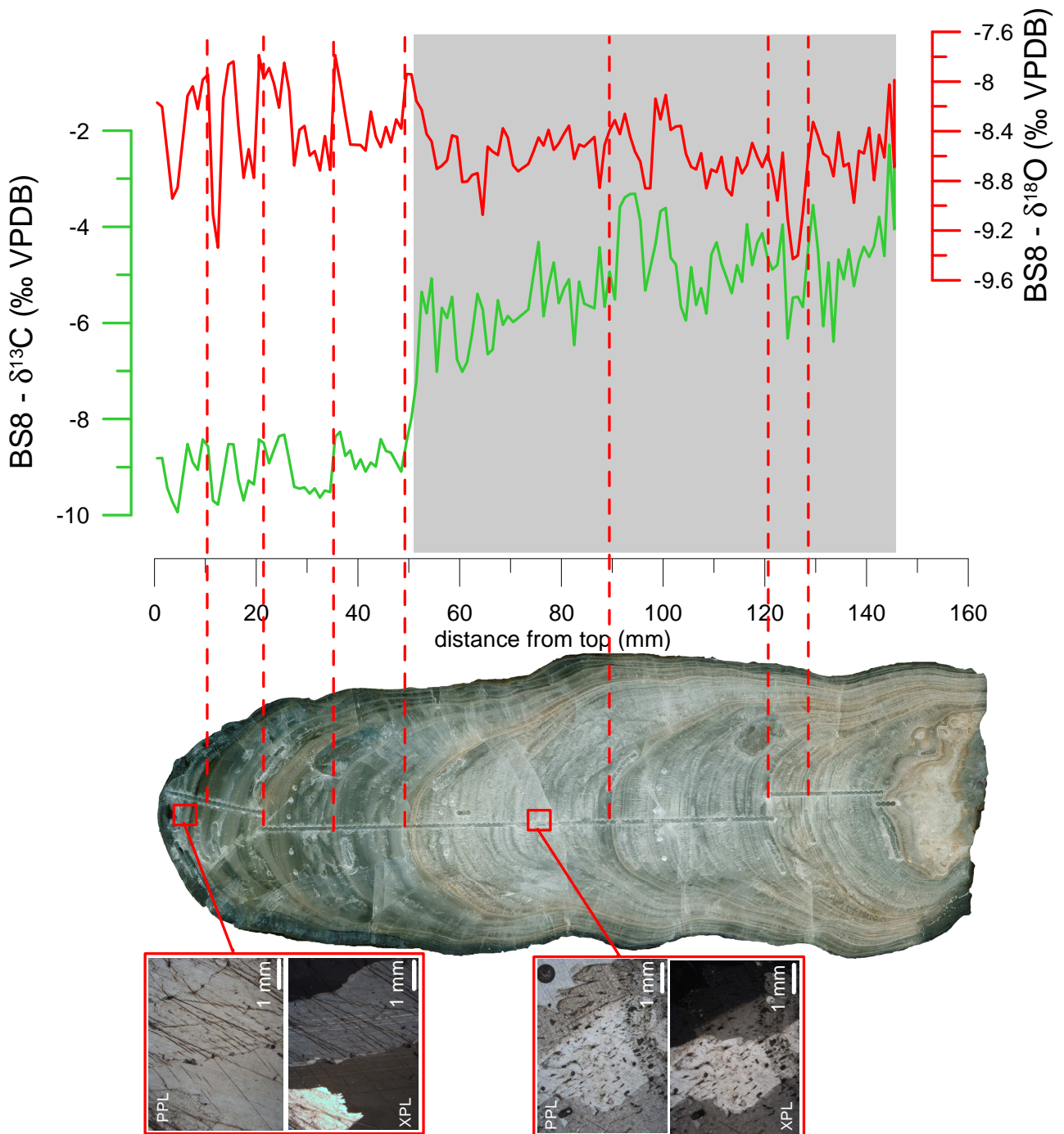


Fig. 6.3.11 Stable isotope profiles compared with calcite fabrics in stalagmite BS8. Data are represented in relation to their distance from the stalagmite top (mm). The red dotted lines indicate hiatuses. Grey box rerepresents the parts of the growth axis made more porous calcite. At the bottom, microphotographs of thin sections (PPL and XPL light) represent, respectively, the compact columnar and open columnar calcite fabrics.

6.3.5 Conclusions

In this Chapter, the studied stalagmites have been examined using a multiproxy approach and applying the new micrologging method proposed in Frisia (2015) to improve the $\delta^{13}\text{C}$ and $\delta^{18}\text{O}$ profile interpretation in terms of palaeoenvironments.

Although it was not possible to demonstrate the presence of equilibrium conditions during the deposition of the studied samples with the Hendy test, the strong noise affecting the stable isotope profiles suggest that isotopic disequilibrium fractionation likely occurred. However, a comparison between stable isotopes, calcite textures and trace elements (BS15) allowed for the interpretation of their variations in terms of hydrological changes, providing information about the presence of drier and wetter periods. In particular, positive correlations were found between $\delta^{13}\text{C}$, calcite textures and Mg associated with a negative correlation between Mg- $\delta^{13}\text{C}$ and Sr. A strong sensitivity of these values to drip-rate variations was identified. The strong relation between textures and drip-rate in stalagmites BS14 and BS15 allowed for the identification of changes in hydrology at the lamina scale, thus demonstrating the strong potential of the petrography micrologging in providing clues for palaeo-environmental investigations. The relation between $\delta^{18}\text{O}$ and petrography is less evident, even if higher $\delta^{18}\text{O}$ values are associated with calcite textures indicating drier conditions. Although disequilibrium fractionation likely occurred, a paleo-environmental signal may still be recorded if disequilibrium fractionation and environmental changes acted in the same direction on the isotopic ratios. In this context, the $\delta^{18}\text{O}$ variations are thought to provide information about the seasonality of aquifer recharge: lower values would indicate a more important winter recharge (possibly associated with summer drought), while higher values would be related to a stronger contribution of summer precipitation.

6.4 The Bosnian Holocene record

6.4.1 Introduction

In this Chapter the environmental signals analysed in the previous Chapter are interpreted in terms of palaeoenvironmental and palaeoclimate fluctuations. Comparison between the five sampled stalagmites allowed for the identification of millennial and decadal-to-centennial climate fluctuations. The obtained palaeoclimate record has been compared with contemporaneous records from the central Mediterranean in order to investigate the meaning of the recorded signal in terms of climate changes occurred at the Mediterranean regional scale.

6.4.2 Interpretation of the analysed record in terms of palaeo-environmental changes during the Holocene in Bosnia

6.4.2.1 Millennial-scale climate trends through the Holocene

The stalagmites sampled in Govještica and Mračna Pećina caves cover almost entirely the Holocene, with the exception of some relatively short periods in which the studied speleothems stopped growing.

- **Stalagmites G5 and BS8 (~9.5 – 6.3 ka)**

Stalagmite G5 started growing during the glacial period at ~73 ka. It stopped between about 12.5 and 10 ka and then it started again until about 6.2 ka. Its definitive growth interruption at ~6.2 ka may be related to the fall of the stalagmite due to natural causes or to changed environmental conditions affecting the feeding system.

Considering that most of the sampled stalagmites in the nearby Mračna Pećina cave grew from about 6 ka, the hypothesis of the occurrence of a major environmental change occurring from this period can be put forward. In addition, the only stalagmite from this cave (BS8), that had started growing earlier, shows a clear change of calcite texture after ~5.7 ka. Unfortunately, the lack of monitoring in the area where stalagmite G5 was found prevented the identification of dripping dynamics (at the time of sampling, July 2014, this area appeared dry). However, the main stalagmite growth phase during a period cooler than today suggests a more efficient aquifer recharge during relatively cooler conditions and the absence of permanently frozen ground during the last glacial in this region. The thicker bedrock cover, the compact and clear calcite forming the

G5 speleothem and the fairly constant growth rate (~ 0.02 mm/yr) suggest longer water residence time if compared with Mračna Pečina cave and a possible diffuse flow dominated system providing a buffered connection with the external environment. Its stable isotope profiles show a weak trend towards higher $\delta^{18}\text{O}$ associated with a trend towards lower $\delta^{13}\text{C}$ between about 10 and 8 ka followed by a slightly increasing trend (Fig. 6.4.1). Unfortunately, the Hendy test was not performed on this stalagmite due to the absence of a clearly visible lamination, thus preventing the identification of calcite deposition at isotopic equilibrium. However, the presence of a compact columnar calcite texture observed on the stalagmite polished section, together with the lack of covariation between $\delta^{13}\text{C}$ and $\delta^{18}\text{O}$ along the growth axis, suggest that conditions at least close to isotopic equilibrium may have occurred.

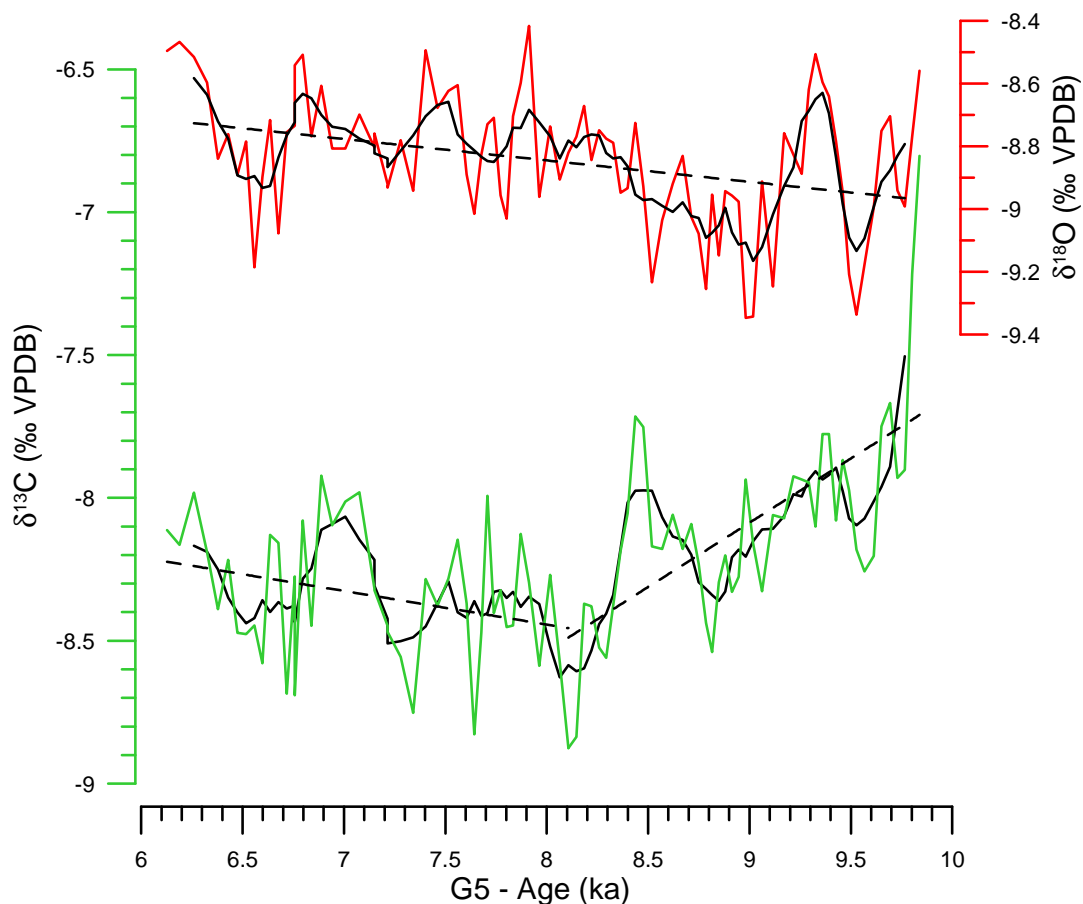


Fig. 6.4.1 – $\delta^{13}\text{C}$ (green) and $\delta^{18}\text{O}$ (red) profiles in stalagmite G5. Black lines represent smoothed isotopic curves (5 points moving averages). Black dotted lines indicate the identified long term trends. Hiatuses not considered in the age-depth model are not represented here.

Starting from the considerations discussed in Chapter 6.3, the weak long term trend towards higher $\delta^{18}\text{O}$ may thus indicate a lower contribute of winter precipitation to aquifer recharge and/or the onset of milder conditions. In stalagmites BS9, BS14 and BS15 sampled in the nearby Mračna Pečina cave the $\delta^{13}\text{C}$ was interpreted as a hydrologic proxy. However the strong trend towards

lower $\delta^{13}\text{C}$ in BS8 (Fig. 6.4.2) during the early Holocene can be interpreted as a progressive soil restoration and development after the last glacial period. Thus, it is unclear whether the $\delta^{13}\text{C}$ weak trend in stalagmite G5 is mainly related to vegetation activity, hydrology or both.

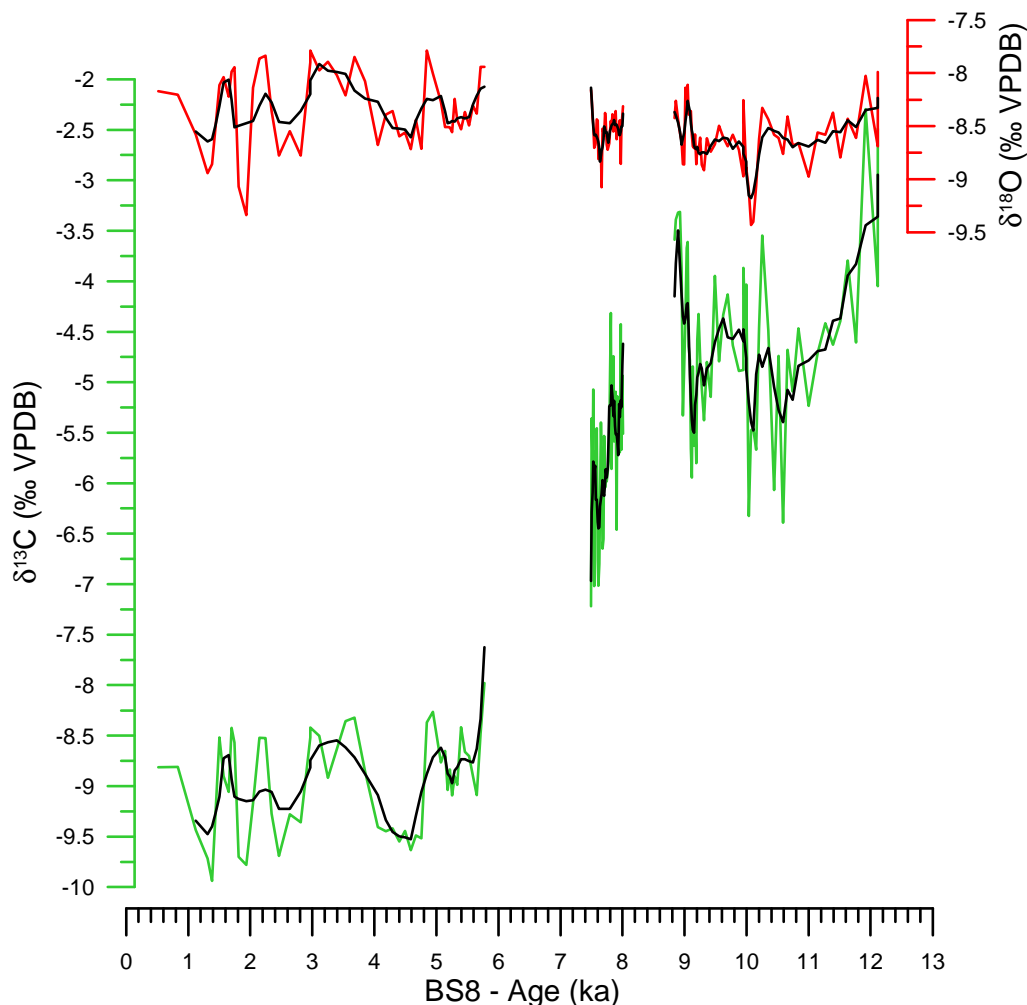


Fig. 6.4.2 - $\delta^{13}\text{C}$ (green) and $\delta^{18}\text{O}$ (red) profiles in stalagmite BS8. Black lines represent smoothed isotopic curves (5 points moving averages). Hiatuses not considered in the age-depth model are not represented here.

Both isotopic signals in BS8 stalagmite are higher than the ones found in G5 during the early to middle Holocene (especially $\delta^{13}\text{C}$: average $\delta^{13}\text{C}_{\text{BS8}} = -5.06 \pm 0.97$ ‰; average $\delta^{13}\text{C}_{\text{G5}} = -8.21 \pm 0.32$ ‰; average $\delta^{18}\text{O}_{\text{BS8}} = -8.59 \pm 0.25$ ‰; average $\delta^{18}\text{O}_{\text{G5}} = -8.84 \pm 0.21$ ‰; Fig. 6.4.3). These differences may be the result of site-specific mechanisms related to groundwater residence time, soil development at aquifer recharge sites and sample location with respect to cave air circulation. The $\delta^{18}\text{O}$ long-term trend in BS8 shows a relative stability suggesting the lack of significant changes in seasonality of aquifer recharge. Unfortunately, the large variability and the low resolution of the $\delta^{18}\text{O}$ time series (especially during the first millennia of the Holocene) prevent any further discussion at the millennial scale.

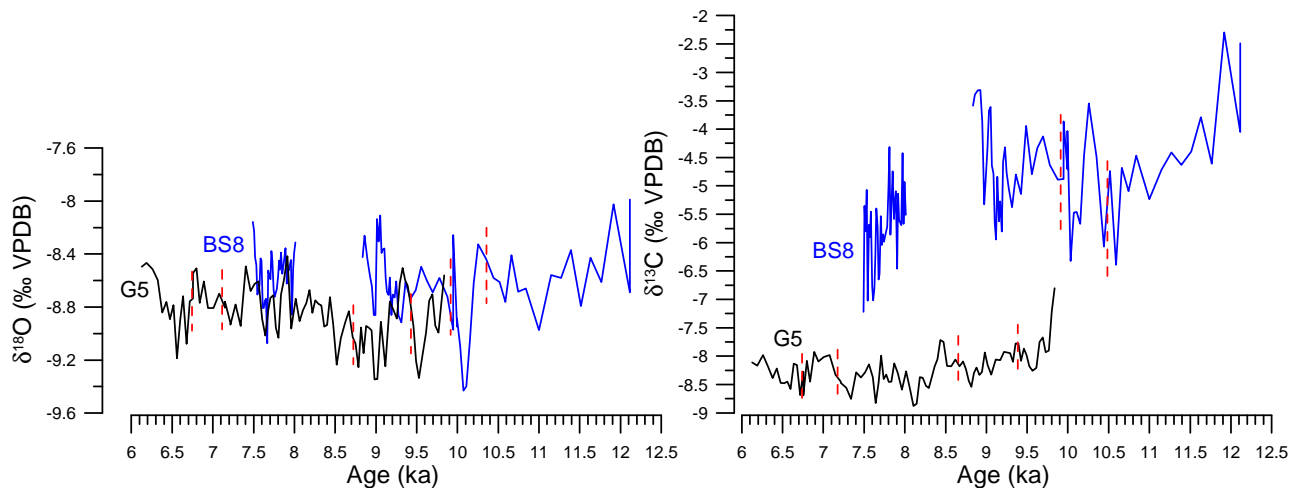


Fig. 6.4.3 – Comparison between $\delta^{18}\text{O}$ (left) and $\delta^{13}\text{C}$ (right) variation recorded during the first half of the Holocene in stalagmites BS8 (blue) and G5 (black). Red dotted lines indicate the hiatuses not entered in the age-depth model.

The low growth rate of BS8 before ~ 10 ka (~ 0.01 mm/yr), period in which G5 was not growing, suggests relatively dry conditions during the first millennia of the Holocene and/or a poorly developed soil overlying the cave. Higher growth rates of ~ 0.03 mm/yr between ~ 9 and 8.8 ka and ~ 0.16 to 0.06 mm/yr between about 8 and 7.5 ka may suggest calcite deposition under faster drip rate indicating wetter conditions.

- **Stalagmites BS8, BS9, BS14 and BS15 ($\sim 6.5 - 0.7$ ka)**

Stable isotope profiles of all the middle to late Holocene stalagmites from Mračna Pećina Cave show comparable $\delta^{18}\text{O}$ range values (Fig. 6.4.4), suggesting that the recorded range-values are not site-dependent but may reflect the composition of the infiltrating water. However, the lack of any marked long term trend of $\delta^{18}\text{O}$ indicates relatively stable seasonality of aquifer recharge and/or temperature during the middle to late Holocene. On the contrary, the $\delta^{13}\text{C}$ profiles present larger fluctuations reflecting the sensitivity of this proxy to site specific conditions (Fig. 6.4.4).

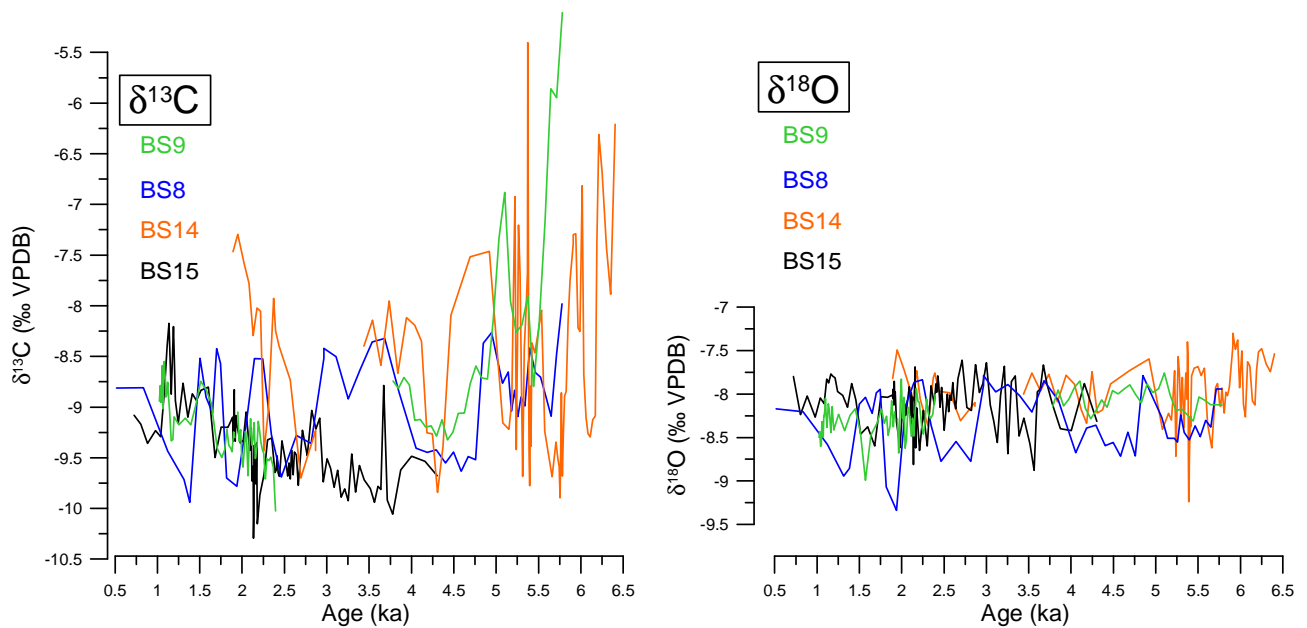


Fig. 6.4.4 - Comparison of $\delta^{18}\text{O}$ (left) and $\delta^{13}\text{C}$ (right) variations between the four Mračna Pečina stalagmites. BS8 isotope profiles are represented only for its middle to late Holocene part. Hiatuses not considered in the age-depth models are not represented here.

After a prolonged hiatus between ~ 7.5 and ~ 5.8 ka, BS8 calcite became more compact suggesting a change of precipitation conditions. This part presents slightly higher $\delta^{18}\text{O}$ (-8.33 ± 0.36 ‰) and remarkably lower $\delta^{13}\text{C}$ (-8.96 ± 0.48 ‰) associated with a slower growth rate (0.02 mm/yr), suggesting a more important soil activity, but a probable lower drip rate.

During the last 4 ka, in stalagmite BS15 is present a trend towards progressively higher $\delta^{13}\text{C}$ values (Fig. 6.4.5). A similar trend is also found in the last 2.5 ka in stalagmites BS9 and BS14. Considering the relation between hydrology and $\delta^{13}\text{C}$ variations (cf. Chapter 6.3), this trend would indicate a tendency towards longer dripping intervals, which may reflect drier conditions as also suggested by the relatively weak long-term trend towards higher Mg values in BS15 (Fig. 6.4.5). In addition the presence of *stricto sensu* microcrystalline calcite during the last 1.5 ka associated with the lack of the brownish lamination, which is believed to be related to organic matter flushing, is also consistent with a lower vegetation activity at that time (cf. Paragraphs 6.3.4.1 and 6.3.4.2).

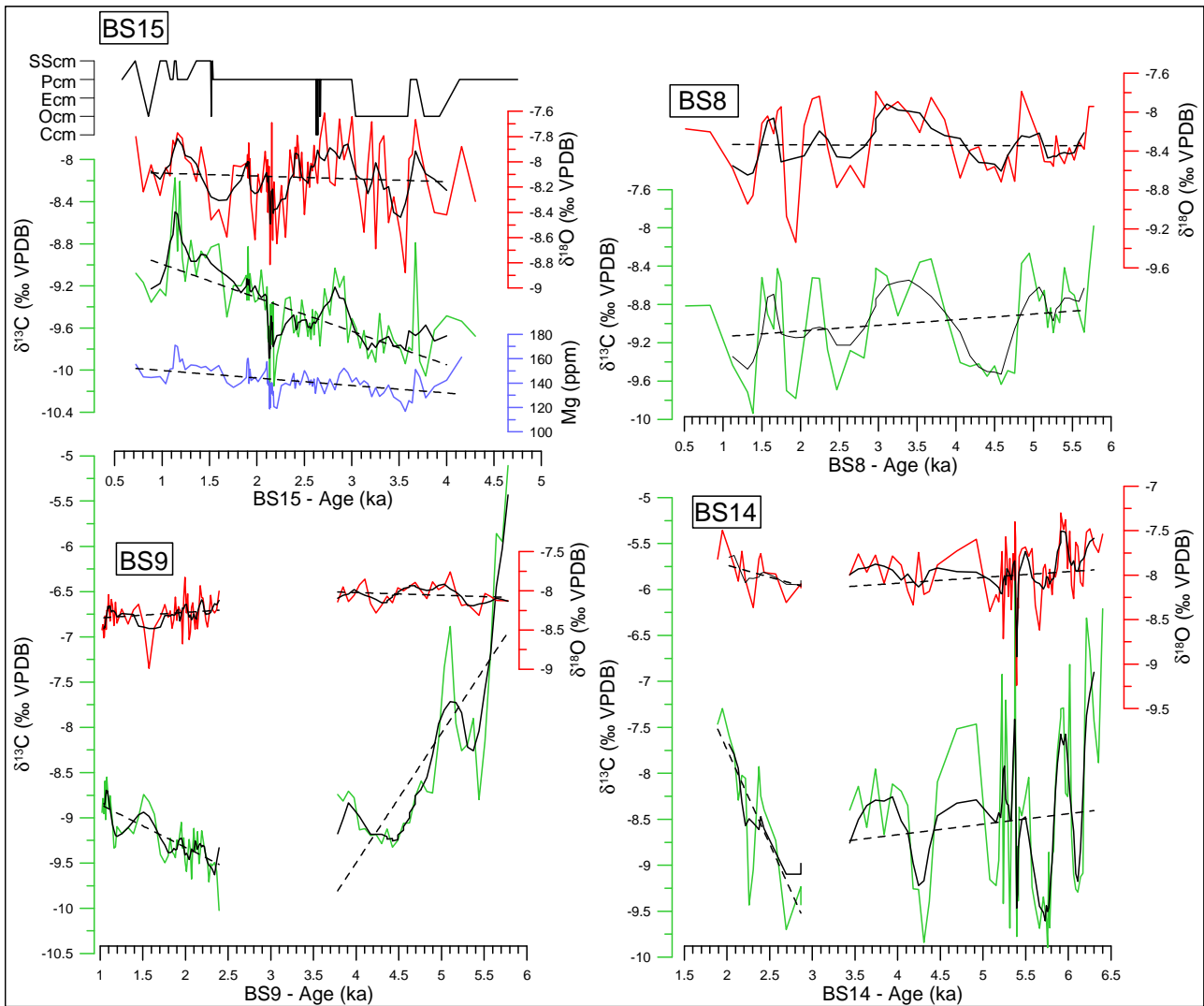


Fig. 6.4.5 – Middle to late Holocene $\delta^{13}\text{C}$ (green) and $\delta^{18}\text{O}$ (red) profiles in stalagmite BS15, BS8, BS9 and BS14, Mg (ppm) concentration variations and petrography variations in BS15. Black lines represent smoothed isotopic curves (5 points moving averages). Black dotted lines are the linear correlation calculated on the smoothed curves to highlight potential long-term trends. Hiatuses not considered in the age-depth model are not represented here.

6.4.2.2 Multi-decadal- to centennial-scale climate changes

- **Early Holocene (~12 – 8.2 ka)**

As showed previously (Paragraph 6.4.2.1), during the early Holocene in the Prača valley area, relatively dry conditions until ~10 ka may have occurred, followed by a trend towards wetter/milder conditions. Among the studied samples, only stalagmites G5 and BS8 were deposited during the early Holocene. The described differences in the duration of the hiatuses (Chapter 6.2) and in calcite patterns suggest the presence of different feeding systems and a stronger connection of stalagmite BS8 with the external environment. In this sample, two growth interruptions between ~5.8 - 7.5 ka and ~8 - 8.8 ka, together with two surfaces possibly referring to short hiatuses at ~10

and 10.3 ka, indicate changed environmental conditions not favourable to speleothem formation, that may suggest drier conditions or changed seasonality of precipitation. Stalagmite G5 started growing after an interruption between ~12.5 ka and 9.5 ka. Faint surfaces possibly indicating short growth interruptions were also found at ~9.4 and 8.7 ka. Unfortunately, the large age uncertainties prevented the identification of the precise duration of the hiatuses and the calculation of a high precision age-depth model for the studied stalagmites. However, according to common features identified in the stable isotope profiles, the hiatus at ~10 ka in BS8 could be correlated with the one found at ~9.5 in G5 (n° 6 in BS8 and n° 4 in G5 in Fig. 6.4.6), since they fall within the same time window identified by the large age uncertainty of the age model, suggesting a drier phase at that time (Fig. 6.4.6 a) and b)).

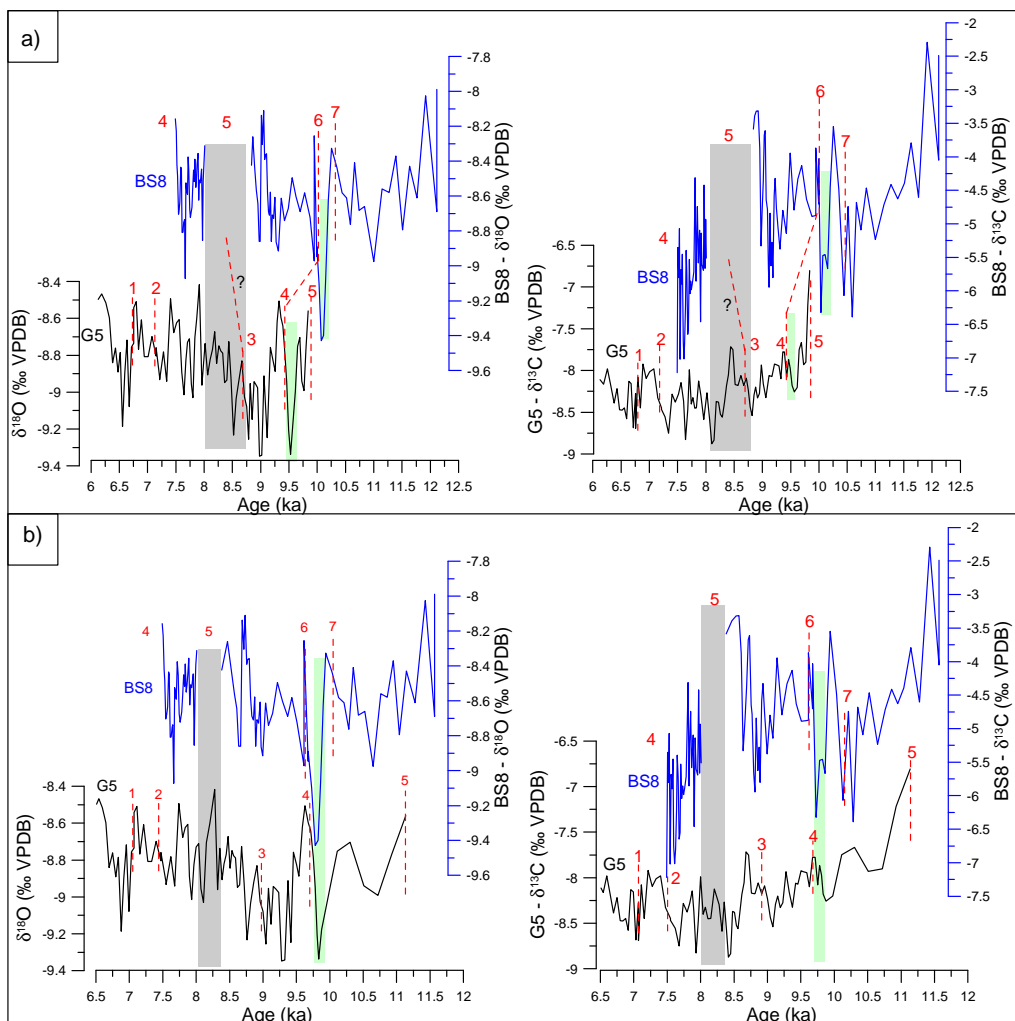


Fig. 6.4.6 – Early to middle Holocene $\delta^{13}\text{C}$ and $\delta^{18}\text{O}$ profiles for stalagmites BS8 (blue) and G5 (black). Red dotted lines indicate the identified growth interruptions; red numbers correspond to the hiatuses in plates 1 and 2 (Chapter 5). The grey box indicates the period in G5 corresponding to BS8 growth interruption. The green boxes indicate a possible correlation among stable isotope profiles. a): stable isotope profiles are plotted in relation to the age model (ages corresponding to the 50th percentile of the age model); b) stable isotope ratios are plotted in relation to the age model error boundaries: for BS8 the lower boundary (i.e. ages corresponding to the 3rd percentile of the age model) has been chosen, for G5 the upper boundary (i.e. ages corresponding to the 97th percentile of the age model) has been considered.

However, the period just before this hiatus (6 in BS8 in Fig. 6.4.6) presents a marked lowering of $\delta^{18}\text{O}$ and $\delta^{13}\text{C}$ values in both stalagmites (green box in Fig. 6.4.6). According to what explained in the previous chapter, the low isotopic values may represent a more important winter recharge (low $\delta^{18}\text{O}$) in a wetter context than the preceding period.

The longer hiatus between $\sim 8.9 \pm 0.4$ and $\sim 8.0 \pm 0.3$ ka in BS8 is less evident in G5 and should correspond to the one at ~ 8.7 ka, however G5 dating results show a continuous growth from ~ 8.6 ka until at least 7.1 ka, but with a slower deposition rate between ~ 7.5 and 7 ka (Fig. 6.4.6 a); Fig. 6.2.1 in Paragraph 6.2.2). This period is recorded differently in the two records probably because of the remarkably longer residence time of G5 feeding system and to its lower sensitivity to seasonal hydrological changes. Considering the large age uncertainty affecting the age model, it is difficult to compare the recorded signals in these two stalagmites. While low correlation among stable isotope profiles is present between profile plotted with their mean age calculated by the age model (Fig. 6.4.6 a)), if we plot the BS8 stable isotope profiles according to the lower boundary of the age model uncertainty (i.e. the ages corresponding to the 3rd percentile) and G5 stable isotope corresponding to the upper boundary of the age model uncertainty (i.e. the ages corresponding to the 97th percentile), good correlation among stable isotope variations are visible, especially during the first millennia of the Holocene (Fig. 6.4.6 b)). It is thus clear the impossibility to precisely individuate the stable isotope patterns in stalagmite G5 corresponding to BS8 prolonged growth interruptions (i.e. the one found between $\sim 8.9 \pm 0.4$ and 8.0 ± 0.3 ka; grey box in Fig. 6.4.6). However, the absence of hiatuses in G5 during that period, suggests the possible occurrence of seasonal changes which did not deeply affect this stalagmite feeding system. Slightly drier and generally cooler winter conditions may have led to the growth interruption in BS8.

- **Middle Holocene ($\sim 8.2 - 4.2$ ka)**

Between ~ 8 and 7.5 ka BS8 started growing again suggesting increased moisture availability during this time window. The age model related to this part is considered reliable. The fast growth rate, associated with the porous fabric, suggest the presence of strong cave ventilation and/or fast and irregular water discharge (Chapter 6.3). This stalagmite portion presents $\delta^{18}\text{O}$ values comparable to the previous periods and lower $\delta^{13}\text{C}$ values. Wetter winter and summer conditions are then inferred for this period. Stalagmite BS8 stopped growing again at ~ 7.5 ka until about 5.7 ka. Two hiatuses are present in G5 at ~ 7.1 and 6.8 ka, and its growth rate decreased between ~ 7.5 and 7 ka, thus suggesting short deterioration of climate conditions. At ~ 6.2 ka, G5 stopped growing definitively indicating changed conditions which were not favourable to its growth. The period comprised

between ~8 and 6 ka in G5 presents relatively higher $\delta^{18}\text{O}$ and lower $\delta^{13}\text{C}$ if compared with older recorded periods. A trend towards wetter summers and/or milder winters is thus inferred.

As previously described, the growth interruption of G5, broadly corresponding to the re-start of BS8 with a more compact texture and lower $\delta^{13}\text{C}$, together with the formation of the other stalagmites sampled in Mračna Pećina cave (BS14 and BS9 first, BS15 then), may be related to climate and/or environmental changes. A decreased cave ventilation, triggered (at least partly) by the occurrence of milder winters and/or by a change in cave dynamics able to modify cave air circulation, may have decreased cave CO_2 sequestration, especially in the area far from the entrance (where G5 was sampled), lowering calcite saturation and speleothem formation. Another option may be represented by the combination of soil/vegetation development above the cave together with relatively drier conditions, which may have caused: 1) the extinction of the drip site feeding stalagmite G5 and 2) an increase in calcite saturation of fast infiltrating water (i.e. drip sites presenting a strong connection with precipitation), leading to the deposition of stalagmites BS9, BS14 and BS15.

The period comprised between ~6 and 4.2 ka is not well recorded by the analysed record. Stalagmite BS8 started growing again at ~5.7 ka after a prolonged hiatus, displaying a more compact texture than its older part (cf. above). According to the age model, a hiatus is present at $\sim 4.8 \pm 0.3$ ka (n° 3 in Fig. 6.4.7 and 6.4.8). However, the age model of BS8 younger part is not accurate and fully reliable due to the presence of large age uncertainties and several hiatuses not considered in the model (Paragraph 6.2.3). Stalagmite BS9 displays a dendritic texture associated with high $\delta^{13}\text{C}$ values until ~5.1 ka (Fig. 6.4.7), when, after a short hiatus, its texture changed to microcrystalline calcite (cf. Paragraph 6.3.4.3). A hiatus occurred after ~4.5 ka and the stalagmite started growing again at ~2.3 ka. Unfortunately its precise duration was not determined due to large age uncertainties. Stalagmite BS14 started growing at $\sim 6.4 \pm 0.7$ ka, displaying noisy $\delta^{13}\text{C}$ and $\delta^{18}\text{O}$ isotope profiles (Fig. 6.4.7 and 6.4.8). It displays the alternation of different calcite textures at the lamina scale (in particular Ccm, Ocm and Pcm; Fig. 6.4.9) suggesting frequent fluctuations in drip rate, possibly related to hydrological instability. At $\sim 4.2 \pm 0.4$ ka a hiatus occurred (n° 3 in Fig. 6.4.7 and 6.4.8). Unfortunately, because of the low reliability of the age models, it is not clear whether the hiatuses identified at ~4.8 ka, after 4.5 ka and at ~4.2 ka in, respectively, BS8, BS9 and BS14 can be correlated or not. Although any marked trend or climate condition can be discussed for the period between ~6 and 4.2 ka due to the data low resolution, the presence of hydrological instability can be inferred.

- **Late Holocene (from ~4.2 ka)**

Despite the relative stability in terms of temperature and/or seasonality of rainfall, a long-term trend towards relatively drier conditions is seen in the last 4 ka (cf. Paragraph 6.4.2.1). Unfortunately, as for the early Holocene (BS8 and G5), large uncertainties affecting the age models complicated the correlation of stable isotope patterns between the studied samples (Fig. 6.4.7 and 6.4.8). High $\delta^{13}\text{C}$ and $\delta^{18}\text{O}$ values are present between about ~3 and 2.3 ka in stalagmite BS15, suggesting the occurrence of a dry phase which lead to the deposition of porous microcrystalline calcite (Pcm; Fig. 6.4.9). At the same time, stalagmite BS9, whose age model, together with the BS15 one, is considered reliable (cf. replication test: Paragraph 6.3.3.1), was not growing (Fig. 6.4.7 and 6.4.8), providing further clues for the occurrence of a dry phase. Similar peaks in $\delta^{13}\text{C}$ and $\delta^{18}\text{O}$ profiles also associated with hiatuses were identified in BS8 and BS14 stable isotope profiles, although with large age offsets, which falls within the age model uncertainties (Fig. 6.4.7 and 6.4.8). The strong co-variation between the two isotopic ratios in these parts of stalagmites BS8 and BS14 may be the result of stalagmite growth under extremely thin film of fluid causing calcite deposition at isotopic disequilibrium.

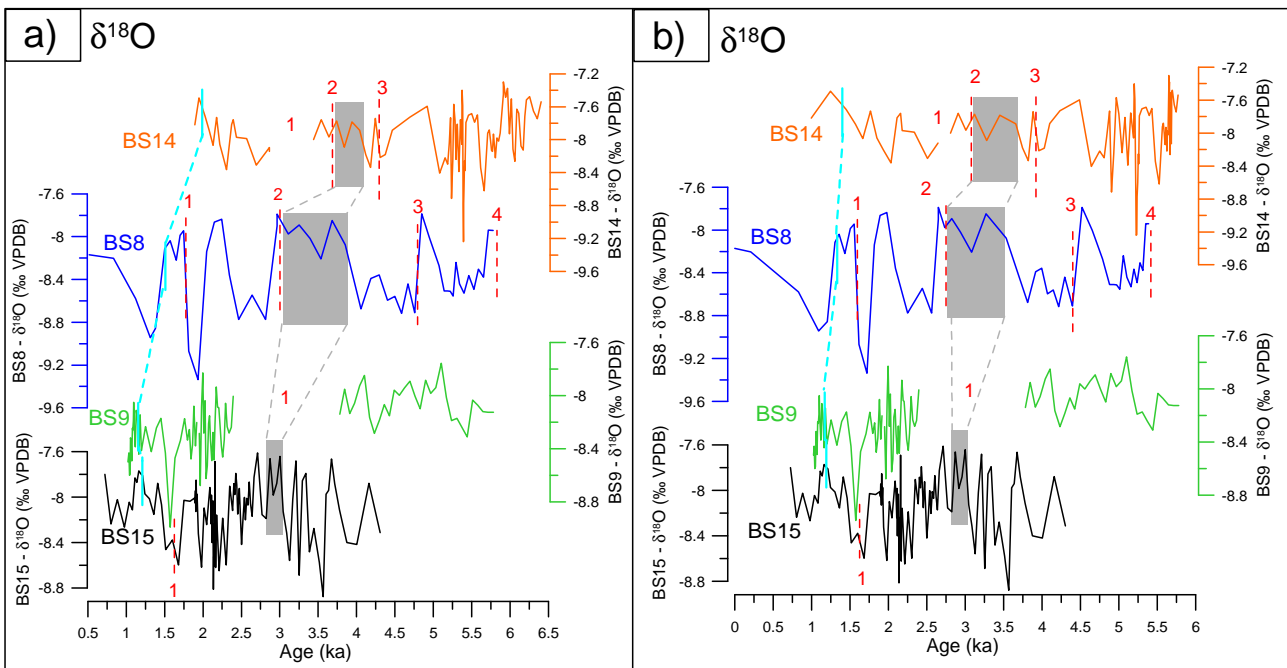


Fig. 6.4.7 – $\delta^{18}\text{O}$ profiles of stalagmites BS8 (top part), BS9, BS14 and B15 covering the second half of the Holocene. Red dotted lines and red numbers represent hiatuses (Plates 2 to 4 in Chapter 5). Light blue dotted line indicates a dark layer found close to the top of all these samples. The grey and the green shades are possible correlations among stable isotope profiles indicating a warmer and/or drier period. a): stable isotope profiles are plotted in relation to the age model (ages corresponding to the 50th percentile of the age model); b) stable isotope ratios are plotted in relation to the age model error boundaries: for BS8 and BS14 the lower boundary (i.e. ages corresponding to the 3rd percentile of the age model) has been chosen, for BS9 and BS15 the ages calculated in the age model are kept (ages corresponding to the 50th percentile of the age model).

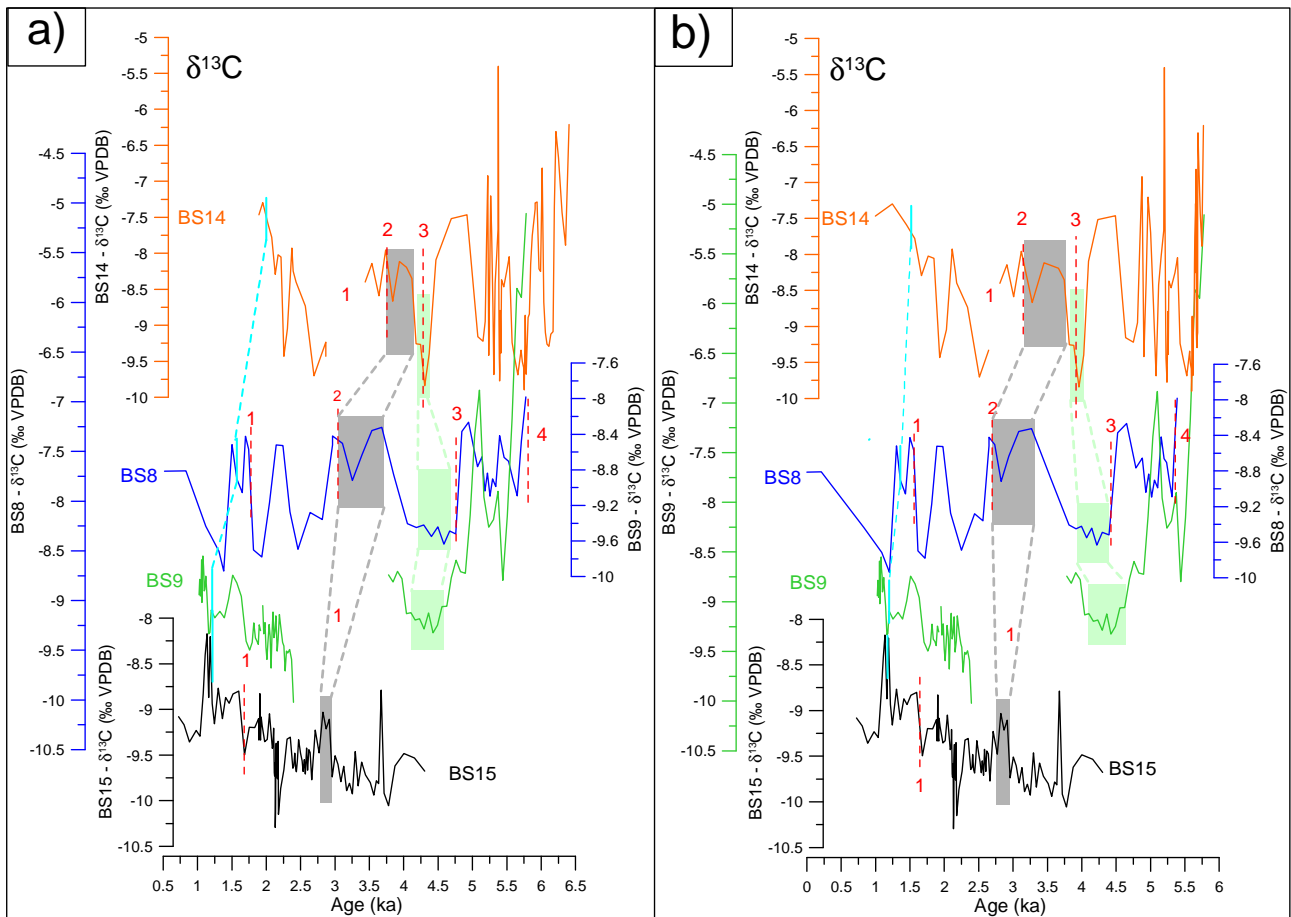


Fig. 6.4.8 – $\delta^{13}\text{C}$ profiles of stalagmites BS8 (top part), BS9, BS14 and B15 covering the second half of the Holocene. Red dotted lines and red numbers represent hiatuses (Plates 2 to 4 in Chapter 5). Light blue dotted line indicates a dark layer found close to the top of all these samples. The grey and the green shades are a possible correlation among stable isotope profiles indicating a warmer and/or drier period. a): stable isotope profiles are plotted in relation to the age model (ages corresponding to the 50th percentile of the age model); b) stable isotope ratios are plotted in relation to the age model error boundaries: for BS8 and BS14 the lower boundary (i.e. ages corresponding to the 3rd percentile of the age model) has been chosen, for BS9 and BS15 the ages calculated in the age model are kept (ages corresponding to the 50th percentile of the age model).

During the long term trend towards more arid conditions a wetter spell probably occurred between about 2.2 and 2.1 ka, when in stalagmite BS15 lower $\delta^{13}\text{C}$ associated with Ccm is present (compact columnar microcrystalline calcite; cf. Paragraph 6.3.3.2; Fig. 6.4.9).

From about 1.5 ka a steepening of $\delta^{13}\text{C}$ trend towards higher values associated with the presence of microcrystalline calcite is present in BS15. This trend may be correlated to the steepening of $\delta^{13}\text{C}$ at the top of stalagmite BS14 (grey shade in Fig. 6.4.9). Large age offset is present between these two $\delta^{13}\text{C}$ patterns which fall only partially within the error of the age model and that would make this correlation unlikely (Fig. 6.4.8b). However, the low reliability of BS14 age model in this part (Paragraph 6.2.5) and the presence of the dark (i.e. soot, cf. Chapter 6.5) layer, which can be considered as an event-marker, make this correlation plausible. This part of BS14 present elongated

microcrystalline to dendritic fabrics which are also indicating dry conditions. The presence of different microcrystalline subtypes in BS15 and BS14 during growth phases that are thought to be coeval can be related to the sensitivity of petrography to drip rate, which in turns depends on the dynamics of the drip site feeding the stalagmite. Indeed, stalagmite BS14 was probably fed by a slower drip site than stalagmite BS15.

The last 1.5 ka in stalagmite BS15 also lacks the brownish lamination suggesting the absence of organic matter flushing events, which is consistent with the identified drier conditions. However, lower vegetation cover allowing for higher soil erosion and transfer of foreign particles (characteristic of this fabric) is not excluded. Indeed, the *strico sensu* microcrystalline calcite deposited at that time is known to be influenced by the presence of foreign particles favouring the formation of crystal defects (cf. Frisia, 2015). Finally, a return towards less dry conditions probably occurred in the last 200 years of stalagmite BS15, where a lowering of $\delta^{13}\text{C}$ values is present.

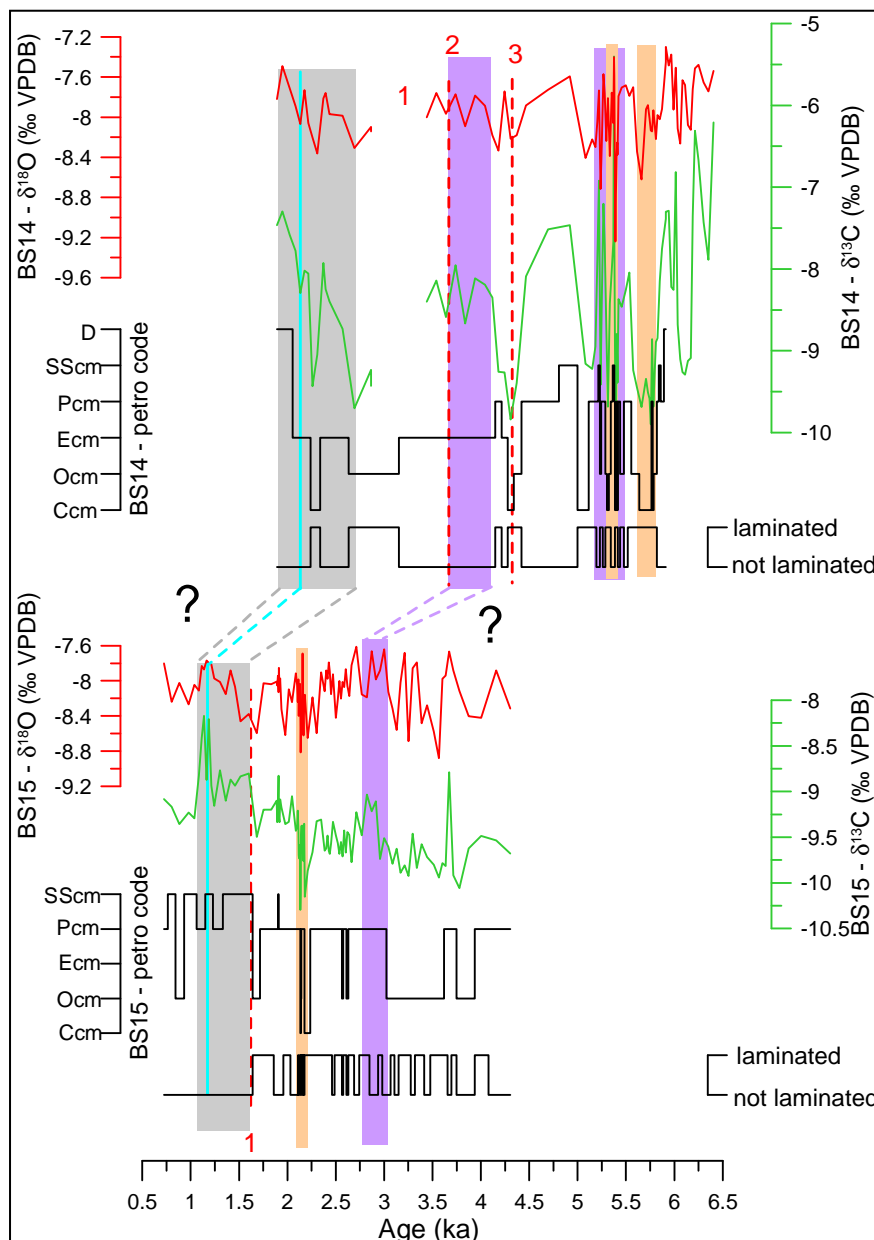


Fig. 6.4.9 – $\delta^{13}\text{C}$, $\delta^{18}\text{O}$ petrography and lamination curves of stalagmites BS14 and BS15 covering the second half of the Holocene. Minor hiatuses are represented with red dotted lines and red numbers (Plate 4 and 5 in Chapter 5). Orange shadows indicate periods of milder and wetter winter climate conditions. Purple shadow indicates a remarkably drier period. Grey shadow indicates a dry period possibly when increased anthropogenic pressure on the overlying plateau possibly occurred.

6.4.3 Comparison with other records and signal interpretation in the wider context of climate variations in the central Mediterranean and the Balkan region

- **Early Holocene (~12-8.2 ka)**

After the last remarkably cold and dry spell represented by the Younger Dryas, the onset of warmer conditions indicating the end of the last glacial period in the Adriatic occurred at ~11.5 ka (Ariztegui et al., 2000). At this point an arboreal cover started developing in the Adriatic basin.

After a relatively dry period during the first millennia of the Holocene, soil restoration and/or wetter conditions are suggested by the Bosnian stalagmites, where a trend towards lower $\delta^{13}\text{C}$ values is present (Paragraph 6.4.2). However, relatively low soil development associated with strong seasonality of precipitation and/or temperature persisted until about ~6 ka, when stalagmite G5 stopped growing and stalagmite BS8 started being deposited, after a prolonged hiatus, with a more compact texture and a slower growth rate. At the same time BS14 and BS9 started growing followed by BS15.

During the early to middle Holocene, in other Balkan records, cold winter conditions were recorded (e.g. Lake Ohrid and Lake Maliq; Bordon et al., 2009; Vogel et al., 2010). This pattern may have been enhanced by high summer insolation associated with low winter insolation during the early Holocene (Fig. 6.4.10). At this time the installation of a positive NAO-type circulation in the North Atlantic Area is also inferred, which, in association with ice-sheet melting and solar forcing, may have been responsible for wetter conditions in the northern European sites and drier conditions in the southern ones (Davis and Brewer, 2009). Around 10 kyrs ago, low $\delta^{18}\text{O}$ and $\delta^{13}\text{C}$ values in both BS8 and G5 stalagmites suggest wetter conditions, similarly to what is observed in the south Mediterranean sites during the same period (south of 40°N; Magny et al., 2013).

The correspondence between the two major growth interruptions identified in stalagmite BS8 and two cold spells recorded in the south Adriatic Sea is particularly interesting (Siani et al., 2013; Fig. 6.4.10). Unfortunately, the precise duration of the hiatuses in the Bosnian stalagmite was not identified because of the large age uncertainties (Paragraph 6.2.3).

The first of these two hiatuses, identified between $\sim 8.9 \pm 0.4$ and 8.0 ± 0.3 ka, comprehends the time window corresponding to the Sapropel S1 deposition interruption which occurred between about 8.2 and 8.0 ka (e.g. Rohling, 1997). Although it is not clear whether this interruption is related to the same 8.2 ka event recorded in Northern Atlantic Ocean sites or not, this temporary return to oxygenated bottom water conditions suggests a decrease fluvial inflow in the Mediterranean Basin (Ariztegui et al., 2000). While this return to cooler and drier conditions has

been recorded by several marine and lake records in the Periadriatic and central Mediterranean area (e.g. Giunta et al., 2003; Bordon et al., 2009; Avramidis et al., 2012; Di Rita and Magri, 2012; Peyron et al., 2013; Siani et al. 2013), it is poorly witnessed in speleothems. No dry/cool phase which may be correlated with the S1 interruption was recorded in stalagmites from Corchia Cave (Tuscany, NW Italy; Zanchetta et al., 2007a) and Savi Cave (Friuli Venezia Giulia, NE Italy; Frisia et al., 2005), while a dry and cool phase centred at ~8.2 ka was recorded in a stalagmite from Carburangeli Cave (Sicily, S Italy; Frisia et al., 2006). In Eastern Europe (Balkans and Carpathian Region) a cooling occurring at ~8.2 ka is clearly documented by lake and pollen records but does not find a correspondence in speleothem $\delta^{18}\text{O}$ ratios (Drăguşin et al., 2014 and reference therein). This difference may reside in the proxy sensitivity to seasonal changes. In particular, in the Romanian record, increased summer precipitation was inferred during this period but any decrease in winter precipitation was identified (Ascusnă Cave, Drăguşin et al., 2014). Lake records from Northern Italy and the central Balkans show relatively drier winters associated with cooler and wetter summers at ~8.2 ka (Lake Ledro, Peyron et al., 2013; Lake Maliq, Bordon et al., 2009).

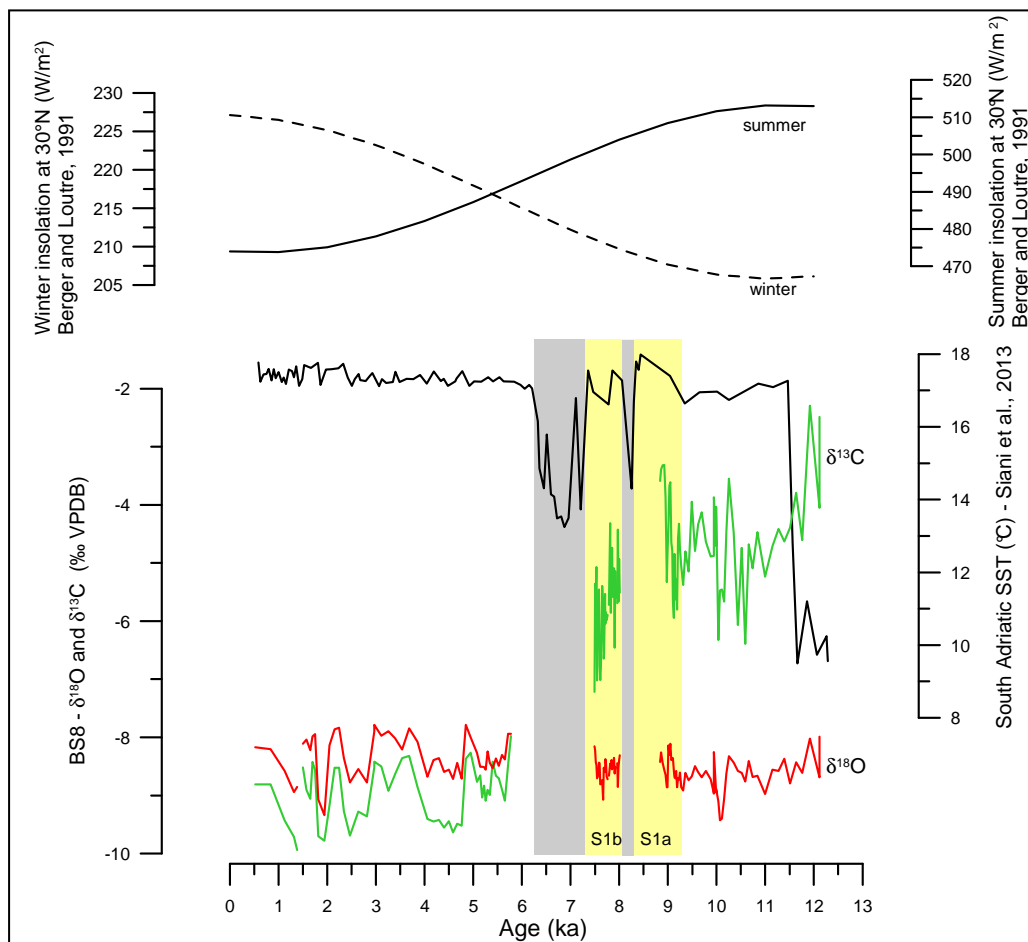


Fig. 6.4.10 – $\delta^{13}\text{C}$ (green) and $\delta^{18}\text{O}$ (red) profiles of stalagmite BS8 and South Adriatic Sea Surface Temperature ($^{\circ}\text{C}$) (Siani et al., 2013); winter and summer insolation variations at 30°N during the Holocene (Berger and Loutre, 1991). Grey shades indicate two marked cold spells of surface water identified in the South Adriatic Sea; yellow shades indicate Sapropel S1a and S1b deposition in the South Adriatic Sea (Siani et al., 2013 and references therein).

Considering the Bosnian record, the continuous growth of stalagmite G5 during the prolonged stalagmite BS8 growth interruption (between ~8.9 and 8 ka) confirms the role of site-specific sensitivity to seasonality. The prolonged and marked hiatus of BS8 suggests the occurrence of slightly drier conditions characterising this period in this area of the Balkans. At the same time, cooler and drier conditions are also recorded at Lake Ohrid (Lacey et al., 2015). The continuous growth of stalagmite G5 would suggest it was not however a marked dry phase, preventing calcite deposition at this site.

- **Middle Holocene (8.2 – 4.2 ka)**

After the 8.2 ka cool and dry phase, the southern Mediterranean basin experienced its wettest phase, which caused the deposition of Sapropel S1b (~8.0-7.4 ka; Siani et al., 2013). This period corresponds to a fast growing phase of stalagmite BS8, while stalagmite G5 did not show any significant change. According to Magny et al. (2013), the deposition of Sapropel S1 has been favoured by increased winter precipitation in the Northern Mediterranean regions and increased winter and summer precipitation in the Southern Mediterranean ones. An important increase in winter precipitation may have had a detectable influence on G5 stable isotope composition as a stronger winter recharge results in lower $\delta^{18}\text{O}$ values. However, only a slight lowering of stable isotope values is recorded in G5 stalagmite during Sapropel S1 deposition. Thus, increased precipitation in both summer and winter season may have occurred, in line with what was recorded at the Southern Mediterranean sites.

The second BS8 growth interruption occurred just after 7.5 ± 0.4 ka. According to the age model, the stalagmite started growing again between ~6.6 and 5.4 ka (Fig. 6.2.2 in Paragraph 6.2.3). The correspondence of this hiatus with the cold sea surface temperature identified in the Adriatic core MD 90-917 by Siani et al. (2013) is remarkable (Fig. 6.3.10). In G5 this period is not recorded as a marked dry phase in the stable isotope record; however, two growth interruptions occurred at ~7.1 and 6.8 ka and the growth rate slowed down. In the central Mediterranean area the presence of a clear climate event during this period is poorly documented. Evidences of a cool and dry phase at ~7.3 and 7.1 ka are found in Slovenia and Croatia (Wunsam et al., 1999; Andrič, 2007), while a decrease in temperate taxa suggests cooler climate conditions between 7.8 and 6.3 in the southern Balkans (Avramidis et al., 2012). Lake records from the central Balkans and the Italian peninsula do not register this cooler phase, which is coeval with the cooling observed in the Aegean Sea. The latter has been related to a multi-decadal period with winter outbreaks of cold and dry north-eastern winds likely induced by a strengthening of the Siberian High (Rohling et al., 2002; Marino et al., 2009). This may have also caused a strengthening of the Bora wind over the Adriatic. A similar

response of the Bora wind to the Siberian High was also supposed by Belli et al. (2013) in Savi Cave, but during the Younger Dryas (cf. Paragraph 2.2.1.1). These winds may have thus influenced the winter climate of the Balkan and central Adriatic area, without evident climatic consequences on the Tyrrhenian side of the Italian Peninsula. Unfortunately, the lack of palaeoclimate records dating back to this period from the Adriatic side of the Italian Peninsula prevents the demonstration of this hypothesis for this area. At present, the Siberian High, which is linked to the EA/WR teleconnection pattern, is thought to be indirectly influenced by the NAO (Krichak and Alpert, 2005; Paragraph 2.1.1). Thus, it not clear whether a strengthening of the NAO in the past may have indirectly influenced the outburst to dry and cold north eastern winds over this region.

The strong sensitivity of stalagmite BS8 to seasonal changes may have thus enabled its recording. However, this phase was probably characterised by less severe conditions than the 8.2 ka cool and dry event, which was documented in several palaeoclimate studies (using different proxies) in the area. For example, comparing the close Lake Ohrid record with the Bosnian one, it is possible to identify a marked reduction of organic matter content at 8.2 ka, while any evidence of a cool phase was recorded after the Sapropel S1b deposition (Fig. 6.4.11). This may be related to a different magnitude of the recorded events and/or to changed seasonality: while the 8.2 ka event probably affected winter and summer precipitation and/or temperature, the second one (post-sapropel S1b) was probably mainly related to winter changes.

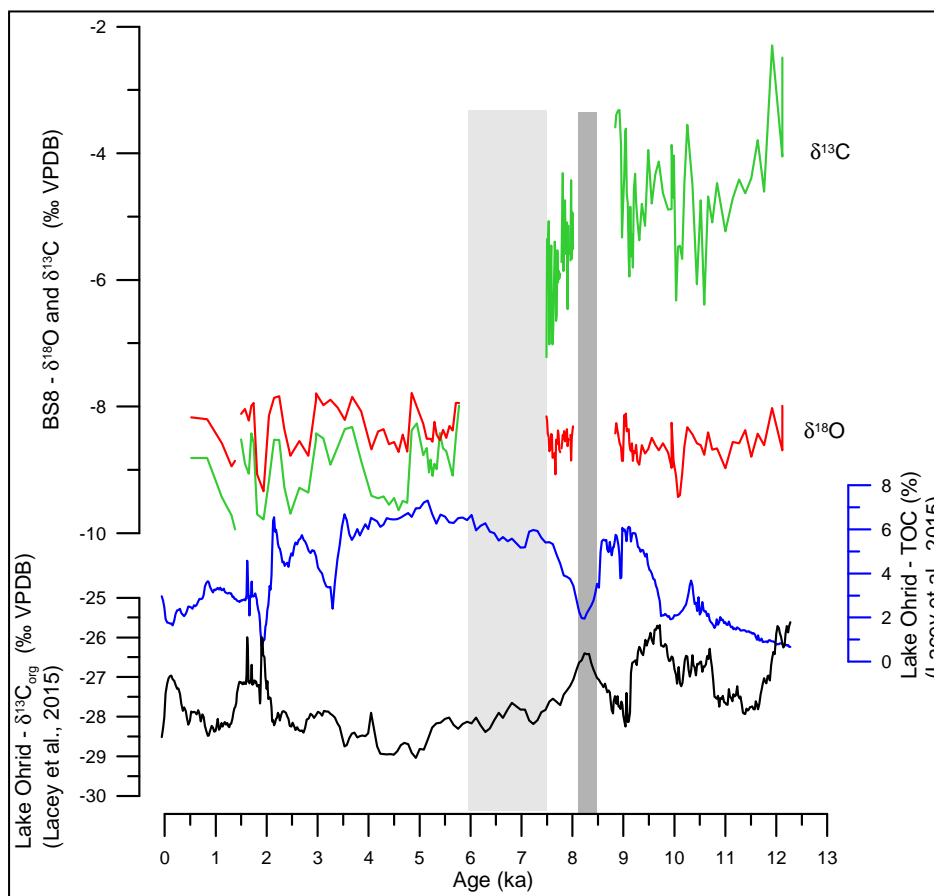


Fig. 6.4.11 – $\delta^{18}\text{O}$ (red) and $\delta^{13}\text{C}$ (green) profiles in stalagmite BS8 and total organic carbon (TOC %; blue) and organic matter $\delta^{13}\text{C}$ (black) of Lake Ohrid (Lacey et al., 2015). Grey box indicates the 8.2 ka cold and dry event, while the light grey box indicates the period of cold sea surface temperature in the South Adriatic Sea (~7.3-6.3 ka; Siani et al., 2013).

At 6.3 ka stalagmite G5 stopped growing definitively, while BS8, after a prolonged interruption, started again at ~5.8 ka with remarkably lower $\delta^{13}\text{C}$ values and a more compact texture (Fig. 6.2.2 in Paragraph 6.2.3 and Fig. 6.3.11 in Paragraph 6.3.4.3). In this period, also stalagmite BS14 (~6.4 ka), followed by BS9 (~5.9 ka) and BS15 (~4.3 ka), started being deposited. The remarkable lowering of $\delta^{13}\text{C}$ ratios found in stalagmite BS8 during the second half of the Holocene may be the result of progressive soil development and vegetation recover after the glacial period. Such a delay of soil development after the severe conditions of the last glacial period has also been recorded in other sites, like stalagmite CC26 from Corchia cave (Fig. 6.4.12), which developed in a similar geological context (Zanchetta et al., 2007).

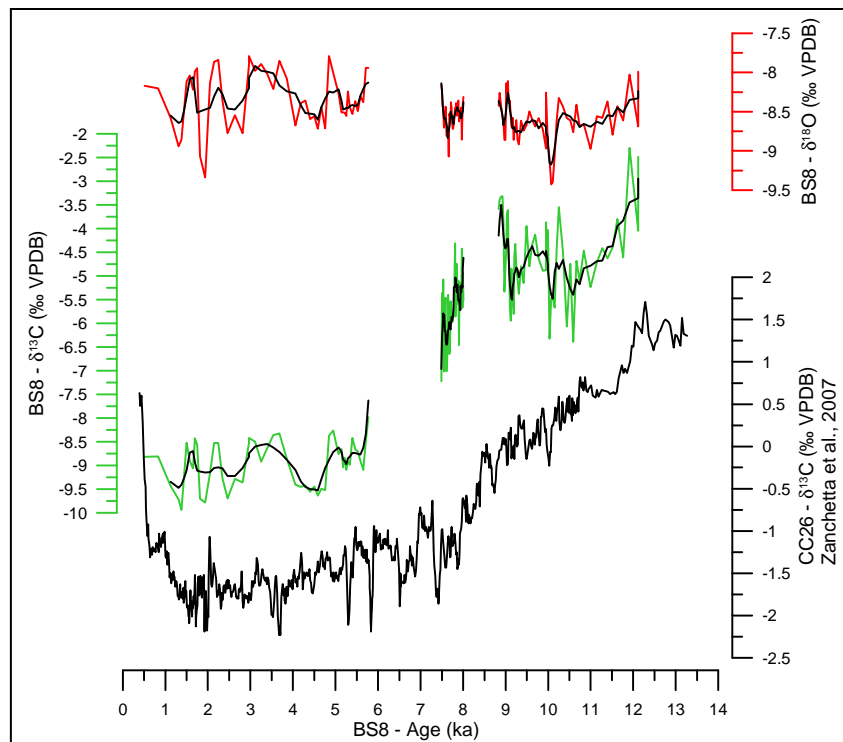


Fig. 6.4.12 – $\delta^{13}\text{C}$ and $\delta^{18}\text{O}$ profiles of stalagmite BS8 and $\delta^{13}\text{C}$ profile of stalagmite CC26 from Corchia Cave (Zanchetta et al., 2007). A similar trend towards lower $\delta^{13}\text{C}$ ratios is present in both stalagmites.

A more soil development, together with improved climate conditions (warmer winters), is reflected by the deposition of stalagmites BS14 and BS9 first, and BS15 later. At the same time, improved climate conditions are also present in the South Adriatic Sea, where the highest sea surface temperature of the last 12 ka are recorded between ~6.9 and 5.6 ka (Siani et al., 2013). Increased salinity at the same site suggests a trend towards drier conditions in the southern Mediterranean area (Siani et al., 2013; Sangiorgi et al., 2003). In the northern Balkans, a forest regeneration occurred at ~7.0 ka and milder conditions favourable to tufa formation developed (Horvatinčić et al., 2003; Andrič et al., 2007). A transitional phase towards a Mediterranean climate is recorded between 6.3 and 5.5 ka in the Croatian coastal areas (Wunsam et al., 1999). Moderate drier and warmer

conditions occurred in the central/southern Balkans between 6.0 and 4.3 ka (Lake Dojran; Francke et al., 2013). However, Lacey et al. (2015) observed relatively wet conditions at Lake Ohrid (west from Lake Dojran) at the same time. In the southern Balkans (Greece), wet and mild winters associated with dry and warm summers dominated this period (Alikes Lagoon; Avramidis et al., 2012).

The Bosnian stalagmites have recorded a certain degree of hydrological instability during this period (between ~6.4 and 4.3 ka), when BS14 witnesses the alternation of relatively mild and wet conditions and slightly drier and/or cooler ones. At the same time, BS9 dendritic texture shows the presence of relatively drier and/or cooler conditions than during the following period.

In northern and southern Periadriatic sites, this period is mainly seen as a transitional phase, which will bring to, respectively, increased aridity in the south and wetter condition in the northern Mediterranean regions (e.g. Desprat et al., 2013).

- **Late Holocene (from 4.2 ka)**

After the improvement of climate conditions, a dry short spell has been recorded by both stalagmites BS8 and BS14. This phase may probably be related to the so-called “4.2 ka event”, even if the large age uncertainties prevent a reliable identification. This dry event was clearly recorded by central/southern Italy (e.g. Renella Cave; Drysdale et al., 2006; Corchia Cave; Regattieri et al., 2014), Balkan and eastern Mediterranean sites, while in northern areas of the central Mediterranean (e.g. Northern Italy) there are no clear evidence of a marked dry spell (Zanchetta et al., 2016 and reference therein). Di Rita and Magri (2009), Zanchetta et al. (2011) and Zanchetta et al. (2016) suggest the origin of this event in the occurrence of longer and drier warm season, without any remarkable change in winter hydrology conditions. Such conditions may also explain the “condensed” calcite growth recorded during this period in both BS8 and BS14 stalagmites. In agreement with what is observed at Lake Shkodra (Sadori et al., 2015), this dry phase was preceded by a wet one that is reflected by BS14 petrography at the same time (Fig. 6.4.9 in Paragraph 6.4.2.2). Interestingly, the Calderone glacier expansion (Southern Appennines; Giraudi et al., 2005), occurring between ~4.5 and ~4.0 ka, corresponds to the period in which stalagmite BS15 started growing. This would indicate the absence of a phase, at 4.2 ka, dry enough to deeply affect calcite precipitation.

The following long-term trend towards higher $\delta^{13}\text{C}$ in BS15 and BS9 has been interpreted as a trend towards increased aridity. This is in agreement with the Lake Ohrid record (central Balkans), where increased calcite $\delta^{18}\text{O}$ and decreased TOC (%) suggest the onset of progressively drier conditions (Fig. 6.4.13; Lacey et al. 2015).

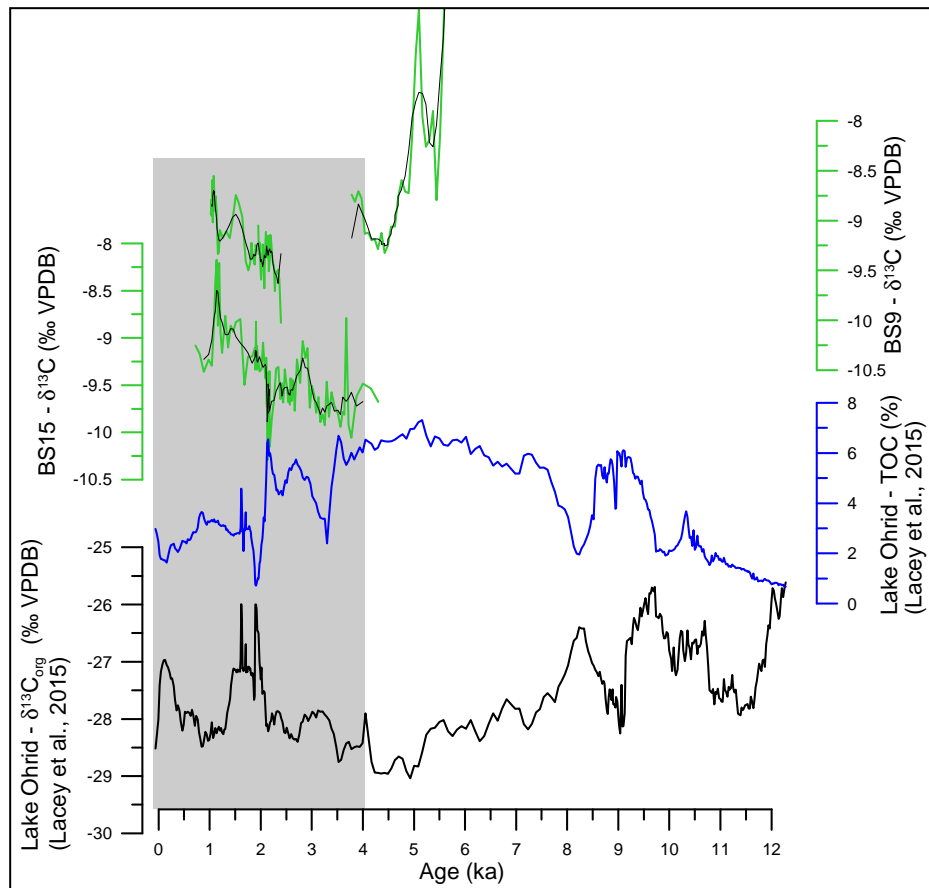


Fig. 6.4.13 – $\delta^{13}\text{C}$ profiles of stalagmites BS9 and BS15 and total organic carbon (TOC %) and organic matter $\delta^{13}\text{C}$ of Lake Ohrid (Lacey et al., 2015). The shaded area indicates the period for which a drying trend is seen.

From ~4.5 ka until present, the opposite trend observed between northern and southern location of the Mediterranean becomes more evident, with increased dryness in the southern and eastern areas and wetter conditions in the northern sites (Magny et al., 2003; Magny and Combourieu, 2013). This period corresponds to the end of the persistent positive NAO-phase recorded during the early Holocene and a southerly migration of the westerlies and of ITCZ in the tropics (Magny et al., 2013 and reference therein).

In the Bosnian stalagmites a remarkably dry phase is found centred at ~3 ka in BS14, BS9 and BS8, while it is less clear in BS15, where any marked growth interruption is seen, but only relatively higher $\delta^{18}\text{O}$ values between about 3 and 2.4 ka (Fig. 6.4.8 in Paragraph 6.4.2.2). The period between ~3.5 and 3 ka corresponds to a marked lowering of TOC (%) at Lake Ohrid, suggesting the occurrence of drier conditions at this site (Lacey et al., 2015). In the central Mediterranean sites no remarkable climate event has been recorded. On the contrary, eastwards in the Southern Carpathians, cold conditions are recorded at ~3.2 ka (Constantin et al., 2007; Drăguşin et al., 2014 and reference therein), suggesting changed hydrology in the Eastern Mediterranean which may have affected also the studied region. In particular, in the southern Carpathians a reduction in winter rainfall and/or increased summer precipitation is inferred at ~3.2 ka (Drăguşin et al., 2014). The

presence of a prolonged hiatus in BS9 in association to the higher $\delta^{18}\text{O}$ and $\delta^{13}\text{C}$ values found in BS15, BS14 and BS8 would agree with this interpretation. This dry phase is followed by relatively wetter conditions (~ 2.6 and between ~ 2.2 and 2.1 ka) recorded in stalagmite BS15 (light blueshades in Fig. 6.4.14), during a period with a less stable NAO-type atmospheric circulation (Fig. 6.4.14; Olsen et al., 2012). According to Magny et al. (2013) and Lamy et al. (2006) changes in NAO-type circulation and solar forcing played an important role in Mediterranean climate fluctuations during the Holocene.

With the exception of another relatively wet spell at ~ 1.6 ka, generally drier conditions followed until a short return to a wetter phase during the last 200 yrs of growth of this stalagmite. According to BS15 age model, this 200 yrs long phase would have started at $\sim 1.0 \pm 0.1$ ka, corresponding to the so-called “Medieval Climate Anomaly”. Thus, the cold conditions brought by the onset of the following “Little Ice Age” at ~ 0.7 ka may have favoured the definitive growth interruption of this sample at $\sim 0.7 \pm 0.3$ ka. Unfortunately, the large age uncertainties prevent the precise temporal identification of these events. Indeed, considering the age uncertainties, the peak of $\delta^{13}\text{C}$ and $\delta^{18}\text{O}$ recorded at $\sim 1.2 \pm 0.2$ ka (Fig. 6.4.14) may instead represent the milder conditions of the “Medieval Climate Anomaly”, while the following drop of $\delta^{13}\text{C}$ and $\delta^{18}\text{O}$ values may be indicative of the onset of the “Little Ice Age”.

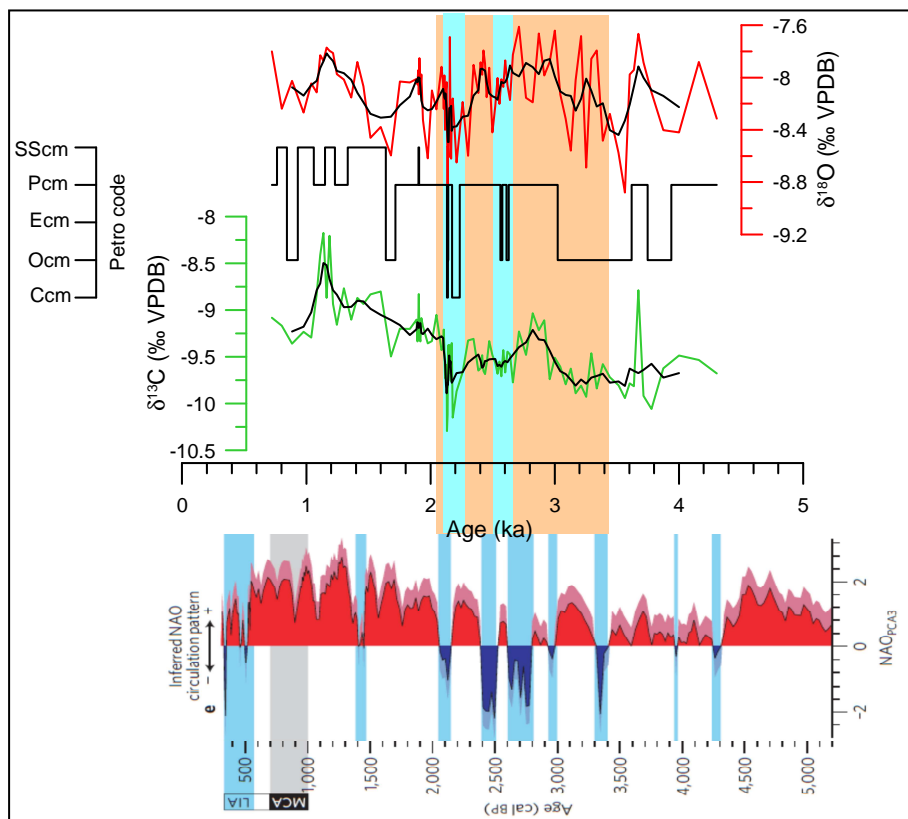


Fig. 6.4.14 – $\delta^{13}\text{C}$, $\delta^{18}\text{O}$ and petrography changes in stalagmite BS15 and NAO oscillation reconstruction for the last 5.2 ka (Olsen et al., 2012). The orange box indicates a phase of less stable NAO phases/regime. The light blue shades indicate wetter phases recorded in stalagmite BS15.

6.4.4 Conclusions

Local conditions (i.e. orography and local soil development) influenced the formation of the Bosnian stalagmites collected in Govještica and Mračna Pećina caves (central Bosnia). Nevertheless, long-term climate trends were identified. Indeed, the Holocene Bosnian record suggests the presence of relatively dry conditions during the first millennia of the Holocene, followed by wetter conditions until ~7.5 ka. A transitional phase led to a long term trend towards more arid conditions during the last 4.2 ka. However, the low resolution of the analysed data must be taken with care and further paleoclimate studies in this region are needed to confirm the identified trend. If this pattern will be verified, it would indicate a Holocene climate response in the central Balkans similar to the one of south Mediterranean sites. However, its location at ~43°N would involve a slight offset for the Balkan region of the boundary between the contrasting Holocene climate patterns, assumed to be located at ~40°N in the Mediterranean (e.g. Magny et al., 2013). Indeed the studied site is located at higher latitude than other central Mediterranean sites (e.g. Lake Accesa; ~42°N) showing climate fluctuations typical of sites from the northern Mediterranean basin. The identified climate trends may be related to the distance of the Balkan region from the NAO influences and a regional sensitivity to eastern Europe atmospheric circulation, which is influenced by variations in the Siberian High. Indeed, even if a possible influence of NAO-type circulation likely influenced the climate pattern in this region during the last 5 ka, marked dry periods, possibly related to the strengthening of the Siberian High, have been individuated as well. Unfortunately, the large age uncertainties affecting the studied speleothems did not allow constraining accurately the timing of climate events. However this study demonstrates the importance and the need for palaeoclimate investigation, at the local scale, to better understand the atmospheric circulation dynamics at the borderline between northern and southern Mediterranean regions, representing a crucial point for the prediction of future atmospheric reorganisation over the Mediterranean basin, in response to global climate changes.

6.5 Archaeological evidence

6.5.1 Introduction

This short Chapter is about a marginal, but nevertheless interesting topic of this study: the origin of the black layer appearing in coeval stalagmites from Mračna Pečina Cave. Trace element analyses, fluorescence microscope observations, FTIR, micro-Raman and SEM analyses were performed to qualify it.

6.5.2 Timing of the black layer in the Mračna Pečina stalagmites

A dark layer presenting a sharp boundary with the underlying calcite layers has been observed in all the studied stalagmites from Mračna Pečina cave (i.e. BS8, BS9, BS14 and BS15; plates 1-4 in Chapter 5). Its presence along a single layer developing over the entire stalagmite surfaces, from the central axis to the speleothem flanks, suggests its origin as a substance that coated the whole stalagmite external surfaces during their growth period.

This layer is found, respectively, at 7, 14, 3 and 10 mm from the top in BS8, BS9, BS14 and BS15 which, according to the age-depth model, correspond respectively to 1.6 ± 0.2 ka (BS8), 1.2 ± 0.1 ka (BS9), 2.1 ± 0.5 ka (BS14) and 1.2 ± 0.1 ka (BS15). Thus, only in stalagmites BS15 and BS9 it appears to be contemporaneous (Fig. 6.5.1).

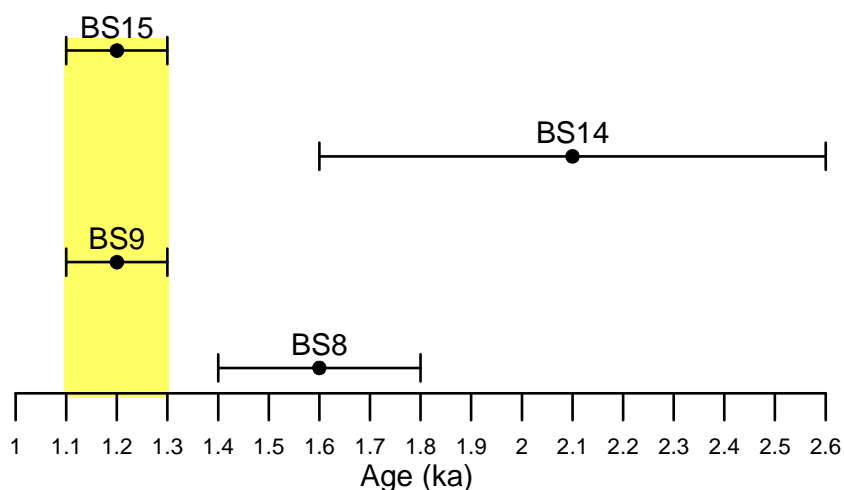


Fig. 6.5.1 – Ages of the black layer in stalagmites BS8, BS9, BS15 and BS14 according to their age-depth models. The yellow box indicates the ages that are contemporaneous.

However, the dating results of the younger portion of stalagmite BS14 were considered unreliable and possible U leaching, inferred from petrographic observations (cf. Chapter 6.2) may have resulted in older-than-expected U-Th ages.

Considering the BS8 age-depth model, problems in obtaining precise results may be due to: 1) large spatial errors in reporting the right distance from the top along the growth axis for samples taken along the flanks; 2) the presence of several hiatuses that have not been considered in the model (cf. Chapter 6.2). The age-depth models of stalagmites BS9 and BS15 were found to be the most precise also according to the good replication of the stable isotope profiles among the two samples (cf. Chapter 6.3). Thus, the age 1.2 ± 0.1 ka can be considered the most probable for the deposition of the black coating.

If we look at the U-Th results of samples before and after the black layer (without considering the age-depth model), it is possible to observe an overlapping of the age error bars in stalagmite BS8, BS9 and BS15 (Fig. 6.5.2), thus confirming the period at 1.2 ± 0.1 ka as the most plausible for the dark layer deposition.

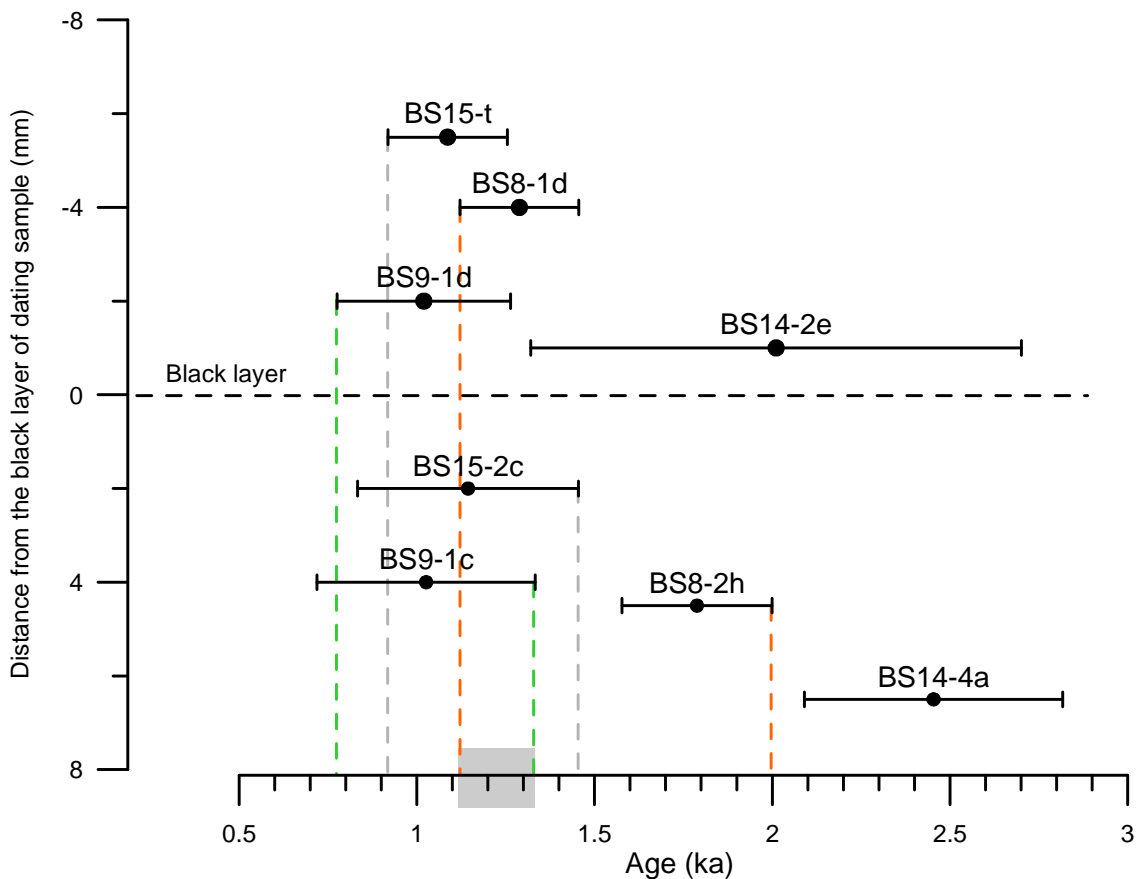


Fig. 6.5.2 – U-Th results for stalagmites BS8, BS9, BS14 and BS15 of samples below and above the black layer. Results are represented as a function of their distance from the black layer in each stalagmite: positive y values represent samples below the black layer; negative y values correspond to result above the black layer. The green, grey and orange vertical dotted lines indicate the projection on the x axis of the lower and upper limit of the age interval in which the black layer was deposited for, respectively, BS9, BS15 and BS8. The grey box on the x-axis indicates the range of ages in which the layer probably formed.

6.5.3 Origin of the black layer

Dark coatings in cave walls and speleothems are often related to manganese and iron oxides. Indeed, a Mn-Fe rich bedrock may provide iron and manganese ions which can be released into water under anoxic conditions. An example is provided in Gázquez et al. (2011) for El Soplao Cave (Spain): cave gallery flooding created the anoxic conditions necessary for manganese and iron ions to be mobilised and dissolved into water. These metals deposited on cave surfaces and their following oxidation under epiphreatic conditions, possibly mediated by microbial activity, caused the formation of black crusts (Gázquez et al. 2011; Northup et al., 2003).

However, there is no evidence of phreatic conditions in Mračna Pečina cave. Furthermore, laser ablation trace element analyses on stalagmite BS15 do not show the presence of significant Mn or Fe content in the dark layer, thus discarding the hypothesis of Mn-Fe coatings composing the black layer formation (Fig. 6.5.3).

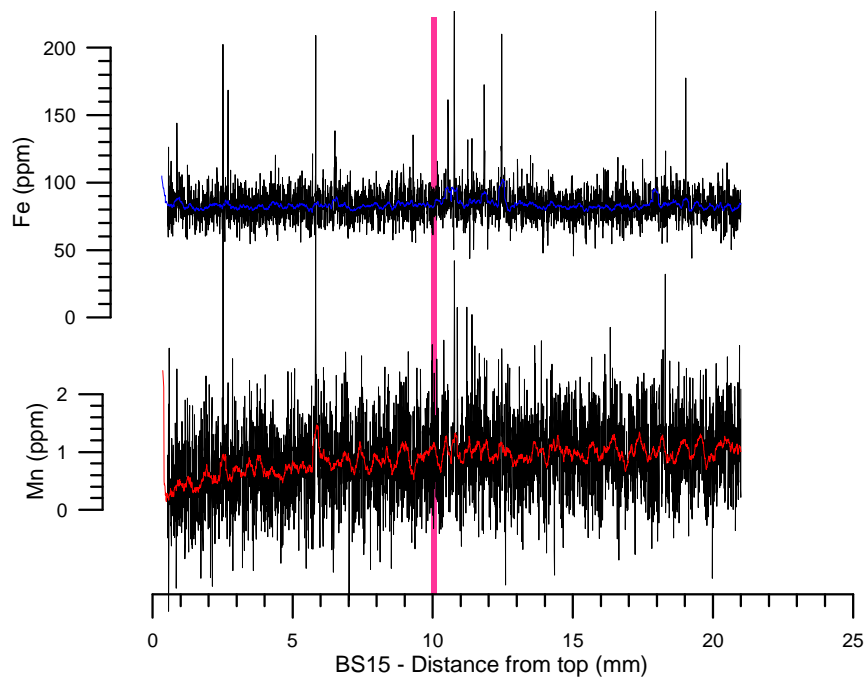


Fig. 6.5.3 – Mn and Fe results from laser ablation on stalagmite BS15. Black lines represent the raw data; red and blue lines are the 31 points moving average smoothed curves. The pink vertical line indicates the black layer on the stalagmite surface.

Thin section examination of the black layer under the petrographic microscope did not show the presence of any visible charcoal, indicating the occurrence of big fires, and particular structures that might be evidence for significant bacterial activity: it only appears as a sharp surface coating the crystals in stalagmites BS15 and BS8, where a short growth interruption is also found, while in stalagmite BS14 this layer is less sharp and seems to have been incorporated into crystal lattices. In

stalagmite BS9 the black layer is not even clearly visible in thin sections (Fig. 6.5.4; plates 1-4 in Chapter 5).

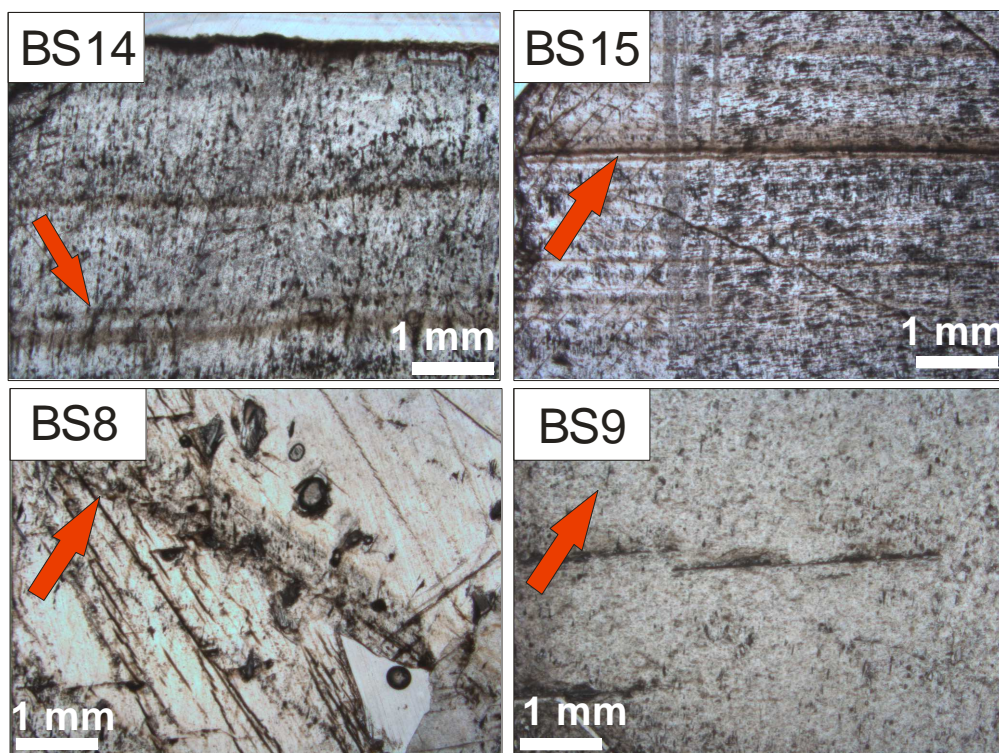


Fig. 6.5.4 – Thin section images (plain polarised light) of the black layer in stalagmites BS14, BS15, BS8 and BS9. The red arrows indicate the black layer.

Both FTIR and micro-Raman analyses did not lead to the identification of the origin of this layer, returning results indicating the detection of calcium carbonate only (Paragraph 5.7). However, the observation under the fluorescence optic microscope showed the presence of fluorescent material forming the black layer, suggesting an organic origin of this lamina (Paragraph 5.7.1). SEM observation on coarse powder drilled on the black layer allowed for the identification of carbon atoms concentrated in the thin black coating of calcite crystals (Fig. 6.5.5).

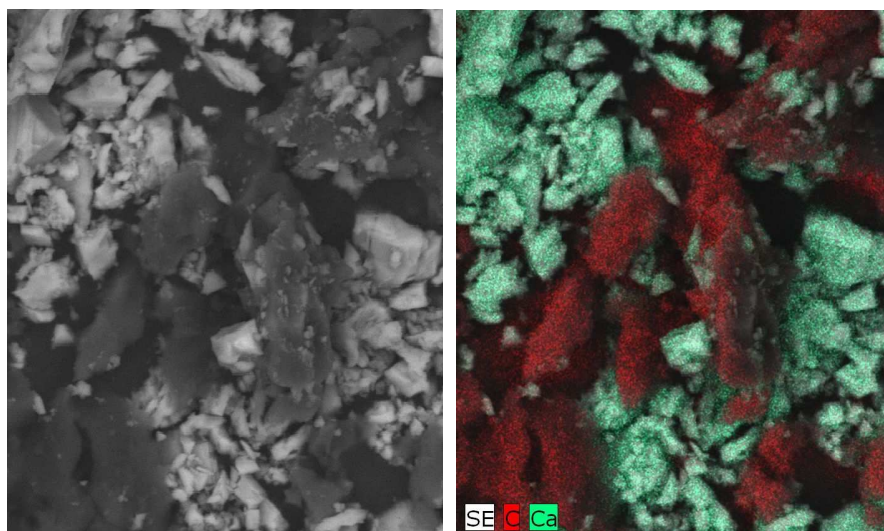


Fig. 6.5.5 – SEM image of calcite coarse powder sampled in the black layer. Left: secondary detector picture. Right: chemical mapping of Ca and C concentration.

Considering that soot produced by candles leads to the formation of fluorescent carbon nanoparticles (Liu et al., 2007), the hypothesis of the origin of the black layer related to candles/torches soot can be put forward.

FTIR analyses did not allow for the identification of this layer probably because of the presence of a calcite signal too strong to allow for the detection of any other carbon-related compounds. The high precision provided by micro-Raman analyses did not lead to any interesting result either: the thinness of the layer and its inclusion into compact calcite crystals probably resulted in the impossibility of its identification on thin section cut perpendicular to lamination.

This finding suggests that intense cave frequentation occurred at $\sim 1.2 \pm 0.1$ ka ($\sim 750 \pm 100$ AD). Interestingly, a cave located in the same region (Golubovici Cave, Gosina plateau, Bosnia and Herzegovina), explored by the Novara caving group between 2003 and 2007 (Cella and Torri, 2006), presents dark surfaces on cave walls and speleothems similar to the ones observed in Mračna Pećina Cave. During the exploration of this cavity, human bones covered by a dark coating resulting from combustion were recovered. Their radiocarbon dating provided an age around $\sim 1180 \pm 80$ cal yr BP, which is synchronous with the deposition of the soot layer in Mračna Pećina Cave speleothems (Cella and Torri, 2006; Cella, personal communication). This historical period corresponds to the massive migration of populations from North-Eastern Europe in the Balkans, between the 5th and 8th centuries (Hines et al., 1999). At the same time, the Western Roman Empire faced its collapse and the Ostrogoth Reign (5th century AD) arose. Its territories were conquered again by the Byzantines in the 6th century. From this period until about the 8th century periodic outbreaks of bubonic plague caused massive deaths in the Byzantine Empire, starting with the Justinian's Flea (541-542 AD; Rosen, 2007).

Unfortunately, the absence of archaeological records dating back to this period in Bosnia prevents the correlation of these findings in the two Bosnian caves to any remarkable historical event. Although it could seem plausible to advance the hypothesis that the burnt bones found in Golubovici Cave may be related to corpse cremation during a plague outbreak, any evidence of this type of corpse burial at that time was found in literature. In addition, any human rest was found in Mračna Pećina Cave so far, so it is not possible to relate the identified soot layer to a burial practice. At present, the cave walls and speleothems in the area closer to the main entrance of this cave present a pervasive dark coating which is believed to be related to intense cave frequentation using torches during the early 20th century, when the cave became accessible for tourists. Thus, a similar context may have caused the deposition of detected soot lamina.

6.5.4 Conclusions

A black layer consisting in a dark coating of stalagmite surfaces during their growth has been observed in all the Holocene stalagmites sampled in Mračna Pećina Cave. U-Th dating suggested its deposition at $\sim 1.2 \pm 0.1$ ka. Several analyses have been performed to identify its composition. Trace element, micro-Raman and FTIR results did not provide any useful information about the nature of the dark lamina. The detection of fluorescent material, together with the identification of carbon atoms concentrated on the coated crystal surfaces, suggests it is composed of organic-rich soot. It could be related to the use of candles/torches or to larger combustion event(s), thus indicating intense cave frequentation during a relatively short time window and/or the use of this environment for activities involving strong combustion of natural material. The comparison with a coeval finding in a nearby cave, witnessing cave frequentation at approximately the same time, possible related to copse cremation, raises questions about a historic correlation between the two discoveries. The absence of archaeological records in this Bosnian region dated from the Early Middle Ages prevents its correlation to any known historic event in the central Balkans. This finding points out speleothems as interesting material not only as palaeo-climate/environmental information archives, but also as potential sources of historical/archaeological information.

VII. CONCLUSIONS

Five Holocene stalagmites sampled in Mračna Pećina and Govještica caves (Prača Valley, Bosnia and Herzegovina) have been studied aiming to reconstruct Holocene climate/environmental fluctuations recorded in the central Balkans. This region, that has scarce palaeoclimate records, is particularly interesting since it is located close to the latitude separating sites of the Mediterranean basin with contrasting climate response during the Holocene. The Balkan region thus represents an ideal target for palaeoclimate investigations.

A multi-proxy approach was adopted to interpret the signals recorded by these samples, which did not display easily interpretable oxygen and carbon stable isotope profiles. A detailed petrographic observation was performed and coupled with trace element composition and calcite $\delta^{13}\text{C}$ and $\delta^{18}\text{O}$ ratios. This approach allowed identifying drip rate as the main forcing factor for both petrography and geochemistry changes, providing information about hydrological fluctuations. In particular, the potential of petrographic observation in providing palaeoenvironmental insights at high resolution was highlighted: even small changes in speleothem feeding system parameters can result in different crystallite arrangements, allowing for the identification of environmental signals, complementary to the information recorded by the stable isotope profiles.

The age models obtained by a Bayesian-Monte Carlo treatment of the U-Th ages were used to time-constrain the geochemical and petrographical information. Unfortunately, the large uncertainties affecting these models prevented the accurate identification of climate events. Nevertheless, palaeohydrological trends similar to the ones in the southern Mediterranean sites were identified. Indeed, relatively dry conditions during the first millennia of the Holocene, followed by a wetter phase until ~4.2 ka, have been identified. From then onwards, the records show a trend towards a progressively drier climate.

This finding, if it is to be confirmed by further studies in this region, would shift to the north (~43°N), in the Balkan region, the border between northern and southern Mediterranean sites presenting contrasting climate response during the Holocene. The influence of the East Atlantic/Western Russia (EA/WR) pattern and the Siberian High in triggering dry phases in the central Balkans is suggested.

Finally, a marginal part of this thesis regarded the identification of a black lamina deposited close to the top of the Holocene stalagmites sampled in Mračna Pećina cave. We demonstrated that it was a soot layer, possibly deposited during a period of intense cave frequentation around ~1.2 ka. Unfortunately, the lack of archaeological records covering this period in central Bosnia does not allow its correlation to any historic event, but it points the attention to speleothems as potential markers for historic/archaeological information.

FINAL REMARKS AND FUTURE DEVELOPMENTS

This project was based on the study of speleothems that were not particularly promising for past climate and/or environmental investigation. However, they were sampled in a region that might be crucial for the understanding of past climate dynamics in the central Mediterranean, and where only few palaeoclimate reconstructions are available. Considering the difficulty in obtaining samples from this area, the decision to keep studying these materials was taken. A multi-proxy approach involving high-resolution petrographic observations allowed extracting palaeoenvironmental information from these stalagmites, thus demonstrating the potential of this method while studying “difficult” speleothems.

Ultimately, our results showed some similarities between Holocene palaeohydrological changes in central Bosnia and the ones typical of southern Mediterranean sites. However, further studies are needed to confirm this result and to increase the spatial resolution of Holocene palaeohydrological patterns. A possible influence of the Siberian High, related to the EA/WR pattern, which, in turns, may be indirectly influenced by the NAO mode, in triggering cold and dry phases in the central Balkans was inferred.

Similarities between the Bosnian record and the one from core MD90-917 in the South Adriatic (Siani et al., 2013) suggest that the Adriatic area may have been influenced by these climate modes too. The question whether these climate patterns may also have influenced the Adriatic coast of the Italian Peninsula arises. In addition, possible influences of these climate modes on palaeohydrological changes during the Holocene to a wider extent in the central Mediterranean region are not excluded. Further studies are necessary to both confirm these hypotheses for the central Balkans and to deeper investigate Holocene climate dynamics in the Periadriatic region. In particular, the central Balkans, from Bosnia to Croatia, and the northern and central region of the Adriatic coast in the Italian Peninsula should be regarded as target regions.

SYNTHESIS IN ITALIAN - Sintesi in Italiano

La regione Mediterranea è un'area densamente popolata caratterizzata da una circolazione atmosferica particolarmente complessa. Piccole modifiche negli equilibri tra le masse d'aria provenienti dal Nord Atlantico e quelle provenienti dalle zone subtropicali e dall'Europa orientale possono condurre ad importanti cambiamenti climatici a scala regionale, soprattutto in termini idrologici. Una profonda comprensione delle fluttuazioni climatiche avvenute in passato è quindi fondamentale per trarre inform-azioni relative a possibili trend futuri.

Le regioni del Mediterraneo centrale, sono state caratterizzate da risposte climatiche contrastanti legate alla riorganizzazione della circolazione atmosferica globale alla fine dell'ultimo periodo glaciale. In particolare, mentre condizioni relativamente aride caratterizzarono la prima metà del periodo olocenico a latitudini superiori a 40°N, condizioni particolarmente umide sono state registrate in siti localizzati a sud di questa latitudine. A partire da circa 5-6 mila anni fa, un periodo di transizione portò all'instaurarsi di condizioni nettamente più umide (da circa 4,5 mila anni fa) nelle regioni settentrionali e più aride in quelle meridionali. Se questi trend sono evidenti nei record continentali e marini della Penisola Italiana e del Mar Adriatico, meno chiare sono le dinamiche climatiche nei Balcani, dove solo alcune ricostruzioni paleoclimatiche sono disponibili.

Con lo scopo di comprendere meglio le fluttuazioni climatiche Oloceniche di questa regione, varie stalagmiti sono state campionate in due grotte in Bosnia Herzegovina (Govještica and Mračna Pećina; Valle di Prača), tagliate longitudinalmente lungo l'asse di crescita e preliminarmente datate nell'ambito di un progetto di dottorato in cotutela tra le Università di Bologna e Communauté Université Grenoble Alpes. Datazioni preliminari, eseguite con la tecnica del disequilibrio U-Th, hanno permesso di scegliere 5 campioni formatisi negli ultimi 12 mila anni.

Formandosi in ambienti protetti dai fenomeni erosivi che avvengono in superficie, gli speleotemi carbonatici possono accrescersi indisturbati per periodi di tempo molto lunghi, registrando nel carbonato di calcio che li compone, informazioni relative all'ambiente esterno.

In particolare, attraverso l'analisi delle concentrazioni nella calcite degli isotopi stabili di ossigeno e carbonio, degli elementi in traccia incorporati nel reticolo cristallino e delle tessiture dei cristalli di carbonato di calcio, è possibile reperire informazioni riguardo variazioni climatiche (precipitazioni e/o temperature) e ambientali (densità e tipo di vegetazione).

Dopo aver individuato i campioni da studiare, un programma di monitoraggio è stato messo in atto in una delle due grotte considerate, al fine di comprendere le dinamiche idrologiche odierne e le

variazioni di temperatura nell'area dove le stalagmiti sono state campionate. Anche le precipitazioni sono state monitorate e campioni d'acqua sia di precipitazione che di stillicidio sono stati prelevati regolarmente per analisi isotopiche, con lo scopo di comprendere il significato del segnale isotopico che viene trasmesso dalle precipitazioni all'ambiente carsico.

In seguito alle datazioni preliminari effettuate per identificare i campioni più promettenti per questo studio, ulteriori campioni di carbonato di calcio sono stati prelevati utilizzando un trapano a colonna a controllo numerico (MicroProto systems MicroMill 2000) al fine di affinare la precisione delle datazioni. I campioni sono stati preparati presso l'Università di Melbourne (Australia). Le polveri carbonatiche sono state dissolte in acido nitrico 105% e una soluzione detta "spike" a contenuto isotopico noto è stata aggiunta. Le soluzioni così ottenute sono state versate in colonne contenenti una resina a scambio ionico. Una serie di lavaggi di queste colonne con acido nitrico, cloridrico e fluoridrico ha poi permesso l'estrazione dell'uranio e del torio dei campioni. I rapporti isotopici di questi campioni, che hanno permesso la determinazione delle età delle stalagmiti, sono stati determinati in spettrometria di massa.

Sfortunatamente, la presenza di una forte contaminazione detritica nella calcite delle stalagmiti studiate, ha portato ad avere barre di errore relativamente ampie sulle date ottenute. Questi risultati sono stati utilizzati per calcolare dei modelli età - profondità delle stalagmiti studiate, attraverso un trattamento statistico dei dati secondo una procedura sviluppata dal dr. John Hellstrom (Università di Melbourne, Australia). Questa procedura ha permesso di ottenere modelli delle età relativamente affidabili, sebbene affetti da margini di errore elevati dovuti all'imprecisione dei risultati delle datazioni e alla presenza di numerosi hiati nei campioni studiati. I modelli così ottenuti sono stati poi utilizzati per interpolare i dati geochimici e le osservazioni petrografiche, permettendo così un'interpretazione paleoambientale dei segnali registrati.

I campioni per le analisi degli isotopi stabili sono stati prelevati ogni millimetro lungo l'asse di crescita delle stalagmiti. Per il campionamento è stato utilizzato lo stesso trapano a colonna a controllo numerico con il quale sono stati prelevati i campioni per le datazioni U-Th. Circa 2 mg di polvere carbonatica sono stati prelevati per ogni campione, utilizzando una punta dal diametro di 1 mm. Le polveri carbonatiche sono state preparate presso il laboratorio della Scuola di Geografia dell'Università di Melbourne e analizzate in spettrometria di massa. Per investigare la presenza o meno di condizioni di equilibrio isotopico durante la formazione delle stalagmiti studiate, alcuni campioni sono stati prelevati lungo 3 lamine di 3 stalagmiti, utilizzando una punta dal diametro di 0,6 mm. Gli elementi in traccia sono stati analizzati in laser ablation lungo l'asse di crescita di una delle 5 stalagmiti studiate, ritenuta la più idonea per questo tipo di analisi.

Sezioni sottili per osservazioni petrografiche sono state realizzate in 4 dei 5 campioni oggetto di questo studio. Le tessiture sono state riconosciute al microscopio petrografico seguendo le linee guida presenti in letteratura. Tuttavia, in due stalagmiti, particolari pattern sono stati osservati a scala della laminazione. Questi sono stati descritti e classificati in base alla micro porosità intra- e inter-cristallina. Per questi due campioni sono stati quindi costruite curve petrografiche.

Infine, con lo scopo di determinare l'origine di un orizzonte nero depositosi circa 1,2 mila anni fa in 4 delle 5 stalagmiti studiate, analisi micro-Raman, FTIR e osservazioni al SEM sono state effettuate.

L'elaborazione dei dati è stata poi suddivisa in tre parti principali, che riguardano: la comprensione di come i segnali isotopici delle precipitazioni vengono trasmessi all'ambiente carsico; l'interpretazione del significato dei dati geochimici e petrografici registrati negli speleotemi; l'interpretazione paleoambientale e/o paeoclimatica del record ottenuto. Una parte marginale, ma non meno interessante, ha riguardato l'esame dell'orizzonte nero depositosi circa 1,2 mila anni fa.

Per quanto riguarda i parametri ambientali odierni monitorati in grotta e all'esterno, è stato possibile identificare una maggiore risposta degli stillicidi monitorati alle precipitazioni autunnali e invernali. I dati isotopici delle precipitazioni campionate sono stati esaminati ed è stata individuata una maggiore dipendenza del valore $\delta^{18}\text{O}$ dell'acqua di precipitazione dalla temperatura, in linea con l'andamento descritto in letteratura in altre località dei Balcani. Considerando che, se la calcite viene depositata in condizioni di equilibrio isotopico può fornire informazioni relative alla composizione isotopica dell'acqua da cui si è formata, si potrebbe ipotizzare la presenza di un segnale relativo alla temperatura nel $\delta^{18}\text{O}$ delle stalagmiti studiate. Tuttavia, l'entità della relazione trovata permetterebbe solo la registrazione di forti cambiamenti di temperatura in speleotemi carbonatici formati in questa regione. Considerando che importanti variazioni di temperatura sono improbabili durante un periodo interglaciale come l'Olocene, non è possibile riferire il $\delta^{18}\text{O}$ della calcite di questi campioni a variazioni di temperatura passate. Il confronto della composizione isotopica delle precipitazioni attuali con quelle dell'acqua di stillicidio ha permesso di identificare una marcata firma isotopica stagionale dell'acqua di infiltrazione. Risulta quindi più plausibile interpretare possibili variazioni isotopiche in calciti deposte in condizioni di equilibrio isotopico in relazione a variazioni di stagionalità nella ricarica dell'acquifero (i.e. maggiore o minore influenza delle precipitazioni autunnali-invernali).

Sfortunatamente, però, non è stato possibile dimostrare la deposizione dei campioni studiati in condizioni di equilibrio isotopico. In particolare, i profili isotopici ($\delta^{13}\text{C}$ e $\delta^{18}\text{O}$) sono risultati essere affetti da un'elevata variabilità e un aspetto a "dente di sega", suggerendo la possibile deposizione di questi campioni in condizioni di disequilibrio isotopico. Mentre non è stato possibile identificare trend specifici associati alle variazioni di $\delta^{18}\text{O}$, un trend verso valori più elevati di $\delta^{13}\text{C}$ è stato identificato negli ultimi 4 mila anni. Al fine di migliorare l'interpretazione di questi profili altrimenti difficilmente interpretabili, un approccio multi-proxy è stato adottato. Le variazioni petrografiche sono state confrontate con le fluttuazioni delle concentrazioni degli elementi in traccia e degli isotopi stabili della calcite delle stalagmiti studiate. In particolare, una stretta relazione è stata trovata tra le variazioni di tessitura a scala millimetrica, $\delta^{13}\text{C}$ e gli elementi in traccia, in particolare magnesio e stronzio, che, nel caso specifico, sono risultati essere dipendenti, rispettivamente, dal tempo di residenza dell'acqua nell'acquifero, e dal tasso di deposizione della calcite. Questo approccio ha permesso di interpretare i profili di $\delta^{13}\text{C}$ in termini idrologici, fornendo informazioni relative all'alternarsi di periodi più o meno aridi durante la formazione degli speleotemi studiati. Questa relazione ha quindi permesso l'identificazione di variazioni idrologiche ad alta risoluzione, permettendo di dimostrare l'utilità di un approccio petrografico a questo tipo di studi. Purtroppo, la mancanza di modelli delle età molto precisi ha impedito l'identificazione temporale esatta di queste variazioni.

Nonostante le elevate incertezze dei modelli delle età, è stato possibile identificare trend specifici nei campioni bosniaci. In particolare, condizioni relativamente aride sono state osservate nel corso dei primi millenni dell'Olocene seguite da un incremento delle precipitazioni. Un trend verso condizioni più aride è stato invece osservato negli ultimi 4 mila anni. Questa risposta climatica apparirebbe quindi in linea con quanto osservato nei siti del Mediterraneo meridionale. Sfortunatamente l'impossibilità di avere datazioni accurate di questi materiali ha impedito la precisa identificazione temporale di questi trend. Nonostante ciò, questo risultato, se sarà confermato da altri studi paleoclimatici in questa regione, sposterebbe a nord ($\sim 43^\circ\text{N}$) nei Balcani il limite attualmente ipotizzato a circa $\sim 40^\circ\text{N}$, che segna il confine tra le regioni meridionali e settentrionali del Mediterraneo caratterizzate da risposte climatiche contrastanti nel corso dell'Olocene. Questa differenza rispetto agli altri siti del Mediterraneo potrebbe essere legata ad una maggiore influenza della circolazione atmosferica dell'Europa orientale (i.e. Alto Siberiano) sulla regione Balcanica. Ulteriori studi paleoclimatici sarebbero necessari nei Balcani centrali e nel versante Adriatico della penisola Italiana al fine di meglio comprendere le risposte climatiche regionali nel Mediterraneo centrale nel corso dell'Olocene e identificarne le cause.

Infine, una parte marginale di questa ricerca ha riguardato l'analisi di un orizzonte nero depositosi circa 1,2 mila anni fa in 4 speleotemi campionati nella stessa grotta. Una serie di analisi è stata effettuata per comprenderne la natura e origine. Nessuna informazione relativa a questo deposito è stata ricavata dai risultati degli elementi in traccia, né dal micro-Raman, né dalla spettroscopia ad infrarosso (FTIR). Osservazioni al microscopio elettronico a trasmissione elettronica (SEM) hanno permesso l'identificazione di atomi di carbonio concentrati sulla patina scura. Questo risultato, in associazione alla presenza di fluorescenza in corrispondenza di questo orizzonte, ha suggerito la presenza di fuliggine in corrispondenza di questo intervallo. L'origine di questo orizzonte scuro potrebbe quindi essere legata ad un'intensa frequentazione della grotta con candele/torce, o all'avvenimento di importanti fenomeni di combustione di materiale organico. Considerando che in una grotta vicina sono state ritrovate ossa umane sottoposte a combustione risalenti allo stesso periodo di questo orizzonte nero, sorge spontaneo chiedersi se i due ritrovamenti possano essere ricollegati a qualche evento storico/culturale oppure se siano eventi scollegati tra loro. Purtroppo l'assenza di testimonianze archeologiche nella regione impedisce il collegamento di questi ritrovamenti ad alcun evento storico riconosciuto.

SYNTHESIS IN FRENCH – Synthèse en Français

La région méditerranéenne est une zone densément peuplée caractérisée par une circulation atmosphérique particulièrement complexe. Des petits changements dans l'équilibre entre les masses d'air provenant de l'Atlantique du Nord et celles des régions subtropicales et de l'Europe de l'Est peuvent conduire à des changements majeurs à l'échelle régionale, notamment en termes hydrologiques. Une compréhension profonde des fluctuations climatiques qui ont eu lieu dans le passé est donc essentielle pour obtenir des informations sur les tendances futures possibles.

Les régions de la Méditerranée centrale ont présenté des réponses climatiques contradictoires à la réorganisation de la circulation atmosphérique globale après la fin de la dernière période glaciaire. En particulier, alors que des conditions relativement arides ont caractérisé la première moitié de la période Holocène à des latitudes supérieures à 40°N, des conditions particulièrement humides sont enregistrées dans des sites situés au sud de cette latitude. À partir d'environ 6-5 mille ans, une période de transition conduit à la mise en place de conditions beaucoup plus humides (il y a environ 4500 ans) dans le Nord et plus sèches dans le Sud. Si ces tendances sont évidentes dans les archives continentales et marines de la péninsule italienne et de la mer Adriatique, la dynamique du climat dans les Balkans, où seules quelques reconstructions paléoclimatiques sont disponibles, sont moins claires.

Dans le but de mieux comprendre les fluctuations climatiques de l'Holocène dans cette région, diverses stalagmites ont été échantillonnées dans deux grottes en Bosnie-Herzégovine (Govještica et Mračna Pečina; Valley Prača). Celles-ci ont fait l'objet de datations préliminaires par U-Th, qui ont permis de choisir les 5 échantillons étudiés dans le cadre de cette thèse de doctorat, dans le cadre d'une cotutelle entre l'Université de Bologne et la Communauté Université Grenoble Alpes (Université Savoie-Mont Blanc).

Les speléothèmes carbonatés, grâce à leur formation dans des environnements protégés des phénomènes érosifs externes, peuvent enregistrer pendant de longues périodes des informations sur le climat et l'environnement de surface

En particulier, à travers l'analyse des rapports isotopiques de l'oxygène et du carbone de la calcite, des concentrations en éléments traces incorporés dans la calcite et de ses textures cristallines, on peut reconstituer certains paramètres climatiques (régime des précipitations et/ou température) ou environnementaux (densité et type de végétation).

Après avoir identifié les échantillons qui feraient l'objet de cette étude, un programme de monitoring a été mis en place dans l'une des deux grottes afin de comprendre la dynamique des

variations hydrologiques actuelles et de la température dans la zone où les stalagmites ont été échantillonnées. Ainsi, les précipitations ont été enregistrées et des échantillons d'eau de pluie et d'eau d'égouttement ont été régulièrement collectés pour l'analyse de leurs isotopes stables ($\delta^{18}\text{O}$ et δD), dans le but de mieux comprendre le sens du signal isotopique transmis par les infiltrations à l'environnement karstique.

Des modèles d'âge pour la croissance des spéléothèmes étudiés ont été construits à partir de nombreuses datations U-Th effectuées sur des échantillons prélevés à l'aide d'une microperceuse à commande numérique (MicroProto system - MicroMill 2000) pour une plus grande résolution spatiale d'échantillonnage. Les datations ont été réalisées à la School of Earth Science, Université de Melbourne (Australie). Le protocole analytique établi par le Dr. John Hellstrom inclut la dissolution totale des échantillons carbonatés et l'incorporation d'un « spike » de composition isotopique connue incluant un isotope artificiel. Les solutions sont ensuite filtrées dans des colonnes grâce à des résines échangeuses d'ions, ce qui permet de n'extraire in fine que l'uranium et le thorium des échantillons. Les rapports isotopiques de ces extractions sont analysés par MC-ICPMS pour déterminer l'âge des échantillons. Malheureusement, les âges obtenus présentent de larges incertitudes à cause de la présence d'une forte contamination détritique dans la calcite des stalagmites étudiées. Ces résultats ont enfin permis de calculer les modèles d'âge - profondeur des stalagmites, grâce à un traitement statistique de type Bayésien-Monte Carlo s'appuyant sur les contraintes stratigraphiques des échantillons. La fiabilité des modèles d'âge obtenus est relativement bonne, malgré des marges d'erreur élevées en raison de l'imprécision des datations et de la présence de nombreuses discontinuités de croissance. Ces modèles ont ensuite été utilisés pour caler chronologiquement les données géochimiques et les observations pétrographiques, permettant une interprétation des signaux paléoenvironnementaux enregistrés.

Les échantillons destinés à l'analyse des isotopes stables ont été prélevés également grâce à un MicroMill, tous les millimètres le long de l'axe de croissance des stalagmites. Environ 2 mg de poudre ont été collectés pour chaque échantillon. Celles-ci ont été analysées à la School of Geography, University of Melbourne, par IRMS. Afin d'étudier les conditions du fractionnement isotopique pendant la précipitation de calcite des stalagmites étudiées, des échantillons ont été prélevés le long de 3 lamines sur chacune des 3 stalagmites.

Les concentrations en éléments traces ont été analysées par ICPMS avec ablation laser le long de l'axe de croissance d'une des stalagmites, sélectionnée pour être la plus adaptée à ce type d'analyse. Des lames minces ont été fabriquées à partir de 4 spéléothèmes de cette étude, pour observations pétrographiques. Les textures ont été étudiées sous un microscope polarisant en suivant les lignes directrices de la littérature. Toutefois, dans deux stalagmites, des textures particulières ont été

observées à l'échelle millimétrique, et ont été décrites et classées en fonction de l'arrangement des cristallites et de leur micro-porosité intra- et inter-cristalline. Pour ces deux échantillons des courbes pétrographiques ont été réalisées.

Enfin, afin de déterminer l'origine d'un horizon noir déposé il y a environ 1200 ans dans les stalagmites de la grotte de Mračna Pečina, des analyses micro-Raman, FTIR et au MEB ont été réalisées.

Le traitement des données a ensuite été divisé en trois parties principales, incluant :

- la compréhension des signaux isotopiques des précipitations transmis à l'environnement karstique ;
- l'interprétation des données pétrographiques et géochimiques enregistrées dans les spéléothèmes étudiés ;
- l'interprétation paléoenvironnementale et/ou paléoclimatique des données obtenues.

En ce qui concerne les paramètres environnementaux actuels, monitorés dans la grotte et à l'extérieur, il a été possible d'identifier une meilleure réponse des égouttements aux précipitations d'automne et d'hiver. Les données isotopiques des précipitations échantillonnées montrent qu'il y a une plus grande dépendance du $\delta^{18}\text{O}$ de l'eau des précipitations à la température, ce qui est cohérent avec ce qui est décrit dans la littérature pour d'autres sites des Balkans. Si la calcite est déposée dans des conditions d'équilibre isotopique, elle peut fournir des informations relatives à la composition de l'eau à partir de laquelle elle s'est formée, et on peut déduire la présence d'un signal de température dans le rapport isotopique $\delta^{18}\text{O}$ des stalagmites étudiées. Cependant, le $\delta^{18}\text{O}$ permettrait seulement d'enregistrer de fortes variations de température dans les spéléothèmes de cette région, alors que d'importantes variations de température sont peu vraisemblables au cours de l'Holocène. La comparaison de la composition isotopique des précipitations avec celles des eaux de percolation a montré une signature isotopique saisonnière de l'infiltration d'eau. Il serait donc plus plausible d'interpréter les variations de $\delta^{18}\text{O}$ dans ces stalagmites en termes de variations saisonnières de la recharge de l'aquifère (c'est à dire en fonction de l'influence plus ou moins grande des précipitations d'automne et d'hiver).

Toutefois, il n'a pas été possible de démontrer que la précipitation des spéléothèmes étudiés avaient eu lieu dans des conditions proches de l'équilibre isotopique. Notamment, les profils isotopiques ($\delta^{13}\text{C}$ et $\delta^{18}\text{O}$) se sont avérés souffrir d'une forte variabilité avec une allure en "dents de scie", suggérant un dépôt hors des conditions d'équilibre isotopique. Le signal du $\delta^{18}\text{O}$ n'a ainsi pas

permis d'identifier de grandes tendances climatiques. En revanche, le signal du $\delta^{13}\text{C}$ a montré une tendance vers des valeurs plus élevées au cours des derniers 4000 ans.

Afin d'améliorer l'interprétation de ces profils isotopiques, une approche multi-proxy a donc été adoptée. Les variations pétrographiques ont été comparées avec les fluctuations des concentrations des éléments traces et des rapports des isotopes stables dans les stalagmites étudiées. Une relation étroite a été établie entre les changements de textures à l'échelle du millimètre, le $\delta^{13}\text{C}$ et les éléments traces, en particulier le magnésium et le strontium. Ces derniers dépendent ici, respectivement, du temps de séjour de l'eau dans l'aquifère, et de la vitesse de précipitation de la calcite. Cette approche a ainsi permis d'interpréter le signal du $\delta^{13}\text{C}$ en termes d'hydrologie, fournissant des informations à haute résolution temporelle relatives à l'alternance de périodes plus ou moins arides lors de la formation des concrétions. Malheureusement, les incertitudes des modèles d'âge ont empêché d'identifier précisément l'âge de ces variations.

Néanmoins, il a été possible d'identifier des tendances climatiques dans ces échantillons de Bosnie. En particulier, des conditions relativement arides ont été observées au cours du premier millénaire de l'Holocène, suivies d'une augmentation des précipitations. Une tendance vers des conditions plus arides a ensuite été observée au cours des derniers 4000 ans. Cette réponse climatique semble cohérente avec ce qui a été observé dans d'autres sites du sud du bassin méditerranéen. Ce résultat, s'il serait confirmé par d'autres études paléoclimatiques dans la région, pourrait déplacer légèrement vers le Nord (à $\sim 43^\circ\text{N}$) dans les Balkans, la limite actuellement envisagée à environ 40°N entre les régions du Sud et du Nord du bassin méditerranéen caractérisées par des réponses climatiques contrastées au cours de l'Holocène. Cette réponse climatique en Bosnie pourrait être liée à une plus grande influence de la circulation atmosphérique d'Europe orientale (i.e. Alto Sibérie) sur la région des Balkans. D'autres études paléoclimatiques seront nécessaires dans les Balkans et sur la côte adriatique de la péninsule italienne, afin de mieux comprendre les réponses climatiques régionales dans le bassin méditerranéen au cours de l'Holocène.

Enfin, une partie marginale de cette recherche s'est intéressée à l'analyse d'un horizon noir déposé il y a environ 1200 ans dans 4 concrétions de la grotte Mračna Pecina. Une série d'analyses a été effectuée afin de connaître sa nature. Aucune réponse n'a pu être obtenue à partir des analyses des éléments traces, ni par spectroscopie micro-Raman et infrarouge (FTIR). Finalement, les observations au microscope électronique à balayage (MEB) ont permis d'identifier des atomes de carbone concentrés sur le dépôt noir. Par ailleurs ce dépôt présentait une forte fluorescence (de matière organique). Ces résultats ont conduit à interpréter cet horizon noir comme un dépôt de suie.

L'origine de ce dépôt pourrait alors être liée à une intense fréquentation de la grotte ou à des épisodes importants de combustion.

ACKNOWLEDGEMENTS

During this 3 year project several people took part to my thesis development. I take this opportunity to forward special thanks to:

- My supervisors Jo De Waele and Isabelle Couchoud, who supported the development of the project;
- Russell Drysdale, who gave me the possibility to visit and spend a few months at his laboratory at the School of Geography (University of Melbourne, Australia) and who financed a part of the geochemical analyses necessary for this project;
- John Hellstrom, who hosted me in his laboratory at the School of Earth Science (University of Melbourne, Australia) showing me the techniques of sample preparation for U-Th dating;
- Petra Bajo (University of Melbourne, Australia), whose support was essential for the calculation of stalagmite age-depth models;
- Simone Milanolo, whose aid in the monitoring program was essential for gaining insight of present day precipitation and cave hydrology;
- Silvia Frisia (University of Newcastle, Australia), who provided her support for petrography observations;
- Emilie Chalmin (University Savoie-Mont Blanc, France), Diego Ercole Angelucci (University of Trento, Italy), Alan Greig and Roland Maas (University of Melbourne, Australia), for the support provided during petrographic and geochemical analyses.
- Fausto De Salvo (University of Bologna, Italy) for the support provided in the statistical analyses;
- Frank McDermott and Christoph Spötl who reviewed the first manuscript and provided useful comments and suggestions for its improvement;
- The “Federazione Speleologica dell’Emilia Romagna (FSER) and the “Gruppo Speleologico Faentino (GSFa)” for the funding provided for U-Th dating;
- The “Gruppo Speleologico-Unione Speleologia Bolognese (GSB-USB)” who provided technical help during sampling campaigns;
- The “Federal Hydrometeorological Institute (BIH)” who provided meteorological data series from Sarajevo.
- The Italo-French University (Turin, Italy) for the assignment of the Vinci grant that partially financed the period spent in France.

Finally, but not less important, I want to thank all the people who supported me during this three year period, where I discovered new languages and new cultures, besides working at my thesis. In particular, I want to thank Agnes Mazót, who helped me in correcting the synthesis of the thesis in French; Camilla Crocker and Benedict Hughes who introduced me to a new culture and new and interesting lifestyles; Elsa Ols, a great flatmate, for her patience in trying to teach me French; Edith Montesinos, Ellen Corrick and Melanie Ferraton, for their support during the months I spent in France. Special thanks go to my family and my partner, Fabio, who has always been there, supporting and encouraging me during the best and the worst moments of this challenging experience.

References

- Affek H. & Zaarur S. (2014) - *Kinetic isotope effect in CO₂ degassing: insight from clumped and oxygen isotopes in laboratory precipitation experiments*. *Geochimica et Cosmochimica Acta*, 142: 319-330.
- Ali S.M., Bonnier F., Lambkin H., Flynn K. and McDonagh V. (2013) - *A comparison of Raman, FTIR and ATR-FTIR micro spectroscopy for imaging human skin tissue sections*. *Analytical Methods*, 5: 2281-2291.
- Allan M., Fagel N., Van Rampelbergh M., Baldini J., Riotte J., Cheng H., Edwards R.L., Gillikin D., Quinif Y. and Verheyden S. (2015) – *Lead concentrations and isotope ratios in speleothems as proxies for atmospheric metal pollution since the industrial revolution*. *Chemical Geology*, 401: 140-150.
- Allen J.R.M., Watts W.A., McGee E. and Huntley B. (2002) – *Holocene environmental variability – the record from Lago Grande di Monticchio, Italy*. *Quaternary International*, 88: 69-80.
- Allison R.B. (1982) – *The relationships between 18O and deuterium in water in sand columns undergoing evaporation*. *Journal of Hydrology*, 55: 163-169.
- Alonso-Zarza A.M. and Wright V. (2010) – *Calcretes*. *Developments in Sedimentology*, 61: 225-267.
- Amorosi A., Pavesi M., Ricci Lucchi M., Sarti G and Piccin A. (2008) – *Climatic signature of cyclic fluvial architecture from the Quaternary of the central Po Plain, Italy*. *Sedimentary Geology*, 209: 58-68.
- Andrič M. (2007) – *Holocene vegetation development in Bela krajina (Slovenia) and the impact of first farmers in the landscape*. *The Holocene*, 17 (6): 763-776.
- Artigiani A., Paschini E., Russo A., Bregant D., Raicich F., and Pinardi N. (1997) – *The Adriatic Sea General Circulation. Part I: Air-Sea Interactions and Water Mass Structure*. *Journal of Physical Oceanography*, 27: 1492-1514.
- Ariztegui D., Asioli A., Lowe J.J., Trincardi F., Vigliotti L., Tamburini F., Chidrogiani C., Accorsi C.A., Bandini Mozzanti M., Mercuri A.M., Van der Kaars S., McKenzie J.A. and Oldfield F. (2000) – *Palaeoclimate and the formation of sapropel S1: inferences from Late Quaternary lacustrine and marine sequences in the central Mediterranean region*. *Palaeogeography, Palaeoclimatology, Palaeoecology*, 158: 215-240.
- Asioli A., Trincardi F., Lowe J.J., Ariztegui D., Langone L. and Oldfield F. (2001) – *Sub-millennial scale climatic oscillations in the central Adriatic during the Lateglacial: palaeoceanographic implications*. *Quaternary Science Reviews*, 20: 1201-1221.
- Aufgebauer A., Panagiotopoulos K., Wagner B., Schaebitz F., Viehberg F.A., Vogel H., Zanhetta G., Sulpizio R., Leng M.J. and Damaschke M. (2012) – *Climate and environmental change in the Balkans over the last 17 ka recorded in sediments from Lake Prespa (Albania/F.Y.R of Macedonia/Greece)*. *Quaternary International*, 274: 122-135.

- Avramidis P., Geraga M., Lazarova M. and Kontopoulos N. (2012) – Holocene record of environmental changes and palaeoclimatic implications in Alykes Lagoon, Zakynthos Island, western Greece, Mediterranean Sea. *Quaternary International*, 293 : 184-195.
- Bailey D.W. (2000) – *Balkan Prehistory. Exclusion, Incorporation and Identity*. Taylor and Francis publications, p.367.
- Baldini L.M., McDermott F., Baldini J.U.L., Fischer M.J. and Möllhoff M. (2010) – *An investigation of the controls on Irish precipitation $\delta^{18}O$ values on monthly and event timescales*. *Climate Dynamics*, 35: 977-993.
- Banks E.D., Taylor N.M., Gulley J., Lubbers B.R., Giarrizzo J.G., Bullen H.A., Hoehler T.M. and Barton H.A. (2010) – *Bacterial calcium carbonate precipitation in cave environments: a function of calcium homeostasis*. *Geomicrobiology Journal*, 27: 444-454.
- Bajo P., Hellstrom J., Frisia S., Drysdale R., Black J., Woodhead J., Borsato A., Zanchetta G., Wallace M.W., Regattieri E. and Haese R. (2016) – « *Cryptic* » diagenesis and its implications for speleothem geochronologies. *Quaternary Science Reviews*, 148 : 17-28.
- Bar Matthews M., Ayalon A., Matthewes A., Sass E. and Halicz L. (1996) – *Carbon and oxygen isotopic study of the active water-carbonate system in a karstic Mediterranean cave: implications for palaeoclimate research in semiarid cave: implications for palaeoclimate research in semiarid regions*. *Geochimica et Cosmochimica Acta*, 60: 337-347.
- Baroni C., Zanchetta G., Fallick A.E. and Longinelli A. (2006) – *Mollusca stable isotope record of a core from Lake Frassino, northern Italy: hydrological and climatic changes during the last 14 ka*. *The Holocene*, 16 (6): 827-837.
- Belli R., Frisia S., Borsato A., Drysdale R., Hellstrom J., Zhao J.-X. and Spötl C. (2013) - *Regional climate variability and ecosystem responses to the last deglaciation in the northern hemisphere from stable isotope data and calcite fabrics in two northern Adriatic stalagmites*. *Quaternary Science Reviews*, 72: 146-158.
- Berger A. and Loutre M.F. (1991) – *Insolation values for the climate of the last 10 million years*. *Quaternary Science Review*, 10(4): 297-317.
- Bisselink B. and Dolman A.J. (2008) – *Precipitation Recycling: Moisture Sources over Europe using ERA-40 Data*. *American Meteorological Society*, 9: 1073-1083
- Boch R., Spötl C. and Frisia S. (2010) – *Origin and palaeoenvironmental significance of lamination in stalagmites from Katerloch Cave, Austria*. *Sedimentology*, 58: 508-531.
- Boistelle R. (1982) – *Mineral crystallization from solutions*. *Estudios Geológicos*, 38: 135-153.
- Bond G., Showers W., Cheseby M., Lotti R., Almasi P., deMenocal P., Priore P., Cullen H., Hajdas I. and Bonani G. (1997) – *A pervasive Millennial-Scale Cycle in North Atlantic Holocene and Glacial Climates*. *Science*, 287: 1257-1266.
- Bordon A., Peyron O., Lézine A.-M., Brewer S. and Fouache E. (2009) – *Pollen-inferred Late Glacial and Holocene climate in southern Balkans (Lake Maliq)*. *Quaternary International*, 200: 19-30.

- Borsato A., Frisia S., Jones B. and van der Borg K. (2000) – *Calcite moonmilk: crystal morphology and environment of formation in caves in the Italian Alps*. *Journal of Sedimentary Research*, 70: 1179-1190.
- Borsato A., Frisia S., Fairchild I.J., Somogyi A. and Susini J. (2007) - *Trace element distribution in annual stalagmite laminae mapped by micrometer-resolution X-ray fluorescence: implications for incorporation of environmentally significant species*. *Geochimica et Cosmochimica Acta*, 71: 1494-1512.
- Borsato A., Frisia S. and Miorandi R. (2015) – *Carbon dioxide concentration in temperate climate caves and parent soils over an altitudinal gradient and its influence on speleothem growth and fabrics*. *Earth Surface Processes and Landforms*, 40(9): 1158-1170.
- Burton W.K., Cabrera N. and Frank F.c. (1951) – *The growth of crystals and the equilibrium structure of their surfaces*. *Philosophical Transactions of the Royal Society of London*, A243: 299-358.
- Buffle J. Wilkinson K.J., Stoll S. Filella M. and Zhang J. (1998) – *A generalized description of aquatic colloidal interactions: the three-colloidal component approach*. *Environmental Science and Technology*, 32: 2887-2899.
- Caddeo G.A., Railsback L.B., De Waele J. and Frau F. (2015) - *Stable isotope data as constraints on models for the origin of coralloid and massive speleothems: the interplay of substrate, water supply, degassing, and evaporation*. *Sedimentary Geology*, 318: 130-141.
- Cañaveras J., Sanchez-Moral S., Soler V. and Saiz-Jimenez C. (2001) – *Microorganisms and microbially induced fabrics in cave walls*. *Geomicrobiological Journal*, 18.
- Caroli I. and Caldara M. (2007) – *Vegetation history of Lago Battaglia (eastern Gargano coast, Abulia, Italy) during the middle-late Holocene*. *Vegetation, History and Archaeobotany*, 16: 317-327.
- Casanueva A., Rodriguez-Puebla C., Frias M.D. & González-Reviriego N., 2014 – *Variability of extreme precipitation over Europe and its relationships with teleconnection patterns*. *Hydrology and Earth System Sciences*, 18: 709-725.
- Cella G.D., Milanolo S., Torre A., Amila Z. () – *La grotte di Golubovici (BIH)*. *Labirinti* 25
- Cerling T.E. (1984) - *The stable isotope composition of modern soil carbonate and its relationship to climate*. *Earth and Planetary Science Letters*, 71: 229-240.
- Cerling T.E. and Quade J. (1993) – *Stable carbon and oxygen isotopes in soil carbonates*. In: Swart P., McKenzie J.A. and Lohman K.C. (eds.): *American Geophysical Union Monograph* 78: 217-231.
- Chapman J. (1990) – *The Neolithic in the Morava-Danube confluence area: a regional assessment of settlement pattern*. In R.E. Tringham and Krštic D. (eds) *Selevac: A Neolithic Village in Yugoslavia*, pp. 13-44, Los Angeles: UCLA.
- Colombaroli D., Tinner W., van Leeuwen J., Noti R., Vscovi E., Vannièrè B., Magny M., Schmidt R. and Bugmann H. (2009) – *Response of broadleaved evergreen Mediterranean forest vegetation to fire disturbance during the Holocene: insights from the peri-Adriatic region*. *Journal of Biogeography*, 36: 314-326.

Constantin S., Bojar A.-V., Lauritzen S.-E. and Lundberg J. (2007) – *Holocene and Late Pleistocene climate in the sub-Mediterranean continental environment : A speleothem record from Poleva Cave (Southern Carpathians, Romania)*. *Palaeogeography, Palaeoclimatology, Palaeoecology*, 243: 322-338.

Combourieu Nebout N., Peyron O., Dormoy I., Desprat S., Beaudouin C., Kotthoff U. and Marret F. (2009) – *Rapid climatic variability in the west Mediterranean during the last 25,000 years from high resolution pollen data*. *Climate of the past*, 5: 503-521.

Combourieu-Nebout N., Peyron O., Bout-Roumazielles, Goring S., Dormoy I., Joannin S., Sadori L., Siani G. and Magnny M. (2013) – *Holocene vegetation and climate changes in the central Mediterranean inferred from a high-resolution marine pollen record (Adriatic Sea)*. *Climate of the Past*, 9: 2023-2042.

Coplen T.B., Herczeg A.L. and Barnes C. (2000) – *Isotope engineering: using stable isotopes of the water molecule to solve practical problems*. In: *Environmental Tracers in Subsurface Hydrology*, ed. By P.G. Cook and A.L.Herczeg, Kluwer Academic Publishers, Boston.

Correggiari A., Cattaneo A. and Trincardi F. (2005) - *Depositional patterns in the Holocene Po Delta system*. In: *River Deltas: Concepts, Models and Examples*, edited by: Bhattacharya, J. P. and Giosan, L., Society of Economic Paleontologists and Mineralogists Special Publication, 83: 365–392.

Couchoud I. (2006) - *Étude pétrographique et isotopique de spéléothèmes du sud-ouest de la France formés en contexte archéologique – Contribution à la connaissance des paléoclimats du stade isotopique 5*. Thèse de doctorat. Université Bordeaux 1, 346 p.

Couchoud I. (2008) - *Les isotopes stables de l'oxygène et du carbone dans les spéléothèmes: des archives paléoenvironnementales*. *Quaternaire*, 19(4): 275-291.

Craig H. (1961) – *Isotopic variations in meteoric waters*. *Science*, 133: 1702-1703.

Curta F. (2013) – *The Beginning of the Middle Ages in the Balkans*. *Millennium* 10 (1): 145-214.

Cvetkoska A., Levkov Z., Reed J.M. and Wagner B. (2014) – *Late Glacial to Holocene climate change and human impact in the Mediterranean: The last ca. 17 ka diatom record of Lake Prespa (Macedonia/Albania/Greece)*. *Palaeogeography, Palaeoclimatology, Palaeoecology*, 406: 22-32.

Daneš J., 1921 - *Pećine u kanjonu Prače i okolini Glasinačkog polja*. *Glasnik Geografskog društva, Beograd*, 5: 139-142.

Davis B.A.S. and Brewer S. (2009) – *Orbital forcing and role of the latitudinal insolation/temperature gradient*. *Climate Dynamics*, 32: 143-165.

Deines P. (1980) – *The isotopic composition of reduced organic carbon*. In: P.Fritz and J.C. Fontes (eds.), *Handbook of Environmental Geochemistry*, Amsterdam, 1: 329-406.

Deininger M., Fohlmeister J., Scholz D. and Mangini A. (2012) – *Isotope disequilibrium effects: The influence of evaporation and ventilation effects on the carbon and oxygen isotope composition of speleothems – A model approach*. *Geochimica et Cosmochimica Acta*, 96: 57-79.

Denèfle M., Lézine A.-M., Fouache É. Dufaure J.-J. (2000) – *A 12000 years pollen recor of Lake Maliq (Albania)*. Quaternary Research, 54: 423-432.

Desprat S., Combourieu-Nebout N., Essallami L., Sicre M.A., Dormoy I., Peyron O., Siani G., Bout Roumazeilles V. and Turon J.L. (2013) – *Deglacial and Holocene vegetation and climatic changes in the southern Central Mediterranean from a direct land-sea correlation*. Climate of the Past, 9 : 767-787.

Dicken A.P. (2005) – Radiogenic Isotope Geology. Cambridge University Press, 2nd edition.

Di Rita F. and Magri D. (2009) – *Holocene drought, deforestation and evergreen vegetation development in the central Mediterranean: a 5500 year record from Lago Alimini Piccolo, Apulia, southeast Italy*. The Holocene 19 (2): 295-306.

Di Rita F., Simone O., Caldara M., Roland Gehrels W. and Magri D. (2011) – *Holocene environmental changes in the coastal Tavoliere Plain (Abulia, southern Italy): A multiproxy approach*. Palaeogeography, Palaeoclimatology, Palaeoecology, 310(1-3): 139-151.

Di Rita F. and Magri D. (2012) – *An overview f the Holocene vegetation history from the central Mediterranean coasts*. Journal of Mediterranean Earth Sciences, 4: 35-52.

Dorale J.A., Gonzalez L.A., Reagan M.K., Pickett D.A., Murrell M.T. and Baker R.G. (1992) - *A high-resolution record of Holocene climate change in speleothem calcite from Cold Water Cave, Northeast Iowa*. Science, 258: 1626-1630.

Dorale J.A, Edwards R.L., Ito E. and Gonzalez L.A. (1998) - *Climate and vegetation history of the mid-continent from 75 to 25 ka: a speleothem record from Crevice Cave, Missouri, USA*. Science, 282: 1871-1874.

Dorale J.E., Edwards R.L. and Onac B.P. (2002) - *Stable isotopes as environmental indicators in speleothems*. In: Yuan D. & Zhang C. (Eds.), *Karst Processes and the Carbon Cycle. Final Report of IGCP 379*, Geological Publishing House, Beijing: 107-120.

Dorale J.A and Liu Z. (2009) - *Limitations of Hendy test criteria in judging the paleoclimatic suitability of speleothems and the need for replication*. Journal of Cave and Karst Studies, 71(1): 73-80.

Dreybrodt W. (1988) - *Processes in Karst Systems*. Springer-Verlag, Berlin, 287 p.

Drăguşin V., Staubwasser M., Hoffmann D.L., Ersek V., Onac B.P. and Veres D. (2014) – *Constraining Holocene hydrological changes in the Carpathians-Balkan region using speleothem $\delta^{18}O$ and pollen-based temperature reconstructions*. Climate of the Past, 10: 1363-1380.

Dreybrodt W. (2008) – *Evolution of the isotopic composition of carbon and oxygen in a calcite precipitating $H_2O-CO_2-CaCO_3$ solution and the related isotopic composition of calcite in stalagmites*. Geochimica et Cosmochimica Acta, 72: 4712-4724.

Dreybrodt W. (2011) - *Comments on processes contributing to the isotope composition of ^{13}C and ^{18}O in calcite deposited in speleothems*. Acta Carsologica, 40(2): 233-238.

- Dreybrodt W. and Scholz D. (2011) - *Climatic dependence of stable carbon and oxygen isotope signals recorded in speleothems: from soil water to speleothem calcite*. *Geochimica et Cosmochimica Acta*, 75: 734-752.
- Drysdale R.N., Zanchetta G., Hellstrom J., Maas R., Fallick A., Pickett M., Cartwright I. And Piccini L. (2006) – *Late Holocene drought responsible for the collapse of Old World civilizations is recorded in an Italian cave flowstone*. *Geology*, 34(2): 101-104.
- Drysdale R.N., Bence T.B., Hellstrom J.C., Couchoud I., Greig A., Bajo P., Zanchetta G., Isola I., Spötl C., Baneschi I., Regattieri E. and Woodhead J.D. (2012) - *Precise microsampling of poorly laminated speleothems for U-series dating*. *Quaternary Geochronology*, 14: 38-47.
- Dunn O.J. (1961) - *Multiple Comparison Among Means*. *Journal of the American Statistical Association*, 56(293): 52-64.
- Dükeloh A. and Jacobeit J., 2003 – *Circulation dynamics of Mediterranean precipitation variability 1948-98*. *International Journal of Climatology*, 23: 1843-1866.
- Fairchild I.J., Borsato A., Tooth A.F., Frisia S., Hawkesworth C.J., Huang Y.-M., McDermott F. and Spiro B. (2000) - *Controls on trace element (Sr-Mg) compositions of carbonate cave waters: implications for speleothem climatic records*. *Chemical Geology*, 166: 255-269.
- Fairchild I.J., Baker A., Borsato A., Frisia S., Hinton R.W., McDermott F. and Tooth A.F. (2001) – *Annual to sub-annual resolution of multiple trace-element trends in speleothems*. *The Geological Society of London*, 158(5): 831-841.
- Fairchild I.J., Smith C.L., Baker A., Fuller L., Spötl C., Matthey D., McDermott F. and EIMF (2006) - *Modification and preservation of environmental signals in speleothems*. *Earth-Science Reviews*, 75: 105-153.
- Fairchild I.J. and McMillan E.A. (2007) – *Speleothems as indicators of wet and dry periods*. *International Journal of Speleology*, 36(2): 69-74.
- Fairchild I.J. and Treble P.C. (2009) - *Trace elements in speleothems as recorders of environmental change*. *Quaternary Science Reviews*, 28: 449-468.
- Fairchild I.J. and Hartland A. (2010) – *Trace element variations in stalagmites: controls by climate and by karst system processes*. *EMU Notes in Mineralogy*, 10(7): 259-287-
- Fairchild I.J. and Baker A. (2012) - *Speleothem science: from process to past environments*. John Wiley & Sons, Oxford, UK, 450 p.
- Farquhar G.D., O’Leary M.H. and Berry J.A. (1982) – *On the Relationships Between Carbon Isotope Discrimination and the Intercellular Carbon Dioxide Concentration in Leaves*. *Australian Journal of Plant Physiology*, 9(2): 121-137.
- Filippi M.L., Heiri O., Arpentini E., Angeli N., Bortolotti M., Lotter A.F. and Van der Borg K. (2005) – *Evoluzione paleoambientale dal Tardoglaciale a oggi ricostruita attraverso lo studio dei sedimenti del Lago di Lavarone (altopiano di Folgaria e Lavarone, Trentino)*. *Studi Trentini di Scienze Naturali, Acta Geologica*, 82: 279-298.

- Fletcher A.J. and Zielhofer C. (2013) – *Fragility of Western Mediterranean landscapes during Holocene Rapid Climate Changes*. *Catena*, 103: 16-29.
- Folk R.L. (1965) – *Some aspects of recrystallization in ancient limestones*. Society of Economic Paleontologists and Mineralogists, Special Publications, 13: 14-48.
- Folk R.L. and Assereto R. (1976) – Comparative fabrics of length-slow and length-fast calcite and calcitized aragonite in a Holocene speleothem, Carlsbad Caverns, New Mexico. *Journal of Sedimentary Research*, 46: 486-496.
- Francke A., Wagner B., Leng M.J. and Rethemeyer J. (2013) – *A Late Glacial to Holocene record of environmental change from Lake Dojran (Macedonia, Greece)*. *Climate of the Past*, 9: 481-498.
- Freytet P. and Verrecchia E. (1999) – *Calcitic radial palisadic fabric in freshwater stromatolites: diagenetic and recrystallized feature or physicochemical sinter crust?* *Sedimentary Geology*, 126: 97-102.
- Frisia S. (1996) – *Petrographic evidences of diagenesis in speleothems: some examples*. *Speleochronos*, 7: 21-30.
- Frisia S., Borsato A., Fairchild I.J. and McDermott F. (2000) - *Calcite fabrics, growth mechanisms, and environments of formation in speleothems from the Italian Alps and Southwestern Ireland*. *Journal of Sedimentary Research*, 70: 1183-1196.
- Frisia S., Borsato A., Preto N. and McDermott F. (2003) – *Late Holocene annual growth in three Alpine stalagmites records the influence of solar activity and the North Atlantic Oscillation on winter climate*. *Earth and Planetary Science Letters*, 216(3): 411-424.
- Frisia F., Borsato A., Spötl C., Villa I.M and Cucchi F. (2005) – *Climate variability in the SE Alps of Italy over the past 17000 years reconstructed from a stalagmite record*. *Boreas*, 34: 445-455.
- Frisia S., Borsato A., Mangini A., Spötl C., Madonia G. and Sauro U. (2006) – *Holocene climate variability in Sicily from a discontinuous stalagmite record and the Mesolithic to Neolithic transition*. *Quaternary Research*, 66 : 388-400.
- Frisia S. and Borsato S. (2010) - *Chapter 6 Karst*. *Developments in Sedimentology*, 61: 269-318.
- Frisia S. (2015) - *Microstratigraphic logging of calcite fabrics in speleothems as tool for palaeoclimate studies*. *International Journal of Speleology*, 44(1): 1-16.
- Fouache E., Desruelles S., Magny M., Bordon A., Oberweiler C., Coussot C., Touchais G., Lera P., Lézine A.-M., Fadin L. and Roger R. (2010) – *Palaeogeographical reconstructions of Lake Maliq (Korça Basin, Albania) between 14,000 BP and 2000 BP*. *Journal of Archaeological Science*, 37 : 525-535.
- Gabitov R.I. and Watson E.B. (2006) – *Partitioning of strontium between calcite and fluid*. *Geochemistry, Geophysics, Geosystems*, 7, Q11004.

Gaetani M., Baldi M., Dalu G.A. & Maracchi G., 2007 – *Connessioni tra il clima della regione Mediterranea e l’Africa Occidentale attraverso la circolazione meridiana di Hadley*. Clima e cambiamenti climatici, i, edited by: Carli, B., Cavarretta, G., Colacino, M. and Fuzzi, S., Roma, Consiglio Nazionale delle Ricerche, 23-26.

Gams I. (1981) – Contributions to morphometrics of stalagmite. Proceedings of the 8th International Congress of Speleology, 276-278.

Gat J.R. and Carmi I. (1970) – *Evolution of the isotopic composition of atmospheric waters in the Mediterranean Sea area*. Journal of Geophysical Research, 75: 3039-3048

Gázquez F., Calaforra J.M., and Forti P. (2011) – *Black Mn-Fe crusts as markers of abrupt palaeoenvironmental changes in El Soplao Cave (Cantabria, Spain)*. International Journal of Speleology, 40(2): 163-169.

Genty D. (1992) – Les spéléothèmes du tunnel de Godrville (Belgique) – un exemple exceptionnel de concrétionnement moderne – intérêt pour l’étude de la cinétique de la précipitation de la calcite et de sa relation avec les variations d’environnement. Speleochronos, 4 : 3-29.

Genty D. and Quinif Y. (1996) – Annually laminated sequences in the internal structure of some Belgian stalagmites: importance for paleoclimatology. Journal of Sedimentary Research, 66: 275-288.

Genty D. and Massault M. (1999) – *Carbon transfer dynamics from bomb ^{14}C and $\delta^{13}\text{C}$ time series of a laminated stalagmite from SW France: modelling and comparison with other stalagmites*. Geochimica, Cosmochimica Acta, 63: 1537-1548.

Genty D., Massault M., Gilmour M., Baker A., Verheyden S. and Keppens E. (1999) – *Calculation of past dead carbon proportion and variability by the comparison of AMS ^{14}C and TIMS U/Th ages of two Holocene stalagmites*. Radiocarbon, 41: 251-270.

Genty D., Baker A., Massault M., Proctor C., Gilmour M., Pons-Branchu E. and Hamelin B. (2001) – *Dead carbon in stalagmites: carbonate bedrock paleodissolution vs. aging of soil organic matter. Implications for ^{13}C variations in speleothems*. Geochimica Cosmochimica Acta, 65: 193-214.

Genty D., Blamart D., Ouahdi R., Gilmour M., Baker A., Jouzel J. and Van-Exter S. (2003) – *Precise dating of Dansgaard-Oeschger climate oscillation in western Europe from stalagmite data*. Nature, 421: 833-837.

Genty D., Blamart D., Ghaleb B., Plagnes V., Causse Ch., Bakalowicz M., Zouari K., Chkir N., Hellstrom J., Wainer K. and Bourges F. (2006) - *Timing and dynamics of the last deglaciation from European and North African $\delta^{13}\text{C}$ stalagmite profiles – comparison with Chinese and South Hemisphere stalagmites*. Quaternary Science Reviews, 25(17-18): 2118-2142.

Geyh M.A. and Schleicher H. (2000) – *Absolute Age Determination*. Springer-Verlag.

Giesler R., Andersson T., Lövgren L. and Persson P. (2005) - *Phosphate sorption in aluminium- and iron-rich humus soils*. Soil Science Society of America Journal, 69: 77-86.

Giorgi F. (2006) – *Climate change hot-spots*. Geophysical Research Letters, 33(8): L08707.

- Giraudi C. (2005) – *Middle to Late Holocene glacial variations, periglacial processes and alluvial sedimentation on the higher Apennine massifs (Italy)*. Quaternary Research, 64: 176-184.
- Giunta S., Negri A., Morigi C., Capotondi L., Combourieu-Neout N., Emeis K.C., Sangiorgi F. and Vigliotti L. (2003) – *Coccolithophorid ecostratigraphy and multi-proxy paleoceanographic reconstruction in the Southern Adriatic Sea during the last deglacial time (Core AD91-17)*. Palaeogeography, Palaeoclimatology, Palaeoecology, 190: 39-59.
- Goede A., McCulloch M., McDermott F. And Hawkesworth C. (1998) – *Aeolian contribution to strontium and strontium isotope variations in a Tasmanian speleothem*. Chemical Geology, 149: 37-50.
- Gonzalez L.A., Carpenter S.J. and Lohmann K.C. (1992) – *Inorganic calcite morphology: roles of fluid chemistry and fluid flow*. Journal of Sedimentary Petrology, 62: 382-399.
- Govedarica B. (2006) – *Find of the Cetina-type in western Balkan hinterland and the issue of culture-historical interpretation in the prehistoric archaeology*.
- Green S.B., Salkind N.J. and Akey T.M. (2008) - *Using SPSS for Windows and Macintosh: Analysing and Understanding Data*. New Jersey, Prentice Hall.
- Grisogono B. and Belušić D. (2009) – *A review of recent advances in understanding the meso- and micro-scale properties of the severe Bora wind*. Tellus A, 61:1-16.
- Grüger E. and Thulin B. (1998) – *First results of biostratigraphical investigations of Lago d'Averno near Naples relating to the period 800 BC-800 AD*. Quaternary International, 47-48: 35-40.
- Hansen M., Dreybrodt W. and Scholz D. (2013) - *Chemical evolution of dissolved inorganic carbon species flowing in thin water films and its implications for (rapid) degassing of CO₂ during speleothem growth*. Geochimica et Cosmochimica Acta, 107: 242-251.
- Hartland A., Fairchild I.J., Lead J.R., Borsato A., Baker A., Frisia S. and Baalousha M. (2012) – *From soil to cave: Transport of trace metals by natural organic matter in karst dripwaters*. Chemical Geology, 304-305: 68-82.
- Hellerman S. and M. Rosenstein (1983) - *Normal monthly wind stress over the world ocean with error estimates*. Journal of Physical Oceanography, 13(1): 1093-1104.
- Hellstrom J., McCulloch M. and Stone J. (1998) - *A detailed 31,000-year record of climate and vegetation change, from the isotope geochemistry of two New Zealand speleothems*. Quaternary Research, 50(2): 167-178.
- Hellstrom J. (2003) - *Rapid and accurate U/Th dating using parallel ion-counting multi-collector ICP-MS*. Journal of Analytical Atomic Spectrometry, 18: 1346-1351.
- Hellstrom J.C. and McCulloch M.T. (2000) – *Multi-proxy constraints on the climatic significance of trace element records from a New Zealand speleothem*. Earth and Planetary Science Letters, 179: 287-297.

- Hellstrom J. (2006) - *U-Th dating of speleothems with high initial ^{230}Th using stratigraphical constraint*. Quaternary Geochronology, 1: 289-295.
- Hendy C.H. (1971) - *The isotopic geochemistry of speleothems-I. The calculation of the effects of different modes of formation on the isotopic composition of speleothems and their applicability as palaeoclimatic indicators*. Geochimica et Cosmochimica Acta, 35: 801-824.
- Hines J., Høilund Nielsen K. and Siegmund F. (1999) – *The pace of change: studies in Early Medieval chronology*. Oxbow Books, p. 93.
- Hodge E., McDonald J., Fischer M., Redwood D., Hua Q., Levchenko V., Drysdale R., Waring C. and Fink D. (2011) – *Using the ^{14}C bomb pulse to date young speleothems*. Radiocarbon, 53 (2): 345-357.
- Hoefs J. (1997) – *Stable Isotope Geochemistry*. 4th ed.. Springer-Verlag, Berlin.
- Horvatinčić N., Krajcar Bronić and Obelić B. (2003) – *Differences in the ^{14}C age, $\delta^{13}\text{C}$ and $\delta^{18}\text{O}$ of Holocene tufa and speleothem in the Dinaric Karst*. Palaeogeography, Palaeoclimatology, Palaeoecology, 193: 139-157.
- Huang Y. and Fairchild I.J. (2001) - *Partitioning of Sr^{2+} and Mg^{2+} into calcite under karst-analogue experimental conditions*. Geochimica et Cosmochimica Acta, 65: 47-62.
- Huang Y., Fairchild I.J., Borsato A., Frisia S., Cassidy N.J., McDermott F. and Hawkesworth C.J., (2001) – *Seasonal variations in Sr, Mg and P in modern speleothems (Grotta di Ernesto, Italy)*. Chemical Geology, 175: 429-448.
- IAEA/WMO (2015) – *Global Network of Isotopes in Precipitation*. The GNIP Database. Accessible at: www.iaea.org/water.
- Jahns S. (2005) – *The Holocene history of vegetation and settlement at the coastal site of Lake Voukaria in Acarnania, western Greece*. Vegetation History and Archaeobotany, 14: 55-66.
- Joannin S., Vannière B., Galop D., Peyron O., Haas J.N., Gilli A., Chapron E., Wirth S.B., Anselmetti F., Desmet M. and Magny M. (2013) – *Climate and vegetation changes during the Lateglacial and early-middle Holocene at Lake Ledro (southern Alps, Italy)*. Climate of the Past, 9: 913-933.
- Kaźmierczak J., Coleman M.L., Gruszczynski M. and Kempe S. (1996) – *Cyanobacterial key to the genesis of micritic and peloidal limestones in ancient seas*. Acta Palaeontologica Polonica, 41: 319-338.
- Kendall A.C. (1993) – *Columnar calcite in speleothems. Discussion*. Journal of Sedimentary Research, 63: 550-553.
- Kendall A.C. and Broughton P.L. (1978) - *Origin of fabrics in speleothems composed of columnar calcite crystals*. Journal of Sedimentary Research, 48: 519-538.
- Kim S.-T. and O'Neil J.R. (1997) – *Equilibrium and nonequilibrium oxygen isotope effects in synthetic carbonates*. Geochimica et Cosmochimica Acta, 61: 3461-3475. Journal of Climate, 28: 505-516.

Kingston D.G., Stagle J.H., Tallaksen L.M. and Hannah D.M. (2015) – *European-Scale Drought: Understanding Connections between Atmospheric Circulation and Meteorological Drought Indices*.

Kinzl H. (1932). *Die grössten nacheiszeitlichen Gletschervorstösse in den Schweizer Alpen und in der Mont Blanc-Gruppe*. Bornträger.

Kim S.-T., O’Neil J.R., Hillaire-Marcel C. and Mucci A. (2007) – *Oxygen isotope fractionation between synthetic aragonite and water: influence of temperature and Mg²⁺ concentration*. *Geochimica et Cosmochimica Acta*, 71: 4704-4715.

Kotthoff U., Koutsodendris A., Pross J., Schmiedl G., Bornemann A., Kaul C., Marino G., Peyron O. and Schiebel R. (2011) – *Impact of Lateglacial cold events on the northern Aegean region reconstructed from marine and terrestrial proxy data*. *Journal of Quaternary Science*, 26: 86-96.

Krichak S.O. & Alpert P., 2005 – *Signatures of the NAO in the atmospheric circulation during wet winter months over the Mediterranean region*. *Theoretical and Applied Climatology*, 82: 27-39.

Milanolo S., Preti N. & Cella G., 2013 - *Govještica Cave – Prača Canyon, BIH*. *Naš Krš Sarajevo*, 23: 43.

Kruskal W.H. and Wallis W.A. (1952) – *Use of ranks in one-criterion variance analysis*. *Journal of the American Statistical Association*, 47(260): 583-621.

Lacey H.J., Francke A., Leng M.J., Vane C.H. and Wagner B. (2015) – *A high-resolution Late Glacial to Holocene record of environmental change in the Mediterranean from Lake Ohrid (Macedonia/Albania)*. *International Journal of Earth Science*, 104: 1623-1638.

Lachniet M.S., 2009 - *Climatic and environmental controls on speleothem oxygen-isotope values*. *Quaternary Science Reviews*, 28: 412-432.

Lamb H. H. (1980). *Weather and climate patterns of the Little Ice Age*. In: *Das Klima* (pp. 149-160). Springer Berlin Heidelberg.

Lamy F., Arz H. W., Bond G. C., Bahr A., and Pätzold J. (2006) - *Multicentennial-scale hydrological changes in the Black Sea and northern Red Sea during the Holocene and the Arctic/North Atlantic Oscillation*. *Paleoceanography*, 21(1): 1-11.

Lead J.R. and Wilkinson K.J. (2006) – *Aquatic colloids and nanoparticles: current knowledge and future trends*. *Environmental Chemistry*, 3: 159-171.

Leng M.J., Wagner B., Boehm A., Panagiotopoulos K., Vane C.H., Snelling A., Haidon C., Woodley E., Vogel H., Zanchetta G., Baneschi I. (2013) - *Understanding past climatic and hydrological variability in the Mediterranean from Lake Prespa sediment isotope and geochemical record over the Last Glacial cycle*. *Quaternary Science Reviews*, 66: 123-136.

Li W.X., Lundberg J., Dickin A.P., Ford D.C., Schwarcz H.P., McNutt R. and Williams D. (1989) – *High-precision mass-spectrometric uranium-series dating of cave deposits and implications for palaeoclimate studies*. *Nature*, 339: 534-536.

Liu H., Ye T. and Mao C. (2007) – *Fluorescent Carbon Nanoparticles Derived from Candle Soot*. *Angewandte Chemie International Edition*, 46: 6473-6475.

- Magny M., Bégeot C., Guiot J. and Peyron O. (2003) – *Contrasting patterns of hydrological changes in Europe in response to Holocene climate cooling phases*. *Quaternary Science Reviews*, 22: 1589-1596.
- Magny M., Joannin S., Galop D., Vannièrè B., Haas J.N., Bassetti M., Bellintani P., Scandolari R. and Desmet M. (2012) – *Holocene palaeohydrological changes in the northern Mediterranean borderlands as reflected by the lake-level record of Lake Ledr, northeastern Italy*. *Quaternary Research*, 77: 382-396.
- Magny M., Combourieu-Nebout N., de Beaulieu J.L., Bout-Roumazièlles V., Colombaroli D., Desprat S., Francke A., Joannin S., Ortu E., Peyron O., Revel M., Sadori L., Siani G., Sicre M.A., Samartin S., Simonneau A., Tinner W., Vannièrè B., Wagner B., Zanchetta G., Anselmetti F., Brugiapaglia E., Chapron E., Debret M., Desmet M., Didier J., Essallami L., Galop D., Gilli A., Haas J.N., Kallel N., Millet L., Stock A., Turon J.L. and Wirth S. (2013) – *North-south palaeohydrological contrasts in the central Mediterranean during the Holocene : tentative synthesis and working hypotheses*. *Climate of the Past*, 9 : 2043-2071.
- Magny M. and Combourieu Nebout N. (2013) – *Holocene changes in environment and climate in the central Mediterranean as reflected by lake and marine records*. *Climate of the Past*, 9: 1447-1454.
- Magri D. and Sadori L. (1999) – *Late Pleistocene and Holocene pollen stratigraphy at Lago di Vico (central Italy)*. *Vegetation History and Archaeobotany*, 8: 247-260.
- Maisch M. (1982) – *Zur Gletscher- und Klimageschichte des alpinen Spätglazials*. *Geographica Helvetica*, 37: 93-104.
- Marino G., Rohling E. J., Sangiorgi F., Hayes A., Casford J. L., Lotter A. F., Kucera M. and Brinkhuis H. (2009) - *Early and middle Holocene in the Aegean Sea: interplay between high and low latitude climate variability*. *Quaternary Science Reviews*, 28: 3246–3262.
- Mattey D., Lowry D., Duffet J., Fisher R., Hodge E. and Frisia S. (2008) – *A 53 year seasonally resolved oxygen and carbon isotope record from a morn Gibraltar speleothem: reconstructed drip water and relationship to local precipitation*. *Earth and Planetary Science Letters*, 269: 80-95.
- Mattey D., Fairchild I.J., Atkinson T.C., Latin J.P., Ainsworth M. and Durell R. (2010) - *Seasonal microclimate control of calcite fabrics, stable isotopes and trace elements in modern speleothems from St. Michaels Cave, Gibraltar*. In: Pedley HM & Rogerson M. (Eds.), *Tufas and speleothems: unraveling the microbial and physical controls*, Geological Society of London Special Publications, 336: 323-344.
- May P. W. (1982) - *Climatological flux estimates in the Mediterranean Sea: Part I. Wind and wind stresses*. *NORDA Rep. 54*: 56 pp.
- Mayewski P.A., Rohling E.E., Stager J.C, Karlén W. Maasch K.A., Meeker L.D., Meyerson E.A., Gasse F., van Kreveland S., Holmgren K., Lee-Thorp J., Rosqvist G., Rack F., Staubwasser M., Schneider R.R., Steig E.J. (2004) – *Holocene climate variability*. *Quaternary Research*, 62: 243-255.

- Mayr F. (1964) - *Untersuchungen über Ausmass und Folgen der Klima und Gletscherschwankungen seit dem Beginn der postglazialen Wärmezeit*. Zeitschrift für Geomorphologie 8: 257–85.
- McDermott F., Frisia S., Huang Y., Longinelli A., Spiro B., Heaton T.H.E., Hawkesworth C.J., Borsato A., Keppens E., Fairchild I.J., van der Bor K., Verheyden S. and Selmo E. (1999) – *Holocene climate variability in Europe: Evidence from $\delta^{18}O$, textural and extension-rate variations in three speleothems*. Quaternary Science Reviews, 18: 1021-1038.
- McDermott F., Matthey D.P. and Hawkesworth C. (2001) – *Centennial-Scale Holocene Climate Variability Revealed by a High-Resolution Speleothem $\delta^{18}O$ Record from SW Ireland*. Science, 294 (5545): 1328-1331.
- McDermott F. (2004) – *Palaeo-climate reconstruction from stable isotope variations in speleothems: a review*. Quaternary Science Reviews, 23(7-8): 901-918.
- Mickler P., Stern L.A. and Banner J. (2006) – *Large kinetic isotope effects in modern speleothems*. Geological Society of America bulletin, 118(1/2): 65-81.
- Milano S., Preti N. and Cella G. (2013) – *Govještica cave – Prača Canyon, BIH*. Naš Krš XXXIII, Sarajevo, 43: 33-44.
- Moore G.W. and Sullivan G.N. (1978) – *Speleology. The study of Caves*. Zephyrus Press, Teaneck (NY).
- Mucci A. and Morse J.W. (1990) - *Chemistry of low-temperature abiotic calcites: experimental studies on coprecipitation, stability, and fractionation*. Reviews in Aquatic Science, 3: 217-254.
- Mühlinghaus C., Scholz D. and Mangini A. (2007) - *Modelling stalagmite growth and $\delta^{13}C$ as a function of drip interval and temperature*. Geochimica et Cosmochimica Acta, 71: 2780-2790.
- Neuser R.D. and Richter D.K. (2007) – *Non-marine radiaxial fibrous calcite – examples of speleothems proved by electron backscatter diffraction*. Sedimentary Geology, 194: 149-154.
- Nicolussi K., Kaufmann M., Patzelt G., van der Plitch J. and Thurner A. (2005) – *Holocene tree-line variability in the Kauner Valley, Central Eastern Alps, indicated by dendrochronological analysis of living trees and subfossil logs*. Vegetation History and Archaeobotany, 14: 221-234.
- Northup D. E., Barns S.M., Yu L.E., Spilde M.N., Schelble R.T., Dano K.E., Crossey L.J., Connolly C.A., Boston P.J., Natvig D.O. and Dahm C.N. (2003) – *Diverse microbial communities inhabiting ferromanganese deposits in Lechuguilla and Spider Caves*. Environmental Microbiology, 5(11): 1071-1086.
- Oldfield F., Asioli A., Accorsi C.A., Mercuri A.M., Juggins S., Langone L., Rolph T., Trincardi F., Wolff G., Gibbs Z., Vigliotti L., Frignani M., van der Post K. and Branch N. (2003) – *A high resolution late Holocene palaeo environmental record from the central Adriatic Sea*. Quaternary Science Reviews, 22: 319-342.
- Olsen J., John Anderson N. and Knudsen M.F. (2012) – *Variability of the North Atlantic Oscillation over the past 5,200 years*. Nature Geoscience, 5: 808-812.

- Orlić M., Gačić M. and La Violette P.E. (1992) – *The currents and circulation of the Adriatic Sea*. *Oceanologica Acta*, 15(2): 109-124.
- Panagiotopoulos K., Aufgebauer A., Schäbitz F. and Wagner B. (2013) – Vegetation and climate history of the Lake Prespa region since the Lateglacial. *Quaternary International*, 293: 157-169.
- Perrette Y., Poulenard J., Saber A.-I., Fanget B., Guittonneau S., Ghaleb B. and Gaeaudee S. (2008) – *Polycyclic Aromatic Hydrocarbons in stalagmites : Occurrence and use for analyzing past environments*. *Chemical Geology*, 251(1-4) : 67-76-
- Perrin J. (1997) – *Géologie et géochimie des eaux dans le réseau du Grand Cor (Valais, Suisse)*. Proc. Of the 12th Int. Congress of Speleology, Chaux-de-Fond, Wsitzerland, 2 : 99102.
- Peyron O., Magny M., Goring S., Joannin S., de Beaulieu J.L., Brugiapaglia E., Sadori L., Garfi G., Kouli K., Ioakim C. and Combourieu-Nebout F. (2013) – *Constrasting patterns of climatic changes during the Holocene across the Italian Peninsula reconstructed from pollen data*. *Climate of the Past*, 9 : 1233-1252.
- Piva A., Asioli A., Trincardi F., Schneider R.R. and Vigliotti L. (2008) – *Late-Holocene climate variabilità in the Adriatic Sea (Central Mediterranean)*. *The Holocene*, 18 (1): 153-167.
- Plagnes V., Causse C., Genty D., Paterne M. and Blamart D. (2002) - *A discontinuous climatic record from 187 to 74 ka from a speleothem of the Clamouse Cave (South of France)*. *Earth and Planetary Science Letters*, 201: 87-103.
- Plummer L.N., 1977 - *Defining reactions and mass transfer in part of the Floridan aquifer*. *Water Resources Research*, 13: 801-812.
- Pučnik, R. (1980) - *Velika knjiga o vremenu*. Cankarjeva založba, Ljubljana, pp. 368.
- Regattieri E-, Zanchetta G., Drysdale R.N., Isola I., Hellstrom J.C. and Dallai L. (2014) – *Lateglacial to Holocene trace element record (Ba, Mg, Sr) from Corchia Cave (Apuan Alps, central Italy): paleoenvironmental implications*. *Journal of Quaternary Science*, 29(4): 381-392.
- Richards D.A. and Dorale J.A. (2003) – Uranium-series chronology and environmental applications of speleothems. *Reviews in Mineralogy & Geochemistry*, 52: 407-460.
- Richter D.K., Gotte T., Niggermann S. and Wurth G. (2004) – *REE³⁺ and Mn²⁺ -activated cathololuminescence in lateglacial and Holocene stalagmites of central Europe: evidence for climatic processes?* *The Holocene*, 14: 759-767.
- Riechelmann D.F.C., Deininger M., Scholz D., Riechelmann S., Schröder-Ritzrau A., Spötl C., Richter D.K., Mangini A. and Immenhauser A. (2013) – *Disequilibrium carbon and oxygen isotope fractionation in recent cave calcite: Comparison of cave precipitates and model data*. *Geochimica et Cosmochimica Acta*, 103:232-244.
- Riechelmann S., Schröder-Ritzrau A., Wassenburg J.A., Schreuer J., Richter D.K., Riechelmann D.F., Terente M., Constantin S., Mangini A. and Immenhauser A. (2014) - *Physicochemical characteristics of drip waters: influence on mineralogy and crystal morphology of recent cave carbonate precipitates*. *Geochimica et Cosmochimica Acta*, 145: 13-29.

- Roberts M.S., Smart P.L. and Baker A. (1998) - *Annual trace element variations in a Holocene speleothem*. Earth and Planetary Science Letters, 154: 237-246.
- Rodwell M.J. and Hoskins B.J. (2001) – *Subtropical Anticyclones and Summer Monsoons*. Journal of Climate, 14: 3192-3211.
- Rohling E.J., Jorissen F.J. and De Stigter H.C. (1997) – *200 Year interruption of Holocene sapropel formation in the Adriatic Sea*. Journal of Micropalaeontology, 16: 97-108.
- Rohling E.J., Mayewski P.A., Zbu-Zied R.H., Casford J.S.L. and Hayes A. (2002) – *Holocene atmosphere-ocean interactions: records from Greenland and the Aegean Sea*. Climate Dynamics, 18: 587-593.
- Rohling E.J. (2013) – *Oxygen isotope composition of seawater*. In: Elias S.A. (ed.) The Encyclopedia of Quaternary Science, vol 2, pp. 915-922. Amsterdam: Elsevier.
- Rosen W. (2007) – *Justinian's Flea: Plague, Empire, and the Birth of Europe*. Viking Adult, p. 367.
- Rossi V. and Vaiani S.C. (2008) – *Benthic foraminiferal evidence of sediment supply changes and fluvial drainage reorganization in Holocene deposits of the Po Delta, Italy*. Marine Micropaleontology, 69(2): 106-118.
- Rudzka D., McDermott F., Baldini L.M., Fleitmann D., Moreno A. and Stoll H. (2011) – *The coupled $\delta^{13}C$ -radiocarbon systematics of three Late Glacial/early Holocene speleothems; insights into soil and cave processes at climatic transitions*. Geochimica et Cosmochimica Acta, 75: 4321-4339.
- Sadori L. and Narcisi B. (2001) – *The Postglacial record of environmental history from Lago di Pergusa, Sicily*. The Holocene, 11(6): 655-670.
- Sadori L., Giardini M., Ghiozzi E., Mazzini I., Sul pizio R., van Welden and Zanchetta G. (2015) – *Vegetation, climate and environmental history of the last 4500 years at lake Shkodra (Albania/Montenegro)*. The Holocene, 25(3): 435-444.
- Sánchez-Moral P.A., Soler V., Cañaveras J.C., Sanz-Rubio E., Van Grieken R. and Gysels K. (1999) – *Inorganic deterioration affecting the Altamira Cave, N Spain : quantitative approach to wall-corrosion (solution-etching) processes induced by visitors*. Science of Total Environment, 243: 67-84.
- Sangiorgi F., Capotondi L., Combourieu Nebout N., Vigliotti L., Brinkhuis H., Giunta S., Lotter A.F., Morigi C., Negri A. and Reichert G.-J. (2003) – *Holocene seasonal sea-surface temperature variations in the southern Adriatic Sea inferred from a multiproxy approach*. Journal of Quaternary Science, 18(8): 723-732.
- Sartori G., Mancabelli A., Wolf U. and Corradini F. (2005) – *Atlante dei suoli del Parco Naturale Adamello-Brenta*. Monografie II, Museo Tridentino di Scienze Naturali, Trento, 239 p..
- Scholz D., Frisia S., Borsato A., Spötl C., Mudelsee M., Miorandi R. and Mangini A. (2012) – *Holocene climate variability in north-eastern Italy: potential influence of the NAO and solar activity recorded by speleothem data*. Climate of the Past, 8: 1367-1383.

Schroedter T.M., Hofmann R., Müller-Scheeddel N., Müller J and Nelle O. (2012) – Late Neolithic vegetation around three sites in the Visoko Basin, Bosnia, based on archaeo-anthracology – spatial variation versus selective wood use. *Wood and Charcoal. Evidence for human and natural history.* SAGVNTVM EXTRA – 13: 53-64.

Sharp Z., (2007) – *Principles of Stable Isotope Geochemistry.* Pearson Prentice Hall, Upper Saddle River, NJ.

Siani G., Magny M., Paterne M., Debret M. and Fontugne M. (2013) – *Paleohydrology reconstruction and Holocene climate variability in the South Adriatic Sea.* *Climate of the Past*, 9: 499-515.

Schmidt R., Müller J., Drescher-Schneider R., Krisai R., Szeroczyńska K. and Barić A. (2000) – *Changes in lake level and trophy at Lake Vrana, a large karstic lake on the Island of Cres (Croatia), with respect to palaeoclimate and anthropogenic impacts during the last approx. 16,000 years.* *Journal of Limnology*, 59 (2): 113-130.

Smith B.N. (1982) – *General characteristics of terrestrial plants (agronomic and forests) – C₃, C₄, and Crassulacean Acid Metabolism plants.* In A. Mitsui and C.C. Black (Eds.), *CRC Handbook of Biosolar Resources*, V. 1, Part 2, CRC Press, Boca Raton, Florida, 99-118.

Spötl C. and Mangini A. (2002) - *Stalagmite from the Austrian Alps reveals Dansgaard–Oeschger events during isotope stage 3:: Implications for the absolute chronology of Greenland ice cores.* *Earth and Planetary Science Letters*, 203(1): 507-518.

Srejić D. (1994) - *Kulture gvozdenog doba na tlu Srbije, Istorija srpskog naroda I*, Srpska književna zadruga, Beograd.

Stefani M. and Vincenti S. (2005) – *The interplay of eustasy, climate and human activity in the late Quaternary depositional evolution and sedimentary architecture of the Po Delta system.* *Marine Geology*, 222-223: 19-48.

Stein A.F., Draxler R.R., Rolph G.D., Stunder B.J.B., Cohen M.D. and Ngan F. (2015) – *NOAA's HYSPLIT atmospheric transport and dispersion modeling system.* *Bulletin of American Meteorological Society*, 96: 2059-2077.

Still C.J., Berry J.A., Collatz G.J. and DeFries R. (2003) – Global distribution of C₃ and C₄ vegetation: Carbon cycle implications. *Global Biogeochemical Cycles*, 17(1): 4-14.

Stipčević A. (1977) – *The Illyrians: history and culture.* Noyes Press, p.108.

Sunagawa I. (1984) – *Growth of crystals in Nature.* In Sunagawa I., ed., *Material Science of the Earth's interior.* Tokyo, Tokyo Scientific Publishing Company, Tokyo, 63-105.

Tang K. and Feng X. (2001) - *The effect of soil hydrology on the oxygen and hydrogen isotopic compositions of plants' source water.* *Earth and Planetary Science Letters*, 185: 355–367.

Thornthwaite C.W. and Mather J.R. (1957) – *Instruction and tables for computing potential evapotranspiration and the water balance.* Publications in climatology, Drexel Institute Technology, Philadelphia, 10, 254p.

- Treble P., Shelley J.M.G. and Chappell J. (2003) - *Comparison of high resolution sub-annual records of trace elements in a modern (1911-1992) speleothem with instrumental climate data from southwest Australia*. Earth and Planetary Science Letters, 216: 141-153.
- Treble P.C., Chappell J. and Shelley J.M.G. (2005) – *Complex speleothem growth processes revealed by trace element mapping and scanning electron microscopy of annual layers*. Geochimica et Cosmochimica Acta, 69(20): 4855-4863.
- Treble P., Shelley J.M.G and Chappell J. (2013) – *Comparison of high resolution sub-annual records of trace elements in a modern (1911-1992) speleothem with instrumental climate data from southwest Australia*. Earth and Planetary Science Letters, 216: 141-153.
- Usdowski E. and Hoefs J. (1990) - *Kinetic $^{13}\text{C}/^{12}\text{C}$ and $^{18}\text{O}/^{16}\text{O}$ effects upon dissolution and outgassing of CO_2 in the system $\text{CO}_2\text{-H}_2\text{O}$* . Chemical Geology, 80: 109-118
- Veggiani A. (1986) - *Le fluttuazioni del clima dal XVIII al XX secolo. I cicli di Bruckner*. Bollettino della società Torricelliana di Scienze e Lettere, 37: 1-56.
- Verheyden S. (2004) – *Trace elements in speleothems. A short review of the state of the art*. International Journal of Speleology, 33(1/4): 95-101.
- Vogel H., Wagner B., Zanchetta G., Sulpizio R. and Rosén P. (2009) – *A paleoclimate record with tephrochronological age control for the last glacial-interglacial cycle from Lake Ohrid, Albania and Macedonia*. Journal of Paleolimnology, 44: 295-310.
- Vreča P., Krajcar Bronić I., Horvatinčić N. and Barešić J. (2006) - *Isotopic characteristics of precipitation in Slovenia and Croatia: comparison of continental and maritime stations*. Journal of Hydrology, 330: 457-469.
- Vujnović L. and Marić J. (1973-1981) – *Sa saradnicima navedenim u ovodu Tumača*. Geoinženjering – OOUR Institut za geologiju, Sarajevo.
- Walker M.J.C., Berkelhammer M., Björck S., Cwynar L.C., Fisher D.A., Long A.J., Lowe J.J., Newnham R.M., Rasmussen S.O. and Weiss H. (2012) – *Formal subdivision of the Holocene Series/Epoch: a Discussion Paper by a Working Group of INTIMATE (Integration of ice-core, marine and terrestrial records) and the Subcommittee on Quaternary Stratigraphy (International Commission on Stratigraphy)*. Journal of Quaternary Science, 27(7): 649-659.
- Wagner B., Lotter A.F., Nowaczyk N., Reed J.M., Schwalb A., Sulpizio R., Valsecchi V., Wessels M. and Zanchetta G. (2009) – *A 40,000-year record of environmental change from ancient Lake Ohrid (Albania and Macedonia)*. Journal of Paleolimnology, 41: 407-430.
- Wang Y.J., Cheng H., Edwards R.L., An Z.S., Wu J.Y., Shen C.-C. and Dorale J.A. (2001) – *A High-Resolution Absolute-Dated Late Pleistocene Monsoon Record from Hulu Cave, China*. Science, 294(5550): 2345-2348.
- Watts W.A. :, Allen J.R.M., Huntley B. and Fritz S.C. (1996) – *Vegetation history and climate of the last 15,000 years at Laghi di Monticchio, Southern Italy*. Quaternary Science Reviews, 15: 113-132.

- Whittle A. (1996) – *Europe in the Neolithic: The Creation of New Worlds*. Cambridge: Cambridge University Press.
- Wiedner E., Scholz D., Mangini A., Polag A., Mühlhous C. and Segl M. (2008) – Investigation of the stable isotope fractionation in speleothems with laboratory experiments. *Quaternary International*, 187: 15-24
- Wigley T.M.L. and Brown M.C. (1976) – *The Physics of Caves*. In: Ford T.D. and Cullingford C.H.D. (eds) *The Science of Speleology*, Academic Press, London, pp. 329-358.
- Willis K.J. (1994) – *The vegetational history of the Balkans*. *Quaternary Science Reviews*, 13: 769-788.
- Williams P.W. (2008) – *The role of the epikarst in karst and cave hydrology: a review*. *International Journal of Speleology*, 37: 1-10.
- White W.M. (1997) – *Geochemistry. Chapter 9: Stable Isotope Geochemistry*. London: Elsevier, 700 p.
- Witkamp M and Frank M.L. (1969) – *Evolution of CO₂ from litter, humus, and subsoil of a pine stand*. *Pedobiologia*, 9: 358-365.
- Woodhead J.D., Hellstrom J., Hergt J.M., Greig A. and Maas R. (2007) - *Isotopic and elemental imaging of geological materials by laser ablation inductively coupled plasma-mass spectrometry*. *Geostandards and Geoanalytical Research*, 31(4): 331-343.
- Wunsam S., Schmidt R. and Müller J. (1999) – *Holocene lake development of two Dalmatian lagoons (Malo and Veliko Jezero, Isle of Mljet) in respect to changes in Adriatic sea level and climate*. *Palaeogeography, Palaeoclimatology, Palaeoecology*, 146: 251-281.
- Wynn P.M., Fairchild I.J., Frisia S., Spötl C., Baker A., Borsato A. And EIMF (2010) – *High-resolution sulphur isotope analysis of speleothem carbonate by secondary ionisation mass spectrometry*. *Chemical Geology*, 271(3-4): 101-107.
- Yurtsever Y. (1975) – *Worldwide survey of stable isotopes in precipitation*. Rep. Sect. Isotope Hydrology, IAEA.
- Zanchetta G., Drysdale R.N., Hellstrom J.C., Fallick A.E., Isola I., Gagan M.K. and Pareschi M.T. (2007) – *Enhanced rainfall in the Western Mediterranean during deposition of sapropel S1 : stalagmite evidence from Corchia cave (Central Italy)*. *Quaternary Science Reviews*, 26: 279-286.
- Zanchetta G., Sulpizio R., Roberts N., Cioni R., Eastwood W.J., Siani G., Caron B., Paterne M. and Santacroce R. (2011) – *Tephrostratigraphy, chronology and climatic events of the Mediterranean basin during the Holocene: An overview*. *The Holocene*, 21(1): 33-52.
- Zanchetta G., Rigattieri E., Isola I., Drysdale R.N., Bini M., Baneschi I., Hellstrom J.C. (2016) – *The so-called “4.2 event” in the Central Mediterranean and its climatic teleconnections*. *Alpine and Mediterranean Quaternary*, 29(1): 2279-7335.
- Zupan Hajna N. (2012) – *Dinaric karst: Geography and Geology*. In: *Encyclopedia of Caves*, 2nd Edn, edited by: White B.W. and Culver C.D., Elsevier, Oxford.